Proximal Sensing For Scalable Mapping Of Shallow Coastal Ecosystems

Elucidating the community structure of coral reefs and mangrove forests through dense and detailed maps and inventories

Daniel Schürholz

Doctoral Dissertation
Date of thesis defense: 09.02.2024

Proximal Sensing For Scalable Mapping Of Shallow Coastal Ecosystems

Elucidating the community structure of coral reefs and mangrove forests through dense and detailed maps and inventories

Universität Bremen

Fachbereich 2: Biologie und Chemie

Proximal Sensing For Scalable Mapping Of Shallow Coastal Ecosystems

Elucidating the community structure of coral reefs and mangrove forests through dense and detailed maps and inventories

Dissertation zur Erlangung des Grades eines Doktors der Naturwissenschaften
– Dr. rer. nat. –

Vorgelegt von: Daniel Schürholz

03. Januar 2024
Datum des Kolloquiums: 09.02.2024

1. Gutachter: PD Dr. Hauke Reuter
2. Gutachter: Dr. Dirk de Beer
Betreuer: Dr. Arjun Chennu

The presented work was conducted from October 2019 to December 2023 at the Microsensor Group at the Max Planck Institute for Marine Microbiology, Bremen and at the Data Science and Technology group at the Leibniz-Centre for Tropical Marine Research (ZMT), Bremen and was part of the Marie Curie Initial Training Network “4D-REEF”.

Daniel Schürholz

Proximal Sensing For Scalable Mapping Of Shallow Coastal Ecosystems

Elucidating the community structure of coral reefs and mangrove forests through dense and detailed maps and inventories

Dissertation zur Erlangung des Grades eines Doktors der Naturwissenschaften – Dr. rer. nat. –

Fachbereich 2: Biologie und Chemie, Universität Bremen, January 2024

Selbstständigkeitserklärung

Erklärung gemäß §7 Abs. 7 Punkte 1 bis 3 der Promotionsordnung der Universität Bremen für den Fachbereich 2 (Biologie/Chemie).

Hiermit versichere ich, dass ich die vorliegende Arbeit

1. ohne unerlaubte fremde Hilfe (selbständig) angefertigt habe,
2. keine anderen als die von mir angegebenen Quellen und Hilfsmittel benutzt habe,
3. die den benutzten Werken wörtliche oder inhaltlich entnommene Stellen als solche kenntlich gemacht habe.

Bremen, den 03. Januar 2024
Datum des Kolloquiums: 09.02.2024

Daniel Schürholz

Abstract

Shallow coastal habitats, such as shallow coral reefs and mangrove forests, provide invaluable services to surrounding ecosystems and coastal human populations. In recent decades, they have experienced rapid decline and are under constant threat from direct and indirect anthropogenic stressors, such as: land run-offs, water pollution, over-fishing, coastal infrastructure development, sea-level rise and ocean acidification due to climate change. Thus, it is critical to understand how these fragile environments are fairing under present-day conditions, and how they can adapt, to be able to design and implement better regulations, protection plans and recovery efforts. Creating platforms fueled by qualitative and quantitative ecological information about the biotic communities is key in the task of posing and answering relevant questions. However, in past decades, survey efforts have struggled to capture thematically detailed, temporally frequent and spatially fine-grained information of ecosystems, partially failing to set concrete baselines. The current accelerated improvement of Artificial Intelligence (AI) algorithms and the increased accessibility of powerful imaging devices provide new tools to significantly reduce the costs of ecosystem monitoring, by automating and scaling up tedious processes. Furthermore, the increase in detail of environmental monitoring introduces the possibility of new discoveries to be made, previous beliefs to be challenged and concrete baselines to be set. This doctoral study identifies the shortcomings of traditional coral reef and mangrove forests surveying methods, on both the proximal sensing scale (e.g., underwater or on-ground sensors) and remote sensing scale (e.g., air- or spaceborne sensors). Furthermore, it shows that through well designed AI workflows, more detail and new insights on these ecosystems can be drawn, while reducing uncertainty. Moving away from sparse sampling towards dense thematic mapping provides a closer view of the underlying biodiversity in shallow coastal ecosystems, captures intra-group composition and configuration patterns, without neglecting rare species or small specimens. An environmental correlation analysis shows that more detailed sampling helps unveil the mechanisms and drivers of shifts in community composition and configuration, as well as the co-occurrence of species and substrate classes. The modern capabilities of AI workflows also enable a shift from purely areal coverage percentage studies towards organism-focused analysis. This not only facilitates in-depth spatial and temporal investigations of individuals within populations, but also reduces the error in ecosystem accounting calculations. The subsequent studies explore the ecological applications of state-of-the-art imaging platforms and novel AI workflows to automatically create habitat maps with thematic detail and individual-organism resolution, as well as showing that these analyses are spatially and thematically scalable.

Chapter 1 introduces shallow coastal ecosystems, specifically coral reefs and mangrove forests and their overall importance, the threats they face in the Anthropocene, their intricate characteristics that complicate their detailed monitoring, and the traditional and current methods used to survey them. Then, the different scales and platforms for ecosystem observation, with image analysis and environmental mapping, are briefly explained. Afterwards, the state-of-the-

art of AI applications in environmental mapping is presented. The lack of scalable dense and organism-focused mapping of habitats is described, followed by an explanation of how this dissertation helps remediate this gap. Finally, current limitations in the literature are explained and the motivations for this doctoral project are outlined.

Chapter 2 presents the design, development and assessment of an AI workflow to leverage underwater hyperspectral image transects with two machine learning algorithms, to produce dense habitat maps of a large subsection of reefs across an island's coastline. The multi-method workflow was used to label large quantities of pixels with very thematic detail for biotic classes, such as corals, algae, sponges, and substrate classes, such as sediment, turf algae and cyanobacterial mats. The workflow enabled accurate survey-scale mapping with low annotation effort and no external data. An assessment of the composition and configuration of the benthic communities was possible, with unprecedented thematic detail and with fine spatial resolution. The dense habitat maps created in this study reveal the inadequacies of traditional point sampling methods to accurately describe reef benthic communities.

Chapter 3 describes a study were an optimized version of the AI workflow presented in Chapter 2 is applied to an island-wide survey to produce 147 habitat maps of benthic coral reef communities along the leeward coast of the Caribbean island of Curaçao. The densely sampled maps provided evidence that deriving community diversity indices from sparse sampling and abstracted thematic labels can mask the true diversity of coral reefs, as well as neglect information about intra-group communities. An environmental statistical analysis provided a unique view into the drivers of community composition and the co-occurrence of biotic and abiotic benthic elements along a complete island-wide gradient. The community description was compared to previous reports on the island and provided a consistent and valuable addition to the reefs' recent natural history.

Chapter 4 focuses on the design and implementation of an AI workflow to produce an inventory of a mangrove forest with dense vegetation, inhabited by two species of mangroves. The AI workflow uses aerial imagery of the mangrove forests captured using a consumer-grade Unoccupied Aerial System (UAS), from which large orthophoto mosaics and digital surface models are built. The workflow accurately delineated individual tree canopies, segmented areas other biotic and abiotic elements of the forests and automatically created a Canopy Height Model (CHM). The workflow shows that the combination of organism-oriented analysis and area cover classifications can be used to create detailed inventories of a mangrove forests, with individual tree height information, crown shape and crown size descriptions. This reduces uncertainty in ecosystem accounting by calculating biomass and carbon stocks on organism level for large forests.

Chapter 5 discusses the next step in the implementation of organism-oriented classification in a shallow coastal ecosystem that presents higher biodiversity: coral reefs in the Coral Triangle. The taxonomic diversity requires spatially and spectrally richer data to be acquired, such that individual biotic organisms can be automatically delineated and classified to finer taxonomic levels through AI workflows. The requirements and a data collections example are shown in this

chapter, laying the ground-work for detailed ecological descriptions of shallow coastal ecosystems.

Chapter 6 presents the merits of the doctoral research in terms of the technical achievements of the AI workflows designed and implemented, the ecological insights gained due to the application of the new methods and the limitations of the workflows. Finally, future work regarding the optimization, the scalability and the adaptation of the workflows to other settings is discussed.

Zusammenfassung

Flache Küstenlebensräume, wie viele Korallenriffe und Mangrovenwälder, erbringen unschätzbare Leistungen für die umliegenden Ökosysteme und für die Küstenbevölkerung. In den letzten Jahrzehnten haben sie einen raschen Rückgang erlebt und sind ständig durch direkte und indirekte anthropogene Stressfaktoren bedroht, wie z. B. Landabfluss, Wasserverschmutzung, Überfischung, Anbau von Küsteninfrastruktur, Anstieg des Meeresspiegels und Versauerung der Meere infolge des Klimawandels. Daher ist es von entscheidender Bedeutung zu verstehen, wie sich diese empfindliche Ökosysteme unter den heutigen Bedingungen verhält und wie sie sich anpassen kann, um bessere Vorschriften, Schutzpläne und Wiederherstellungsmaßnahmen entwerfen und umsetzen zu können. Die Schaffung von Plattformen, die sich auf qualitative und quantitative ökologische Informationen über die Lebensgemeinschaften stützen, ist der Schlüssel, um relevante Fragen zu stellen und zu beantworten. In den vergangenen Jahrzehnten haben sich die Erhebungen jedoch schwer getan, thematisch detaillierte, zeitlich häufige und räumlich feinkörnige Informationen über Ökosysteme zu erfassen, so dass es teilweise nicht gelungen ist, konkrete Grundlinien festzulegen. Die derzeitige beschleunigte Verbesserung von Algorithmen der künstlichen Intelligenz (KI) und die zunehmende Verfügbarkeit leistungsfähiger Bildgebungsgeräte bieten neue Werkzeuge, um die Kosten der Ökosystemüberwachung durch die Automatisierung und Skalierung langwieriger Prozesse erheblich zu senken. Darüber hinaus bietet die zunehmende Detailliertheit der Umweltüberwachung die Möglichkeit, neue Entdeckungen zu machen, frühere Annahmen in Frage zu stellen und konkrete Ausgangspunkte festzulegen. In dieser Doktorarbeit werden die Unzulänglichkeiten herkömmlicher Vermessungsmethoden für Korallenriffe und Mangrovenwälder aufgezeigt, und zwar sowohl auf der Ebene der Naherkundung (z. B. Unterwasser- oder Bodensensoren) als auch auf der Ebene der Fernerkundung (z. B. luft- oder weltraumgestützte Sensoren). Außerdem wird hier zeigt, dass durch gut konzipierte KI-Workflows Arbeitsabläufe mehr Details und neue Erkenntnisse über diese Ökosysteme gewonnen werden können und gleichzeitig die Fehlerquote gesenkt werden kann. Die Abkehr von spärliche Probenahmen hin zu einer dichten thematischen Kartierung ermöglicht einen genaueren Blick auf die zugrunde liegende biologische Vielfalt in flachen Küstenökosystemen und erfasst die Zusammensetzung innerhalb von Gruppen und Konfigurationsmuster, ohne seltene Arten oder kleine Exemplare zu vernachlässigen. Eine korrelative Analyse von Umweltfaktoren zeigt, dass eine detailliertere Probenahme dazu beiträgt, die Mechanismen und Triebkräfte von Veränderungen in der Zusammensetzung und Konfiguration von Gemeinschaften sowie das gemeinsame Auftreten von Arten und Substratklassen aufzudecken. Diese Doktorarbeit zeigt auch, dass die modernen Leistungsfähigkeiten von KI-Workflows eine Verlagerung von rein flächenbezogenen Studien hin zu organismusorientierten Analysen ermöglichen. Dies erleichtert tiefgreifende räumliche und zeitliche Untersuchungen von Individuen innerhalb von Populationen, verringert aber auch den Fehler bei Berechnungen der Ökosystembilanz. Die nachfolgenden Studien untersuchen die ökologischen Anwendungen modernster Bildgebungsplattformen und neuartiger KI-Workflows zur au-

tomatischen Erstellung von Habitatkarten mit thematischer Detailgenauigkeit und mit einzelne Organismen-Auflösung, und zeigen, dass diese Analysen räumlich und thematisch skalierbar sind.

Kapitel 1 stellt flache Küstenökosysteme vor, insbesondere Korallenriffe und Mangrovenwälder, ihre Bedeutung, die Bedrohungen, denen sie im Anthropozän ausgesetzt sind, ihre Merkmale, die ihre detaillierte Überwachung erschweren, sowie die traditionellen und aktuellen Methoden zu ihrer Überwachung. Dann werden die verschiedenen Maßstäbe und Plattformen für die Beobachtung von Ökosystemen mit Bildanalyse und Umweltkartierung kurz erläutert. Anschließend wird der Stand der Technik bei KI-Anwendungen in der Umweltkartierung vorgestellt. Der Mangel an skalierbaren, dichten und auf Organismen fokussierten Kartierungen von Lebensräumen wird beschrieben, und dann, wie diese Dissertation dazu beiträgt, diese Lücke zu schließen. Abschließend werden die derzeitigen Einschränkungen in der Literatur erläutert und die Motivation für dieses Promotionsprojekt dargelegt.

Kapitel 2 präsentiert die Konzeption, Entwicklung und Bewertung eines KI-Arbeitsablaufs zur Nutzung von Unterwasser-Hyperspektralbild-Transekten und zwei Algorithmen für maschinelles Lernen, um dichte Habitatkarten eines großen Abschnitts von Korallenriffen entlang der Küstenlinie einer Insel zu erstellen. Der Multi-Methoden-Workflow wurde verwendet, um große Mengen von Pixeln mit sehr detaillierten thematischen Angaben für biotische Klassen wie Korallen, Algen und Schwämme sowie für Substratklassen wie Sediment, Turf-Algen und Cyanobakterienmatten zu kennzeichnen. Der Arbeitsablauf ermöglichte eine genaue Kartierung im Untersuchungsmaßstab mit geringem Anmerkungsaufwand und ohne externe Daten. Eine Bewertung der Zusammensetzung und Konfiguration der benthischen Lebensgemeinschaften war möglich, und zwar mit einer noch nie dagewesenen thematischen Detailliertheit und einer feinen räumlichen Auflösung. Die dicht-geprobten Habitatkarten, die in dieser Studie erstellt wurden, zeigen die Unzulänglichkeiten herkömmlicher Punktprobenmethoden zur genauen Beschreibung benthischer Korallenriffgemeinschaften.

Kapitel 3 beschreibt eine Studie, bei der eine optimierte Version des in Kapitel 2 vorgestellten KI-Arbeitsablaufs auf eine inselweite Erhebung angewendet wurde, um 147 Habitatkarten von benthischen Korallenriffgemeinschaften entlang der Leeseite der Karibikinsel Curaçao zu erstellen. Die dicht geprobte Karten lieferten den Beweis, dass die Ableitung von Indizes der Gemeinschaftsvielfalt aus spärlichen Probenahmen und abstrakten thematischen Bezeichnungen die wahre Vielfalt von Korallenriffen verschleiern und Informationen innerhalb Funktionelle-Gruppen in Gemeinschaften vernachlässigen kann. Eine statistische Analyse von Umweltfaktoren ermöglichte einen einzigartigen Einblick in die Triebkräfte der Gemeinschaftszusammensetzung und das gemeinsame Vorkommen biotischer und abiotischer benthischer Elemente entlang eines kompletten inselweiten Gradienten. Die Beschreibung der Lebensgemeinschaften wurde mit früheren Berichten über die Insel verglichen und lieferte eine konsistente und wertvolle Ergänzung zur jüngsten Naturgeschichte der Riffe.

Kapitel 4 konzentriert sich auf die Entwicklung und Umsetzung eines KI-Arbeitsablaufs zur

Erstellung einer Bestandsaufnahme eines Mangrovenwaldes mit dichter Vegetation, der von zwei Mangrovenarten bewohnt wird. Der KI-Arbeitsablauf verwendet Luftbilder der Mangrovenwälder, die mit einem unbesetzten Luftfahrtsystem (UAS) der Verbraucherklasse aufgenommen wurden, aus denen große Orthofoto-Mosaike und digitale Oberflächenmodelle erstellt werden. Der Arbeitsablauf ermöglichte eine genaue Abgrenzung der einzelnen Baumkronen, die Segmentierung von Gebieten mit anderen biotischen und abiotischen Elementen der Wälder und die automatische Erstellung eines Baumkronenhöhenmodells (CHM). Diese Studie zeigt, dass die Kombination aus organismusorientierter Analyse und Flächendeckungsklassifizierungen verwendet werden kann, um detaillierte Bestandsaufnahmen eines Mangrovenwaldes mit Informationen über die Höhe einzelner Bäume, die Kronenform und die Kronengröße zu erstellen. Dies verringert die Unsicherheit bei der Ökosystembilanzierung durch die Berechnung von Biomasse und Kohlenstoffvorräten auf Organismusebene für große Waldflächen.

Kapitel 5 erörtert die nächste Schritte bei der Umsetzung der organismusorientierten Klassifizierung in einem flachen Küstenökosystem, das eine größere Artenvielfalt aufweist: Korallenriffe im Korallendreieck. Die taxonomische Vielfalt erfordert die Erfassung räumlich und spektral reichhaltigerer Daten, so dass einzelne biotische Organismen durch KI-Workflows automatisch abgegrenzt und auf feineren taxonomischen Ebenen klassifiziert werden können. In diesem Kapitel werden die Anforderungen und ein Beispiel für Datensammlungen vorgestellt, die die Grundlage für detaillierte ökologische Beschreibungen von flachen Küstenökosystemen bilden.

Kapitel 6 präsentiert die Erreichungen der Doktorarbeit im Hinblick auf: die technischen Leistungen der entwickelten und implementierten KI-Workflows, die durch die Anwendung der neuen Methoden gewonnenen ökologischen Erkenntnisse und die Grenzen der Workflows. Abschließend werden zukünftige Arbeiten hinsichtlich der Optimierung, der Skalierbarkeit und der Anpassung der Arbeitsabläufe an andere Umgebungen diskutiert.

Curriculum Vitae

Daniel Schürholz

Leibniz Centre for
Tropical Marine Research (ZMT)
Farenheitstr. 6
28359 Bremen

daniel.schuerholz@leibniz-zmt.de
daniel.schurholz@gmail.com
+49 151 25073504

Education

2019 - 2024 (expected)	**Early Stage Researcher – Marie Curie Fellow** Initial Training Network: 4DREEF Doctoral candidate at Universität Bremen Max Planck Institute for Marine Microbiology, Germany
2017 - 2019	**Erasmus Mundus Master of Science in Software Engineering** Joint Programme in Pervasive Computing and Communications for sustainable development (PERCCOM) Deakin University, Melbourne, Australia Luleå University of Technology, Skellefteå, Sweden Lappeenranta University of Technology, Lappeenranta, Finland Université de Lorraine, Nancy, France Graduated, ***Grade 4.49/5***
2009 - 2014	**Bachelor of Science in Computer Science** Universidad Católica San Pablo Graduated, ***GPA: 3.9/4.0***

Scholarships

2019-2022	EU Marie Curie fellowship as Early Stage Researcher
2017-2019	EU Erasmus Mundus fellowship for graduate course
2009-2014	Full-Scholarship for outstanding academic performance during Bachelor of Science

Publications

2023	Seeing the Forest for the Trees: Mapping Cover and Counting Trees from Aerial Images of a Mangrove Forest Using Artificial Intelligence, Remote Sensing, 15-13, p.3334. DOI:10.3390/rs15133334
2022	Digitizing the coral reef: Machine learning of underwater spectral images enables dense taxonomic mapping of benthic habitats. In: *Methods in Ecology and Evolution*, 14-2, pp.596–613. DOI: 10.1111/2041-210X.14029
2020	Artificial intelligence-enabled context-aware air quality prediction for smart cities. In: *Journal of Cleaner Production*, 271, p.121941. DOI:10.1016/j.jclepro.2020.121941
2019	MyAQI: Context-aware Outdoor Air Pollution Monitoring System. In: *Proceedings of the 9th International Conference on the Internet of Things (IoT '19)*, 13, pp.1–8. DOI:10.1145/3365871.3365884
2019	Context- and Situation Prediction for the MyAQI Urban Air Quality Monitoring System. In: *Internet of Things, Smart Spaces, and Next Generation Networks and Systems (ruSMART 2019)*, v11660. DOI:10.1007/978-3-030-30859-9_7

Courses & certifications

2023	Matching Talents and Desires in your Career Naturalis Museum, Leiden, Netherlands
2022	Remote Sensing and Mapping for Coral Reef Conservation (Online Course) The Nature Conservancy
2022	Carbonate Sedimentation and Ancient Reefs Course Universidad de Granada, Carboneras, Spain
2021	Steps into Academic Teaching Course Max Planck Institute for Marine Microbiology, Germany
2020	Peer Review for Early Stage Researchers Max Planck Institute for Marine Microbiology, Germany
2018	ITMO International Seminar in Green IT and Sustainable Development Saint Petersburg, Russia

Conferences & workshops

Jul 2023	Marine Atlas and GIS Workshop Instituto del Mar del Perú (IMARPE), Lima, Peru (oral presentation/lecturer)
Jan 2023	Leibniz Centre for Tropical Marine Research (ZMT) Annual Conference Bremen, Germany (oral presentation)
Sep 2022	Annotation of underwater orthomosaic images Hassanudin University UNHAS, Makassar, Indonesia (4DREEF field workshop)
Jul 2022	International Coral Reef Symposium (ICRS) Universität Bremen, Bremen Germany (oral presentation & external organization committee)
Jul 2021	International Coral Reef Symposium (ICRS) (online conference) Universität Bremen, Bremen Germany (oral presentation)
Sep 2019	IEEE Whispers Amsterdam, Netherlands

Research Experience

2023	Consulting GIS expert and data scientist for Peruvian Marine Atlas development (PARAWET project) Leibniz Centre for Tropical Marine Research (ZMT), Bremen, Germany
2022	Spectral and color image acquisition of 13 coral reefs with HyperDiver device Spermonde Archipelago, South Sulawesi, Indonesia
2022	Multispectral camera addition to HyperDiver device and field test Los Gigantes, Tenerife, Spain
2022	Setup of AI workflows on HPC-Clusters Leibniz Centre for Tropical Marine Research (ZMT) Datalab
2021	European Scientific Diver training Leibniz Centre for Tropical Marine Research (ZMT), Bremen, Germany
2020	Stereo-camera addition to HyperDiver device and surveying protocol development Max Planck Institute for Marine Microbiology, Germany

Acknowledgements

I am very grateful for the support I have received from supervisors, friends, colleagues, collaborators and kind strangers. During this doctoral project, I have had great guidance and encouragement from many people, who have made the difficulties more navigable and the successes more enjoyable.

First, I would like to thank Arjun Chennu for his constant support and guidance during the day-to-day work. I am very grateful for the patience in the beginning of the project, when I seemingly did not understand a thing, and the trust in later stages, where I was encouraged take the lead in research projects. While writing this dissertation I have noticed how much I have learnt during my PhD, and a great deal of that knowledge has come from our daily conversations and knowledge exchange on many topics, from disentangling Snakemake graphs to describing the drivers of coral reef community composition. The supervision has been an example for me of true scientific spirit, and has given me the motivation to continue developing tools to better understand our natural world.

I would also like to thank my first group leader, Dirk de Beer, for allowing this computer scientist to join the Microsensors group in a microbiology institute. The openness of Dirk to supervise a variety of seemingly unrelated topics provided a great atmosphere of transdisciplinarity in the group, where ideas stemming from various perspectives inspired great breakthroughs and collaborations. I also cherish the advice he has given me for this thesis project and for my career in general, and for the patience while waiting for ecological insights and not only methodological work, it did pay off in the end. Similarly, I would like to thank Hauke Reuter for accepting to lead my PhD thesis committee and providing deep insights into the direction of my project. He has also shown great patience throughout the stages of learning I underwent in the project. I am grateful for his openness and support to changes in research directions during the thesis project, specially those incurred due to the pandemic. Also, thanks to Martin Zimmer and Martin Diekmann for agreeing to be a part of the examination committee.

During my project I have worked and shared working groups with so many wonderful colleagues and friends. My time at the Microsensors group and MPI Bremen has been great, even with that small pandemic-interruption. I would like to thank my “tocayo” Daniel for weathering the hardships of a PhD life through a pandemic with me, so far away from our South-American homes; the conversations shared with him and Seba reminded me a bit of being back-home. I am grateful for having had Elisa, Andrea, Marit, Lauren and Olivia as colleagues and friends at the MPI, and all the fun moments in- and outside of work. At the ZMT I was lucky to have Fridolin Haag as a colleague and friend, sharing many insightful conversations, on a variety of research- and life topics; setting the bar quite high for future office-mates. Similarly, I cherish all the shared experiences with my colleagues in the Datech group at ZMT: Khishma, Azelea, Dominic, Michelia and Eugene. Many other workers, collaborators, postdocs, PhD and master

students at both institutes have, with small encounters throughout these 4 years, cheered my spirit up and replenished my energy.

I am happy to have been part of the 4D-REEF Marie Curie ITN, where I have met another group of great people that have helped endure the hardships of a PhD. Thanks to all ESRs for always making the training activities twice as fun and full of laughter. I also have a special place in my heart for the Indonesian people I met during the project's field work, those 5 weeks have taught me almost the same as 4 years of studying. Estra, Masdar, Agus, Agung, Gunawan and Phita were all great role-models for improving myself in every aspect, and an inspiration to want to help my own country through hard work and good science. A big thanks also goes to Sebastian Ferse for his invaluable advice on the field site and on my PhD thesis committee meetings, helping me cement my new acquired knowledge about coral reef ecology.

I am very grateful for the research and education initiatives by the European Commission, whose support allowed me to kick-start my graduate education endeavours in Europe. My Erasmus Mundus fellowship (PERCCOM) allowed me to become familiar with the excellency in education offered across European universities and also to meet many international people, whose friendship I still cherish to this day. This foundation allowed me to navigate and succeed as an early stage researcher in a completely new field of study as part of the 4D-REEF Marie Curie ITN. The funding and support received from the network has been very valuable.

During my stay in Bremen I have met so many kind people and made amazing friends that allowed me to escape the incessant work related thoughts, and gave me a sentiment of belonging to this city. I thank my Roundnet gang for providing an escape into competitive sports and fun weekend activities, and the Uni-Bremen-masters gang for all the fun Kohltours, parties and outdoor activities we have shared.

Finally, without the constant support of my family and friends back in Peru, none of this would have been possible. I am lucky to have a family that has always supported my numerous changes in career paths, from professional footballer to marine scientist. My parents have been an example of perseverance an hard work throughout my life, and they continue to inspire me and my siblings. My siblings have always motivated me to reach for higher goals and always offered their love and understanding during the highs and lows of this enterprise. As any self-respecting latino would do, I also have to thank my large extended family, all the "tíos", "tías", "primos" and "sobrinos" in Peru and Germany, all of them share a bit of this success through the warmth they have always shown me. Specially, I would like to thank Martin Silva for continuously being an impromptu therapist for me, setting me right back on course during times of self-doubt. Finally, to all my friends in Peru: Ignacio, Luis, Oscar, Chemo, Alfredo, Victor and many more, a huge "gracias" for being there for me, even if sometimes I had to miss some of their most important life-events to pursue this dream of mine.

Contents

List of Figures

List of Tables

List of Algorithms

Part I

Introduction

Chapter 1

Scalable observations in shallow coastal ecosystems

Sight has played a major role in the human capacity to navigate and remember their environment, and the temporal changes within it. As our understanding of the natural world expands and the visual tools to measure its features improve, it becomes more complex to mentally retain every observed detail. In this context, maps have emerged as preferred models to help us visually portray advanced information about our environment, helping researchers and policymakers better understand the spatial distribution of environmental variables such as biotic communities, land cover, vegetation, terrain, anomalies, among many more (Lecours 2017; Maes et al. 2012).

In the past, field observations were made with visual identification followed by notebook-annotations or hand-drawn sketches of the spatial distribution of biotic and abiotic elements (Duyl 1985; Goreau 1959). With the advent of modern imaging technologies and platforms, increasingly more complex photographs and models are being used to capture snapshots of entire ecosystems at different scales (Alonso et al. 2019; Goldberg et al. 2020; Lassalle et al. 2022; UNEP-WCMC et al. 2010). The ecological analyses that these models unlock, provide groundbreaking insights into the functioning of the natural world. On their own, the image snapshots are useful for an offline visual reference of the captured ecosystems, but visually identifying all target features to the highest detail possible, would take an extraordinary amount of effort. Furthermore, considering that these data-acquisition platforms are starting to cover larger spatial- and more frequent temporal scales, analysis by human-experts alone can become a bottleneck (Beijbom et al. 2015). Thus, the sheer amount of incoming raw data precludes the extraction of important information, when counting only with the capacity of human observers. The finer the detail that is to be extracted from an ecosystems' community characteristics, from the distribution of its biotic communities to their changes over time, the more reliance is to be had on technological advances that can automate and scale-up the observation process.

Technological advances in computer-based image analysis and AI promise to aid in the daunting

task of analysing a large number of field observations, but many ecosystems manifest complex settings that create a set of difficulties to be correctly surveyed and analysed. Shallow coastal ecosystems are no exception, as they present challenging settings for traditional and current observation methods to accurately capture and describe their biotic communities and the structure of their habitats. In the following sections, the characteristics of these ecosystems are explained, the traditional techniques for surveying their biotic and abiotic features are explored, the scales of modern imaging techniques are listed, and the trends in environmental mapping and analysis using AI are discussed.

1.1 Shallow coastal ecosystems

Tropical shallow coastal ecosystems, such as coral reefs and mangrove forests, are distributed across many tropical and a few sub-tropical regions of the world (Figure 1.1). Coral reefs help maintain the health of marine environments and provide numerous services to terrestrial ecosystems, as well as to many human populations (Moberg and Rönnbäck 2003). They play a major role in stabilizing the global climate, despite their rather reduced cover of Earth's surface. Coral reefs provide critically important habitats, thus understanding the intricate composition of biotic communities in these ecosystems and their interactions with their abiotic environment is very relevant, as it facilitates the development of strategies for conservation, sustainable management and restoration efforts (Lecours 2017).

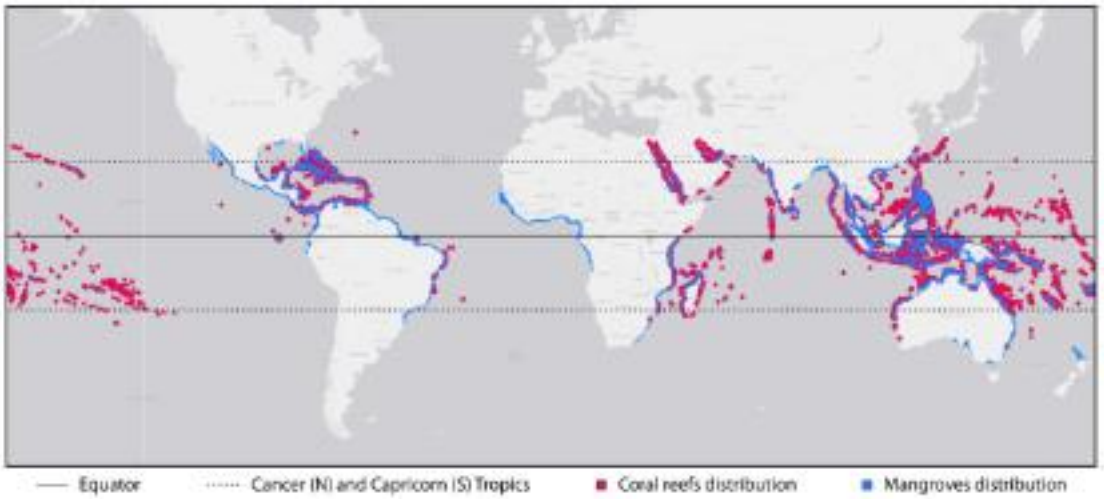

Figure 1.1 Worldwide distribution map of coral reefs and mangrove forests. Coral reef distribution data was taken from the UN Environment Programme - World Conservation Monitoring Centre (UNEP-WCMC), WorldFish Centre, World Resources Institute (WRI), The Nature Conservacy (TNC) (UNEP-WCMC et al. 2010) and mangrove forest data from the Global Mangrove Watch Version 3.0 (Bunting et al. 2022).

1.1.1 Shallow coral reef ecosystems

Coral reefs provide essential habitats for a wide variety of marine species, including fish, crustaceans, mollusks, and various other invertebrates. While occupying just $0.1 - 0.5\%$ of the ocean floor, these ecosystems serve as habitats for nearly a third of marine fish species and other marine biota (MacNeil et al. 2015; M. D. Spalding et al. 1997). The complex structure of scleractinian corals in healthy reefs offers shelter, breeding grounds, and food sources, supporting a rich diversity of life (Connell 1978; Grigg et al. 1984; Plaisance et al. 2011). Coral reef ecosystems also provide many direct and indirect services to human populations (Moberg and Folke 1999; Moberg and Rönnbäck 2003). Many commercially important fish species use coral reefs as nurseries and breeding grounds, helping in the recruitment and maintenance of fish populations, supporting the sustainability of fisheries (Costanza et al. 1997; Moberg and Rönnbäck 2003; Nagelkerken, Velde, et al. 2000). Coral reefs often attract tourism, generating revenue for local economies (M. Spalding et al. 2017). They also provide protection of coastal shorelines from storms and erosion, allowing coastal settlement and development. The degradation and loss of coral reefs could have devastating effects on all other ecosystems and populations depending on these listed services.

Coral reefs are currently under increased pressures as a consequence of human activities. Large changes in community composition and disruptions of the trophic hierarchy are prompted by activities like over-fishing, pollution, eutrophication, coastal development, diving tourism, and the introduction of invasive species (T. P. Hughes et al. 2003; Terence P. Hughes 1994; Terence P. Hughes et al. 2007; Terry P. Hughes, Barnes, et al. 2017; J. B. C. Jackson et al. 2001; Lamb et al. 2014; Pandolfi et al. 2003). Already weakened reefs fail to cope with other stresses coming from indirect factors as a consequence of climate change, such as rising sea levels, rising water temperatures and ocean acidification (D. R. Bellwood et al. 2004; Terry P. Hughes, Barnes, et al. 2017; Pandolfi et al. 2003).

Among the biogeographic regions containing coral reefs, the Caribbean presents a large number of deteriorated reefs. In recent decades, reefs in the Caribbean have seen the loss of vast numbers of *Acroporid* specimens and other reef-building species, inducing a loss in reef complexity (Alvarez-Filip et al. 2009; Gardner et al. 2003; Precht et al. 2006). Exploding human populations in urban areas, added to large numbers of tourists yearly visiting Caribbean beaches, have significantly contributed to this deterioration (Fund 2017; Hawkins et al. 1999). Given that these reefs contain lower biodiversity than reefs in other biogeographic regions, such as the Indo-Pacific, their resilience is diminished by the lack of functional redundancy (D. R. Bellwood et al. 2004; David R. Bellwood et al. 2003; E. J. Jackson et al. 2014). Reefs once dominated by *Orbicella*, *Acropora* and *Diploria* scleractinian corals are shifting to macroalgae dominated reefs, and if further deteriorated, to bacteria-dominated ecosystems (Bak et al. 2005; Brocke et al. 2015; De Bakker, Meesters, et al. 2016; De Bakker, Van Duyl, et al. 2017; Reverter et al. 2022).

Reefs in the Coral Triangle, located in the Indo-Pacific biogeographic region, usually contain a much higher scleractinian coral diversity, with up to 605 species (Veron et al. 2011). This boosts their resilience to changes due to functional redundancy. However, the region has also experienced a high increase in human population and number of coastal of settlements, with countries like Indonesia increasing from 87.75 Million to 275.50 Million inhabitants from 1950 to 2022[1]. The demand for fish as basic diet has increased on-par with the population, and illegal fishing techniques (e.g., blast fishing) have become pervasive in the region, debilitating reefs by directly breaking their structure or removing large numbers of grazers, leading to algal overgrowth (Hampton-Smith et al. 2021; Pauly et al. 1989). Mass coral bleaching events and band-disease outbreaks have further decimated some of the already weakened coral reefs in the region (Terry P. Hughes, Anderson, et al. 2018; McManus et al. 2020; Peñaflor et al. 2009). This increase in human population, has also elevated eutrophication levels in shallow coral reefs due to agricultural and industrial run-offs and sewage output from cities. Under these conditions, certain genera of scleractinian corals have adapted to conditions with high concentration of suspended particles and turbidity, forming turbid reefs, which are being studied as possible coral havens under more extreme future conditions (Browne et al. 2012; Evans et al. 2020; Perry et al. 2012; Sully et al. 2020).

The current state of coral reefs globally, added to the harsh conditions predicted in the future, increase the importance of constantly surveying these reefs as a mean to monitor, protect and recover them, as well as to set detailed baselines on different spatial scales. However, coral reefs present complicated conditions for observation methods.

1.1.1.1 Environmental settings of shallow coral reefs

The exact depth until which a coral reef is deemed as shallow is a debated topic, but usually reefs within the first 30 meters below sea-level are considered as shallow. These reefs are located in the euphotic zone and are usually found in oligotrophic environments with clear water. Despite having high levels of incident sunlight, they present difficult environments to be visually surveyed while underwater. For example, because of their complex 3D structure, many benthic organisms are occluded by geomorphic structures or other superposing organisms (Kornder et al. 2021). In reef slopes, light attenuation along the depth gradient influences the visibility and reduces discernability between organisms, specially those with similar colors and morphologies. The high taxonomic diversity of benthic organisms in coral reefs also increases the difficulty of visually identifying separating between species and sometimes even genera, prompting the use of molecular methods (Fabricius 2006). The medium itself presents another limit for human observers, given that divers have a limited air-supply and have to control the length and depth of the underwater activities to avoid dive-related illnesses. Turbid reefs present another limitation, with suspended particles significantly reducing underwater visibility by reflecting much of

[1] https://www.worlddata.info/asia/indonesia/populationgrowth.php, visited on: 17/12/23

the incoming light. Out-of-water observation methods have the added difficulty of the air-water interface, with light attenuation, glint, light refraction and increased distance to target, limiting the visibility to a certain depth. All the aforementioned characteristics change with the reef geomorphology, the geographic location and the distance-to-shore of each coral reef. For example, reef flats, reef crests and lagoons typically receive more direct sunlight, while deeper outer reefs and reef slopes see a rapid decrease with depth of incident sunlight.

Despite the challenging environmental conditions to survey reefs, researchers have found innovative ways to describe large sections of coral reefs worldwide (Reverter et al. 2022; Sandin, Alcantar, et al. 2022; Sandin, Smith, et al. 2008). However, the use of an array of different surveying methods, lack of standardized surveying protocols, the shift/lack of baselines and the lack of reported uncertainty values, has resulted in only $0.01 - 0.1\%$ of reefs having been quantitatively described (Estes et al. 2018; Hochberg et al. 2021; Muldrow et al. 2020). Thus, standardization of survey methods with clear uncertainty values, are imperative to scale up observation across time and space.

1.1.1.2 Benthic surveying methods in coral reefs

Since the invention of the Self-Contained Underwater Breathing Apparatus (SCUBA) for independent diving, scientists have developed a number of quantitative and semi-quantitative methods to survey benthic sessile communities in coral reefs, capturing the diversity and community composition of large stretches of reefs while being underwater (Urbina-Barreto et al. 2021) (Figure 1.2). Methods, such as Line Intersect Transect (LIT) or point-sampling with photoquadrats have been implemented to sample representative sparse points along a series of underwater transects (Kohler et al. 2006; Loya 1972). These methods have the advantage of reducing the survey and analysis time, by largely under-sampling the reef, while reporting numbers of percentage cover, mostly of dominant classes. Nonetheless, studies have shown that with these methods, rare and smaller species are usually neglected (Pante et al. 2012; Perkins et al. 2016). Random sampling in photoquadrat point-counts also has also been questioned as to its ability to truly represent the taxon richness (Cao et al. 2002). Another caveat of these methods is that all annotations are carried out by human experts, which can introduce biases influenced by their level and field of expertise (Beijbom et al. 2015; Misra et al. 2016). LIT annotations are also problematic given the fact that they cannot be revisited by multiple experts, because the identification and annotation of benthic targets takes place underwater.

More modern techniques rely on Structure-from-Motion (SfM) software to build photogrammetric models from large numbers of co-registered top-down images taken with submersible or aerial imaging platforms. The resulting models are ortho-rectified photomosaics (or orthomosaics), which are top-down views of entire scenes, 3D models, which can be meshes or point-clouds and digital surface models (DSMs), that provide topographic or bathymetric information. These

models provide detailed information on the distribution of elements in a scene and on the complexity of the 3D structure of coral reefs (Carlot et al. 2020; Ferrari et al. 2016; Fukunaga et al. 2019; Storlazzi et al. 2016). Novel annotation tools (e.g., TagLab (Pavoni, Corsini, Ponchio, et al. 2022)) can aid human experts in labeling analytical targets in the benthic communities within the photogrammetric models. This "dry" annotation process of underwater ecosystems remove the air-time restriction of purely diver-oriented methods, allowing multiple experts to concentrate on targets of their own field of expertise. However, as camera platforms and SfM software become more accessible, increasingly larger areas are being captured and with more frequency, and automated scalable workflows are required to meet the demand for annotation effort.

A pervasive problem when undertaking submersed surveys of underwater environments, is the lack of precise georeferencing of samples. Geo-positional systems, such as GPS, do not work below the water surface, as the signal is scattered through the medium. This difficults survey repetition and photogrammetric model co-registration on a site, hindering temporal analyses. Low-tech solutions exist, but are not very precise. For example, GPS receivers are inserted in a surface buoy that is dragged by a diver while doing a line transect. In contrast, high-end robotic systems like Autonomous Underwater Vehicles (AUVs) and rovers, can have underwater positioning systems, that rely on a connection to a surface vessel, but this survey setting can be prohibitively expensive for small-scale operations. Aerial platforms (such as Unoccupied Aerial Systems (UASs)) or surface platforms (such as boats with cameras attached to their hulls) have the advantage of carrying GPS devices, which automatically georeferences all their products.

1.1.2 Mangrove ecosystems

Many services provided by coral reefs are also provided by mangrove forests, as they have a similar worldwide bio-geographical distribution (Figure 1.1). Mangroves, and other coastal vegetation, act as natural buffers in the sea-land interface, providing protection against storm surges, hurricanes, and tsunamis (Bimrah et al. 2022; Getzner et al. 2020; M. Brander et al. 2012). The intricate root systems of mangroves stabilize coastlines, reduce erosion, and mitigate the impacts of extreme weather events, contributing to the overall resilience of coastal areas. Mangroves and seagrasses, play a vital role in carbon sequestration, as they absorb large amounts of carbon dioxide from the atmosphere and store it in their biomass and sediments, providing better storage than other forest types (S. E. Hamilton and Friess 2018). This sequestered carbon has been coined "blue carbon". It helps mitigate climate change and is an asset that is gaining importance in international environmental management in recent decades (Macreadie et al. 2019; Ouyang et al. 2023). Mangroves also act as natural filters, trapping sediments and pollutants and improving water quality overall, helping maintain the balance of nutrients in coastal waters. They also provide a similar volume of nursery space for important fish species as coral reefs

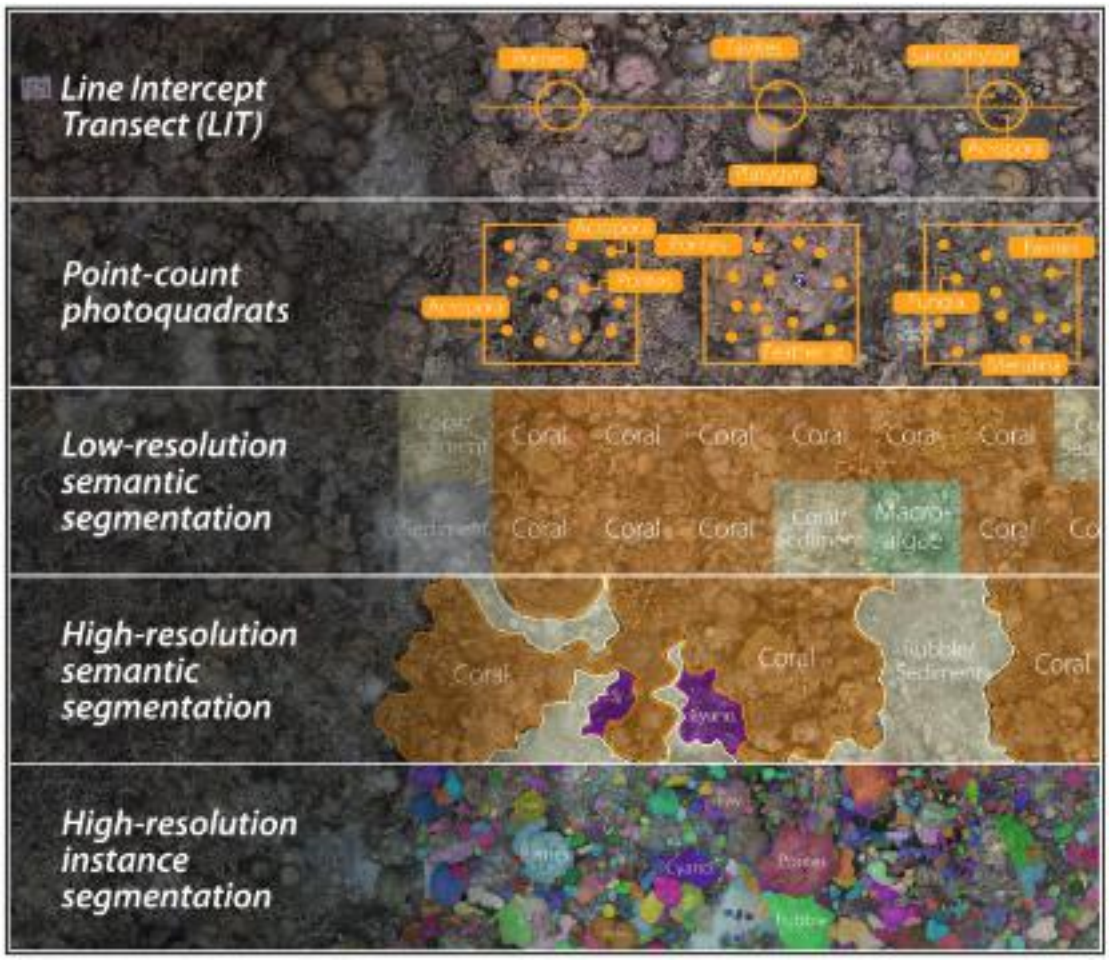

Figure 1.2 Comparison of coral reef benthic surveying methods. All 5 methods sample at different spatial and thematic scales. The LIT method produces spatially sparse samples that have no spatial coordinate system, but the thematic scale can be very detailed, depending on the expertise of the human observer. Photoquadrat sampling produces similar samples as LIT, but the use of images allows for annotation revisiting, contextual information and partial automation through AI. Low-resolution semantic mapping densely samples the seafloor, but lumps many benthic targets into large squares, while high-resolution semantic mapping provides better delineation of biotic and abiotic targets. Lastly, instance segmentation can detect and contour individual organisms, the thematic detail then depends on the identification capabilities of the (human or automated) annotator.

(Castellanos-Galindo, Krumme, et al. 2013; Nagelkerken and Velde 2002; Nagelkerken, Velde, et al. 2000). In some biogeographic regions mangroves provide habitat for unique and endemic terrestrial species (i.e., proboscis monkeys – *Nasalis larvatus* – in mangroves in Sarawak, Malaysia) and nesting places for marine birds (e.g., frigate birds – *Fregata magnificens* – in mangroves in Tumbes, Peru).

Despite the valuable services they provide, mangroves forest areas have shrunk by approximately 20% – 35% over the last 50 years (Polidoro et al. 2010). From 1996 to 2020, the greatest losses have occurred in Southeast Asia (loss of 4.8%) and in North and Central America and the Caribbean (loss of 4.7%) (Leal et al. 2022). The loss of mangrove forests has been mainly driven by coastal infrastructure development, particularly aquaculture farms and palm oil plantations (Goldberg et al. 2020; S. Hamilton 2013; Lai et al. 2015). In certain regions, mangrove forests are used for timber and firewood (Castellanos-Galindo, Cantera, et al. 2015). In the past 7 years, the aggregate global loss of mangrove cover has come to a halt. This has been mainly due to the increased awareness of the importance of mangroves in regulating global climate and of the service they provides to other coastal ecosystems and communities, prompting several restoration projects (Gerona-Daga et al. 2022; Goldberg et al. 2020; Leal et al. 2022). For example, 100% of mangrove forests in Ecuador and at least 75% of mangroves in Brazil have some degree of protected status (S. E. Hamilton and Lovette 2015; Magris et al. 2010).

Despite their recent improved conditions, these ecosystems still require further monitoring and restoration efforts, under increasingly harsher coastal conditions worldwide. Effective mangrove surveying is nonetheless difficult, as in coral reefs, because of the complex environmental settings that these ecosystems present.

1.1.2.1 Environmental settings of mangrove forests

Mangrove forests are a difficult habitat to survey, specially from the ground. They are generally located in remote coastal areas, that are only accessible by boat or several days of car travel (Castellanos-Galindo, Cantera, et al. 2015; Mejía-Rentería et al. 2018). Mangroves usually grow between coral reefs and dense terrestrial forests and, having adapted to brackish waters, they are found on river mouths and deltas. They can be found in mudflats that experience high tidal fluctuations, reducing their accessibility, both by foot or by boat. Many mangrove tree species present intricate aerial root systems, sometimes with bush-like sizes and branches, obstructing the passage through tree stands.

Mangrove forests can be composed by a variety of mangrove tree species, and communities differ across biogeographic regions. Mangrove forests in the Indo-Pacific region, for example, contain a high diversity of mangrove tree species in their forests with up to 42 species, while forests in the Atlantic-East-Pacific (AEP) region have a lower diversity, with up to 12 species (Barth 1982). The high heterogeneity within a forest can hinder the discernability between species, given their similar phenotype. Some mangrove forests also present dense tree stands (which results in dense overlapping crowns in canopies) from which it is difficult to differentiate between individual trees from aerial images. For example, mangrove forests in the Colombian Pacific Coast have very dense sections of canopies with low species diversity, mainly inhabited by the endemic "tea mangrove" species (*Pelliciera Rhizophorae*). These forests present many of the

hindering conditions that difficult surveying it from the ground. They are located in very remote coastal regions with no viable road infrastructure. They also present strong tidal fluctuations, intricate root systems and present some of the tallest mangrove specimens in the world (>30 meters) (Mejía-Rentería et al. 2018).

1.1.2.2 Mangrove forest surveys

Throughout decades, researchers have ventured into mangrove forests and acquired on-ground measurements, despite the complex in-situ conditions. The traditional approach for creating a forest inventory has been to sample dozens of smaller plots (e.g., 35×35 meters). The samples consist of tree counts (only trees greater than a preset size) within each plot and measuring their heights and Diameter at Brest Height (DBH) (Ravindranath et al. 2008) (Figure 1.3). Allometric equations are usually then applied, in which tree height, DBH and a species-specific wood density constant are used to calculate the Above Ground Biomass (AGB), which in turn is used to calculate above-ground carbon stocks. Generally, the resulting numbers are then extrapolated from the sub-sample units (plots) to the total area covered by the forest. The exact forest area has been generally derived from Earth observation products (satellite imagery).

In the procedure of creating a mangrove forest inventory with these traditional methods, the number of factors contributing to uncertainty are high. For example, DBH and height measurements can be difficult to capture accurately (Zang et al. 2023), as some mangrove species present complex morphologies. Due to poor planning, lack of funding or inaccessibility, the selected sampling subplots might not represent accurately the tree distribution in the total forest extent (Cao et al. 2002). These errors accumulate and are extrapolated from field estimates to larger areas, rapidly increasing the uncertainty, and recent studies have pointed out this growing problem for global mangrove ecosystem accounting (Mejía-Rentería et al. 2018; Persson et al. 2022; Zang et al. 2023). See (Persson et al. 2022) for a complete description on the uncertainties that arise during this process.

Modern techniques are trying to overcome this shortcoming, producing complete inventories of mangrove forests using aerial or high-resolution satellite imagery. These platforms cover large areas and produce SfM products that can be further used with manual annotation of experts or machine learning algorithms, for automated mapping (Lassalle et al. 2022; Navarro et al. 2020; Otero et al. 2018; Ruwaimana et al. 2018; Wirasatriya et al. 2022). Furthermore, other sensors, such as Light Detection and Ranging (LiDAR), multispectral and hyperspectral cameras are used to improve the height measurements and to provide richer data, to visually identify the species of mangrove trees. Nonetheless, the cost of specialized sensors quickly becomes prohibitive, specially for entities in remote areas in tropical countries, where mangroves are usually located. Consumer-grade UASs prices on the contrary, have become more accessible, providing a promising tool for monitoring large extents of mangrove forests, even in remote locations. Hence, the products of

SfM on consumer-grade UAS imagery of dense mangrove forest canopies provide a cost-accessible entry point for detailed mangrove forest monitoring across the tropics (Castellanos-Galindo, Casella, et al. 2019; Joyce et al. 2023).

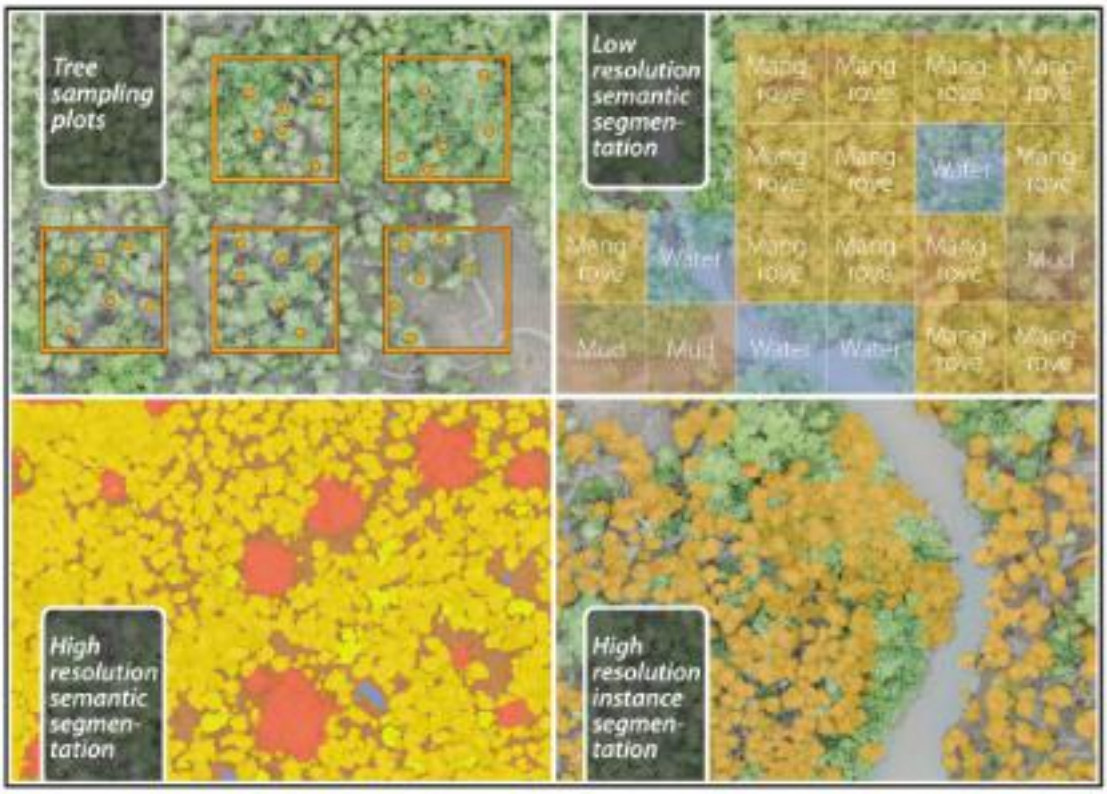

Figure 1.3 Comparison of mangrove forest surveying methods. All 4 methods sample at different spatial and thematic scales. The tree plots method produces spatially sparse samples inside subplots of forests, by counting a subset of trees and measuring their DBH and height. Low-resolution semantic mapping (usually from satellite imagery) densely samples the mangrove forests, but lumps forest targets together into large pixels, while high-resolution semantic mapping provides better delineation of biotic and abiotic targets. Lastly, instance segmentation can detect and contour individual organisms, the thematic detail then depends on the identification capabilities of the (human or automated) annotator.

1.2 The scales of ecosystem observation through imaging

One aim of effective ecosystem mapping is to provide multi-scale resolution, which hinges on the acquisition of fine-grained detail to allow for higher-level abstractions, thus encompassing processes across different scales (Sparrow et al. 2020). Ecosystem observation with imaging sensors

is constrained by a set of scales that determine the level of detail that can be extracted. Sensors can be mounted on mobile or static platforms, and both their specifications define their range within scales, such as: spatial cover, spatial resolution, temporal frequency, spectral resolution and thematic detail. The capabilities of each imaging technology and the possible downstream analysis on their data product, are set from a trade-off between these scales.

1.2.1 Spatial and temporal scales

Spatial cover and resolution vary from micro-scale point samples on individual organisms to meter-scale global-wide coverage (Figure 1.4). Spatial cover will determine how much of an ecosystem is considered in the analysis, while the resolution will determine how much detail can be extracted. Ecosystem observation platforms are categorized in a gradient between proximal sensing and remote sensing.

Proximal sensing techniques acquire information close to the targets, gathering information on cells, tissues, organs, individuals and up to a group of individuals (i.e., a stand of trees), with a large number of samples (i.e., pixels in images) per organism (Figure 1.4) (Tao et al. 2022). Examples of these technologies are imagers mounted on AUVs and UASs, hovering close to the surveyed targets. The emergence of UASs has improved the flexibility of low-altitude observations and greatly reduced data costs, becoming a promising solution for coastal ecosystem surveying (Joyce et al. 2023). One current disadvantage of UASs is their short battery life and reduced load capacity. Other ground platforms, such as handheld devices, fixed tripods, mobile gantries, and ground vehicles can be used to measure certain aspects of an ecosystem with high detail, but with limited mobility and cover.

Remote sensing platforms are airborne or spaceborne platforms that have a higher flying altitude, which facilitates covering complete landscapes up to global scales. Although most satellite platforms have a relatively low spatial resolution, some low-orbit satellite platforms are showing promising sub-meter resolution (e.g., WorldView-4, GeoEye-1, PlanetLab's SKYSAT, and GF-2). Airborne platforms (e.g., planes) have the benefit of covering large areas of a specific ecosystem on-demand, and they have an augmented carrying capacity for an array of complex sensors (e.g., hyperspectral imagers or LiDAR sensors). A disadvantage of remote sensing solutions is that the price of these platforms (or of the captured data products) can sometimes be prohibiting for low-budget monitoring projects. Furthermore, the coarser resolution of images from remote sensing platforms has the effect of grouping one or more survey subjects within a single pixel, and signal unmixing techniques have to be applied to discern between compounding signals (Figure 1.2 & Figure 1.3). Another disadvantage is that cloud cover can interfere with direct line-of-sight to the studied targets. A great benefit of remote sensing is that worldwide distribution maps can be attained, but generally on-ground validation surveys, undertaken with proximal sensing platforms, are still required to confirm estimations and reduce uncertainty (B. Lyons et al. 2020;

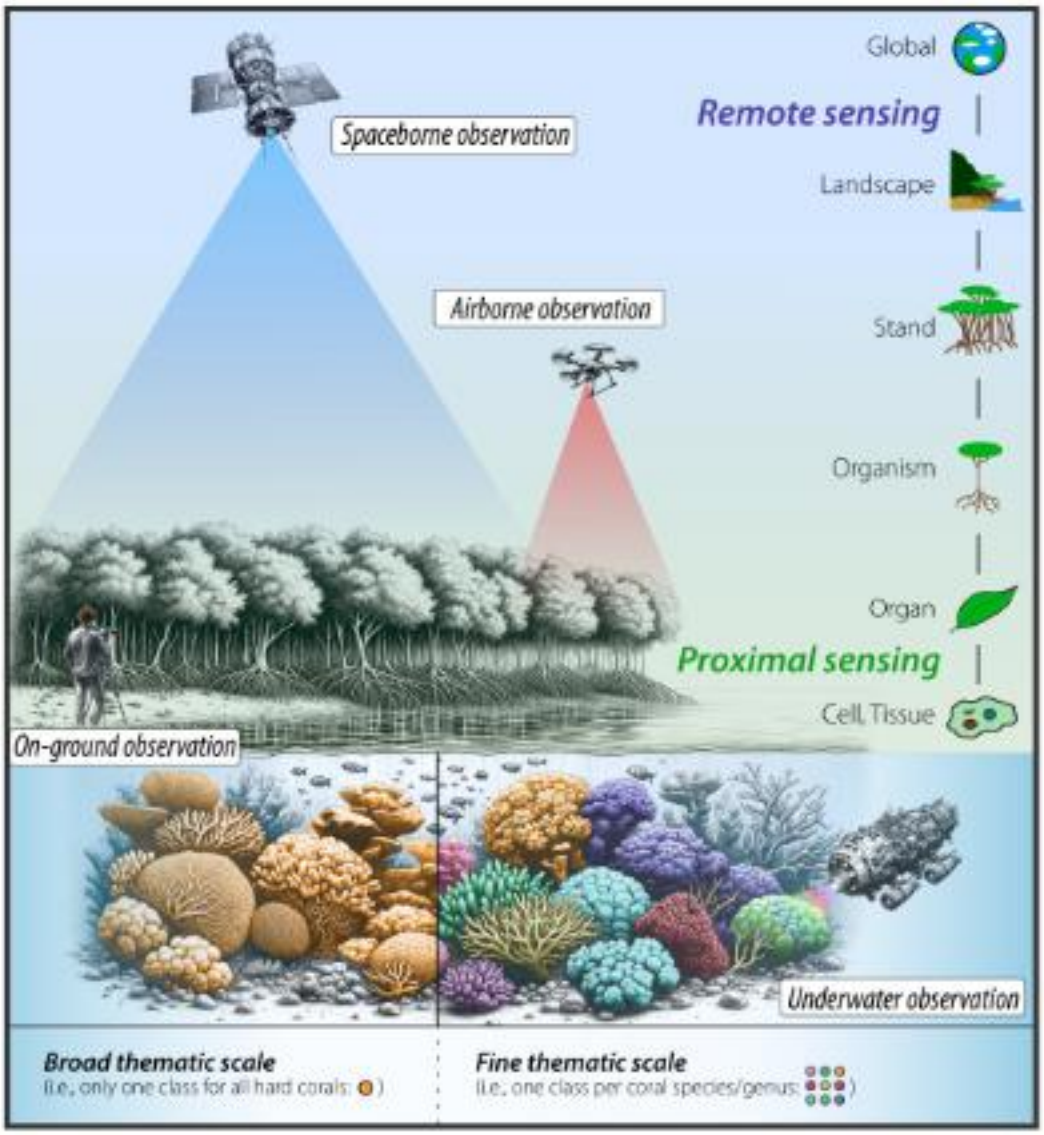

Figure 1.4 Spatial and thematic scales in ecosystem observation. Observational methods can capture different levels of detail in ecosystems, depending on the spatial resolution and cover, temporal frequency and spectral detail they provide. The interactions between these scales are often a trade-off. Satellite imaging, for example, covers large areas, but provides broader pixel-resolutions between 0.5 to 10 meters. The finest thematic scales attainable depends on the given grain of spatial and spectral detail, and represents the detail of the labelset that describes the habitat/community. For example, describing all scleractinian corals as only one class, removes all the detail of the intra-class taxonomic differences like genera or species. Spatial scale descriptions are adapted from (Tao et al. 2022).

Estes et al. 2018; Hochberg et al. 2021; Lecours 2017; Stehman et al. 2019).

Selecting the proper spatial scale for identifying ecological patterns in an ecosystem is paramount for the success of a study, and ideally multiple scales are used to gain a better characterization of species−habitat relationships (Congalton 1991; Lecours, Brown, et al. 2016; Lecours, Devillers, et al. 2015; Riitters 2019; Sparrow et al. 2020). Nonetheless, narrowing each survey to answer a reduced set of questions removes the possibility of reusing a dataset, and thus, it is important that all the information possible is extracted from observation products (Sparrow et al. 2020).

The temporal scale varies with the deployment type that different observation platforms have. For example, satellites can have near-daily temporal resolution (e.g., AVHRR/MODIS, WorldView-4, and SuperView-1), and after deployment, the effort to keep this frequency is low. Other survey-oriented platforms (e.g., UASs) depend on the logistics and structure of the project or framework they are deployed under and the associated costs (Joyce et al. 2023). To monitor the community composition of a coral reef for example, annual surveys might suffice, unless specific events break out (e.g. mass-bleaching), in which case higher frequency is required to gain detailed insights to specific processes. Also, the comparability of time point measurement is very relevant. Standardization and consistency between observations and meta-data, such as geo-referencing, is paramount to enable temporal comparisons (Mayr et al. 2019).

1.2.2 Spectral scale

The spectral information of an image adds richness to each pixel, that is very useful for automatic classification analysis, specially for habitat maps on any spatial scale (Chennu et al. 2017; Guanter et al. 2015; La Rosa et al. 2021; Lodhi et al. 2018; Mills et al. 2023; Rashid et al. 2020; Rast et al. 2019). Spectral imaging is a combination of spectroscopic analysis and imaging. Optical imaging captures the light reflected or emitted by an object, forming a visual representation of its size, shape, or layout. The light information is captured by a sensor into a grid of pixels, that represent the scene in a 2D-model. How much information of the light spectrum is captured, determines the spectral type of the sensor. Color cameras reduce the electromagnetic visible-light spectrum to only three values (Red-Green-Blue). In contrast, spectral imaging works by capturing light at every spatial point in an image with specific spectral details. Multi-spectral sensors, for example, capture light in spectral bands of varying bandwidths that are not necessarily contiguous, while hyperspectral imaging involves narrow, usually contiguous spectral bands, including possibly hundreds or thousands of spectra. This means that each pixel in an image has an almost continuous spectrum, providing rich information. Analyzing these spectral images helps to combine spectroscopic data (such as the function of a material) with spatial data (like its shape). The combination of fine spatial and spectral resolutions is the goal of improvements in the development of spectral imaging sensors. The cost of spectral sensors is steep compared to consumer-grade color sensors, although multi-spectral sensors are becoming more accessible in recent years.

1.2.3 Thematic scale

The thematic scale is defined as the level of classification detail of the sampling units (Buyantuyev et al. 2007). For example, mapping all scleractinian corals under a single class constitutes a broader scale in contrast to mapping each coral species/genus separately, which defines a finer thematic scale (Figure 1.4). The influence of thematic resolution in ecological analysis derived from mapping products has only recently started to be investigated and its importance to be highlighted (Bailey et al. 2007; Lechner et al. 2016). It has been observed that using broad classes for describing groups of taxonomically or morphologically similar organisms can mask intra-group specific processes and dynamics (Brito-Millán et al. 2019).

The granularity of the attainable classification detail in habitat maps is tightly related to the spatial and spectral scales, given that the discernability between many organisms – by a human expert or automated workflow – requires rich descriptive information. In some cases, the achievable level of detail is not possible even with the most advanced imaging technologies, and in those cases molecular methods have to be applied. Nonetheless, for any mapping effort the most detailed thematic level possible should be targeted, to produce reusable datasets that can be applied to answer questions at many scales, given that finer thematic scales can usually be abstracted to broader or intermediate scales. Producing a set of abstractable/hierarchical categories within maps allows to cater to different possible users of mapping products, from ecologists to policy makers (Kennedy et al. 2021; Lecours 2017).

Another important consideration when selecting a thematic scale is the use of standardized classification labelsets. This allows for consistency between revisits of the same ecosystems and temporal comparisons between mappings. Openly available, standardized libraries are recommended, such as the World Register of Marine Species (WORMS) for marine flora and fauna, and the Collaborative and Automated Tools for Analysis of Marine Imagery (CATAMI) for underwater mapping of habitats with labels for biota, bedforms, relief and substrates (Althaus et al. 2015; WoRMS 2023).

1.2.4 Automation and scalability through Artificial Intelligence

Imaging technologies for ecosystem observation can cover larger areas at a high spatial, spectral and temporal resolution, resulting in large datasets of photographic data being captured for survey projects and earth observation efforts. This results in an ever-growing flow of incoming raw data that synchronously grows the demand for expert time for analysis, and if the demand is not met, large datasets remain unanalysed or under-analysed. Thus, automated and scalable analysis pipelines, that extract as much detail as possible from observations have to be researched.

AI has shown to be a promising tool in automating and scaling up the analysis of environmental datasets. For a few decades already, feature engineering, Object-Based Image Analysis (OBIA)

and computer vision algorithms have been applied to satellite imagery, providing Land Use/Land Cover (LULC) classifications, habitat maps, bio-physical and physical-chemical maps. LULC maps, for example, are provided by the the European Space Agency (ESA) World Cover (2020–2021) (*ESA WorldCover* 2020; *ESA WorldCover* 2021), the National Aeronautics and Space Administration (NASA) MCD12Q1 500 m resolution dataset 6 (2001–2018) (Friedl et al. 2022; Sulla-Menashe et al. 2019), and Copernicus Global Land Service (CGLS) Land Cover 100 m dataset (from 2015 to 2019) (Buchhorn, Lesiv, et al. 2020; Buchhorn, Smets, et al. 2020). ML approaches were also used to create global coral reef habitat maps and reef geomorphology maps (B. Lyons et al. 2020; Kennedy et al. 2021; Roelfsema et al. 2020). Similar approaches have been applied at survey scales, for example, to detect tree crowns in mangrove forests (Miraki et al. 2021; Navarro et al. 2020; Otero et al. 2018). Early ML techniques provided accurate classification results, but require large training datasets and do not generalize well. This means that when applied on new raw data that has not been used during training, their performance drops significantly.

Deep Convolutional Neural Networks (CNNs) have become very popular in recent years for their capacity to provide good predictions and better generalization. Their application is already widespread in numerous ecosystem mapping scenarios, specially on photographic data taken during ecosystem surveys (Alonso et al. 2019; Beijbom et al. 2015; Kattenborn et al. 2021; Lassalle et al. 2022; Paoletti et al. 2019; Pavoni, Corsini, Callieri, et al. 2020; Schiefer et al. 2020). CNNs provide an end-to-end framework, meaning that feature extraction from raw images is done by the algorithm all the way down to the classification task. They also provide different levels of classification granularity depending on their network architecture (Figure 1.2 & Figure 1.3). Image (or image-patch) classification predicts a label for the whole image or an image-patch. Image-patch classification can expedite automatic labelling of coral point samples collected with sparse photoquadrat techniques (Beijbom et al. 2015; Williams et al. 2019). Semantic segmentation networks predict a label for every single pixel in an image, producing densely classified/sampled images. Large orthomosaics can be annotated with these networks resulting in detailed community distribution maps (Hopkinson et al. 2020; Schiefer et al. 2020). Instance segmentation networks also delineate the boundaries of different objects in images, before classifying them. These networks can also be applied on images or orthomosaics to detect individual organisms, such as mangrove trees (Lassalle et al. 2022), and produce detailed inventories of the surveyed environment (Tucker et al. 2023).

1.2.5 Current limitations

Many ecosystem observations have been executed with sparse sampling and with a variety of methodologies making it rather difficult to reliably compare between reported values (Hochberg et al. 2021; Reverter et al. 2022). The analysis workflows to produce community and habitat

maps also rely on different methodologies with custom settings, and resulting publications failed to report uncertainty values. Standardized solutions are necessary to provide consistent baselines as validation for future global mapping efforts.

State-of-the-art AI workflows can produce accurate habitat maps, but they generally include low thematic detail and do not consider organism-wise segmentation. The level of thematic detail and the accuracy in delineating organisms within a habitat/community map, heavily relies on the richness of the captured image data – the spatial and spectral resolution. Hence, as highlighted by Kattenborn et al. 2021, to produce detailed ecosystem-wide inventories and consistent habitat/community maps, ecosystem survey workflows have to consider an end-to-end process, which starts with rich data acquisition, leverages on novel AI algorithms and finally validates its products with ecological assessments.

1.3 Motivation of the doctoral thesis

As outlined so far, shallow coastal ecosystems are critically important to the health of our planet. Despite their small global cover, they provide important services for other adjacent ecosystems and coastal human populations, besides helping regulate the global climate. Anthropogenic stressors are decimating coral reef biotic communities worldwide and reducing mangrove forest extents. Hence, constant surveying of their state and deepening our knowledge about their intricate processes is paramount to enact effective protective and restorative measures.

There is a lack of effective and consistent surveying of coral reefs and mangroves that can integrally set the baselines of local biodiversity, community composition and habitat structures, for future comparisons and more accurate ecological analysis (Brito-Millán et al. 2019; Flower et al. 2017; Hochberg et al. 2021; Reverter et al. 2022). Most monitoring reports on shallow coastal ecosystems are analysed into very broad thematic groupings, spatially sparse samplings and/or low spatial resolution, masking local ecological phenomena and intra-group specific processes (Brito-Millán et al. 2019; Reverter et al. 2022). Even to understand patterns occurring at large scales, such as those reported in most global or continental mapping efforts, effects observed at smaller scales should be considered (Levin 1992; Underwood et al. 2000).

Habitat maps that describe ecosystems with fine-grained community composition and configuration descriptions, can provide key information to understand their health, and to predict past occurrences and future scenarios. These maps unlock more intricate spatio-temporal analysis such as those already being applied on terrestrial ecosystems at landscape scale, moving beyond simple percentage cover reporting (Nowosad et al. 2019; Riitters 2019). Riitters 2019 mentions that landscape pattern analysis fundamentally provides information about landscape composition and landscape configuration, which vary continuously over geographic space and

observation scale. Thus, observations must be captured across many scales, not only spatially, but also thematically.

At a local survey scale (e.g., the coral reefs on an island), there has been a lack of fine-grained mapping products. This can be attributed to the low resolution of Earth observation imaging technologies, the high cost of aerial and submersible platforms, the cost of specialized sensors and the nonexistence of automated workflows for mapping large quantities of acquired image data. However, the astounding current progress in observation platforms and in computational resources is prompting many researchers to revisit the creation and use of densely annotated habitat maps.

Information rich habitat maps can provide the opportunity to deepen our understanding of shallow coastal ecosystems and to revisit past beliefs. Previous descriptions of coral reef community compositions across environmental gradients have many times neglected intra-group diversity and the configurational patterns, focusing mostly on point-sample abundance and/or on abundance of dominant reef groups (De Bakker, Meesters, et al. 2016; De Bakker, Van Duyl, et al. 2017; Reverter et al. 2022; Sandin, Smith, et al. 2008; Teichberg et al. 2018). Dense and thematic detailed maps would allow for fine-scaled co-occurrence analysis of biotic organisms (down to genus and species level) and substrate classes. Tracking temporal shifts in composition and configuration of an ecosystem's community, with replacement analysis and fragmentation indices of patch communities would be possible. Species-specific growth and accretion rates of scleractinian corals could be studied in more detail, which are key indicators for coral reef health (Flower et al. 2017).

Individual organism detection and analysis on a large scale has not been easily achievable in the past and is still a daunting task. In traditional mangrove forest surveys only a subset of trees are usually measured and used as a proxy in allometric equations to calculate AGB estimates for large forested areas (Goldberg et al. 2020; Ravindranath et al. 2008). This produces significant uncertainty in regional, continental and global estimates (Marvin et al. 2016; Vorster et al. 2020). Detailed inventories with geo-located individual mangrove trees would narrow the error from allometric equations and better account for stored above ground carbon in forests (Tucker et al. 2023). The capability to identify organisms in images would also allow to track events over time, quantifying different aspects of change in biological and ecological settings (Keefe et al. 2022).

All the aforementioned needs motivate the technical and scientific goals of this doctoral project: design and implement AI workflows to produce dense and thematically detailed habitat maps of surveys in a shallow coastal ecosystems to describe in detail their community composition and configuration and apply it in a case study. Furthermore, produce habitat maps with organisms delineated and classified on large surveyed areas, to improve derived ecosystem accounting statistics in shallow coastal ecosystems. Finally, comment on the future of ecosystem mapping through an example of the ideal dataset collected to provide habitat maps with organisms delineated and

labelled, abiotic elements segmented and classified, all to the most detailed level possible.

References

Alonso, Iñigo, Matan Yuval, Gal Eyal, Tali Treibitz, and Ana C. Murillo (2019). "CoralSeg: Learning coral segmentation from sparse annotations". In: *Journal of Field Robotics* 36.8, pp. 1456–1477. DOI: *https://doi.org/10.1002/rob.21915*.

Althaus, Franziska, Nicole Hill, Renata Ferrari, Luke Edwards, Rachel Przeslawski, Christine H. L. Schönberg, Rick Stuart-Smith, Neville Barrett, Graham Edgar, Jamie Colquhoun, Maggie Tran, Alan Jordan, Tony Rees, and Karen Gowlett-Holmes (2015). "A Standardised Vocabulary for Identifying Benthic Biota and Substrata from Underwater Imagery: The CATAMI Classification Scheme". In: *PLOS ONE* 10.10, e0141039. DOI: *10.1371/journal.pone.0141039*.

Alvarez-Filip, Lorenzo, Nicholas K. Dulvy, Jennifer A. Gill, Isabelle M. Côté, and Andrew R. Watkinson (2009). "Flattening of Caribbean coral reefs: region-wide declines in architectural complexity". In: *Proceedings of the Royal Society B: Biological Sciences* 276.1669, pp. 3019–3025. DOI: *10.1098/rspb.2009.0339*.

B. Lyons, Mitchell, Chris M. Roelfsema, Emma V. Kennedy, Eva M. Kovacs, Rodney Borrego-Acevedo, Kathryn Markey, Meredith Roe, Doddy M. Yuwono, Daniel L. Harris, Stuart R. Phinn, Gregory P. Asner, Jiwei Li, David E. Knapp, Nicholas S. Fabina, Kirk Larsen, Dimosthenis Traganos, and Nicholas J. Murray (2020). "Mapping the world's coral reefs using a global multiscale earth observation framework". In: *Remote Sensing in Ecology and Conservation*. Ed. by Nathalie Pettorelli and Vincent Lecours, rse2.157. DOI: *10.1002/rse2.157*.

Bailey, Debra, Felix Herzog, Isabel Augenstein, Stéphanie Aviron, Regula Billeter, Erich Szerencsits, and Jacques Baudry (2007). "Thematic resolution matters: Indicators of landscape pattern for European agro-ecosystems". In: *Ecological Indicators* 7.3, pp. 692–709. DOI: *10.1016/j.ecolind.2006.08.001*.

Bak, Rolf P. M., Gerard Nieuwland, and Erik H. Meesters (2005). "Coral reef crisis in deep and shallow reefs: 30 years of constancy and change in reefs of Curacao and Bonaire". In: *Coral Reefs* 24.3, pp. 475–479. DOI: *10.1007/s00338-005-0009-1*.

Barth, Hartmut (1982). "The biogeography of mangroves". In: *Contributions to the ecology of halophytes*. Ed. by David N. Sen and Kishan S. Rajpurohit. Tasks for vegetation science. Dordrecht: Springer Netherlands, pp. 35–60. DOI: *10.1007/978-94-009-8037-2_4*.

Beijbom, Oscar, Peter J. Edmunds, Chris Roelfsema, Jennifer Smith, David I. Kline, Benjamin P. Neal, Matthew J. Dunlap, Vincent Moriarty, Tung-Yung Fan, Chih-Jui Tan, Stephen Chan, Tali Treibitz, Anthony Gamst, B. Greg Mitchell, and David Kriegman (2015). "Towards Automated Annotation of Benthic Survey Images: Variability of Human Experts and Operational Modes of Automation". In: *PLOS ONE* 10.7, e0130312. DOI: *10.1371/journal.pone.0130312*.

Bellwood, D. R., T. P. Hughes, C. Folke, and M. Nyström (2004). "Confronting the coral reef crisis". In: *Nature* 429.6994, pp. 827–833. DOI: *10.1038/nature02691*.

Bellwood, David R., Andrew S. Hoey, and J. Howard Choat (2003). "Limited functional redundancy in high diversity systems: resilience and ecosystem function on coral reefs". In: *Ecology Letters* 6.4, pp. 281–285. DOI: *10.1046/j.1461-0248.2003.00432.x*.

Bimrah, Kanika, Rajarshi Dasgupta, Shizuka Hashimoto, Izuru Saizen, and Shalini Dhyani (2022). "Ecosystem Services of Mangroves: A Systematic Review and Synthesis of Contemporary Scientific Literature". In: *Sustainability* 14.19, p. 12051. DOI: *10.3390/su141912051*.

Brito-Millán, Marlene, Mark J. A. Vermeij, Esmeralda A. Alcantar, and Stuart A. Sandin (2019). "Coral reef assessments based on cover alone mask active dynamics of coral communities". In: *Marine Ecology Progress Series* 630, pp. 55–68. URL: *https://www.jstor.org/stable/26920540* (visited on 12/10/2023).

Brocke, Hannah J., Lubos Polerecky, Dirk de Beer, Miriam Weber, Joachim Claudet, and Maggy M. Nugues (2015). "Organic Matter Degradation Drives Benthic Cyanobacterial Mat Abundance on Caribbean Coral Reefs". In: *PLOS ONE* 10.5, e0125445. DOI: *10.1371/journal.pone.0125445*.

Browne, N.K., S.G. Smithers, and C.T. Perry (2012). "Coral reefs of the turbid inner-shelf of the Great Barrier Reef, Australia: An environmental and geomorphic perspective on their occurrence, composition and growth". In: *Earth-Science Reviews* 115.1, pp. 1–20. DOI: *10.1016/j.earscirev.2012.06.006*.

Buchhorn, Marcel, Myroslava Lesiv, Nandin-Erdene Tsendbazar, Martin Herold, Luc Bertels, and Bruno Smets (2020). "Copernicus Global Land Cover Layers—Collection 2". In: *Remote Sensing* 12.6, p. 1044. DOI: *10.3390/rs12061044*.

Buchhorn, Marcel, Bruno Smets, Luc Bertels, Bert De Roo, Myroslava Lesiv, Nandin-Erdene Tsendbazar, Martin Herold, and Steffen Fritz (2020). *Copernicus Global Land Service: Land Cover 100m: collection 3: epoch 2019: Globe*. Version V3.0.1. DOI: *10.5281/zenodo.3939050*.

Bunting, Pete, Ake Rosenqvist, Lammert Hilarides, Richard M. Lucas, Nathan Thomas, Takeo Tadono, Thomas A. Worthington, Mark Spalding, Nicholas J. Murray, and Lisa-Maria Rebelo (2022). "Global Mangrove Extent Change 1996–2020: Global Mangrove Watch Version 3.0". In: *Remote Sensing* 14.15, p. 3657. DOI: *10.3390/rs14153657*.

Buyantuyev, Alexander and Jianguo Wu (2007). "Effects of thematic resolution on landscape pattern analysis". In: *Landscape Ecology* 22.1, pp. 7–13. DOI: *10.1007/s10980-006-9010-5*.

Cao, Yong, D. Dudley Williams, and David P. Larsen (2002). "Comparison of Ecological Communities: The Problem of Sample Representativeness". In: *Ecological Monographs* 72.1, pp. 41–56. DOI: *10.1890/0012-9615(2002)072[0041:COECTP]2.0.CO;2*.

Carlot, J., A. Rovère, E. Casella, D. Harris, C. Grellet-Muñoz, Y. Chancerelle, E. Dormy, L. Hedouin, and V. Parravicini (2020). "Community composition predicts photogrammetry-based structural complexity on coral reefs". In: *Coral Reefs* 39.4, pp. 967–975. DOI: *10.1007/s00338-020-01916-8*.

Castellanos-Galindo, Gustavo A., Jaime R. Cantera, Ulrich Saint-Paul, and Daniella Ferrol-Schulte (2015). "Threats to mangrove social-ecological systems in the most luxuriant coastal forests of the Neotropics". In: *Biodiversity and Conservation* 24.3, pp. 701–704. DOI: *10.1007/s10531-014-0827-y*.

Castellanos-Galindo, Gustavo A., Elisa Casella, Juan Carlos Mejía-Rentería, and Alessio Rovere (2019). "Habitat mapping of remote coasts: Evaluating the usefulness of lightweight unmanned aerial vehicles for conservation and monitoring". In: *Biological Conservation* 239, p. 108282. DOI: *10.1016/j.biocon.2019.108282*.

Castellanos-Galindo, Gustavo A., Uwe Krumme, Efrain A. Rubio, and Ulrich Saint-Paul (2013). "Spatial variability of mangrove fish assemblage composition in the tropical eastern Pacific Ocean". In: *Reviews in Fish Biology and Fisheries* 23.1, pp. 69–86. DOI: *10.1007/s11160-012-9276-4*.

Chennu, Arjun, Paul Färber, Glenn De'ath, Dirk de Beer, and Katharina E. Fabricius (2017). "A diver-operated hyperspectral imaging and topographic surveying system for automated mapping of benthic habitats". In: *Scientific Reports* 7.1, pp. 1–12. DOI: *10.1038/s41598-017-07337-y*.

Congalton, Russell G. (1991). "A review of assessing the accuracy of classifications of remotely sensed data". In: *Remote Sensing of Environment* 37.1, pp. 35–46. DOI: *10.1016/0034-4257(91)90048-B*.

Connell, Joseph H. (1978). "Diversity in Tropical Rain Forests and Coral Reefs". In: *Science* 199.4335, pp. 1302–1310. DOI: *10.1126/science.199.4335.1302*.

Costanza, Robert, Ralph d'Arge, Rudolf de Groot, Stephen Farber, Monica Grasso, Bruce Hannon, Karin Limburg, Shahid Naeem, Robert V. O'Neill, Jose Paruelo, Robert G. Raskin, Paul Sutton, and Marjan van den Belt (1997). "The value of the world's ecosystem services and natural capital". In: *Nature* 387.6630, pp. 253–260. DOI: *10.1038/387253a0*.

De Bakker, Didier M., Erik H. Meesters, Rolf P. M. Bak, Gerard Nieuwland, and Fleur C. Van Duyl (2016). "Long-term Shifts in Coral Communities On Shallow to Deep Reef Slopes of Curaçao and Bonaire: Are There Any Winners?" In: *Frontiers in Marine Science* 3. DOI: *10.3389/fmars.2016.00247*.

De Bakker, Didier M., Fleur C. Van Duyl, Rolf P. M. Bak, Maggy M. Nugues, Gerard Nieuwland, and Erik H. Meesters (2017). "40 Years of benthic community change on the Caribbean reefs of Curaçao and Bonaire: the rise of slimy cyanobacterial mats". In: *Coral Reefs* 36.2, pp. 355–367. DOI: *10.1007/s00338-016-1534-9*.

Duyl, Fleur (1985). "Atlas of the living reefs of Curaçao and Bonaire (Netherlands Antilles) /". In: *Studies of Flora and Fauna of Surinam and the Netherlands Antilles* 117, 1–37 plus maps.

ESA WorldCover (2020). URL: *https://worldcover2020.esa.int/* (visited on 12/18/2023).

ESA WorldCover (2021). URL: *https://worldcover2021.esa.int/* (visited on 12/18/2023).

Estes, Lyndon, Peng Chen, Stephanie Debats, Tom Evans, Stefanus Ferreira, Tobias Kuemmerle, Gabrielle Ragazzo, Justin Sheffield, Adam Wolf, Eric Wood, and Kelly Caylor (2018). "A large-

area, spatially continuous assessment of land cover map error and its impact on downstream analyses". In: *Global Change Biology* 24.1, pp. 322–337. DOI: *10.1111/gcb.13904*.

Evans, Richard D., Shaun K. Wilson, Rebecca Fisher, Nicole M. Ryan, Russ Babcock, David Blakeway, Todd Bond, Passang Dorji, Francois Dufois, Peter Fearns, Ryan J. Lowe, Jim Stoddart, and Damian P. Thomson (2020). "Early recovery dynamics of turbid coral reefs after recurring bleaching events". In: *Journal of Environmental Management* 268, p. 110666. DOI: *10.1016/j.jenvman.2020.110666*.

Fabricius, Katharina E. (2006). "Effects of irradiance, flow, and colony pigmentation on the temperature microenvironment around corals: Implications for coral bleaching?" In: *Limnology and Oceanography* 51.1, pp. 30–37. DOI: *10.4319/lo.2006.51.1.0030*.

Ferrari, Renata, David McKinnon, Hu He, Ryan N. Smith, Peter Corke, Manuel González-Rivero, Peter J. Mumby, and Ben Upcroft (2016). "Quantifying Multiscale Habitat Structural Complexity: A Cost-Effective Framework for Underwater 3D Modelling". In: *Remote Sensing* 8.2, p. 113. DOI: *10.3390/rs8020113*.

Flower, Jason, Juan Carlos Ortiz, Iliana Chollett, Sabah Abdullah, Carolina Castro-Sanguino, Karlo Hock, Vivian Lam, and Peter J. Mumby (2017). "Interpreting coral reef monitoring data: A guide for improved management decisions". In: *Ecological Indicators* 72, pp. 848–869. DOI: *10.1016/j.ecolind.2016.09.003*.

Friedl, Mark and Damien Sulla-Menashe (2022). *MODIS/Terra+Aqua Land Cover Type Yearly L3 Global 500m SIN Grid V061*. DOI: *10.5067/MODIS/MCD12Q1.061*.

Fukunaga, Atsuko, John H. R. Burns, Brianna K. Craig, and Randall K. Kosaki (2019). "Integrating Three-Dimensional Benthic Habitat Characterization Techniques into Ecological Monitoring of Coral Reefs". In: *Journal of Marine Science and Engineering* 7.2, p. 27. DOI: *10.3390/jmse7020027*.

Fund, United Nations Population (2017). *State of World Population 2017: Worlds Apart - Reproductive Health and Rights in an Age of Inequality*. United Nations. DOI: *10.18356/b19523c6-en*.

Gardner, Toby A., Isabelle M. Côté, Jennifer A. Gill, Alastair Grant, and Andrew R. Watkinson (2003). "Long-Term Region-Wide Declines in Caribbean Corals". In: *Science* 301.5635, pp. 958–960. DOI: *10.1126/science.1086050*.

Gerona-Daga, Maria Elisa B. and Severino G. Salmo (2022). "A systematic review of mangrove restoration studies in Southeast Asia: Challenges and opportunities for the United Nation's Decade on Ecosystem Restoration". In: *Frontiers in Marine Science* 9. URL: *https://www.frontiersin.org/articles/10.3389/fmars.2022.987737* (visited on 12/11/2023).

Getzner, Michael and Muhammad Shariful Islam (2020). "Ecosystem Services of Mangrove Forests: Results of a Meta-Analysis of Economic Values". In: *International Journal of Environmental Research and Public Health* 17.16, p. 5830. DOI: *10.3390/ijerph17165830*.

Goldberg, Liza, David Lagomasino, Nathan Thomas, and Temilola Fatoyinbo (2020). "Global declines in human-driven mangrove loss". In: *Global Change Biology* 26.10, pp. 5844–5855. DOI: *10.1111/gcb.15275*.

Goreau, Thomas F. (1959). "The Ecology of Jamaican Coral Reefs I. Species Composition and Zonation". In: *Ecology* 40.1, pp. 67–90. DOI: *10.2307/1929924*.

Grigg, Richard W., Jeffrey J. Polovina, and Marlin J. Atkinson (1984). "Model of a coral reef ecosystem". In: *Coral Reefs* 3.1, pp. 23–27. DOI: *10.1007/BF00306137*.

Guanter, Luis, Hermann Kaufmann, Karl Segl, Saskia Foerster, Christian Rogass, Sabine Chabrillat, Theres Kuester, André Hollstein, Godela Rossner, Christian Chlebek, Christoph Straif, Sebastian Fischer, Stefanie Schrader, Tobias Storch, Uta Heiden, Andreas Mueller, Martin Bachmann, Helmut Mühle, Rupert Müller, Martin Habermeyer, Andreas Ohndorf, Joachim Hill, Henning Buddenbaum, Patrick Hostert, Sebastian Van der Linden, Pedro J. Leitão, Andreas Rabe, Roland Doerffer, Hajo Krasemann, Hongyan Xi, Wolfram Mauser, Tobias Hank, Matthias Locherer, Michael Rast, Karl Staenz, and Bernhard Sang (2015). "The EnMAP Spaceborne Imaging Spectroscopy Mission for Earth Observation". In: *Remote Sensing* 7.7, pp. 8830–8857. DOI: *10.3390/rs70708830*.

Hamilton, Stuart (2013). "Assessing the Role of Commercial Aquaculture in Displacing Mangrove Forest". In: *Bulletin of Marine Science* 89.2, pp. 585–601. DOI: *10.5343/bms.2012.1069*.

Hamilton, Stuart E. and Daniel A. Friess (2018). "Global carbon stocks and potential emissions due to mangrove deforestation from 2000 to 2012". In: *Nature Climate Change* 8.3, pp. 240–244. DOI: *10.1038/s41558-018-0090-4*.

Hamilton, Stuart E. and John Lovette (2015). "Ecuador's Mangrove Forest Carbon Stocks: A Spatiotemporal Analysis of Living Carbon Holdings and Their Depletion since the Advent of Commercial Aquaculture". In: *PLOS ONE* 10.3, e0118880. DOI: *10.1371/journal.pone.0118880*.

Hampton-Smith, Melissa, Deborah S. Bower, and Sarah Mika (2021). "A review of the current global status of blast fishing: Causes, implications and solutions". In: *Biological Conservation* 262, p. 109307. DOI: *10.1016/j.biocon.2021.109307*.

Hawkins, Julie P., Callum M. Roberts, Tom Van'T Hof, Kalli De Meyer, Jamie Tratalos, and Chloe Aldam (1999). "Effects of Recreational Scuba Diving on Caribbean Coral and Fish Communities". In: *Conservation Biology* 13.4, pp. 888–897. DOI: *10.1046/j.1523-1739.1999.97447.x*.

Hochberg, Eric J. and Michelle M. Gierach (2021). "Missing the Reef for the Corals: Unexpected Trends Between Coral Reef Condition and the Environment at the Ecosystem Scale". In: *Frontiers in Marine Science* 8, p. 1191. DOI: *10.3389/fmars.2021.727038*.

Hopkinson, Brian M., Andrew C. King, Daniel P. Owen, Matthew Johnson-Roberson, Matthew H. Long, and Suchendra M. Bhandarkar (2020). "Automated classification of three-dimensional reconstructions of coral reefs using convolutional neural networks". In: *PLOS ONE* 15.3, e0230671. DOI: *10.1371/journal.pone.0230671*.

Hughes, T. P., A. H. Baird, D. R. Bellwood, M. Card, S. R. Connolly, C. Folke, R. Grosberg, O. Hoegh-Guldberg, J. B. C. Jackson, J. Kleypas, J. M. Lough, P. Marshall, M. Nyström, S. R. Palumbi, J. M. Pandolfi, B. Rosen, and J. Roughgarden (2003). "Climate Change, Human

Impacts, and the Resilience of Coral Reefs". In: *Science* 301.5635, pp. 929–933. DOI: *10.1126/science.1085046*.

Hughes, Terence P. (1994). "Catastrophes, Phase Shifts, and Large-Scale Degradation of a Caribbean Coral Reef". In: *Science* 265.5178, pp. 1547–1551. DOI: *10.1126/science.265.5178.1547*.

Hughes, Terence P., Maria J. Rodrigues, David R. Bellwood, Daniela Ceccarelli, Ove Hoegh-Guldberg, Laurence McCook, Natalie Moltschaniwskyj, Morgan S. Pratchett, Robert S. Steneck, and Bette Willis (2007). "Phase Shifts, Herbivory, and the Resilience of Coral Reefs to Climate Change". In: *Current Biology* 17.4, pp. 360–365. DOI: *10.1016/j.cub.2006.12.049*.

Hughes, Terry P., Kristen D. Anderson, Sean R. Connolly, Scott F. Heron, James T. Kerry, Janice M. Lough, Andrew H. Baird, Julia K. Baum, Michael L. Berumen, Tom C. Bridge, Danielle C. Claar, C. Mark Eakin, James P. Gilmour, Nicholas A. J. Graham, Hugo Harrison, Jean-Paul A. Hobbs, Andrew S. Hoey, Mia Hoogenboom, Ryan J. Lowe, Malcolm T. McCulloch, John M. Pandolfi, Morgan Pratchett, Verena Schoepf, Gergely Torda, and Shaun K. Wilson (2018). "Spatial and temporal patterns of mass bleaching of corals in the Anthropocene". In: *Science* 359.6371, pp. 80–83. DOI: *10.1126/science.aan8048*.

Hughes, Terry P., Michele L. Barnes, David R. Bellwood, Joshua E. Cinner, Graeme S. Cumming, Jeremy B. C. Jackson, Joanie Kleypas, Ingrid A. van de Leemput, Janice M. Lough, Tiffany H. Morrison, Stephen R. Palumbi, Egbert H. van Nes, and Marten Scheffer (2017). "Coral reefs in the Anthropocene". In: *Nature* 546.7656, pp. 82–90. DOI: *10.1038/nature22901*.

Jackson, Edited Jeremy, Mary Donovan, Katie Cramer, and Vivian Lam (2014). *Status and trends of caribbean coral reefs: 1970-2012*. International Union for Conservation of Nature (IUCN).

Jackson, Jeremy B. C., Michael X. Kirby, Wolfgang H. Berger, Karen A. Bjorndal, Louis W. Botsford, Bruce J. Bourque, Roger H. Bradbury, Richard Cooke, Jon Erlandson, James A. Estes, Terence P. Hughes, Susan Kidwell, Carina B. Lange, Hunter S. Lenihan, John M. Pandolfi, Charles H. Peterson, Robert S. Steneck, Mia J. Tegner, and Robert R. Warner (2001). "Historical Overfishing and the Recent Collapse of Coastal Ecosystems". In: *Science* 293.5530, pp. 629–637. DOI: *10.1126/science.1059199*.

Joyce, Karen E., Kate C. Fickas, and Michelle Kalamandeen (2023). "The unique value proposition for using drones to map coastal ecosystems". In: *Cambridge Prisms: Coastal Futures* 1, e6. DOI: *10.1017/cft.2022.7*.

Kattenborn, Teja, Jens Leitloff, Felix Schiefer, and Stefan Hinz (2021). "Review on Convolutional Neural Networks (CNN) in vegetation remote sensing". In: *ISPRS Journal of Photogrammetry and Remote Sensing* 173, pp. 24–49. DOI: *10.1016/j.isprsjprs.2020.12.010*.

Keefe, Robert F., Eloise G. Zimbelman, and Gianni Picchi (2022). "Use of Individual Tree and Product Level Data to Improve Operational Forestry". In: *Current Forestry Reports* 8.2, pp. 148–165. DOI: *10.1007/s40725-022-00160-3*.

Kennedy, Emma V., Chris M. Roelfsema, Mitchell B. Lyons, Eva M. Kovacs, Rodney Borrego-Acevedo, Meredith Roe, Stuart R. Phinn, Kirk Larsen, Nicholas J. Murray, Doddy Yuwono,

Jeremy Wolff, and Paul Tudman (2021). "Reef Cover, a coral reef classification for global habitat mapping from remote sensing". In: *Scientific Data* 8.1, p. 196. DOI: *10.1038/s41597-021-00958-z*.

Kohler, Kevin E. and Shaun M. Gill (2006). "Coral Point Count with Excel extensions (CPCe): A Visual Basic program for the determination of coral and substrate coverage using random point count methodology". In: *Computers & Geosciences* 32.9, pp. 1259–1269. DOI: *10.1016/j.cageo.2005.11.009*.

Kornder, Niklas A., Jose Cappelletto, Benjamin Mueller, Margaretha J. L. Zalm, Stephanie J. Martinez, Mark J. A. Vermeij, Jef Huisman, and Jasper M. de Goeij (2021). "Implications of 2D versus 3D surveys to measure the abundance and composition of benthic coral reef communities". In: *Coral Reefs* 40.4, pp. 1137–1153. DOI: *10.1007/s00338-021-02118-6*.

La Rosa, Laura Elena Cué, Camile Sothe, Raul Queiroz Feitosa, Cláudia Maria de Almeida, Marcos Benedito Schimalski, and Dário Augusto Borges Oliveira (2021). "Multi-task fully convolutional network for tree species mapping in dense forests using small training hyperspectral data". In: *ISPRS Journal of Photogrammetry and Remote Sensing* 179, pp. 35–49. DOI: *10.1016/j.isprsjprs.2021.07.001*.

Lai, Samantha, Lynette H. L. Loke, Michael J. Hilton, Tjeerd J. Bouma, and Peter A. Todd (2015). "The effects of urbanisation on coastal habitats and the potential for ecological engineering: A Singapore case study". In: *Ocean & Coastal Management* 103, pp. 78–85. DOI: *10.1016/j.ocecoaman.2014.11.006*.

Lamb, Joleah B., James D. True, Srisakul Piromvaragorn, and Bette L. Willis (2014). "Scuba diving damage and intensity of tourist activities increases coral disease prevalence". In: *Biological Conservation* 178, pp. 88–96. DOI: *10.1016/j.biocon.2014.06.027*.

Lassalle, Guillaume, Matheus Pinheiro Ferreira, Laura Elena Cué La Rosa, and Carlos Roberto de Souza Filho (2022). "Deep learning-based individual tree crown delineation in mangrove forests using very-high-resolution satellite imagery". In: *ISPRS Journal of Photogrammetry and Remote Sensing* 189, pp. 220–235. DOI: *10.1016/j.isprsjprs.2022.05.002*.

Leal, Marice and Mark D. Spalding (2022). *The State of the World's Mangroves 2022*. Mangrove Alliance. URL: *https://www.mangrovealliance.org/wp-content/uploads/2022/09/The-State-of-the-Worlds-Mangroves-Report_2022.pdf* (visited on 12/11/2023).

Lechner, Alex Mark and Jonathan R. Rhodes (2016). "Recent Progress on Spatial and Thematic Resolution in Landscape Ecology". In: *Current Landscape Ecology Reports* 1.2, pp. 98–105. DOI: *10.1007/s40823-016-0011-z*.

Lecours, Vincent (2017). "On the Use of Maps and Models in Conservation and Resource Management (Warning: Results May Vary)". In: *Frontiers in Marine Science* 4, p. 288. DOI: *10.3389/fmars.2017.00288*.

Lecours, Vincent, Craig J. Brown, Rodolphe Devillers, Vanessa L. Lucieer, and Evan N. Edinger (2016). "Comparing Selections of Environmental Variables for Ecological Studies: A Focus on Terrain Attributes". In: *PLOS ONE* 11.12, e0167128. DOI: *10.1371/journal.pone.0167128*.

Lecours, Vincent, Rodolphe Devillers, David C. Schneider, Vanessa L. Lucieer, Craig J. Brown, and Evan N. Edinger (2015). "Spatial scale and geographic context in benthic habitat mapping: review and future directions". In: *Marine Ecology Progress Series* 535, pp. 259–284. DOI: *10.3354/meps11378*.

Levin, Simon A. (1992). "The Problem of Pattern and Scale in Ecology: The Robert H. MacArthur Award Lecture". In: *Ecology* 73.6, pp. 1943–1967. DOI: *10.2307/1941447*.

Lodhi, Vaibhav, Debashish Chakravarty, and Pabitra Mitra (2018). "Hyperspectral Imaging for Earth Observation: Platforms and Instruments". In: *Journal of the Indian Institute of Science* 98.4, pp. 429–443. DOI: *10.1007/s41745-018-0070-8*.

Loya, Y. (1972). "Community structure and species diversity of hermatypic corals at Eilat, Red Sea". In: *Marine Biology* 13.2, pp. 100–123. DOI: *10.1007/BF00366561*.

M. Brander, Luke, Alfred J. Wagtendonk, Salman S. Hussain, Alistair McVittie, Peter H. Verburg, Rudolf S. de Groot, and Sander van der Ploeg (2012). "Ecosystem service values for mangroves in Southeast Asia: A meta-analysis and value transfer application". In: *Ecosystem Services* 1.1, pp. 62–69. DOI: *10.1016/j.ecoser.2012.06.003*.

MacNeil, M. Aaron, Nicholas A. J. Graham, Joshua E. Cinner, Shaun K. Wilson, Ivor D. Williams, Joseph Maina, Steven Newman, Alan M. Friedlander, Stacy Jupiter, Nicholas V. C. Polunin, and Tim R. McClanahan (2015). "Recovery potential of the world's coral reef fishes". In: *Nature* 520.7547, pp. 341–344. DOI: *10.1038/nature14358*.

Macreadie, Peter I., Andrea Anton, John A. Raven, Nicola Beaumont, Rod M. Connolly, Daniel A. Friess, Jeffrey J. Kelleway, Hilary Kennedy, Tomohiro Kuwae, Paul S. Lavery, Catherine E. Lovelock, Dan A. Smale, Eugenia T. Apostolaki, Trisha B. Atwood, Jeff Baldock, Thomas S. Bianchi, Gail L. Chmura, Bradley D. Eyre, James W. Fourqurean, Jason M. Hall-Spencer, Mark Huxham, Iris E. Hendriks, Dorte Krause-Jensen, Dan Laffoley, Tiziana Luisetti, Núria Marbà, Pere Masque, Karen J. McGlathery, J. Patrick Megonigal, Daniel Murdiyarso, Bayden D. Russell, Rui Santos, Oscar Serrano, Brian R. Silliman, Kenta Watanabe, and Carlos M. Duarte (2019). "The future of Blue Carbon science". In: *Nature Communications* 10.1, p. 3998. DOI: *10.1038/s41467-019-11693-w*.

Maes, Joachim, Benis Egoh, Louise Willemen, Camino Liquete, Petteri Vihervaara, Jan Philipp Schägner, Bruna Grizzetti, Evangelia G. Drakou, Alessandra La Notte, Grazia Zulian, Faycal Bouraoui, Maria Luisa Paracchini, Leon Braat, and Giovanni Bidoglio (2012). "Mapping ecosystem services for policy support and decision making in the European Union". In: *Ecosystem Services* 1.1, pp. 31–39. DOI: *10.1016/j.ecoser.2012.06.004*.

Magris, Rafael Almeida and Raquel Barreto (2010). "Mapping and assessment of protection of mangrove habitats in Brazil". In.

Marvin, David C. and Gregory P. Asner (2016). "Spatially explicit analysis of field inventories for national forest carbon monitoring". In: *Carbon Balance and Management* 11.1, p. 9. DOI: *10.1186/s13021-016-0050-0*.

Mayr, Stefan, Claudia Kuenzer, Ursula Gessner, Igor Klein, and Martin Rutzinger (2019). "Validation of Earth Observation Time-Series: A Review for Large-Area and Temporally Dense Land Surface Products". In: *Remote Sensing* 11.22, p. 2616. DOI: *10.3390/rs11222616*.

McManus, Lisa C., Vítor V. Vasconcelos, Simon A. Levin, Diane M. Thompson, Joan A. Kleypas, Frederic S. Castruccio, Enrique N. Curchitser, and James R. Watson (2020). "Extreme temperature events will drive coral decline in the Coral Triangle". In: *Global Change Biology* 26.4, pp. 2120–2133. DOI: *10.1111/gcb.14972*.

Mejía-Rentería, Juan C., Gustavo A. Castellanos-Galindo, Jaime R. Cantera-Kintz, and Stuart E. Hamilton (2018). "A comparison of Colombian Pacific mangrove extent estimations: Implications for the conservation of a unique Neotropical tidal forest". In: *Estuarine, Coastal and Shelf Science* 212, pp. 233–240. DOI: *10.1016/j.ecss.2018.07.020*.

Mills, Matthew S., Mischa Ungermann, Guy Rigot, Joost den Haan, Javier X. Leon, and Tom Schils (2023). "Assessment of the utility of underwater hyperspectral imaging for surveying and monitoring coral reef ecosystems". In: *Scientific Reports* 13.1, p. 21103. DOI: *10.1038/s41598-023-48263-6*.

Miraki, Mojdeh, Hormoz Sohrabi, Parviz Fatehi, and Mathias Kneubuehler (2021). "Individual tree crown delineation from high-resolution UAV images in broadleaf forest". In: *Ecological Informatics* 61, p. 101207. DOI: *10.1016/j.ecoinf.2020.101207*.

Misra, Ishan, C. Lawrence Zitnick, Margaret Mitchell, and Ross Girshick (2016). "Seeing Through the Human Reporting Bias: Visual Classifiers From Noisy Human-Centric Labels". In: Proceedings of the IEEE Conference on Computer Vision and Pattern Recognition, pp. 2930–2939. URL: *https://www.cv-foundation.org/openaccess/content_cvpr_2016/html/Misra_Seeing_Through_the_CVPR_2016_paper.html* (visited on 12/17/2023).

Moberg, Fredrik and Carl Folke (1999). "Ecological goods and services of coral reef ecosystems". In: *Ecological Economics* 29.2, pp. 215–233. DOI: *10.1016/S0921-8009(99)00009-9*.

Moberg, Fredrik and Patrik Rönnbäck (2003). "Ecosystem services of the tropical seascape: interactions, substitutions and restoration". In: *Ocean & Coastal Management* 46.1, pp. 27–46. DOI: *10.1016/S0964-5691(02)00119-9*.

Muldrow, Milton, Edward C. M. Parsons, and Robert Jonas (2020). "Shifting baseline syndrome among coral reef scientists". In: *Humanities and Social Sciences Communications* 7.1, pp. 1–8. DOI: *10.1057/s41599-020-0526-0*.

Nagelkerken, I. and G. van der Velde (2002). "Do non-estuarine mangroves harbour higher densities of juvenile fish than adjacent shallow-water and coral reef habitats in Curaçao (Netherlands Antilles)?" In: *Marine Ecology Progress Series* 245, pp. 191–204. URL: *https://www.jstor.org/stable/24866404* (visited on 12/10/2023).

Nagelkerken, I., G. van der Velde, M. W. Gorissen, G. J. Meijer, T. Van't Hof, and C. den Hartog (2000). "Importance of Mangroves, Seagrass Beds and the Shallow Coral Reef as a Nursery for Important Coral Reef Fishes, Using a Visual Census Technique". In: *Estuarine, Coastal and Shelf Science* 51.1, pp. 31–44. DOI: *10.1006/ecss.2000.0617*.

Navarro, Alejandro, Mary Young, Blake Allan, Paul Carnell, Peter Macreadie, and Daniel Ierodiaconou (2020). "The application of Unmanned Aerial Vehicles (UAVs) to estimate above-ground biomass of mangrove ecosystems". In: *Remote Sensing of Environment* 242, p. 111747. DOI: *10.1016/j.rse.2020.111747*.

Nowosad, Jakub and Tomasz F. Stepinski (2019). "Information theory as a consistent framework for quantification and classification of landscape patterns". In: *Landscape Ecology* 34.9, pp. 2091–2101. DOI: *10.1007/s10980-019-00830-x*.

Otero, Viviana, Ruben Van De Kerchove, Behara Satyanarayana, Columba Martínez-Espinosa, Muhammad Amir Bin Fisol, Mohd Rodila Bin Ibrahim, Ibrahim Sulong, Husain Mohd-Lokman, Richard Lucas, and Farid Dahdouh-Guebas (2018). "Managing mangrove forests from the sky: Forest inventory using field data and Unmanned Aerial Vehicle (UAV) imagery in the Matang Mangrove Forest Reserve, peninsular Malaysia". In: *Forest Ecology and Management* 411, pp. 35–45. DOI: *10.1016/j.foreco.2017.12.049*.

Ouyang, Xiaoguang, Erik Kristensen, Martin Zimmer, Carol Thornber, Zhifeng Yang, and Shing Yip Lee (2023). "Response of macrophyte litter decomposition in global blue carbon ecosystems to climate change". In: *Global Change Biology* 29.13, pp. 3806–3820. DOI: *10.1111/gcb.16693*.

Pandolfi, John M., Roger H. Bradbury, Enric Sala, Terence P. Hughes, Karen A. Bjorndal, Richard G. Cooke, Deborah McArdle, Loren McClenachan, Marah J. H. Newman, Gustavo Paredes, Robert R. Warner, and Jeremy B. C. Jackson (2003). "Global Trajectories of the Long-Term Decline of Coral Reef Ecosystems". In: *Science* 301.5635, pp. 955–958. DOI: *10.1126/science.1085706*.

Pante, Eric and Phillip Dustan (2012). "Getting to the Point: Accuracy of Point Count in Monitoring Ecosystem Change". In: *Journal of Marine Biology* 2012, e802875. DOI: *10.1155/2012/802875*.

Paoletti, M. E., J. M. Haut, J. Plaza, and A. Plaza (2019). "Deep learning classifiers for hyperspectral imaging: A review". In: *ISPRS Journal of Photogrammetry and Remote Sensing* 158, pp. 279–317. DOI: *10.1016/j.isprsjprs.2019.09.006*.

Pauly, Daniel, Geronimo Silvestre, and Ian R. Smith (1989). "On Development, Fisheries and Dynamite: A Brief Review of Tropical Fisheries Management". In: *Natural Resource Modeling* 3.3, pp. 307–329. DOI: *10.1111/j.1939-7445.1989.tb00084.x*.

Pavoni, Gaia, Massimiliano Corsini, Marco Callieri, Giuseppe Fiameni, Clinton Edwards, and Paolo Cignoni (2020). "On Improving the Training of Models for the Semantic Segmentation of Benthic Communities from Orthographic Imagery". In: *Remote Sensing* 12.18, p. 3106. DOI: *10.3390/rs12183106*.

Pavoni, Gaia, Massimiliano Corsini, Federico Ponchio, Alessandro Muntoni, Clinton Edwards, Nicole Pedersen, Stuart Sandin, and Paolo Cignoni (2022). "TagLab: AI-assisted annotation for the fast and accurate semantic segmentation of coral reef orthoimages". In: *Journal of Field Robotics* 39.3, pp. 246–262. DOI: *10.1002/rob.22049*.

Peñaflor, E. L., W. J. Skirving, A. E. Strong, S. F. Heron, and L. T. David (2009). "Sea-surface temperature and thermal stress in the Coral Triangle over the past two decades". In: *Coral Reefs* 28.4, pp. 841–850. DOI: *10.1007/s00338-009-0522-8*.

Perkins, Nicholas R., Scott D. Foster, Nicole A. Hill, and Neville S. Barrett (2016). "Image subsampling and point scoring approaches for large-scale marine benthic monitoring programs". In: *Estuarine, Coastal and Shelf Science* 176, pp. 36–46. DOI: *10.1016/j.ecss.2016.04.005*.

Perry, Chris, Scott Smithers, Pauline Gulliver, and Nicola Browne (2012). "Evidence of very rapid reef accretion and reef growth under high turbidity and terrigenous sedimentation". In: *Geology* 40, pp. 719–722. DOI: *10.1130/G33261.1*.

Persson, Henrik Jan, Magnus Ekström, and Göran Ståhl (2022). "Quantify and account for field reference errors in forest remote sensing studies". In: *Remote Sensing of Environment* 283, p. 113302. DOI: *10.1016/j.rse.2022.113302*.

Plaisance, Laetitia, M. Julian Caley, Russell E. Brainard, and Nancy Knowlton (2011). "The Diversity of Coral Reefs: What Are We Missing?" In: *PLoS ONE* 6.10, e25026. DOI: *10.1371/journal.pone.0025026*.

Polidoro, Beth A., Kent E. Carpenter, Lorna Collins, Norman C. Duke, Aaron M. Ellison, Joanna C. Ellison, Elizabeth J. Farnsworth, Edwino S. Fernando, Kandasamy Kathiresan, Nico E. Koedam, Suzanne R. Livingstone, Toyohiko Miyagi, Gregg E. Moore, Vien Ngoc Nam, Jin Eong Ong, Jurgenne H. Primavera, Severino G. Salmo Iii, Jonnell C. Sanciangco, Sukristijono Sukardjo, Yamin Wang, and Jean Wan Hong Yong (2010). "The Loss of Species: Mangrove Extinction Risk and Geographic Areas of Global Concern". In: *PLOS ONE* 5.4, e10095. DOI: *10.1371/journal.pone.0010095*.

Precht, William F. and Richard B. Aronson (2006). "Death and resurrection of Caribbean coral reefs: a palaeoecological perspective". In: *Coral Reef Conservation*. Ed. by Isabelle M. Côté and John D. Reynolds. Conservation Biology. Cambridge: Cambridge University Press, pp. 40–77. DOI: *10.1017/CBO9780511804472.004*.

Rashid, Ahmad Rafiuddin and Arjun Chennu (2020). "A Trillion Coral Reef Colors: Deeply Annotated Underwater Hyperspectral Images for Automated Classification and Habitat Mapping". In: *Data* 5.1, p. 19. DOI: *10.3390/data5010019*.

Rast, Michael and Thomas H. Painter (2019). "Earth Observation Imaging Spectroscopy for Terrestrial Systems: An Overview of Its History, Techniques, and Applications of Its Missions". In: *Surveys in Geophysics* 40.3, pp. 303–331. DOI: *10.1007/s10712-019-09517-z*.

"Methods for Estimating Above-Ground Biomass" (2008). In: *Carbon Inventory Methods Handbook for Greenhouse Gas Inventory, Carbon Mitigation and Roundwood Production Projects*. Ed. by N. H. Ravindranath and Madelene Ostwald. Advances in Global Change Research. Dordrecht: Springer Netherlands, pp. 113–147. DOI: *10.1007/978-1-4020-6547-7_10*.

Reverter, Miriam, Stephanie B. Helber, Sven Rohde, Jasper M. de Goeij, and Peter J. Schupp (2022). "Coral reef benthic community changes in the Anthropocene: Biogeographic het-

erogeneity, overlooked configurations, and methodology". In: *Global Change Biology* 28.6, pp. 1956–1971. DOI: *10.1111/gcb.16034*.

Riitters, Kurt (2019). "Pattern metrics for a transdisciplinary landscape ecology". In: *Landscape Ecology* 34.9, pp. 2057–2063. DOI: *10.1007/s10980-018-0755-4*.

Roelfsema, Chris M., Eva M. Kovacs, Juan Carlos Ortiz, David P. Callaghan, Karlo Hock, Mathieu Mongin, Kasper Johansen, Peter J. Mumby, Magnus Wettle, Mike Ronan, Petra Lundgren, Emma V. Kennedy, and Stuart R. Phinn (2020). "Habitat maps to enhance monitoring and management of the Great Barrier Reef". In: *Coral Reefs* 39.4, pp. 1039–1054. DOI: *10.1007/s00338-020-01929-3*.

Ruwaimana, Monika, Behara Satyanarayana, Viviana Otero, Aidy M. Muslim, Muhammad Syafiq A, Sulong Ibrahim, Dries Raymaekers, Nico Koedam, and Farid Dahdouh-Guebas (2018). "The advantages of using drones over space-borne imagery in the mapping of mangrove forests". In: *PLOS ONE* 13.7, e0200288. DOI: *10.1371/journal.pone.0200288*.

Sandin, Stuart A., Esmeralda Alcantar, Randy Clark, Ramón de León, Faisal Dilrosun, Clinton B. Edwards, Andrew J. Estep, Yoan Eynaud, Beverly J. French, Michael D. Fox, Dave Grenda, Scott L. Hamilton, Heather Kramp, Kristen L. Marhaver, Scott D. Miller, Ty N. F. Roach, Gisette Seferina, Cynthia B. Silveira, Jennifer E. Smith, Brian J. Zgliczynski, and Mark J. A. Vermeij (2022). "Benthic assemblages are more predictable than fish assemblages at an island scale". In: *Coral Reefs* 41.4, pp. 1031–1043. DOI: *10.1007/s00338-022-02272-5*.

Sandin, Stuart A., Jennifer E. Smith, Edward E. DeMartini, Elizabeth A. Dinsdale, Simon D. Donner, Alan M. Friedlander, Talina Konotchick, Machel Malay, James E. Maragos, David Obura, Olga Pantos, Gustav Paulay, Morgan Richie, Forest Rohwer, Robert E. Schroeder, Sheila Walsh, Jeremy B. C. Jackson, Nancy Knowlton, and Enric Sala (2008). "Baselines and Degradation of Coral Reefs in the Northern Line Islands". In: *PLOS ONE* 3.2, e1548. DOI: *10.1371/journal.pone.0001548*.

Schiefer, Felix, Teja Kattenborn, Annett Frick, Julian Frey, Peter Schall, Barbara Koch, and Sebastian Schmidtlein (2020). "Mapping forest tree species in high resolution UAV-based RGB-imagery by means of convolutional neural networks". In: *ISPRS Journal of Photogrammetry and Remote Sensing* 170, pp. 205–215. DOI: *10.1016/j.isprsjprs.2020.10.015*.

Spalding, M. D. and A. M. Grenfell (1997). "New estimates of global and regional coral reef areas". In: *Coral Reefs* 16.4, pp. 225–230. DOI: *10.1007/s003380050078*.

Spalding, Mark, Lauretta Burke, Spencer A. Wood, Joscelyne Ashpole, James Hutchison, and Philine zu Ermgassen (2017). "Mapping the global value and distribution of coral reef tourism". In: *Marine Policy* 82, pp. 104–113. DOI: *10.1016/j.marpol.2017.05.014*.

Sparrow, Ben D., Will Edwards, Samantha E.M. Munroe, Glenda M. Wardle, Greg R. Guerin, Jean-Francois Bastin, Beryl Morris, Rebekah Christensen, Stuart Phinn, and Andrew J. Lowe (2020). "Effective ecosystem monitoring requires a multi-scaled approach". In: *Biological Reviews* 95.6, pp. 1706–1719. DOI: *10.1111/brv.12636*.

Stehman, Stephen V. and Giles M. Foody (2019). "Key issues in rigorous accuracy assessment of land cover products". In: *Remote Sensing of Environment* 231, p. 111199. DOI: *10.1016/j.rse.2019.05.018*.

Storlazzi, Curt D., Peter Dartnell, Gerald A. Hatcher, and Ann E. Gibbs (2016). "End of the chain? Rugosity and fine-scale bathymetry from existing underwater digital imagery using structure-from-motion (SfM) technology". In: *Coral Reefs* 35.3, pp. 889–894. DOI: *10.1007/s00338-016-1462-8*.

Sulla-Menashe, Damien, Josh M. Gray, S. Parker Abercrombie, and Mark A. Friedl (2019). "Hierarchical mapping of annual global land cover 2001 to present: The MODIS Collection 6 Land Cover product". In: *Remote Sensing of Environment* 222, pp. 183–194. DOI: *10.1016/j.rse.2018.12.013*.

Sully, Shannon and Robert van Woesik (2020). "Turbid reefs moderate coral bleaching under climate-related temperature stress". In: *Global Change Biology* 26.3, pp. 1367–1373. DOI: *10.1111/gcb.14948*.

Tao, Haiyu, Shan Xu, Yongchao Tian, Zhaofeng Li, Yan Ge, Jiaoping Zhang, Yu Wang, Guodong Zhou, Xiong Deng, Ze Zhang, Yanfeng Ding, Dong Jiang, Qinghua Guo, and Shichao Jin (2022). "Proximal and remote sensing in plant phenomics: 20 years of progress, challenges, and perspectives". In: *Plant Communications*. Focus Issue on Tree Biology 3.6, p. 100344. DOI: *10.1016/j.xplc.2022.100344*.

Teichberg, Mirta, Christian Wild, Vanessa N. Bednarz, Hauke F. Kegler, Muhammad Lukman, Astrid A. Gärdes, Jasmin P. Heiden, Laura Weiand, Nur Abu, Andriani Nasir, Sara Miñarro, Sebastian C. A. Ferse, Hauke Reuter, and Jeremiah G. Plass-Johnson (2018). "Spatio-Temporal Patterns in Coral Reef Communities of the Spermonde Archipelago, 2012–2014, I: Comprehensive Reef Monitoring of Water and Benthic Indicators Reflect Changes in Reef Health". In: *Frontiers in Marine Science* 5. DOI: *10.3389/fmars.2018.00033*.

Tucker, Compton, Martin Brandt, Pierre Hiernaux, Ankit Kariryaa, Kjeld Rasmussen, Jennifer Small, Christian Igel, Florian Reiner, Katherine Melocik, Jesse Meyer, Scott Sinno, Eric Romero, Erin Glennie, Yasmin Fitts, August Morin, Jorge Pinzon, Devin McClain, Paul Morin, Claire Porter, Shane Loeffler, Laurent Kergoat, Bil-Assanou Issoufou, Patrice Savadogo, Jean-Pierre Wigneron, Benjamin Poulter, Philippe Ciais, Robert Kaufmann, Ranga Myneni, Sassan Saatchi, and Rasmus Fensholt (2023). "Sub-continental-scale carbon stocks of individual trees in African drylands". In: *Nature* 615.7950, pp. 80–86. DOI: *10.1038/s41586-022-05653-6*.

Underwood, A. J, M. G Chapman, and S. D Connell (2000). "Observations in ecology: you can't make progress on processes without understanding the patterns". In: *Journal of Experimental Marine Biology and Ecology* 250.1, pp. 97–115. DOI: *10.1016/S0022-0981(00)00181-7*.

UNEP-WCMC, WorldFish, World Resources Institute, and The Nature Conservancy (2010). *Global Distribution of Coral Reefs*. Version 4.1. DOI: *10.34892/T2WK-5T34*.

Urbina-Barreto, Isabel, Rémi Garnier, Simon Elise, Romain Pinel, Pascal Dumas, Vincent Mahamadaly, Mathilde Facon, Sophie Bureau, Christophe Peignon, Jean-Pascal Quod, Eric

Dutrieux, Lucie Penin, and Mehdi Adjeroud (2021). "Which Method for Which Purpose? A Comparison of Line Intercept Transect and Underwater Photogrammetry Methods for Coral Reef Surveys". In: *Frontiers in Marine Science* 8. URL: *https://www.frontiersin.org/articles/10.3389/fmars.2021.636902* (visited on 12/10/2023).

Veron, John (Charlie) E. N., Lyndon M. DeVantier, Emre Turak, Alison L. Green, Stuart Kininmonth, M. Stafford-Smith, and N. Peterson (2011). "The Coral Triangle". In: *Coral Reefs: An Ecosystem in Transition*. Ed. by Zvy Dubinsky and Noga Stambler. Dordrecht: Springer Netherlands, pp. 47–55. DOI: *10.1007/978-94-007-0114-4_5*.

Vorster, Anthony G., Paul H. Evangelista, Atticus E. L. Stovall, and Seth Ex (2020). "Variability and uncertainty in forest biomass estimates from the tree to landscape scale: the role of allometric equations". In: *Carbon Balance and Management* 15.1, p. 8. DOI: *10.1186/s13021-020-00143-6*.

Williams, Ivor D., Courtney S. Couch, Oscar Beijbom, Thomas A. Oliver, Bernardo Vargas-Angel, Brett D. Schumacher, and Russell E. Brainard (2019). "Leveraging Automated Image Analysis Tools to Transform Our Capacity to Assess Status and Trends of Coral Reefs". In: *Frontiers in Marine Science* 6. DOI: *10.3389/fmars.2019.00222*.

Wirasatriya, Anindya, Rudhi Pribadi, Sigit Bayhu Iryanthony, Lilik Maslukah, Denny Nugroho Sugianto, Muhammad Helmi, Raditya Rizki Ananta, Novi Susetyo Adi, Terry Louise Kepel, Restu N. A. Ati, Mariska A. Kusumaningtyas, Rempei Suwa, Raghab Ray, Takashi Nakamura, and Kazuo Nadaoka (2022). "Mangrove Above-Ground Biomass and Carbon Stock in the Karimunjawa-Kemujan Islands Estimated from Unmanned Aerial Vehicle-Imagery". In: *Sustainability* 14.2, p. 706. DOI: *10.3390/su14020706*.

WoRMS, Editorial Board (2023). *World Register of Marine Species*. URL: *https://www.marinespecies.org* (visited on 11/13/2023).

Zang, Jingrong, Shichao Jin, Songyin Zhang, Qing Li, Yue Mu, Ziyu Li, Shaochen Li, Xiao Wang, Yanjun Su, and Dong Jiang (2023). "Field-measured canopy height may not be as accurate and heritable as believed: evidence from advanced 3D sensing". In: *Plant Methods* 19.1, p. 39. DOI: *10.1186/s13007-023-01012-2*.

Part II

Doctoral Research

Overview of chapters

This doctoral dissertation is a cumulative thesis consisting of the complete versions of three manuscripts prepared for publication in international journals (Chapters 2, 3 and 4) and the abstract of a manuscript in preparation (Chapter 5). Of these, two are already published (Chapters 2 & 4), one is ready for submission (Chapter 3) and one is in preparation (Chapter 5).

Chapter 2 – DIGITIZING THE CORAL REEF: MACHINE LEARNING OF UNDERWATER SPECTRAL IMAGES ENABLES DENSE TAXONOMIC MAPPING OF BENTHIC HABITATS
Daniel Schürholz and Arjun Chennu. (see Author contributions)

Published in *Methods in Ecology and Evolution* 2023. 14.2, pp. 596–613.

Chapter 3 – CURAÇAO REEFS UNDER THE HYPERSPECTRAL LENS: DETAILED MAPPING REVEALS REEFSCAPE PATTERNS OF COMMUNITY COMPOSITION AND ENVIRONMENTAL DRIVERS
Daniel Schürholz and Arjun Chennu. (see Author contributions)

Prepared for submission to *eLife journal*.

Chapter 4 – SEEING THE FOREST FOR THE TREES: MAPPING COVER AND COUNTING TREES FROM AERIAL IMAGES OF A MANGROVE FOREST USING ARTIFICIAL INTELLIGENCE
Daniel Schürholz, Gustavo Adolfo Castellanos-Galindo, Elisa Casella, Juan Carlos Mejía-Rentería and Arjun Chennu. (see Author contributions)

Published in *Remote Sensing* 15.13. p. 3334.

Chapter 5 – REMOVING THE TURBID VEIL: ARE TURBID REEFS A REFUGIA FOR CORALS IN AN ADVERSE FUTURE?
Daniel Schürholz, Andi Muh. Agung Pratama, Gunawan Syafruddin, Puspita Lestari Kanna, Estradivari Estradivari, Dino Angelo Ramos and Arjun Chennu. (see Author contributions)

In preparation for submission to *Coral Reefs*.

Chapter 2

Digitizing the coral reef: Machine learning of underwater spectral images enables dense taxonomic mapping of benthic habitats

Daniel Schürholz [1,2] *and Arjun Chennu* [2]

Manuscript status

Published as Daniel Schürholz and Arjun Chennu (2023). "Digitizing the coral reef: Machine learning of underwater spectral images enables dense taxonomic mapping of benthic habitats". In: *Methods in Ecology and Evolution* 14.2, pp. 596–613. doi: 10.1111/2041-210X.14029.

[1]Max Planck Institute for Marine Microbiology, 28359 Bremen, Germany
[2]Leibniz Centre for Tropical Marine Research (ZMT), 28359 Bremen, Germany

2.1 Abstract

1: Coral reefs are the most biodiverse marine ecosystems, and host a wide range of taxonomic diversity in a complex spatial community structure. Existing coral reef survey methods struggle to accurately capture the taxonomic detail within the complex spatial structure of benthic communities.

2: We propose a workflow to leverage underwater hyperspectral image transects and two machine learning algorithms to produce dense habitat maps of 1150 m^2 of reefs across the Curaçao coastline. Our multi-method workflow labelled all 500+ million pixels with one of 43 classes at taxonomic family, genus or species level for corals, algae, sponges, or to substrate labels such as sediment, turf algae and cyanobacterial mats.

3: With low annotation effort (2% pixels) and no external data, our workflow enables accurate (Fbeta 87%) survey-scale mapping, with unprecedented thematic and spatial detail. Our assessments of the composition and configuration of the benthic communities of 23 image transects showed high consistency.

4: Digitizing the reef habitat and community structure enables validation and novel analysis of pattern and scale in coral reef ecology. Our dense habitat maps reveal the inadequacies of point sampling methods to accurately describe reef benthic communities.

2.2 Introduction

Under rapidly changing environmental conditions, the need for accurate and speedy ecological assessment of marine and freshwater ecosystems has greatly increased. This is particularly pressing for coral reefs, which are the most biologically diverse marine ecosystems on the planet, but have suffered significant deterioration in recent years due to a variety of stressors, such as tourism overuse, destructive fishing practices, land-based pollution and climate change (Cesar et al. 2003; Hughes et al. 2021). Continued stress on coral reefs deteriorates their health, leading to increased coral bleaching, coral mortality, disease outbreaks, loss of coral dominance and diversity loss (Burke et al. 2004). In turn, the deterioration of coral reef health world-wide will endanger the ecosystem services that these reefs provide (i.e. shoreline protection, bioprospecting, food production, etc.) to coastal populations and other associated systems (Hoegh-Guldberg et al. 2017; Moberg et al. 1999). Furthermore, this long-term degradation of reefs confounds an inter-generational understanding of baseline reef health that informs reef restoration and management interventions (Muldrow et al. 2020), thus highlighting the need for objective assessments of reef health through monitoring.

Modern reef monitoring efforts focus on the creation of benthic habitat maps, as they capture the

spatial distributions of species and habitat features (Guisan et al. 2013; Roelfsema, Kovacs, et al. 2020). Such information captured over a long time series forms the basis of scientific evaluation of the ecosystem's evolution, and underpins the decisions for management, conservation and restoration (Foo et al. 2019). The spatial, temporal and thematic scales of ecosystem mapping have a critical influence on the viability of specific scientific analyses (Lecours 2017), such as elucidating functional drivers, detecting community phase shifts or signalling deterioration of habitats. Most reef inventories compiled from in-situ surveys lack sufficient taxonomic and spatial detail, and have been carried out in only 0.01%–0.1% of coral reef regions world-wide (Eric J. Hochberg et al. 2021). In addition, many surveys do not report any uncertainty information that limits the utility of the data for scaling up studies to the ecosystem-level (Reverter et al. 2022). Thus, a priority for future in-situ reef surveys should be wider biogeographic coverage, clearer uncertainty estimates and deeper taxonomic and spatial detail at the survey scale.

Satellites are increasingly used to map shallow benthic habitats and analyse regional and global phenomena affecting coral reefs (Hedley et al. 2016; Heron et al. 2016). With recent enhanced spectral and spatial resolutions of remotely sensed images (0.5–10 m per pixel), better reef monitoring products have been enabled, such as geomorphological zonation of reefs (Kennedy et al. 2021) and benthic habitat maps (B. Lyons et al. 2020; Roelfsema, Lyons, et al. 2021). However, validating the accuracy of satellite-derived maps is a difficult task, impeded by the lack of in-situ validation datasets and the lack of error estimation in existing datasets (Eric J. Hochberg et al. 2021; Phinn et al. 2012). While remote sensing offers a viable approach for large scale analyses of reefs, current satellite sensors lack spatial resolution to represent small organisms (<0.5 m) and the spectral resolution to potentially differentiate organisms to a deep taxonomic description (Eric J Hochberg et al. 2003; Muller-Karger et al. 2018). In contrast, in-situ surveys can provide enhanced spatial and spectral resolutions in underwater imagery, made available by advancements in instrumentation and robotic platforms (Chennu, Färber, et al. 2017), both aerial (Casella et al. 2017) and underwater (Armstrong et al. 2019). Improvements ML, especially with the application of artificial neural networks, have contributed to better accuracy and throughput of efforts in automated classification (Beijbom et al. 2015; González-Rivero et al. 2020) and semantic segmentation (Alonso et al. 2019; Pavoni et al. 2020) of benthic images. Carefully designed 'ground-truthing', produced from images acquired via underwater/proximal sensing, and mapped through scalable and automated workflows, can provide a consistent source of validation for current and upcoming ecosystem-level studies.

Deriving validation support from in-situ surveys requires careful design conformity between the proximal and remote sensing campaigns (Roelfsema and Phinn 2013). For example, the lack of conformity in the set of labels used between satellite and in-situ studies is a major confounding factor (Foody 2004). The labelspace of global maps usually include broad reefgroups (coral, algae, sediment, etc.), some status indicators (dead, alive, bleached) or morphological descriptions (branching, massive, weedy; Kennedy et al. 2021). This multi-faceted and easy-to-interpret view

of the reef structure is useful for coastal management (Roelfsema, Kovacs, et al. 2020). However, describing the reef community with broad reefgroups can hide intra-group shifts and conceal key dynamics of coral reef communities (Brito-Millán et al. 2019). To enable these analyses, in-situ studies leverage thematic scales that identify organisms down to genus or species level, as well as different substrata (sand, rock, rubble) and the substrate-associated communities (cyanobacterial mats, turf algae), rendering a detailed view of the biotic and abiotic components (Althaus et al. 2015). Capturing community structure with a detailed labelspace is typically limited by the availability of expert time or by logistical constraints. For this reason, reef community structure, as assessed in a majority of reef studies, is severely undersampled—both spatially and thematically—with respect to habitat complexity, neglecting spatial distributions and locations of benthic components.

Here we demonstrate how to produce dense and detailed maps of coral reef habitats from underwater surveys (Figure 2.1). Dense means that all regions/pixels in each image transect are assigned a (biotic or abiotic) habitat label, resulting in full semantic segmentation of the transect without any 'background' or 'unknown' labels. Detailed refers to the thematic detail that is captured by the labels, either being taxonomic (species, genus, etc) or broad reefgroups (corals, sponges, etc). We leverage ML to automate the classification of underwater hyperspectral image transects captured over multiple weeks and locations along the coast of the Caribbean island of Curaçao (Chennu, Färber, et al. 2017; Rashid et al. 2020). Our workflow description (Figure 2.1) considers all the steps from the field survey to the classification of 500+ million pixels to the validation of aggregate habitat descriptions derived from the detailed habitat maps. We show how dense maps can be produced, with clear assessments of accuracy, into multiple thematic scales, either at a broad ('reefgroups') or taxonomic ('detailed') labelspace. By implementing two independent ML methods (neural networks and object-based ensemble classification) in parallel, we provide an assessment of the consistency between the reef community structures as described by the maps produced with each ML method. These ML methods can be used to rapidly convert transect spectral data into habitat maps at the survey scale, without the need to augment the training data with external datasets. Finally, we exploit the dense habitat maps of island-wide transects to reveal the inadequacies of sparse point sampling methods to accurately describe reef benthic communities.

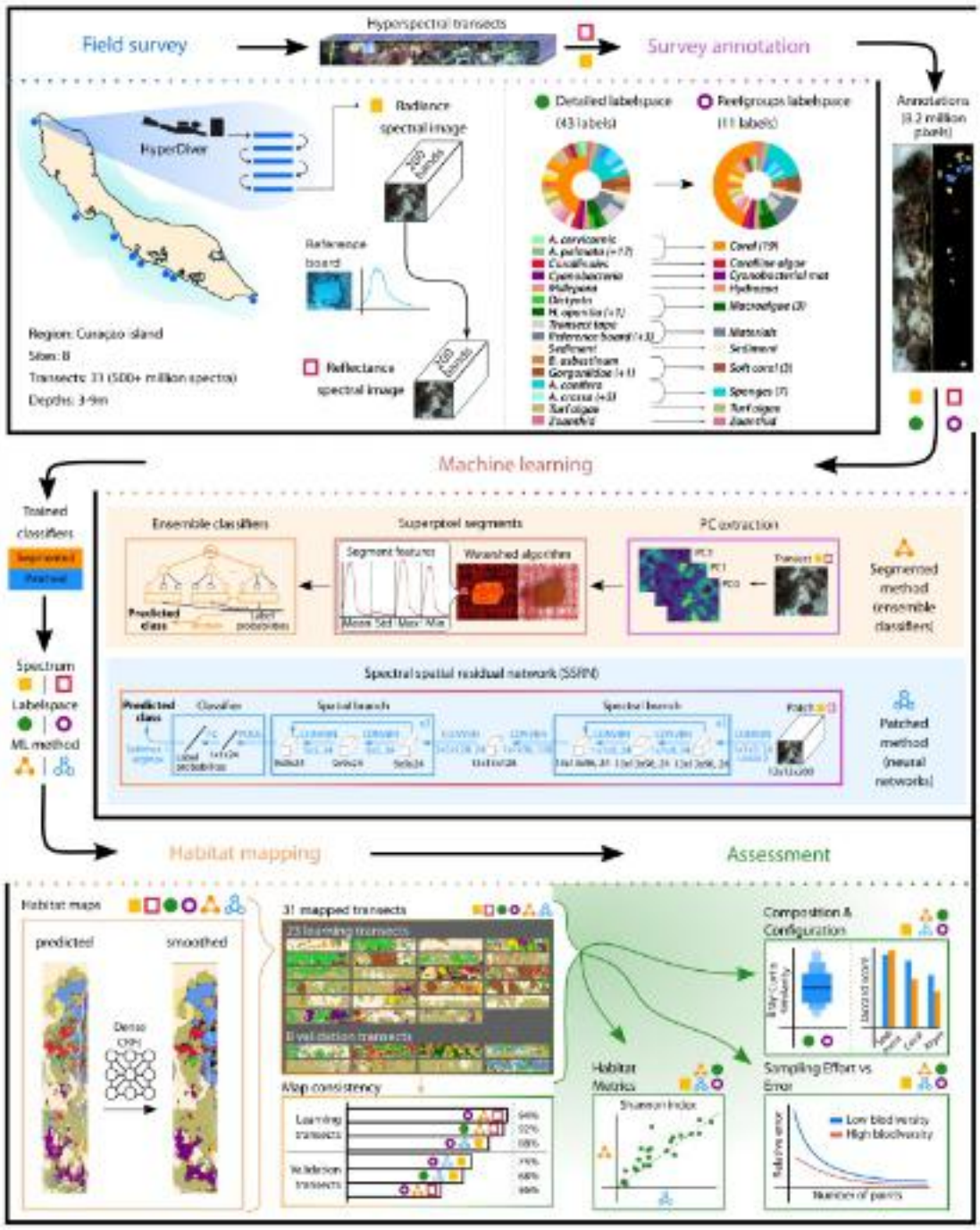

Figure 2.1 Schematic of scalable acquisition-mapping-assessment workflow for digitizing reef community structure. (Caption continues on next page)

Figure 2.1 The underwater survey with the HyperDiver at eight study sites over 147 transects (50 m each) in Curaçao produced radiance and reflectance spectral images. A subset of 31 transect images was annotated into the detailed (43 classes) labelspace and aggregated into the reefgroups (11 classes) labelspace (see Figure A.3 for complete labelspaces). Labelspaces can be adapted to encompass the underlying benthic community being studied. Annotated regions from 23 transects were used in two separate machine learning methods to classify each region of the spectral images into each labelspace independently. The segmented method used ensemble learning on image superpixel features, while the patched method used spatial-spectral neural network learning of image patches. The modular architecture of our workflow facilitates the usage of other ML models that produce probabilistic predictions. The classifiers were used to predict the label probabilities at each of 500+ million pixels in all 31 transects. The classifier-predicted probability maps were contextually smoothed and converted into densely labelled habitat maps. The habitat maps were assessed for their consistency with reference annotations as well as their ability to describe the composition and configuration of the benthic communities in the transects. The effort-versus-error relationship for point-count sampling of the reef habitats was assessed using virtual sampling of the 23 dense habitat maps.

2.3 Materials and Methods

2.3.1 Underwater hyperspectral surveying

Underwater hyperspectral transects were acquired with the HyperDiver surveying system (Chennu, Färber, et al. 2017), and a detailed description of the acquisition and processing is available in a data descriptor (Rashid et al. 2020). A brief overview is provided here.

Hyperspectral transects were acquired in a survey conducted along the leeward coastline of the Caribbean island of Curaçao (Figure 2.1 "Field Survey"). At each of the eight survey sites, 10 to 20 transect images of $50m \times 1m$ area were acquired by divers at varying depths (3 m to 9 m range). The resulting dataset contains 147 hyperspectral transects, from which 31 transects were selected for testing the proposed workflow. The 31 transects were comprised by 23 transects selected from the 3 m, 6 m and 9 m depth for each site (except for one site where the 6m transect was missing), and 8 additional transects randomly selected across the depth gradient. The hyperspectral push-broom imager captures lines of 640 pixels at a time. Each pixel contained 12-bits of radiometric information for each of the 480 wavelength bands in the 400-800 nm range. The spectral images were interpolated and reduced to 200 bands of 8-bit radiometric precision. Although the spectral transect images contain 60 times more colour information per pixel, the overall data size is smaller or comparable to high resolution colour photography used in reef surveys.

The hyperspectral transect images were captured as radiance data under natural and varying light conditions due to depth, cloud cover, water surface conditions, etc. To be independent of these lighting conditions,each transect's radiance image was converted to pseudo-reflectance

images (for brevity we refer to pseudo-reflectance as reflectance for the rest of this manuscript) by dividing out the average radiance signal of a gray reference board present at the ends of each transect plot.

2.3.2 Benthic annotation and thematic flexibility

Annotations were created by human experts to support automated classification of the transects by ML methods. The annotations consisted of 2089 small polygons covering 8.2 million pixels with a corresponding habitat label across the 31 transects (Figure A.1,A.2; Figure 2.1 "Survey annotation"). Biotic classes were annotated to the deepest taxonomic level possible, such as family, genus or species. Substrate classes are represented as sediment, cyanobacterial mat or turf algae. Survey materials were also included to give semantic labels to any object found in the transects, i.e. transect tape or reference board. Three classes were removed given their very low representation in the selected transects (<2 annotated regions). The resulting "detailed" labelspace had 43 final labels (Figure A.3). Loosely speaking, the detailed labelspace describes the habitat in the perspective of a reef ecologist, aiming for full taxonomic resolution of the studied reef community.

From the perspective of a reef manager, typically interested in the broad demographic description of a reef, taxonomic detail is not useful or a detriment to management analysis. We created a labelspace to serve the perspective of a reef manager, by abstracting each label in the detailed labelspace to a corresponding broad reef group class (Figure A.3). For example, the 19 coral species and genera were abstracted to a class called "Coral". The 11 resulting classes formed the "reefgroups" labelspace. This thematic flexibility allowed us to run the ML setup with annotations in either labelspace, to measure the workflow's ability to classify into both labelspaces correctly. To compare classifications across labelspaces, we created an abstracted "detailed-to-reefgroups" version of the detailed lablespace maps, that is, assigning all labels to their corresponding reefgroups label. Then the reef community composition was compared between the detailed-to-reefgroups maps and the reefgroups maps.

The reference annotations were created with a bias towards reducing human effort rather than providing uniform coverage of samples across the survey data (ibid.). This resulted in a ML dataset with a relatively high degree of label imbalance, both when considered as a set of polygons or as a set of pixels across the annotated transects (Figure A.1,A.2). The degree of imbalance meant that, for example, the 5 most abundant classes (*Sediment*, *Turf algae Diploria strigosa*, *Dictyota*, *Siderastrea siderea*) had 789 polygons and 3.16 million pixels, while the 5 rarest classes (*Aplysina cauliformis*, *Briareum asbestinum*, *Dichocoenia stokesii*, *Zoanthid*, *Lobophora variegata*) had only 14 polygons and 18464 pixels.

The annotated data consisted of 23 "learning transects" (373+ million pixels), that were used to train and test classifiers in the ML steps of our workflow, and 8 separate "validation transects"

(150+ million pixels) that were used to assess the performance of our workflow on unseen data outside the learning transects. Overall, it was possible to represent each annotated transect with two types of signal (radiance or reflectance) and labelspaces (detailed or reefgroups) for ML towards automated classification. The automation of mapping steps in our workflow (i.e., ML classifier training, map creation and assessment) was implemented with the snakemake workflow management system (Mölder et al. 2021).

2.3.3 Machine learning for benthic mapping

ML classifiers were then created to predict the identity of each image region based on its spectral-spatial features (Figure 2.1 "Machine learning"). Two separate ML methods – "patched" and "segmented" – were independently implemented for each combination of signal type (radiance, reflectance) and labelspace (detailed, reefgroups). The predictions of both methods for each image region were a probability value for each label/class in a labelspace.

For the patched method, a deep learning network called spectral-spatial residual network (Zhong et al. 2018) – was used to train a classifier. This network identifies spectral and spatial features by first convolving 1D filters in a spectral branch and then convolving 2D filters in a spatial branch over square patches from the hyperspectral image. Our hyperparameter tuning experiments indicated good performance for parameter values close to original study (see Supplement). For each pixel in the image, the probability of labels is predicted for the central pixel based on the neighbouring pixels in a regular image patch (hence the name "patched"). The image was padded with reflection of border pixels to enable selection of patches at the image edges. After training, each transect was mapped by passing every image patch through the trained network to obtain the predicted label probabilities for the central pixel.

The segmented method consisted of three sequential processes to obtain the the label probabilities for each image region (Figure 2.1). The first step was to reduce each transect image to six principal components and calculate the mean at each pixel. The second step was superpixel over-segmentation of the transect using the mean image as input to the watershed algorithm. The parameters for the watershed algorithm were a batch size of 2000×640 pixels, 12000 markers per batch and a compactness of 1000. This reduced the transect image into a set of irregularly shaped superpixels, which were contiguous image segments of similar pixels (hence the name "segmented"). Descriptors for each hyperspectral image segment were calculated for each spectral band: mean, standard deviation, minimum and maximum values. There were concatenated into a feature vector of 800 features for each image segment. These vectors were then used as input samples for the random forest ensemble classifier in the scikit-learn library. The parameters for the classifier used for transect mapping were 300 base estimators, 2 minimum leaves per tree, 25 as the maximum tree depth and a minimum of 3 samples per tree split. The function used to measure the quality of a split was the Gini inequality function and the class weights were

adjusted inversely to the class abundance in the samples. The classifier output was the label probabilities for an image segment, which were assigned to all the pixels within the segment to generate the class probability map of each transect.

Both methods were set up to take as input an image segment/patch from either of the signal types and produce the same output: an array of probability values for each label in the labelspace linked to all pixels inside a segment or the central pixel in a patch. The predictive performance of the trained classifiers was tested on a set of image annotations, which was spatially disjoint (no shared pixels) from the annotations used for training, as recommended in recent reviews (Paoletti et al. 2019). This testing set comprised of 15496 image segments for the segmented method and 50000 pixels for the patched method. The ML setup allowed us to utilize the segmented method (ensemble classifiers) and the patched method (deep learning) as interchangeable ML components in the workflow for scalable reef mapping.

The performance metrics used to evaluate the classifiers on the testing dataset were: overall accuracy (OA), recall (or producer accuracy), precision (or user accuracy), Fbeta (or F1-score) and Cohen's kappa (Figure 2.2; Table 2.1). OA was calculated by dividing the number of correctly predicted by total predicted segments/pixels. Recall, precision and Fbeta values were calculated for each class separately, and then aggregated using weighted averaging, with weights corresponding to the inverse of the class proportion in the testing dataset. Recall was calculated as the fraction of segments/pixels of a given class that were correctly classified. Precision for a class was the fraction of predicted segments/pixels that were annotated as that class. Fbeta is the harmonic mean of recall and precision. Cohen's kappa measures the performance of a classifier as a distance to an uninformed classifier (value of 0) and to a perfect classifier (value of 1), considering the dataset class imbalance.

Method	Label-space	Signal type	Overall accuracy	Precision	Recall	Fbeta	Cohen's Kappa
patched	*detailed*	*radiance*	0.767	0.779	0.769	0.769	0.760
		reflectance	0.715	0.723	0.720	0.720	0.708
	reefgroups	*radiance*	0.869	0.871	0.869	0.869	0.829
		reflectance	0.841	0.841	0.841	0.841	0.793
segmented	*detailed*	*radiance*	0.772	0.779	0.771	0.771	0.755
		reflectance	**0.846**	**0.848**	**0.845**	**0.845**	**0.835**
	reefgroups	*radiance*	0.792	0.796	0.794	0.794	0.737
		reflectance	**0.875**	**0.876**	**0.875**	**0.875**	**0.841**

Table 2.1 Classifiers performance. Comparison of the performance of each ML method in combination with each labelspace and each signal type. The classifiers were tested on disjoint datasets of 50000 patches for the patched method and 15946 segments for the segmented method. The best performing classifiers are highlighted in boldface for the detailed and reefgroups labelspace.

We studied how both classifiers performed depending on the quantity and quality of annotated spectral pixels (Figure 2.3A,B). The quantity of annotated data was measured as unique pixels (in each patch or segment) used during training. Classifier performance was measured by training on various quantities of data but keeping the amount of computing effort constant (see Supplement). Furthermore, to measure the effect of the quality of the spectral information on the classifiers' performance, a subset (N=[10, 25, 50, 100, 150]) of equally-spaced spectral bands were selected (out of the original 200 bands) from the transect images (Figure 2.3C). Each method was separately trained and tested on the transect images with the subsampled spectral bands.

The class probability maps of each transect from either ML method were smoothed by refining the probabilities with Dense Conditional Random Fields (DCRF) (Krähenbühl et al. 2011). DCRF were used to update the probability of each pixel based on the surrounding context, i.e. label probabilities. DCRF interconnect every pixel in an image through a graph model, thus allowing fusing of long-range and short-range context within the image. The class probability maps were used as unary potential inputs to the DCRF, to obtain the smoothed probability maps (Figure 2.1 "Habitat mapping"; Figure 2.4A,B; Figure 2.5).

Each class probability map – from either ML method and with or without smoothing – was converted to a class map by assigning the identity of the class with the highest probability at each transect image location. The result was a categorical habitat map where every pixel was assigned to one label in the labelspace of the trained classifier.

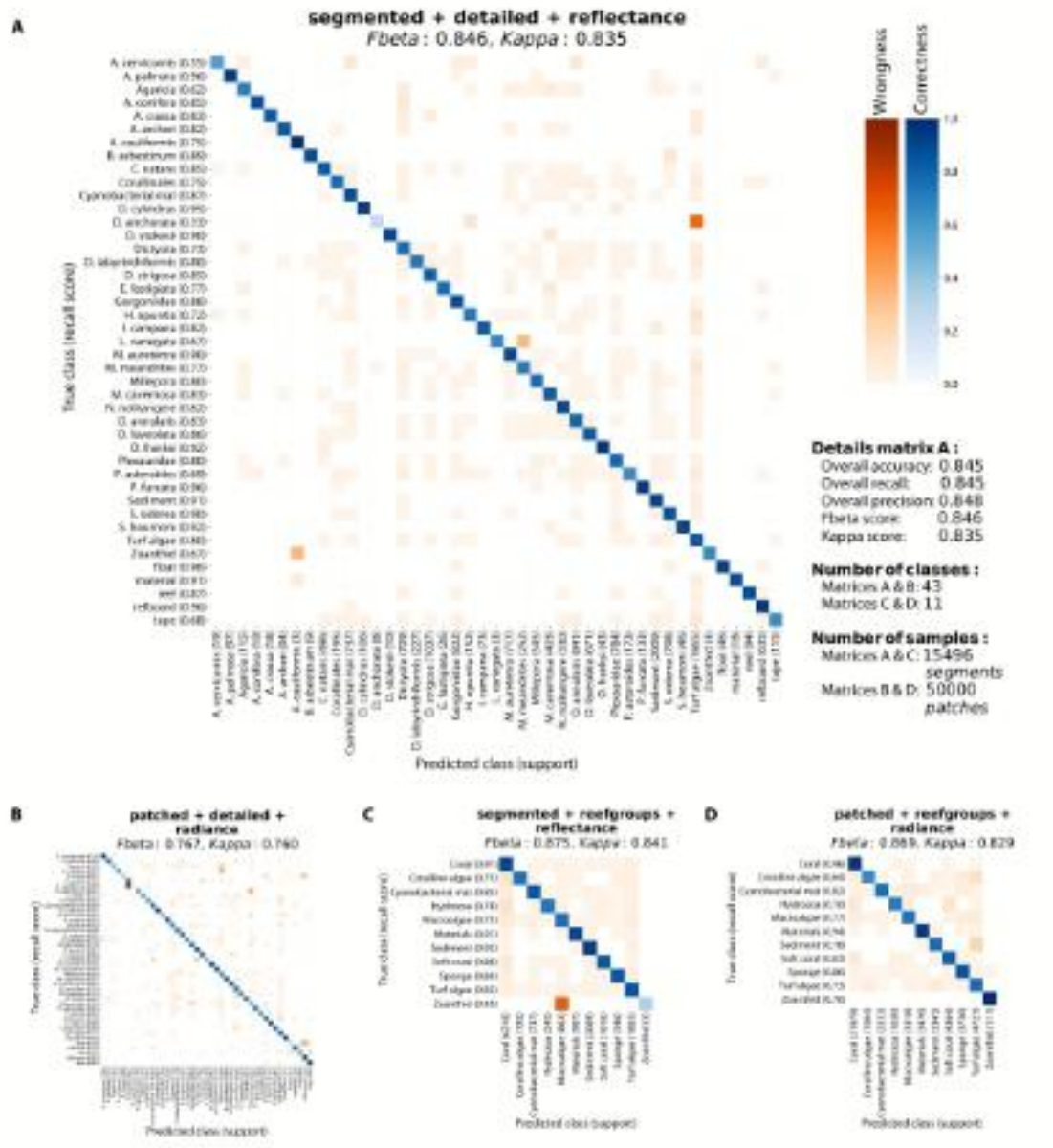

Figure 2.2 Performance evaluation of classifiers in detailed and reefgroups labelspaces. (Caption continues on next page)

2.3.4 Comparison of community structure

We assessed and compared the compositional and configurational structures of the reef benthos from the 23 (learning) transects distributed across Curaçao island (Figure 2.1 “Assessment”;

Figure 2.2 Performance evaluation of classifiers in detailed and reefgroups labelspaces. Recall confusion matrices of classifiers from a subset of ML method+labelspace+signal-type combinations were used to asses performance on a held-out testing set. The segmented method (A) had an excellent overall performance (84.6% Fbeta score; other metrics shown in the side notes) on the detailed labelspace. It presented little (<3%) to minor (<20%) confusions for the rare classes such as *Zoanthid* and *D. anchorata*. The patched method (B) showed a lower overall performance (Fbeta of 76.7%) in the detailed labelspace; with similar confusion for rare classes, such as *A. cauliformis* and *refboard*. On the reefgroup labelspace, both the segmented (C) and patched (D) methods showed excellent overall performance (87.5% and 86.9% Fbeta, respectively), with high recall (92%) shown by the segmented method for *Sediment* and similarly by the patched method for *Coral* (96%). The segmented method showed some relevant confusion between the *Zoanthid* and *Macroalgae* classes, due to the rarity (only three segments) of *Zoanthids* in the dataset.

Figure 2.6). Since both ML methods independently generated habitat maps in each labelspace of each transect, the habitat maps derived from each method were used for pairwise comparisons of the transect's community structures. For each transect the percentage cover (P_i) was calculated as:

$$P_i = 100 \times (\frac{C_i}{N})$$

where C_i is the count of pixels of class i in the transect and N is the total pixel count in the transect.

As a diversity measure for each transect we used Shannon diversity index (H'), defined as:

$$H' = -\sum_{i=1}^{R} p_i \ln p_i$$

where p_i is the proportion of elements of a class i and R is the total number of classes in the labelspace.

To identify biases in the ML methods, we applied a Bland-Altman analysis on the habitat metrics derived for the transects from each ML method (Figure 2.6A-D). This analysis consists of two plots that help identify agreement between two quantitative methods of measurement. The first plots the values of both methods for the specific variable – percentage cover of a class or Shannon diversity index – against each other, to identify values deviating from the one-to-one correlation line. In the second plot the differences of the paired measurements are plotted against their averages, to identify the mean of the difference and its ±1.96 standard deviation lines. The bias is read as the gap between the mean of the difference and the 0 difference line. The two methods

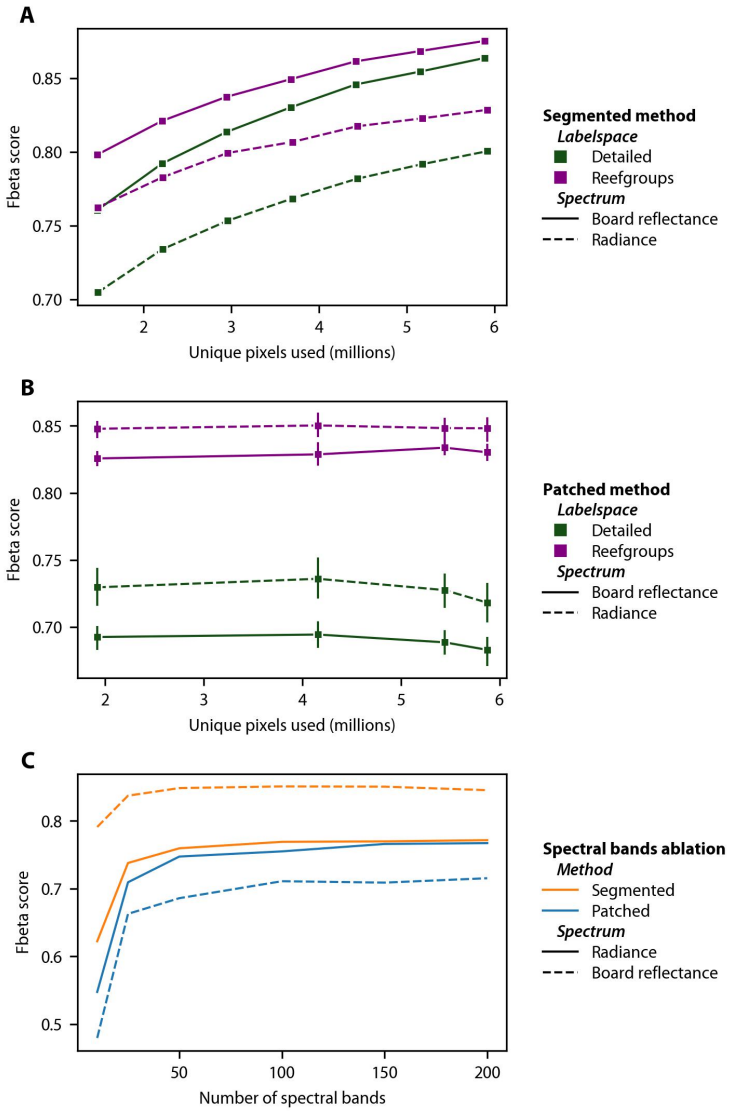

Figure 2.3 Effect of quantity and quality of spectral data on classifier performance. The effects of increasing the unique number of pixels in the data, but training the ML models with the same computational effort, were measured (Fbeta score) for both methods and labelspaces. The segmented method (A) showed improved performance whereas the patched method (B) showed little change in performance. Both methods performed better at predicting into the reefgroup labelspace (with 11 classes) than the detailed labelspace (with 43 classes) irrespective of the spectral signal type. (C) Both methods performed better when using an increasing number of (uniformly sampled) spectral bands for training, with limited improvement beyond 50 spectral bands.

are considered to be in agreement if 95% of the values lie within the standard deviation lines in the second plot.

To measure the compositional similarity between two classified maps we used the Bray–Curtis similarity (BCS) index defined as:

$$BCS = 1 - \frac{\sum_{i=1}^{R} |A_i - B_i|}{\sum_{i=1}^{R} |A_i + B_i|}$$

where A_i is the count of pixels of class i in map A and B_i is the count of pixels of class i in map B. R is the total number of classes in the labelspace. We used the "braycurtis" function from scipy python library (Virtanen et al. 2020). The closer the BCS value is to 1 the more similar the composition of the two compared communities.

We measured the similarity in the configuration of the communities between each reefgroups habitat map and their corresponding detailed-to-reefgroups map provided by each method, by calculating the Jaccard score for each reefgroups class. The Jaccard score (J) is defined as:

$$J_i = \frac{A_i \cap B_i}{A_i \cup B_i}$$

When the Jaccard score is 1, then the two maps are identical in configuration and when the score is 0 then the maps are entirely dissimilar. A high Jaccard score requires that across the habitat maps from both ML methods, both the identity and the location of the pixels are a match. Thus, it is a stringent measure of the similarity between two maps or sets.

2.3.5 Effort-vs-error of point-count sampling

We conducted simulations to estimate the error associated with a certain level of sampling effort in assessing the diversity and coverage of key groups through sparse point sampling of transects. For this simulated experiment, we selected 4 transects with Shannon diversity index from low to high ($H' = \{0.61, 1.26, 1.6, 2.64\}$). Each transect was divided into 50 non-overlapping quadrats of size 640 pixels × 406–705 pixels. Each of these quadrats was sparsely sampled with N = {5, 10, 20, 40, 80 ,160, 240, 320, 480, 640, 960} randomly selected points. For example, this means that when N = 5 points, 250 points (50 quadrats × 5 points) were randomly selected from the habitat map of the transect. The random sampling of the quadrats was conducted 250 times for each effort level. From each set of subsampled points in each transect, the coral coverage, sediment coverage and Shannon diversity index were calculated. For each metric, the relative deviation of the value obtained from the subsampled points from the value obtained from all the points in each transect was calculated. We selected 5% relative error as the limit for acceptable error, similar to a previous simulation study (Pante et al. 2012). The resulting error from changing

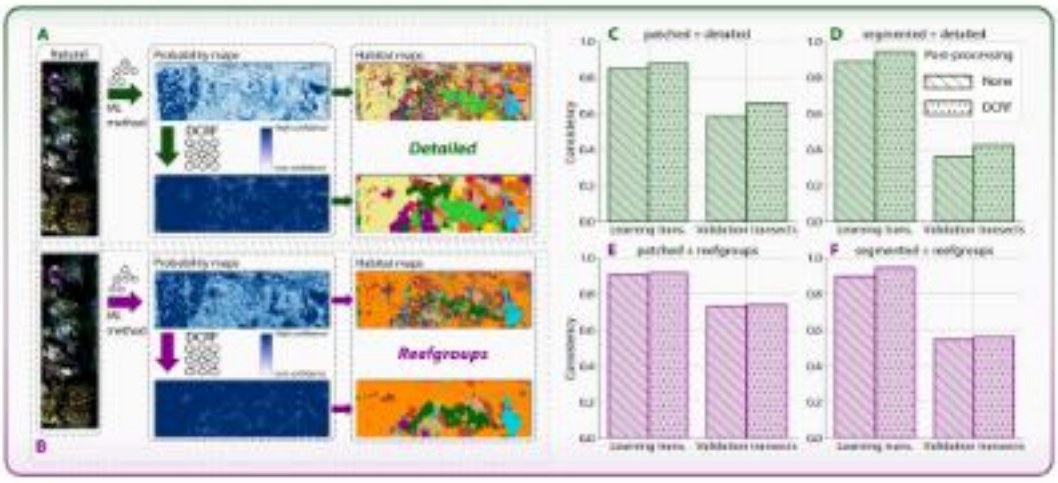

Figure 2.4 Smooth and consistent habitat mapping. The process of producing consistent habitat maps in the detailed (A) and reefgroups (B) labelspaces. Habitat maps produced from the classifiers' probability maps exhibit small-scale spatial noise and regions of low confidence. Smoothing the label probabilities with DCRF renders spatially cohesive maps. (See Figure A.3 for colour legend.) (C-F) The use of DCRF improved the map consistency in all cases. The patched method was better than the segmented method at generalization and was more accurate at mapping the validation transects, which were completely disjoint from the learning transects used for training the ML classifiers.

sampling effort was compared for each of the transects containing a significantly different species diversity and coverage distribution (Figure 2.7).

2.4 Results

2.4.1 Automated workflow for scalable benthic mapping

To measure the performance of the ML methods on the expert annotations several experiments with combinations of signal type and labelspace were executed (see Methods and Materials). For the detailed labelspace, the segmented+reflectance combination had the best predictive performance with an Fbeta score of 84.5% (Figure 2.2A; Table 2.1). The classifier had 80% to 96% recall for a majority of the 43 labels with sufficient data support (see diagonal of Figure 2.2A). Some labels with low data support showed excellent recall (*Aplysina archeri*, *Aiolochroia crassa*, *B. asbestinum* and *D. stokesii*), while others showed significant errors (*Zoanthid*, *L. variegata* and *Desmapsamma anchorata*). Despite having to distinguish between 43 labels, the segmented+reflectance classifier had a high Cohen's kappa coefficient indicating performance which is 83.5% of a perfect classifier (Figure 2.2A; Table 2.1). For the same labelspace,

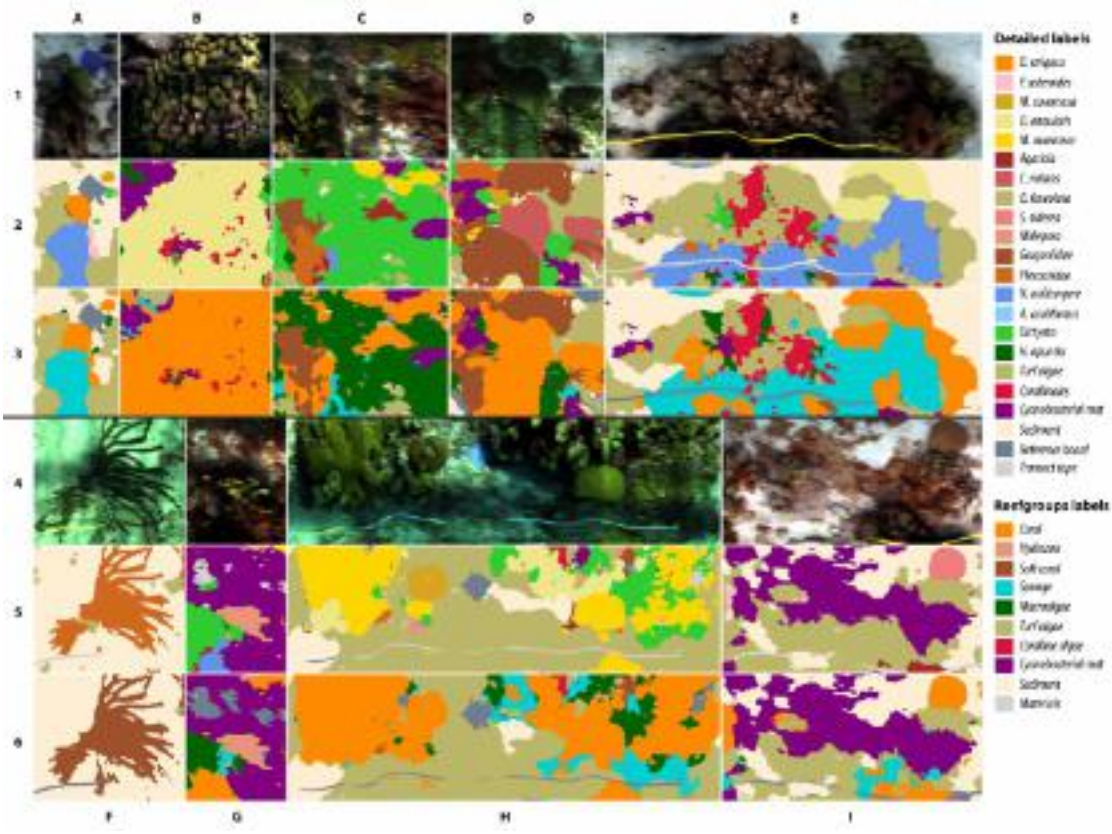

Figure 2.5 The rich structure of a digitized reef community. Sections of habitat maps produced with the patched ML method, with colours corresponding to classes from each labelspace (see legend and Figure A.3). Rows 1 and 4 are the natural view, as would be seen by a human observer. Rows 2 and 5 show the sections in the detailed labelspace and rows 3 and 6 in the reefgroups labelspace. Our proposed workflow accurately discerns among a large labelspace and delineates complicated shapes of reef biota. In image A:2 and A:3, the habitat maps show correctly classified and well delineated instances of three coral species (*D. strigosa*, *P. asteroides* and *M. cavernosa*), a sponge (*N. nolitangere*) as well as regions of *Sediment*, *Turf algae* and *Dictyota* macroalgae. The maps in F:5 and F:6 show another example of fine-grained segmentation of the branches of a specimen of the *Plexauridae* soft coral family. Comparing the maps in D:2 and D:3, or in H:5 and H:6, shows the number of different coral species that can be identified under the broad *Coral* group (in orange). Small encrusting taxa such as *Coralline algae* are visible in B:2 and E:2. The delineation of *Cyanobacterial mat* in G:2 and I:2, along with the many regions of *Sediment* and *Turf algae* represent substrate and microbial components of coral reef benthos.

the patched+radiance combination (Figure 2.2B; larger version in Figure A.4) performed with a 9% lesser Fbeta score (76.7%). Most classes had a recall value between 70% and 90%, with some rare classes, such as *A. cauliformis* and *B. asbestinum*, having significant errors.

For the reefgroups labelspace, the best predictive performance was 87.5% in the segmented+reflectance

combination (Figure 2.2C) followed closely by the patched+radiance combination with 86.9% (Figure 2.2D). The latter showed high recall values for all 11 classes, even reaching 96% correctness for the *Coral* class – which consists of 19 different coral genera and species (Figure A.3). The highest confusion occurred between *Turf algae* and *Sediment* classes. For both ML methods classifiers had a Cohen's kappa score of 83% towards a perfect classifier (Figure 2.2; Table 2.1). Overall, both ML methods showed Fbeta scores between 72% to 87% with better performances on the reefgroups labelspace than on the detailed labelspace (Figure 2.2; Figure A.4-Figure A.8; Table 2.1).

Both classifiers had different responses to the amount of unique input data seen during training. The classifier performance in the segmented method improved significantly with greater quantities of training data (Figure 2.3A). The greatest improvement was an Fbeta from 76% with 1.47 million pixels to 86% with 5.89 million pixels seen in the detailed labelspace using reflectance spectra. The performance also improved with greater quantities of radiance spectra, but overall the segmented method performed better on reflectance rather than radiance spectra. In contrast, the patched method showed no improvement with larger quantities of training data (Figure 2.3B). Instead, the performance in the detailed labelspace showed a 1% deterioration when the same computing effort was distributed over all the available data (5.93 million pixels). This seemingly unexpected result of poorer performance with more data can be understood by considering the lower number of training iterations over the larger dataset to maintain the same computing effort.

The impact of data quality, or spectral resolution, on predictive performance was assessed by using a subset of 10-100 spectral bands in the training data. In both the segmented and patched methods (Figure 2.3C), the predictive performance showed a strong 5% to 15% improvement when the number of spectral bands was increased from 10 to 25 with diminishing improvements when using 50+ spectral bands. Overall, the availability of greater spectral resolution, even when the bands were chosen without special consideration, had a large effect on the performance of the ML methods.

To produce habitat maps for further analysis, we selected one patched classifier that was trained on all 200 bands and with 62500 patches (4.1 million unique pixels) and one segmented classifier that was trained on all 200 bands and with 62332 segments (5.8 million unique pixels).

2.4.2 Smooth habitat maps to digitize reef community structure

The label probability map obtained directly from the classifier's prediction showed generally noisy spatial distribution, with many areas of low confidence (Figure 2.4). This effect of low and noisy confidence was larger in the detailed than the reefgroups labelspace. Processing the predicted probability map with DCRF produced a more uniform map of probabilities with high confidence except for the border pixels between adjacent targets (Figure 2.4C,E). The habitat maps from

the DCRF-processed probability maps better delineated the benthic scene with smooth and contiguous regions (Figure 2.4A-B).

Beyond the visual cohesiveness, the smoothed habitat maps were quantitatively more consistent than the raw habitat maps in all combinations of ML methods and labelspaces for transects (Figure 2.4C,F; Figure A.9A-B). The map consistency was measured as the average of the label accuracy in each of the annotation regions in all of the annotated transects, i.e. regions used for both training and testing the ML methods. The consistency of the habitat maps in the regions of the validation transects were lower than in the learning transects (Figure 2.4C-F): consistency for the segmented method dropped from 94% to 43% and from 95% to 56% with the detailed and reefgroups labelspaces (Figure 2.4D,F), respectively, and from 88% to 66% and from 92% to 74% for the patched method (Figure 2.4C,E). This indicated that the patched method (convolutional neural networks) was better than the segmented method (ensemble object classifiers) at generalizing to unseen data. Classification of transects with the reflectance signals resulted in a large drop of consistency, with a worst case change from 92% for the learning transects to 18% for the validation transects (Figure A.9). Overall, the best predictive performance on data from the validation transects, which was not used in any ML step, was from the patched method.

Smooth habitat maps in both labelspaces were produced for all 31 transects. With each transect approximately 50 m $\times$ 1 m in size, this task involved assigning each of the 500+ million spectral pixels to one of 43 labels (detailed) or one of 11 labels (reefgroups) independently. Montages of the habitat maps for all transects were visualized (Figure A.10-A.13). A selection of interesting sections of these habitat maps were visualized (Figure 2.5) with the natural view (rows 1 and 4), the detailed map (rows 2 and 5) and the reefgroups map (rows 3 and 6) shown together. Despite overall conformity, the habitat map sections also display some confusions: different sections of the same colony in C:2 are assigned to *Plexauridae* and *Gorgoniidae*, which are both soft coral families with similar digitate morphologies, while in C:3 this same colony is assigned between *Coral* and *Soft coral*. The incorrectly labelled regions of *Neofibularia nolitangere* sponge in E:2 (and *Sponge* in E:3) along the image edge are also errors. These errors likely occur due to the poorly illuminated shadow regions that received predictions with low confidence, and then got reassigned to the *Sponge* class by the DCRF process due to nearby high-confidence regions. Note however that this did not occur for the Transect tape in the shadow regions which was predicted with high confidence.

2.4.3 Assessing the community structure

A Bland-Altman analysis of the coral coverage (Figure 2.6A,B) and the Shannon diversity index (Figure 2.6C,D) from the reefgroups labelspace maps showed a high degree of correlation and low bias between the segmented and patched methods. The coverage of all other reefgroups classes, except for *Sponges*, derived from either mapping method, were comparable across the

range of values in all the transects (Figure A.14). The Bray-Curtis similarity, which compares the compositional structure between the communities in the maps of both methods, had a median value of 82% in the detailed and reefgroups labelspaces with a quartile range of 72%–89% and 75%–90%, respectively (Figure 2.6E). With the *Sediment* and *Turf algae* substrate classes merged together, the median value for the similarity rose to 89% for the detailed and reefgroups labelspaces, with a quartile range of 78%–92% and 79%–94%, respectively. This improvement in the similarity index indicates a large effect of the inherent definition problem of *Turf algae* on reef habitat mapping.

The similarity assessment across the learning transects for the patched method showed an 88% similarity median value with a quartile range of 84%–92%, while the segmented method showed an 87% median value with a quartile range of 77–91%. With the *Sediment* and *Turf algae* classes merged, the patched method showed a similarity median of 90% (quartile range 88%–97%), whereas the segmented method showed a barely improved median similarity of 88% (quartile range 77%–93%). Our proposed workflow recovered a reef community composition that was highly consistent between the taxonomic and broad reef group descriptions of the reef benthos.

The spatial configuration analysis between the detailed-to-reefgroups and reefgroups maps showed that three classes had higher configurational similarity for the patched method than for the segmented method: *Cyanobacterial mat* (64% vs. 40%), *Coral* (74% vs. 57%) and *Macroalgae* (51% vs. 29%) (Figure 2.6F). Two classes showed higher configurational similarity for the segmented method than the patched method: *Sediment* (83% vs. 78%) and *Turf algae* (72% vs. 67%). The Jaccard score was lower for both methods on rarer classes (Figure A.15).

2.4.4 Evaluating the effort-vs-error compromise in reef sampling

We exploited our dense and accurate habitat maps to revisit the effort-vs-error relationship of sparser reef sampling techniques (see Methods for point selection). The number of random point samples required to achieve a relative error lesser than 5% was assessed (Figure 2.7). To recover the hard coral coverage in transect T1 – which had low biodiversity ($H' = 0.6$) and low coral coverage (2.3%) – 960 random points per quadrat were required (Figure 2.7B,C). For the transect T4, with $H' = 2.6$ and coral coverage of 34.2%, 80 random points per quadrat were sufficient. Similarly, 960 points per quadrat were needed to recover the sediment coverage in transect T4, where sediment covers only 2% of the benthos (Figure 2.7D,E). In contrast, only 5 points per quadrat were required to capture the sediment coverage in transect T1, which has the highest sediment coverage (84.6%). The Shannon index was recovered with 10 sampling points per quadrat for transect T4 ($H' = 2.6$), with 40 points per quadrat for the transects T2 ($H' = 1.6$) and T3 ($H' = 1.3$), and with 160 points per quadrat for transect T1 ($H' = 0.6$) (Figure 2.7F,G). Overall, higher sampling effort was required to accurately recover the coverage of rare species or to capture the Shannon biodiversity index of scenes with low biotic coverage.

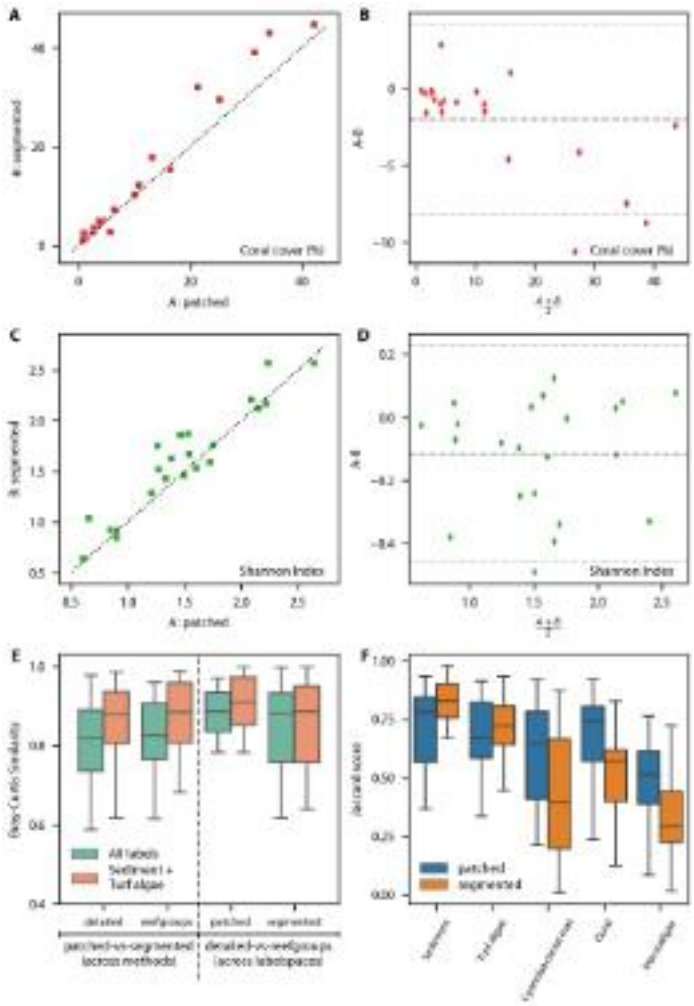

Figure 2.6 Assessing the benthic community structure from dense maps. (A) Coral cover of 22 learning transects was compared from the habitat maps for each ML method. The segmented method predicted slightly more coral cover than the patched method in the transects. (B) No clear bias was noted for either method in the Bland-Altman plot. (C) The Shannon index values for 22 compared transects were highly correlated between the maps from the segmented and patched methods. The segmented method produced habitat maps with slightly higher Shannon diversity. (D) No significant bias was found in either ML method for the Shannon index comparison. (E) The median Bray-Curtis similarity between the mapped communities was 80% across ML methods and 88% across labelspaces. Note that the orange bars refer to a labelspace where *Sediment* and *Turf algae* were combined into a single class, resulting in a higher compositional similarity. (F) Configurational similarity assessed using the Jaccard index between the reefgroups and detailed-to-reefgroups habitat maps for the top-five dominant labels are shown. Given the 500+ millions of pixels in this assessment, the maps showed very good consistency in configuration.

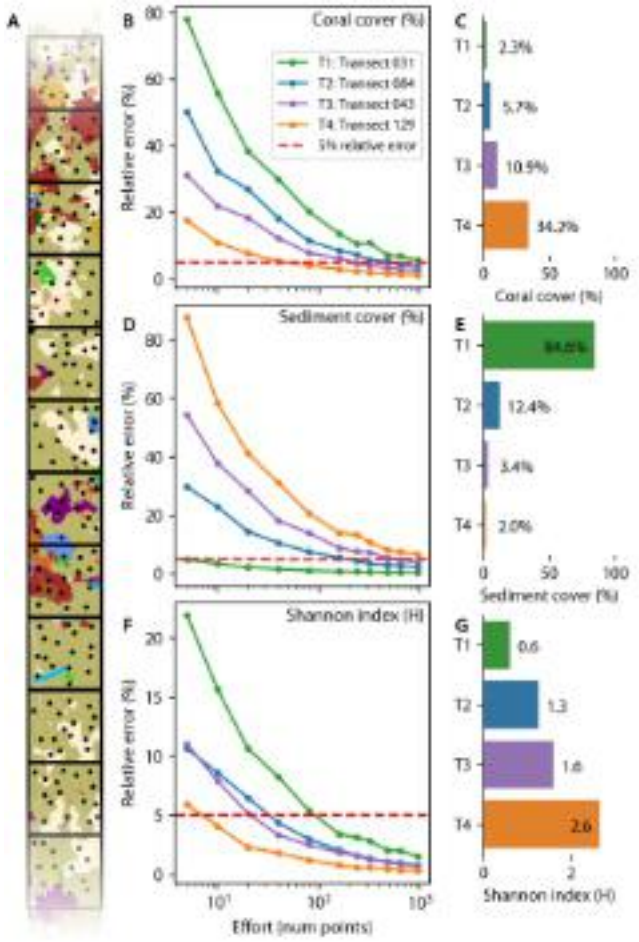

Figure 2.7 Effort-vs-error analysis for point-count sampling of reef community structure. (A) Schematic of the simulations of quadrat-wise random sparse sampling of dense habitat maps to estimate metrics (coverage or Shannon index) through point-count estimates of four transects with different biodiversity values (H = 0.61, 1.26, 1.6, 2.64). The error in the habitat metric from sparse random points relative to the metric of the full map was calculated from repeated trials. The number of point samples per quadrat required to achieve a relative error lesser than 5% (dashed red line) was assessed. (B, C) The transect with the least coral coverage (T1) required more than 960 points per quadrat to estimate it within the 5% error limit, whereas the transect with the highest coral coverage (T4) required 80 or less points per quadrat. (D, E) The transect with the least sediment coverage (T4) required more than 960 points per quadrat to estimate sediment coverage within the 5% error limit, whereas the transect with the highest sediment coverage (T1) required only 5 points per quadrat. (F, G) The least diverse transect (T1) required 160 points, compared to 40 points per quadrat for the more diverse transect (T4), to estimate the Shannon diversity index within the 5% error limit. These results suggest that rarer species require more sampling effort and that over 80 points per quadrat should be used to estimate habitat metrics in reef transects where the expected diversity or coverage is not previously known.

2.5 Discussion

2.5.1 Dense and detailed mapping of benthic communities

The presented reef mapping workflow was able to produce dense habitat maps with an unprecedented degree of thematic (43 labels) detail and high spatial (2.5 cm/pixel) resolution. The rich spectral detail in the HyperDiver data was leveraged by ML classifiers to produce highly accurate habitat maps (87% Fbeta) with little annotation effort (2% pixels in 20 hours). The two labelspaces used in the maps describe the reef benthic biodiversity down to genus and species level as well as abiotic and microbial components, such as sediment, turf algae and cyanobacterial mats. Our habitat maps provide a no-pixel-left-behind dense view of entire 50 m long transects, which allowed us to identify, localize and delineate the components of the surficial reef benthic community. Two ML methods with different complexities were used independently to produce dense and detailed habitat maps, thus facilitating objective comparison of reef descriptions at big data scale. Our workflow provides a deep description of community structure (diversity, coverage, composition and configuration), which demonstrated high convergence between both ML methods. Nonetheless, our detailed assessment indicates that deep learning classifiers (i.e. the patched method) are better at generalizing towards new and unseen datasets under comparable annotation and computational effort.

We designed the thematic detail in our workflow to target multiple user groups. Our workflow uses a detailed thematic scale in the form of 43 benthic categories that describe biotic and abiotic components of the reef habitat. Subsequently, a reefgroups labelspace, comprised of broad groups of reef biodiversity, was abstracted from the taxonomically detailed labelspace through interconnected ontologies, similar to hierarchical geomorphic zones developed previously (Kennedy et al. 2021). By independently mapping into the reefgroups labelspace we showed that the workflow consistently retrieved the composition and configuration of the reef transects across thematic resolutions (Figure 2.6E,F). This enables comparisons between our maps and previous/historical datasets which may have different thematic resolutions, as well as allowing for the workflow to 'translate' between the needs of different expert groups, such as reef ecologists or managers (Lecours et al. 2015; Roelfsema, Lyons, et al. 2021). We incorporated this thematic flexibility in our workflow, so that it can be reused in other benthic mapping scenarios (i.e., other coral reef sites, seagrass meadows, rocky reef sites).

2.5.2 Comparison of machine learning methods

To automate the digitization of reef communities and community structure, careful consideration of workflow parameters is recommended. In our workflow, we independently utilized two ML approaches: one based on object-based image analysis (i.e., segmented method) and the other on deep neural networks (i.e., patched method). Continual increase in complexity and specificity

of ML tasks for automation impedes a clear judgment of an ML method's ability to generalize (Paoletti et al. 2019). We tested two ML methods with different operational paradigms on a non-overlapping dataset to explore the trade-off in performance vs. complexity of automation. Both segmented and patched methods showed 80% ± 5% Fbeta scores in both labelspaces (Figure 2.2), the segmented approach performing better with reflectance data and the patched method with radiance data. We do not consider this to be generally indicative for future efforts, because both our ML models have no consideration of the optical physics between the two signal types. Another work targeting a similar sized labelspace (35 labels) achieves a mean pixel accuracy of 49.9% with a deep semantic segmentation network (DeepLabV3+) on sparse samples in 729 test images of coral reef orthomosaics (Alonso et al. 2019). Given only 2% of annotated pixels, our workflow mapped, with higher accuracy on 43 labels, underwater transects with high natural variability. We show that both ML methods can produce accurate mapping of reef transects, apparently due to the spectral detail (Figure 2.3C). Nonetheless, we found significant differences in the data requirements of both ML methods, and in their generalization abilities.

To determine the data requirements for the ML algorithms, we assessed the performance of both methods – under a constant computational effort – based on the number of unique pixels (in segments or patches) used for training (Figure 2.3A,B). The patched method needed less data to achieve its peak performance under the same amount of computing power and annotation effort. Despite the variable lighting conditions and methodological artefacts between training and validation transects , the patched method classified into both labelspaces more consistently (Figure 2.4C-F). Although classifier performance metrics on the training transects are better for the segmented method (Figure 2.2), the patched method was 23% better at classifying out-of-distribution data (i.e., validation transects) in the detailed labelspace and 18% better in the reefgroups labelspace than the segmented method (Figure 2.4C-D). Given that expert annotation is the biggest bottleneck for reef survey analysis (Beijbom et al. 2015; Roelfsema and Phinn 2013), the patched method, with its better generalization capability, provides better performance-per-human-effort compared to the segmented method.

2.5.3 How well do the habitat maps capture the community structure?

The smoothed habitat maps from our workflow show spatial and thematic detail of the structure of the coral reef benthic community (Figure 2.5). Benthic targets are clearly separated into meaningful regions, which represent different substrata, different organisms of various sizes. Small coral colonies and intricate shapes of branching corals, soft corals and sponges, and even transect tapes are correctly delineated and classified. Our workflow is able to accurately map bare sediment, turf algae and cyanobacterial mats achieving a previously missing capability in reef habitat mapping: dense mapping of the microbial components of reef substrata, while integrating them into a benthic community labelspace. This can be used to quantify changes in

abundance of cyanobacterial mats or turf algae, usually an indicator of reef deterioration (De Bakker et al. 2017).

The primary focus of our workflow development was to convert underwater spectral images into dense habitat maps. The target of our assessment was to go beyond comparing classifier-level metrics, and assess the final habitat maps for consistency and accuracy. We considered the goal of comparing the densely classified maps to photo-quadrats with point-count estimates (Rashid et al. 2020), but the large difference in sample sizes – 2000 quadrat points vs. millions of classified points – made the experiment statistically unsound. Given that 98% pixels (out of 500+ million) do not have reference label annotations and the complex spatial structure of the transects (Figure A.10-A.13), it is difficult to assess the maps accuracy on a pixel level. To overcome this limitation, we exploited the fact that the two ML methods produced the same type of output, but worked fully independent of each other in terms of method, input signal and parametrization. We compared the community structure of the dense maps in describing the same physical transect of the seafloor. To achieve this we used coverage, as well as composition and configuration metrics, which are key descriptors of community structure (Nowosad et al. 2019; Riitters 2019). We consider that if the statistical properties of the habitat maps from independent methods are similar, our workflow will have succeeded in representing the true composition and configuration of the coral reef transects captured by the underwater surveys.

The Bland-Altman analysis showed that the habitat maps agree on coverage and diversity metrics, except for some small discrepancies (Figure 2.6A,B; Figure A.14). These discrepancies are noticeable in coverage of corals, sponges and cyanobacterial mats which were overestimated by the segmented method in a few transects (Figure A.14 I-J). The demographic composition of the communities between pairs of dense habitat maps (considering all pixels) was highly similar as shown by the Bray-Curtis similarity index (Figure 2.6E). This shows that both ML methods independently ascribe similar classes and a similar number of those classes to the same transect. Furthermore, the assessment of the communities between the two labelspaces was also very similar (Figure 2.6E), providing confidence in the thematic flexibility of our workflow. We infer that automated mapping with ML methods of underwater hyperspectral transects can handle intra-class variability (detailed labelspace) as well as inter-group variability (reefgroups labelspace) with high accuracy.

Going beyond the composition, we also assessed the spatial configuration similarity of the benthic community in the transects described by both ML methods using the Jaccard index. The regions from the abstracted detailed-to-reefgroups maps and direct reefgroups maps yielded Jaccard scores over 60% for the dominant labels (Figure 2.6F). Given that these comparisons are across hundreds of millions of pixels and over 43 different labels, these results indicate high configurational similarity between the maps. Therefore, our workflow is able to correctly localize and delineate important targets in benthic habitat maps, despite the degree of thematic detail. Nonetheless, these assessments are inter-comparisons within our workflow and a correct assess-

ment of the configuration of the community structure would require dense manual annotations of the transects. The high degree of convergence in the community structure mapped independently by the two ML methods using two different hyperspectral signal types gives confidence in the ability of the workflow to produce accurate in-situ descriptions of coral reef habitats with high detail and analytical throughput.

2.5.4 The effect of sampling effort on community structure

There has been some debate about the amount of sampling effort necessary to accurately measure reef community structure. In benthic surveys with photo-quadrats, the 'adequate' number of samples (points-per-quadrat or quadrat-per-area) to accurately describe the community has been a topic of debate (Dumas et al. 2009; Pante et al. 2012; Perkins et al. 2016). The goal is to find a good balance between expert effort (labelling the sampling units in images) and reliability in the derived scene description. At the reef area scale, the number of quadrats per area (i.e, sampling density) is an important determinant of the precision of coverage estimations (Lechene et al. 2019; Perkins et al. 2016). At the quadrat scale, various studies have used different numbers of points per quadrat (from 5 to 99) within indeterminate quadrat distributions, and hence, a similar analysis at the point scale is valuable. Simulations of sampling synthetic habitat maps, based on normal distribution of class abundances, to recover the coral and sponge coverage estimates with less than 5% relative error, revealed that the optimal number of points per quadrat ranged between 13 points for a heterogeneous area with high coral coverage and over 600 points for a very homogeneous region with low coral coverage (Pante et al. 2012). The recommended number of points per quadrat was 80 for transects of unknown community structure, but generally depended on the true underlying diversity and dispersion of the community configuration.

We contribute to the debate with a reef-scale analysis based on empirical community structure derived from our benthic habitat maps (Figure 2.7). We simulated quadrat sampling with various degrees of sampling effort, and found that higher densities of sampling points reduced the estimation error, similar to the results at the quadrat scale (Lechene et al. 2019). The number of point per quadrat to accurately recover the coverage of rare classes exceeded the recommended values in the literature. Even with 1000 sampling points per quadrat, rare classes at the transect level could not be detected within the 5% relative error limit (Figure 2.7B,D). In contrast to the coverage of individual classes, the Shannon diversity index was captured within 5% relative error with 160 sampling points per quadrat (Figure 2.7E). We demonstrate that the rarity and skewness of occurrence significantly impacts the error associated with a constant sampling effort. Ultimately, the precision of survey estimations is determined by the tension between distribution and density of sampling units, whether points or quadrats. When dense mapping at new sites is not possible and logistics constrain the number of quadrats , we recommend to sample over 160 points per quadrat during generation of baseline data, as well as to communicate the uncertainty

generated from the sampling design (Eric J. Hochberg et al. 2021).

2.5.5 Limitations and outlook

Although the results of our workflow are encouraging enough to recommend the different methods applied in this work, some limitations are noteworthy. For example, the nature of the images gathered by the push-broom hyperspectral camera (without georeferencing) meant that the resulting transects are not ideal for photogrammetric techniques. This hinders the generation of 3D models and orthomosaics, which provide a more comprehensive view of reef sites and facilitate temporal studies through georeferencing. Recent studies are investigating novel techniques to overcome this limitation of hyperspectral push-broom sensors and have succeeded in producing rectified orthomosaics of hyperspectral transects (Jurado et al. 2021; Moroni et al. 2012). Similarly, new robotic platforms, survey methods and data sources are being developed to improve benthic habitat mapping. We believe that the future direction of reef mapping is to develop end-to-end workflows that can handle mapping at the reefscape scale, with thematic and technical flexibility. Our workflow lays the groundwork for such end-to-end frameworks, where spectrally rich data flows are leveraged for mapping coral reefs.

It is also important to note, that the ML methods presented in this study are tailored for hyperspectral data and would not produce similarly high performance on RGB images. Another limitation of our ML methods is that they show low classification confidence in darkened areas (i.e., shadows). Thus, caution is advised when measuring small changes in temporal studies or reporting size of benthic organisms. A simple solution would be to group such problematic regions in a "Shadow" class of the labelspace. It must also be mentioned, that deep neural networks require high computational power to train and predict on hyperspectral data within reasonable time frames.

Regardless of the imaging techniques and ML methods used in reef surveys, we consider it important to evaluate the dense habitat maps (and not the classifiers) in terms of accuracy and completeness, as the measure of progress. To disentangle the effects of changes in ML methods and data, we urge that the original images and annotations be made publicly available so that they can be re-evaluated independently. We have made the complete datasets (Chennu, Rashid, et al. 2020; Schürholz et al. 2022a) and source code available to reproduce the results presented in this work (Schürholz et al. 2022b).

Even though our workflow produces dense habitat maps with species level resolution in several reef groups, it is not a replacement for biodiversity assessments, where every species is recorded. New ML paradigms might be necessary to resolve the taxonomical hierarchy within reef organisms. Habitat descriptions that are derived from purely surficial surveys neglect cryptic biota, which can account for as much as half of the reef community and are hence critical to biodiversity assessments (Kornder et al. 2021). Further development of interdisciplinary efforts intersecting

ML, computer vision, robotics, environmental DNA analysis and reef ecology will be required to automate survey outputs that directly enable biodiversity assessments and detailed reef inventories.

2.6 Conclusions

Our proposed workflow showcases a way to generate dense habitat maps of coral reefs with flexible thematic detail. This thematic and spatial detail in the maps enables fine-grained analyses of coral reef functions and community dynamics by coral reef ecologists. We seek to contribute to unifying the perspective of ecologists, environmental managers, remote sensing and ML communities involved in the study of coral reefs. Particularly for ecologists and managers, our approach provides a consistent habitat description with adaptive thematic detail. Between remote sensing and machine learning experts, it offers a perspective on bridging the 'measurement gap' between ML classifiers and the ultimate data products, i.e. habitat maps. The consistency achieved by our mapping workflow, and the patched method in particular, is related to the richness in spectral detail and the spatial acuity of our proximal sensing vantage point of underwater surveys (Chennu, Färber, et al. 2017; Rashid et al. 2020). When certain limitations are overcome and with improvements in cost and performance of underwater spectral surveying technology, it will become feasible to integrate it as a standard in-situ reef monitoring technique. The widespread use of underwater spectral surveying and automated benthic habitat mapping promises to provide the best validation data for aerial Earth observation efforts to map coral reefs globally. The integration of thematic detail into global habitat mapping promises to enable novel analyses of pattern and scale in coral reef ecology.

2.7 Acknowledgements

We would like to thank Carsten John and Oliver Artmann at the Max Planck Institute for Marine Microbiology for their IT support. This project has received funding from the European Union's Horizon 2020 research and innovation programme under the Marie Sklodowska-Curie grant agreement number 813360 "4D-REEF".

2.8 Author contributions

Daniel Schürholz – Methodology, Software, Validation, Formal analysis, Investigation, Data curation, Writing – Original Draft, Writing – Review & Editing, Visualization, Project adminis-

tration.

Arjun Chennu – Conceptualization, Methodology, Software, Validation, Formal analysis, Investigation, Data curation, Writing – Original Draft, Writing – Review & Editing, Visualization, Supervision, Project administration, Funding acquisition.

References

Alonso, Iñigo, Matan Yuval, Gal Eyal, Tali Treibitz, and Ana C. Murillo (2019). "CoralSeg: Learning coral segmentation from sparse annotations". In: *Journal of Field Robotics* 36.8, pp. 1456–1477. DOI: *https://doi.org/10.1002/rob.21915*.

Althaus, Franziska, Nicole Hill, Renata Ferrari, Luke Edwards, Rachel Przeslawski, Christine H. L. Schönberg, Rick Stuart-Smith, Neville Barrett, Graham Edgar, Jamie Colquhoun, Maggie Tran, Alan Jordan, Tony Rees, and Karen Gowlett-Holmes (2015). "A Standardised Vocabulary for Identifying Benthic Biota and Substrata from Underwater Imagery: The CATAMI Classification Scheme". In: *PLOS ONE* 10.10, e0141039. DOI: *10.1371/journal.pone.0141039*.

Armstrong, Roy A., Oscar Pizarro, and Christopher Roman (2019). "Underwater Robotic Technology for Imaging Mesophotic Coral Ecosystems". In: *Mesophotic Coral Ecosystems*. Ed. by Yossi Loya, Kimberly A. Puglise, and Tom C.L. Bridge. Coral Reefs of the World. Cham: Springer International Publishing, pp. 973–988. DOI: *10.1007/978-3-319-92735-0_51*.

B. Lyons, Mitchell, Chris M. Roelfsema, Emma V. Kennedy, Eva M. Kovacs, Rodney Borrego-Acevedo, Kathryn Markey, Meredith Roe, Doddy M. Yuwono, Daniel L. Harris, Stuart R. Phinn, Gregory P. Asner, Jiwei Li, David E. Knapp, Nicholas S. Fabina, Kirk Larsen, Dimosthenis Traganos, and Nicholas J. Murray (2020). "Mapping the world's coral reefs using a global multiscale earth observation framework". In: *Remote Sensing in Ecology and Conservation*. Ed. by Nathalie Pettorelli and Vincent Lecours, rse2.157. DOI: *10.1002/rse2.157*.

Beijbom, Oscar, Peter J. Edmunds, Chris Roelfsema, Jennifer Smith, David I. Kline, Benjamin P. Neal, Matthew J. Dunlap, Vincent Moriarty, Tung-Yung Fan, Chih-Jui Tan, Stephen Chan, Tali Treibitz, Anthony Gamst, B. Greg Mitchell, and David Kriegman (2015). "Towards Automated Annotation of Benthic Survey Images: Variability of Human Experts and Operational Modes of Automation". In: *PLOS ONE* 10.7, e0130312. DOI: *10.1371/journal.pone.0130312*.

Brito-Millán, Marlene, Mark J. A. Vermeij, Esmeralda A. Alcantar, and Stuart A. Sandin (2019). "Coral reef assessments based on cover alone mask active dynamics of coral communities". In: *Marine Ecology Progress Series* 630, pp. 55–68. URL: *https://www.jstor.org/stable/26920540* (visited on 12/10/2023).

Burke, Lauretta and Jon Maidens {and} contributing authors: Mark Spalding (2004). *Reefs at Risk in the Caribbean*. URL: *https://www.wri.org/research/reefs-risk-caribbean* (visited on 07/27/2022).

Casella, Elisa, Antoine Collin, Daniel Harris, Sebastian Ferse, Sonia Bejarano, Valeriano Parravicini, James L. Hench, and Alessio Rovere (2017). "Mapping coral reefs using consumer-grade drones and structure from motion photogrammetry techniques". In: *Coral Reefs* 36.1, pp. 269–275. DOI: *10.1007/s00338-016-1522-0*.

Cesar, H.S.J., L. Burke, and L. Pet-Soede (2003). *The Economics of Worldwide Coral Reef Degradation*. Cesar Environmental Economics Consulting (CEEC). URL: *https://books.google.de/books?id=WicVAQAAIAAJ*.

Chennu, Arjun, Paul Färber, Glenn De'ath, Dirk de Beer, and Katharina E. Fabricius (2017). "A diver-operated hyperspectral imaging and topographic surveying system for automated mapping of benthic habitats". In: *Scientific Reports* 7.1, pp. 1–12. DOI: *10.1038/s41598-017-07337-y*.

Chennu, Arjun, Ahmad Rafiuddin Rashid, Joost den Haan, and Dirk de Beer (2020). *Taxonomically annotated underwater hyperspectral and color images of coral reef transects from Curaçao*. DOI: *10.1594/PANGAEA.911300*.

De Bakker, Didier M., Fleur C. Van Duyl, Rolf P. M. Bak, Maggy M. Nugues, Gerard Nieuwland, and Erik H. Meesters (2017). "40 Years of benthic community change on the Caribbean reefs of Curaçao and Bonaire: the rise of slimy cyanobacterial mats". In: *Coral Reefs* 36.2, pp. 355–367. DOI: *10.1007/s00338-016-1534-9*.

Dumas, Pascal, Arnaud Bertaud, Christophe Peignon, Marc Leopold, and Pelletier Dominique (2009). "A "quick and clean"photographic method for the description of coral reef habitats". In: *Journal of Experimental Biology and Ecology* 368, pp. 161–168. DOI: *10.1016/j.jembe.2008.10.002*.

Foo, Shawna A. and Gregory P. Asner (2019). "Scaling Up Coral Reef Restoration Using Remote Sensing Technology". In: *Frontiers in Marine Science* 6.79. URL: *https://www.frontiersin.org/article/10.3389/fmars.2019.00079* (visited on 03/01/2022).

Foody, Giles M. (2004). "Thematic Map Comparison". In: *Photogrammetric Engineering & Remote Sensing* 70.5, pp. 627–633. DOI: *10.14358/PERS.70.5.627*.

González-Rivero, Manuel, Oscar Beijbom, Alberto Rodriguez-Ramirez, Dominic E. P. Bryant, Anjani Ganase, Yeray Gonzalez-Marrero, Ana Herrera-Reveles, Emma V. Kennedy, Catherine J. S. Kim, Sebastian Lopez-Marcano, Kathryn Markey, Benjamin P. Neal, Kate Osborne, Catalina Reyes-Nivia, Eugenia M. Sampayo, Kristin Stolberg, Abbie Taylor, Julie Vercelloni, Mathew Wyatt, and Ove Hoegh-Guldberg (2020). "Monitoring of Coral Reefs Using Artificial Intelligence: A Feasible and Cost-Effective Approach". In: *Remote Sensing* 12.3, p. 489. DOI: *10.3390/rs12030489*.

Guisan, Antoine, Reid Tingley, John B. Baumgartner, Ilona Naujokaitis-Lewis, Patricia R. Sutcliffe, Ayesha I. T. Tulloch, Tracey J. Regan, Lluis Brotons, Eve McDonald-Madden, Chrystal Mantyka-Pringle, Tara G. Martin, Jonathan R. Rhodes, Ramona Maggini, Samantha A. Setterfield, Jane Elith, Mark W. Schwartz, Brendan A. Wintle, Olivier Broennimann, Mike Austin, Simon Ferrier, Michael R. Kearney, Hugh P. Possingham, and Yvonne M. Buckley

(2013). "Predicting species distributions for conservation decisions". In: *Ecology Letters* 16.12, pp. 1424–1435. DOI: *10.1111/ele.12189*.

Hedley, John D., Chris M. Roelfsema, Iliana Chollett, Alastair R. Harborne, Scott F. Heron, Scarla Weeks, William J. Skirving, Alan E. Strong, C. Mark Eakin, Tyler R. L. Christensen, Victor Ticzon, Sonia Bejarano, and Peter J. Mumby (2016). "Remote Sensing of Coral Reefs for Monitoring and Management: A Review". In: *Remote Sensing* 8.2, p. 118. DOI: *10.3390/rs8020118*.

Heron, Scott F., Lyza Johnston, Gang Liu, Erick F. Geiger, Jeffrey A. Maynard, Jacqueline L. De La Cour, Steven Johnson, Ryan Okano, David Benavente, Timothy F. R. Burgess, John Iguel, Denise I. Perez, William J. Skirving, Alan E. Strong, Kyle Tirak, and C. Mark Eakin (2016). "Validation of Reef-Scale Thermal Stress Satellite Products for Coral Bleaching Monitoring". In: *Remote Sensing* 8.1, p. 59. DOI: *10.3390/rs8010059*.

Hochberg, Eric J, Marlin J Atkinson, and Serge Andréfouët (2003). "Spectral reflectance of coral reef bottom-types worldwide and implications for coral reef remote sensing". In: *Remote Sensing of Environment* 85.2, pp. 159–173. DOI: *10.1016/S0034-4257(02)00201-8*.

Hochberg, Eric J. and Michelle M. Gierach (2021). "Missing the Reef for the Corals: Unexpected Trends Between Coral Reef Condition and the Environment at the Ecosystem Scale". In: *Frontiers in Marine Science* 8, p. 1191. DOI: *10.3389/fmars.2021.727038*.

Hoegh-Guldberg, Ove, Elvira S. Poloczanska, William Skirving, and Sophie Dove (2017). "Coral Reef Ecosystems under Climate Change and Ocean Acidification". In: *Frontiers in Marine Science* 4. URL: *https://www.frontiersin.org/article/10.3389/fmars.2017.00158* (visited on 03/01/2022).

Hughes, Terence P and Jason E Tanner (2021). "Recruitment Failure, Life Histories, and Long-Term Decline of Caribbean Corals". In: p. 15.

Jurado, Juan M., Luís Pádua, Jonas Hruška, Francisco R. Feito, and Joaquim J. Sousa (2021). "An Efficient Method for Generating UAV-Based Hyperspectral Mosaics Using Push-Broom Sensors". In: *IEEE Journal of Selected Topics in Applied Earth Observations and Remote Sensing* 14, pp. 6515–6531. DOI: *10.1109/JSTARS.2021.3088945*.

Kennedy, Emma V., Chris M. Roelfsema, Mitchell B. Lyons, Eva M. Kovacs, Rodney Borrego-Acevedo, Meredith Roe, Stuart R. Phinn, Kirk Larsen, Nicholas J. Murray, Doddy Yuwono, Jeremy Wolff, and Paul Tudman (2021). "Reef Cover, a coral reef classification for global habitat mapping from remote sensing". In: *Scientific Data* 8.1, p. 196. DOI: *10.1038/s41597-021-00958-z*.

Kornder, Niklas A., Jose Cappelletto, Benjamin Mueller, Margaretha J. L. Zalm, Stephanie J. Martinez, Mark J. A. Vermeij, Jef Huisman, and Jasper M. de Goeij (2021). "Implications of 2D versus 3D surveys to measure the abundance and composition of benthic coral reef communities". In: *Coral Reefs* 40.4, pp. 1137–1153. DOI: *10.1007/s00338-021-02118-6*.

Krähenbühl, Philipp and Vladlen Koltun (2011). "Efficient inference in fully connected CRFs with Gaussian edge potentials". In: *Proceedings of the 24th International Conference on Neural*

Information Processing Systems. NeurIPS. NIPS'11. Red Hook, NY, USA: Curran Associates Inc., pp. 109–117. (Visited on 03/22/2022).

Lechene, Marine Anna Alice, Anna Julia Haberstroh, Maria Byrne, Will Figueira, and Renata Ferrari (2019). "Optimising Sampling Strategies in Coral Reefs Using Large-Area Mosaics". In: *Remote Sensing* 11.24, p. 2907. DOI: *10.3390/rs11242907*.

Lecours, Vincent (2017). "On the Use of Maps and Models in Conservation and Resource Management (Warning: Results May Vary)". In: *Frontiers in Marine Science* 4, p. 288. DOI: *10.3389/fmars.2017.00288*.

Lecours, Vincent, Rodolphe Devillers, David C. Schneider, Vanessa L. Lucieer, Craig J. Brown, and Evan N. Edinger (2015). "Spatial scale and geographic context in benthic habitat mapping: review and future directions". In: *Marine Ecology Progress Series* 535, pp. 259–284. DOI: *10.3354/meps11378*.

Moberg, Fredrik and Carl Folke (1999). "Ecological goods and services of coral reef ecosystems". In: *Ecological Economics* 29.2, pp. 215–233. DOI: *10.1016/S0921-8009(99)00009-9*.

Mölder, Felix, Kim Philipp Jablonski, Brice Letcher, Michael B. Hall, Christopher H. Tomkins-Tinch, Vanessa Sochat, Jan Forster, Soohyun Lee, Sven O. Twardziok, Alexander Kanitz, Andreas Wilm, Manuel Holtgrewe, Sven Rahmann, Sven Nahnsen, and Johannes Köster (2021). *Sustainable data analysis with Snakemake*. 10:33. F1000Research. DOI: *10.12688/f1000research.29032.2*.

Moroni, Monica, Carlo Dacquino, and Antonio Cenedese (2012). "Mosaicing of Hyperspectral Images: The Application of a Spectrograph Imaging Device". In: *Sensors (Basel, Switzerland)* 12.8, pp. 10228–10247. DOI: *10.3390/s120810228*.

Muldrow, Milton, Edward C. M. Parsons, and Robert Jonas (2020). "Shifting baseline syndrome among coral reef scientists". In: *Humanities and Social Sciences Communications* 7.1, pp. 1–8. DOI: *10.1057/s41599-020-0526-0*.

Muller-Karger, Frank E., Erin Hestir, Christiana Ade, Kevin Turpie, Dar A. Roberts, David Siegel, Robert J. Miller, David Humm, Noam Izenberg, Mary Keller, Frank Morgan, Robert Frouin, Arnold G. Dekker, Royal Gardner, James Goodman, Blake Schaeffer, Bryan A. Franz, Nima Pahlevan, Antonio G. Mannino, Javier A. Concha, Steven G. Ackleson, Kyle C. Cavanaugh, Anastasia Romanou, Maria Tzortziou, Emmanuel S. Boss, Ryan Pavlick, Anthony Freeman, Cecile S. Rousseaux, John Dunne, Matthew C. Long, Eduardo Klein, Galen A. McKinley, Joachim Goes, Ricardo Letelier, Maria Kavanaugh, Mitchell Roffer, Astrid Bracher, Kevin R. Arrigo, Heidi Dierssen, Xiaodong Zhang, Frank W. Davis, Ben Best, Robert Guralnick, John Moisan, Heidi M. Sosik, Raphael Kudela, Colleen B. Mouw, Andrew H. Barnard, Sherry Palacios, Collin Roesler, Evangelia G. Drakou, Ward Appeltans, and Walter Jetz (2018). "Satellite sensor requirements for monitoring essential biodiversity variables of coastal ecosystems". In: *Ecological Applications* 28.3, pp. 749–760. DOI: *10.1002/eap.1682*.

Nowosad, Jakub and Tomasz F. Stepinski (2019). "Information theory as a consistent framework for quantification and classification of landscape patterns". In: *Landscape Ecology* 34.9, pp. 2091–2101. DOI: *10.1007/s10980-019-00830-x*.

Pante, Eric and Phillip Dustan (2012). "Getting to the Point: Accuracy of Point Count in Monitoring Ecosystem Change". In: *Journal of Marine Biology* 2012, e802875. DOI: *10.1155/2012/802875*.

Paoletti, M. E., J. M. Haut, J. Plaza, and A. Plaza (2019). "Deep learning classifiers for hyperspectral imaging: A review". In: *ISPRS Journal of Photogrammetry and Remote Sensing* 158, pp. 279–317. DOI: *10.1016/j.isprsjprs.2019.09.006*.

Pavoni, Gaia, Massimiliano Corsini, Marco Callieri, Giuseppe Fiameni, Clinton Edwards, and Paolo Cignoni (2020). "On Improving the Training of Models for the Semantic Segmentation of Benthic Communities from Orthographic Imagery". In: *Remote Sensing* 12.18, p. 3106. DOI: *10.3390/rs12183106*.

Perkins, Nicholas R., Scott D. Foster, Nicole A. Hill, and Neville S. Barrett (2016). "Image subsampling and point scoring approaches for large-scale marine benthic monitoring programs". In: *Estuarine, Coastal and Shelf Science* 176, pp. 36–46. DOI: *10.1016/j.ecss.2016.04.005*.

Phinn, Stuart R., Chris M. Roelfsema, and Peter J. Mumby (2012). "Multi-scale, object-based image analysis for mapping geomorphic and ecological zones on coral reefs". In: *International Journal of Remote Sensing* 33.12, pp. 3768–3797. DOI: *10.1080/01431161.2011.633122*.

Rashid, Ahmad Rafiuddin and Arjun Chennu (2020). "A Trillion Coral Reef Colors: Deeply Annotated Underwater Hyperspectral Images for Automated Classification and Habitat Mapping". In: *Data* 5.1, p. 19. DOI: *10.3390/data5010019*.

Reverter, Miriam, Stephanie B. Helber, Sven Rohde, Jasper M. de Goeij, and Peter J. Schupp (2022). "Coral reef benthic community changes in the Anthropocene: Biogeographic heterogeneity, overlooked configurations, and methodology". In: *Global Change Biology* 28.6, pp. 1956–1971. DOI: *10.1111/gcb.16034*.

Riitters, Kurt (2019). "Pattern metrics for a transdisciplinary landscape ecology". In: *Landscape Ecology* 34.9, pp. 2057–2063. DOI: *10.1007/s10980-018-0755-4*.

Roelfsema, Chris M., Eva M. Kovacs, Juan Carlos Ortiz, David P. Callaghan, Karlo Hock, Mathieu Mongin, Kasper Johansen, Peter J. Mumby, Magnus Wettle, Mike Ronan, Petra Lundgren, Emma V. Kennedy, and Stuart R. Phinn (2020). "Habitat maps to enhance monitoring and management of the Great Barrier Reef". In: *Coral Reefs* 39.4, pp. 1039–1054. DOI: *10.1007/s00338-020-01929-3*.

Roelfsema, Chris M., Mitchell Lyons, Nicholas Murray, Eva M. Kovacs, Emma Kennedy, Kathryn Markey, Rodney Borrego-Acevedo, Alexandra Ordoñez Alvarez, Chantel Say, Paul Tudman, Meredith Roe, Jeremy Wolff, Dimosthenis Traganos, Gregory P. Asner, Brianna Bambic, Brian Free, Helen E. Fox, Zoe Lieb, and Stuart R. Phinn (2021). "Workflow for the Generation of Expert-Derived Training and Validation Data: A View to Global Scale Habitat Mapping". In:

Frontiers in Marine Science 8. URL: *https://www.frontiersin.org/article/10.3389/fmars.2021.643381* (visited on 03/01/2022).

Roelfsema, Chris M. and Stuart R. Phinn (2013). "Validation". In: *Coral Reef Remote Sensing: A Guide for Mapping, Monitoring and Management*. Ed. by James A. Goodman, Samuel J. Purkis, and Stuart R. Phinn. Dordrecht: Springer Netherlands, pp. 375–401. DOI: *10.1007/978-90-481-9292-2_14*.

Schürholz, Daniel and Arjun Chennu (2022a). *Dense and taxonomically detailed habitat maps of coral reef benthos machine-generated from underwater hyperspectral transects in Curaçao*. DOI: *10.1594/PANGAEA.946315*.

– (2022b). *Digitizing the coral reef: a complete workflow for dense taxonomic mapping of benthic habitats with machine learning of underwater hyperspectral images*. DOI: *10.5281/zenodo.7185108*.

Virtanen, Pauli, Ralf Gommers, Travis E. Oliphant, Matt Haberland, Tyler Reddy, David Cournapeau, Evgeni Burovski, Pearu Peterson, Warren Weckesser, Jonathan Bright, Stéfan J. van der Walt, Matthew Brett, Joshua Wilson, K. Jarrod Millman, Nikolay Mayorov, Andrew R. J. Nelson, Eric Jones, Robert Kern, Eric Larson, C J Carey, İlhan Polat, Yu Feng, Eric W. Moore, Jake VanderPlas, Denis Laxalde, Josef Perktold, Robert Cimrman, Ian Henriksen, E. A. Quintero, Charles R. Harris, Anne M. Archibald, Antônio H. Ribeiro, Fabian Pedregosa, Paul van Mulbregt, and SciPy 1.0 Contributors (2020). "SciPy 1.0: Fundamental Algorithms for Scientific Computing in Python". In: *Nature Methods* 17, pp. 261–272. DOI: *10.1038/s41592-019-0686-2*.

Zhong, Zilong, Jonathan Li, Zhiming Luo, and Michael Chapman (2018). "Spectral–Spatial Residual Network for Hyperspectral Image Classification: A 3-D Deep Learning Framework". In: *IEEE Transactions on Geoscience and Remote Sensing* 56.2, pp. 847–858. DOI: *10.1109/TGRS.2017.2755542*.

Chapter 3

Curaçao reefs under the hyperspectral lens: detailed mapping reveals reefscape patterns of community composition and environmental drivers

Daniel Schürholz [1,2] *and Arjun Chennu* [2]

Manuscript status

In preparation for submission to *eLife journal*.

[1]Max Planck Institute for Marine Microbiology, 28359 Bremen, Germany
[2]Leibniz Centre for Tropical Marine Research (ZMT), 28359 Bremen, Germany

3.1 Abstract

The current accelerated improvement of artificial intelligence (AI) algorithms provides a new tool to significantly reduce the costs of coral reef monitoring, whilst also allowing for improvements in the detail of the thematic, spatial and temporal scales. In this study we use AI to provide an island-wide description of coral reef benthic communities along the leeward coast of the Caribbean island of Curaçao. We apply a machine learning workflow that uses hyperspectral transects, acquired in 2016 with the HyperDiver method, to produce densely-classified thematically-detailed community maps covering approximately 74 *ha* of reefs (over 2.2 billion samples) and 20 *ha* (over 600 million samples) after filtering by prediction confidence. Furthermore, paired with depth readings for each sample, we provide a detailed community distribution analysis across the depth-gradient down to 18 meters. With our densely sampled maps, we provide evidence that deriving community diversity indices from sparse sampling and abstracted thematic labels can mask the true diversity of the coral reef, as well as lose information about intra-class dynamics. Combining dense community sampling with an environmental statistical analysis, we explore the possible drivers of the community compositions along the coastline of the island. The reef communities in sites situated towards the southern tip of the island show higher cover and diversity of corals, possibly driven by being farther away from coastal infrastructure, trash and sewage pollution. Sites in the northern most tip, despite being similarly distant to these stressors, showed a deteriorated state, with higher abundance of macroalgae and sponges, and a lack of reef-building corals. Reefs in the center of the island, closer to the capital city Willemstad were most deteriorated, dominated by cyanobacterial mats, turf algae and large stretches of bare sediment, and reduced diversity in corals.

3.2 Introduction

Tropical coral reefs have undergone significant degradation in recent decades, caused by direct and indirect stressors (Erftemeijer et al. 2012; Fabricius 2005; Hughes et al. 2003; Wilkinson 1999). As stressors become more acute, coral reef communities shift towards more degraded states, becoming dominated by algae and bacteria, at the cost of reef-building organisms such as scleractinian corals (De Bakker, Van Duyl, et al. 2017; Heery et al. 2018; Knowlton et al. 2008). The loss of structurally complex corals causes significant degradation or cessation of the services that reefs provide for other sessile and many motile organisms (e.g., fish hideouts, fish nurseries), as well as services that they provide for coastal human populations (e.g., wave breakers, fishing grounds) (Moberg et al. 1999; Pratchett et al. 2014). Surveying and monitoring the state and trajectories of coral reefs is paramount to set concrete baselines and implement effective management plans (Camacho et al. 2020; Muldrow et al. 2020; Sandin, Smith, et al. 2008).

Caribbean reefs have been specially affected by the expansion of the human population and industrial expansions in the region. It is estimated that mean scleractinian coral cover between 0 – 20 m depth has decreased by up to 80% on many reefs, from 35% areal cover in the 1970s to only 15% in 2014 (Gardner et al. 2003; Jackson et al. 2015). In the same time span, the benthic real estate vacated by corals was initially taken over by fleshy macroalgae and their abundance rose by 7% to 23% (Jackson et al. 2015), in what is known as the coral-macroalgae phase shift. However, in more recent studies it was demonstrated that the eventual benefactor of the vacated benthic space are bacterial mats and bacteria-algae symbiotic communities, such as turf algae (Brocke et al. 2015; De Bakker, Van Duyl, et al. 2017; Ford et al. 2018; Paerl et al. 2012).

In the islands of the Leeward Antilles located in the southern Caribbean Sea, this trend has been convincingly demonstrated based on a compendium of detailed studies of reef communities spanning over 40 years (Bak 1977; Bak and Luckhurst 1980; Bak, Nieuwland, et al. 2005; De Bakker, Van Duyl, et al. 2017; Van Duyl 1985). Based on reef monitoring data spanning from 1973 to 2013 it is shown that coral reefs in 3 locations of Curaçao and one location in Bonaire experience rise and decline of turf algae, followed by a rapid expansion of cyanobacterial mats covering up to 22.2% of their 10-40 m deep quadrats in 2013 (from 0.1% in 1973). Macroalgal cover and sponge cover also increased from 1973 to 2013, although far less: from 0% to 2% and from 0.5% to 2.3% cover, respectively. In contrast, scleractinian corals showed a loss of up to 71% from 1973 to 2013. While this represents the most detailed temporal study of the island's reefs, it was spatially constrained to a small section of the Curaçaoan leeward coastline, with the 3 studied locations in Curaçao clustered very close to CARMABI Research Station (see Figure 3.1). The proximity of this study site to Willemstad (capital of Curçao and only major city on the island) does not capture the variety of reef environments and communities to be found on the rest of the island's coast.

In the Waitt Institute's report titled "The State of Curaçao's Coral Reefs" (WAITTS-Institute 2017), the authors present the percentage cover of the most dominant functional groups along the island. Similarly, a 2015 study (Sandin, Alcantar, et al. 2022) of benthic assemblages along the island found more scleractinian coral cover on the south side, with small pockets of high cover of hard coral in the center and north of the coastline. Although the spatial extent of the studies is quite large (148 sites for (WAITTS-Institute 2017) and 122 for (Sandin, Alcantar, et al. 2022)), the sampling density within each site is low. Following the Global Coral Reef Monitoring Network (GCRMN) guidelines for benthic cover surveys, both studies (WAITTS-Institute 2017) and (Sandin, Alcantar, et al. 2022) recorded 25 random points within each of the 15 photo-quadrats (0.9 m × 0.6 m) acquired along 5 line transects of 30 meters length for each site, calculating percentage covers from only 1875 sampled points per site with an area of 300 m^2 each. The thematic resolution of the studies were broad benthic groups, such as hard coral, macroalgae, sponges, Crustose Coralline Algae (CCA), turf algae, cyanobacteria, soft corals, etc.

Sparse spatial sampling, coupled with broad thematic labelsets, can lead to the occlusion of rare

species and the masking of intra-group dynamics (Brito-Millán et al. 2019; Hochberg et al. 2021; Pante et al. 2012; Schürholz et al. 2023). Scleractinian corals, for example, are composed by many genera and species in the Caribbean (*Corals of the World* 2016). If only overall coral cover is reported, the actual diversity (or lack thereof) within this benthic group is obscured. A detailed study with the same photoquadrat data as in (De Bakker, Van Duyl, et al. 2017) focused on the scleractinian coral community changes, from 1973 to 2014, adding one site in the south of the island as comparison (De Bakker, Meesters, et al. 2016). They show that hard coral communities between 10 – 20 m became dominated by the massive frame-building *Orbicella spp.*, the opportunistic digitate *Madracis spp.* and the submassive/encrusting *Stephanocoenia michelini* species, whereas the communities down to 40 m shifted towards encrusting/foliose *Agaricia spp.*. Branching corals, such as *Acropora spp.*, critical for maintaining the 3D complexity of reefs, have lost the most benthic coverage and can only be found in the shallower parts (≤ 8 meters) of more protected reefs in the south of Curaçao (WAITTS-Institute 2017). Not many studies exist that cover several reefs across the leeward side of Curaçao and study its community with thematic detail.

The distribution of benthic groups and coral genera/species along the island is affected by environmental conditions and (physical and anthropogenic) stressors (Sandin, Alcantar, et al. 2022; WAITTS-Institute 2017). The human population in the Caribbean increased from 27 million in 1973 to approximately 43 million in 2016, while Curaçao's population also increased by 9.4% from 154,000 to 170,000 in the same time period (United Nations et al. 2015). The consequences of the population expansion and industrial development are more polluted water run-offs, over-fishing and coastal building encroachments, which pressure the biotic communities of coral reefs(Heery et al. 2018). It is also believed that the abundance of *Acroporid* species has dramatically reduced due to the presence of increased human settlements since the 1950s (Cramer et al. 2020). Curaçao receives a high influx of tourists through cruises and airline passengers, totaling over a million visitors in 2016 alone (*Curaçao Tourist Board - Annual Report* 2016). This increased the amount trash, waste water efflux and diving activities near coral reefs. Further negative impacts to reef health can come from physical factors driven by global climate change, such as more frequent hurricanes, increasing sea water temperature and levels (Crabbe 2008). As a consequence, several coral bleaching events have been recorded within the last 30 years in Caribbean reefs (Alemu et al. 2014; R. Aronson et al. 2002; Bries et al. 2004; Donner et al. 2017; Eakin et al. 2010; Muñiz-Castillo et al. 2019), as well as rapid spread of Band Diseases which has greatly reduced the cover of *Acropora spp.* from the late seventies to the mid-eighties (R. B. Aronson et al. 2001; Gladfelter 1982).

The influence of environmental factors on the Curaçaoan reefs has to be further investigated in relation to detailed accounting of their communities. Dense habitat maps with thematic and spatial detail of large stretches of coral reefs provide the opportunity to implement in-depth analyses of community composition and configuration (Nowosad et al. 2019; Riitters 2019; Riitters and

Vogt 2023; Schürholz et al. 2023). In this study we present a detailed analysis of the states of the coral reef benthic communities in 8 sites along the leeward coast of Curaçao. Expanding on machine learning of underwater hyperspectral images captured in 2016 (Schürholz et al. 2023), we created dense and detailed habitat maps derived from high-resolution (cm-scale) sampling of large areas of the reef floor. The benthic maps have thematic detail of up to 39 taxonomic and 3 substrate classes, with 19 scleractinian coral species/genera mapped separately. With this information we aim at (1) determining the spatial (latitudinal and depth-wise) distribution of benthic groups along the island, (2) similarly determining the distribution of coral species along the island coast, (3) connect the groups' distribution to previously reported information and (4) correlate the distribution information to environmental (physical and anthropogenic) factors along the island, taken from (WAITTS-Institute 2017). Through our analysis and data presentation, we provide an independent measure the coral communities in Curaçao and an insightful complement to previous studies of these reef communities.

3.3 Materials and Methods

3.3.1 Study site

Between the 4th and 26th of August of 2016, underwater hyperspectral image transects were captured using the HyperDiver device in 8 sites along the coast of Curaçao Island in the Dutch Caribbean (Chennu et al. 2017; Rashid et al. 2020) (see Figure 3.2 & Figure 3.1 and Table 3.1). In total, 147 transects were captured and processed Table 3.1.

Table 3.1 Study sites locations and characteristics of acquired transect data.

	Number of transects	Number of samples[1]	Latitude	Longitude	Island zones[2]	Depth range (m)
Playa Kalki	20	60,666,270	12.375344°N	69.158931°W	7	3.6 – 16.2
Habitat	22	75,742,973	12.197850°N	69.079558°W	6	4.2 – 14.1
Kokomo	20	118,301,180	12.160331°N	69.005403°W	5	5.3 – 10.9
Carmabi	22	120,961,636	12.122331°N	68.969234°W	4	3 – 14
Water Factory	10	52,838,930	12.109989°N	68.956258°W	4	4.8 – 11.2
Marie Pampoen	18	79,908,190	12.091894°N	68.907918°W	4	5.3 – 12.8
Sea Aquarium	15	59,273,382	12.083234°N	68.895114°W	3,4	4.1 – 11.7
East Point	20	72,022,092	12.042249°N	68.745104°W	2	4 – 12

[1] *Number of samples* is the number of pixels in all transects in a site after the reliability filtering process.

[2] *Island zones* taken from (WAITTS-Institute 2017).

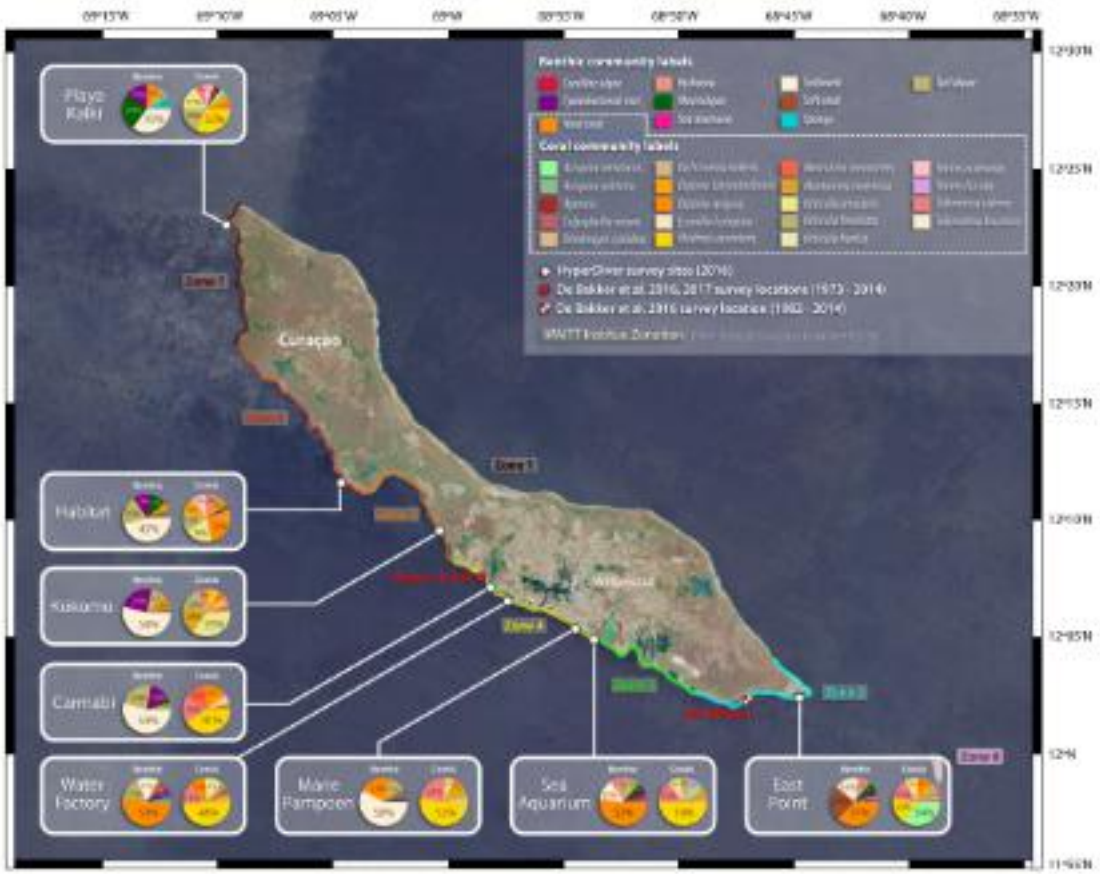

Figure 3.1 Benthic *reefgroups* and coral community abundances across our 8 survey sites. The four southernmost sites have a high cover of *Coral* (scleractinian corals). From the Carmabi site northwards larger areas of *Cyanobacterial mat* and *Turf algae* are found. Playa Kalki,in the far north, presents the highest abundance of *Macroalgae* and *Sponge*. The coral communities of Playa Kalki, Carmabi, Water Factory, Marie Pampoen and Sea Aquarium are dominated by *Madracis auretenra*. *Orbicella annularis*, *Orbicella faveolata*, *Siderastrea siderea* and *Montastrea cavernosa* show high abundances in all sites. East Point in the south, shows the only Acroporid dominated community, with 34% *Acropora cervicornis*. Coastline zones are taken from (WAITTS-Institute 2017). Study sites described in (De Bakker, Meesters, et al. 2016; De Bakker, Van Duyl, et al. 2017) shown with red squares.

3.3.1.1 Environmental factors

The 8 study sites were selected to represent different states of environmental gradients on Curaçao's coastline. The report "The State of Curaçao's Coral Reefs" (WAITTS-Institute 2017) provided a detailed zonation of the island in terms of the type and level of different stressors (Table 3.2). The island is divided into 8 zones, and our sites are situated within zones 2-7 on the leeward side of Curaçao main island. The windward side (zone 8) was not surveyed, because it is

exposed to strong winds and currents. The smaller "Klein Curaçao" island – zone 1 – was out of scope for the survey's purpose. The southern end of the island (zone 2) is the most isolated area, given its distance to urban settlements and road inaccessibility. The central region (zones 3-5) of the island are the most affected by human activities from nearby coastal settlements, such as farming, sewage and coast-infrastructure development, producing elevated sedimentation and eutrophication. The northern part of the island (zones 6, 7) receives the most tourists, and thus is affected by anthropogenic stressors: such as diving tourism, trash agglomeration and sewage run-offs.

Table 3.2 Environmental variables, taken from The State of Curaçao's Coral Reefs report by the Waitt Institute (WAITTS-Institute 2017).

	Anthropogenic factors					*Fish Biomass*		
	Sewage	Pollu-tion	Infra-struc-ture	Diving use	Fishing use	Total	Herbi-vorous	Carni-vorous
Playa Kalki	Low	Very high	Very low	Very high	Very high	Very low	Very low	Low
Habitat	Very low	High	Very low	Below average	Below average	Very low	Very low	Very low
Kokomo	Low	Very high	Low	Low	Below average	Very high	Very high	Very high
Carmabi	Very high	High	Very high	Above average	Very low	Above average	Above average	High
Water Factory	Very high	High	Very high	Above average	Very low	Above average	Above average	High
Marie Pampoen	Very high	High	Very high	Above average	Very low	Above average	Above average	High
Sea Aquarium	Below average	Above average	Below average	Very high	Below average	Very high	High	Very high
East Point	Low	Very low	Very low	Low	Very low	Very high	Below average	Above average

In Figure 3.1 we also show the study locations from de Bakker et al 2016 (De Bakker, Meesters, et al. 2016) & de Bakker et al (De Bakker, Van Duyl, et al. 2017). These studies provided a thorough temporal analysis of the community shifts of dominant benthic classes and coral communities from 1973 until 2014, respectively. Three of their sites (Buoy I, II, & III) are located close to our *Carmabi* site in zone 4, while the site Awa Blancu (AB) is located closer to our *East Point* site in zone 2. Their analysis spans 4 depth zones – 10, 20, 30 & 40 meters – while our transects were captured in a depth between 3 to 16 meters.

3.3.2 Detailed thematic benthic habitat maps

The captured hyperspectral transects were used as input to an AI workflow to create spatially and thematically detailed benthic community maps (Figure 3.2).

3.3.2.1 Spectral-spatial deep learning of hyperspectral transects

In total 147 benthic maps were predicted, each 640 pixels wide and with lengths from 6,090 to 40,720 pixels, with a mean of 24,352 pixels. Each of the approximately 2.X Billion pixels was classified to one of 48 classes (see Figure 3.3). In total, 4224 polygons were manually annotated across all transects to one of the 48 labels. This subset containing 35 million pixels was used to train an AI workflow with multiple spectral-spatial residual neural networks (SSRNs) at its core (Zhong et al. 2018). We modified the workflow presented in Schürholz and Chennu 2023 (Schürholz et al. 2023) to include 5 ensemble SSRN networks. Ensemble networks have been shown to improve the prediction accuracy of AI workflows by introducing voting mechanisms that remove the biases of single networks (Ganaie et al. 2022; Wyatt et al. 2022). The networks predicted the softmax probabilities for each label in each pixel. Biotic elements on the benthos were predicted to the highest taxonomic detail possible (one out of 39 possible classes) following the World Registry of Marine Species (WORMS) database (Marine Species 2023). Substrates were classified to one of three classes (*Turf algae*, *Cyanobacterial mat* or *Sediment*) following the Collaborative and Automated Tools for Analysis of Marine Imagery (CATAMI) standard (Althaus et al. 2015); coral rubble was initially classified independently as a substrate, but later merged in to the *Turf algae* class (Schürholz et al. 2023). The remaining 6 classes were 5 survey materials (transect *tape*, transect *reel*, reference board – *refboard*, floating marker – *float* and other *material*) introduced in the scenes and appearing on the spectral transects plus one class called *Shadow* for regions too dark to distinguish the true cover. These last classes were masked out for community analyses.

We tested the AI workflow's performance through an experiment, in which a subset of approximately 105,000 annotated pixels were separated as a testing set, and then predicted with the ensemble networks trained on another subset of 293,427 annotated pixels. The overall prediction accuracy was of 90.8%, with 43 out of the 48 classes being predicted with over 80% recall (Figure 3.4). Only the sponge genus *Hyrtios* was completely confused with the sponge species *Neofibularia nolitangere* and the sponge species *Aplysina cauliformis* was confused with the *Aplysina archeri* species, but since they were rare species, this error was neglected. The result of the AI workflow were 147 predicted habitat maps with each pixel labeled by class.

The AI workflow was implemented using the PyTorch machine learning Python package (Paszke et al. 2019), Sci-kit Learn package (Pedregosa et al. 2011) and the Snakemake workflow management tool (Mölder et al. 2021).

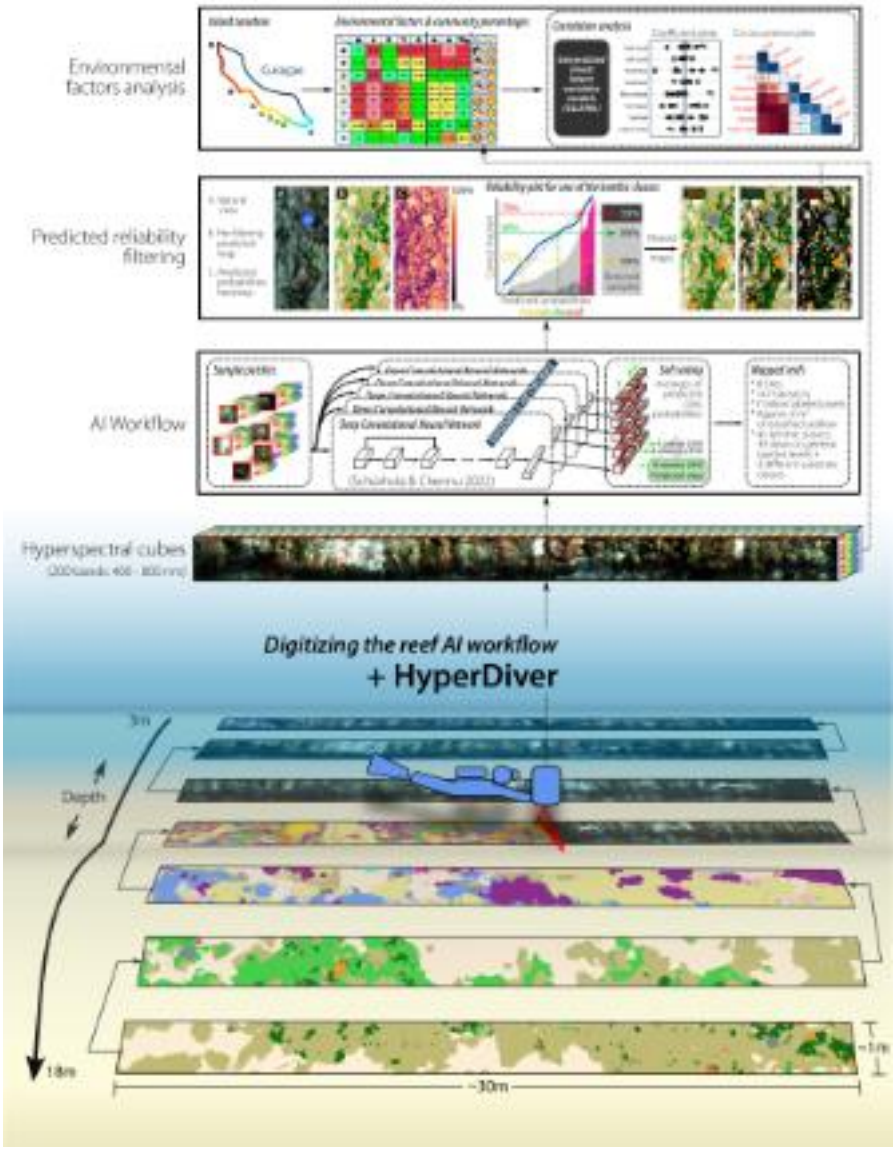

Figure 3.2 Schematic of the methodology. The reefs in each site were surveyed using the HyperDiver methodology. The acquired hyperspectral transects with 200 spectral bands (evenly spaced between 400 and 800nm) were used as input to an ensemble deep neural network AI workflow. The resulting habitat maps had every pixel assigned to one of 48 labels, with 42 reef community biotic and substrate classes. We further filtered the predictions through a reliability analysis for each label. Around 25% of pixels (640 Million) were retained across 147 transects approximately covering approximately 20 hectares of seafloor. The class abundance number were used as input to a Generalized Linear Latent Variable Model (GLLVM) and correlated to environmental variables taken from WAITTS-Institute 2017.

Figure 3.3 Labelsets used in this study. The *Detailed* labelset (A) lists all classes that were annotated on the hyperspectral transects and predicted by the trained AI workflow. The *Reefgroups* labelset (B) presents broader benthic groups into which the detailed labels were abstracted. Colors are consistent throughout all figures in this study. Shapes inside the rectangles map the detailed labels to their abstracted reefgroups class.

3.3.2.2 Per-class reliability filtering of predicted maps

Deep neural networks have greater generalization capabilities than other machine learning techniques, when applied to habitat mapping (Schürholz et al. 2023). Similar to Mills et al. 2023 Mills et al. 2023, we assessed the uncertainty in the prediction accuracy of the out-of-distribution (not used in the training process) pixels, because only 1.5% of pixels out of the 2.3 billion in the dataset were used to train the networks. After a detailed visual inspection some errors were found, and to avoid counting these in the final community descriptions we performed a network-confidence-driven pixel filtering (Figure 3.2).

Due to the large number of pixels in the dataset, we inspected the frequency distribution of the probabilities with which each class was predicted in the annotated pixels and compared it to the empirical correctness of the predictions. From this distribution, we calculated a threshold probability for each class to retain a parameterized "correct fraction" of all pixels. We tested with correct fraction values of 5% up to 95% with increments of 5%, and found that the threshold value that retained the best visual consistency was 75% for 40 out of the 42 classes. Only for the *Orbicella annularis* and *Porites asteroides* fraction values of 60% and 50% were selected, respectively (see all reliability plots in Figure B.1). We also calculated the abstracted reliability plots for the reefgroups labelset, by selecting the label with the highest predicted probability within each dominant benthic class (Figure 3.5).

After applying the filtering to the 147 habitat maps, we retained 639,714,653 pixels, which we

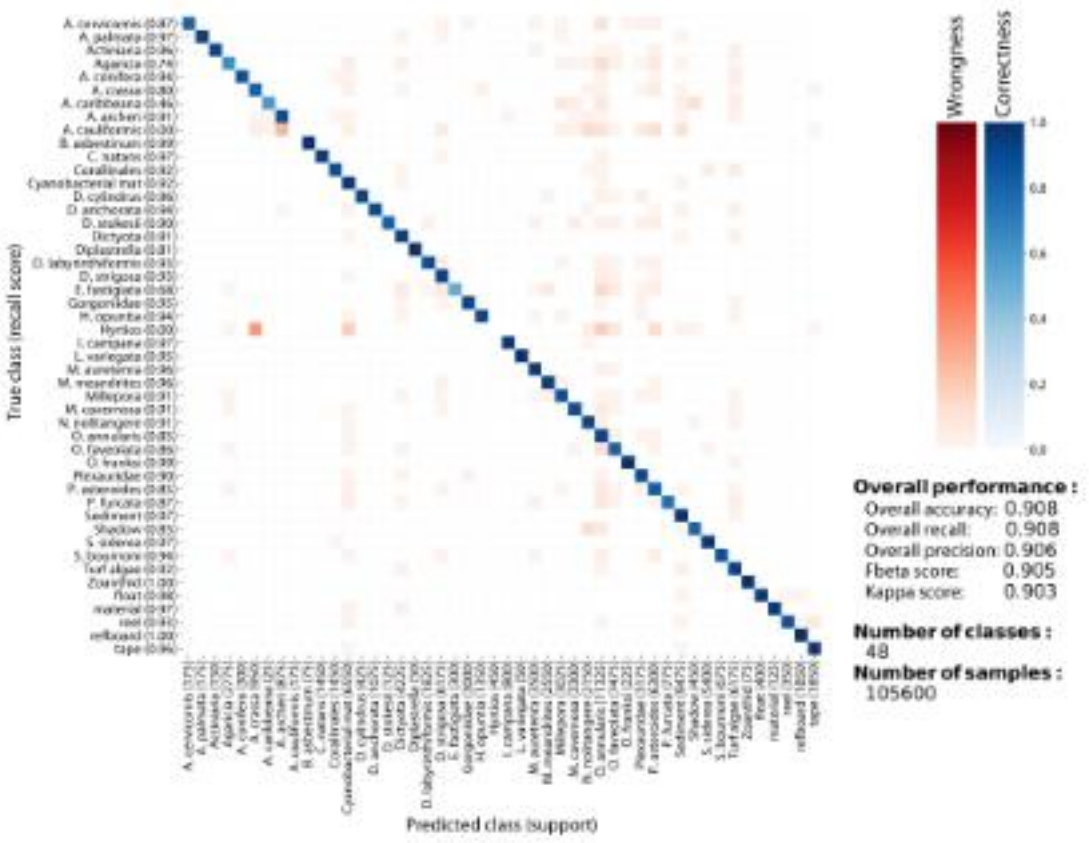

Figure 3.4 Recall confusion matrix for the *detailed* labelspace. The AI workflow classified the 48 classes with 90.8% accuracy, 90.8% recall and 90.6% precision on the out-of-distribution assessment set (with 105,600 samples). 43 classes were predicted with over 80% recall. 16 out of 19 coral species/genera were classified with over 80% recall. The other three classes were confused with *Orbicella annularis* a very abundant species in the reefs. Only *Aplysina cauliformis* and *Hyrtios* had 0% recall, likely due to its similarities with other sponge classes and their low number of available training samples.

call samples hereafter. The per-site distribution of final filtered samples are in Table 3.1. We utilized these filtered samples for all further statistical analyses in the study. All analysis were carried out in one of three labelsets (Figure 3.3). The "*detailed*" labelset contains the 42 low-level classes. Each label in this labelset was then abstracted to higher-level benthic groups, in what we called the "*reefgroups*" labelset. The subset of scleractinian coral genera and species formed the "*coral community*" labelset.

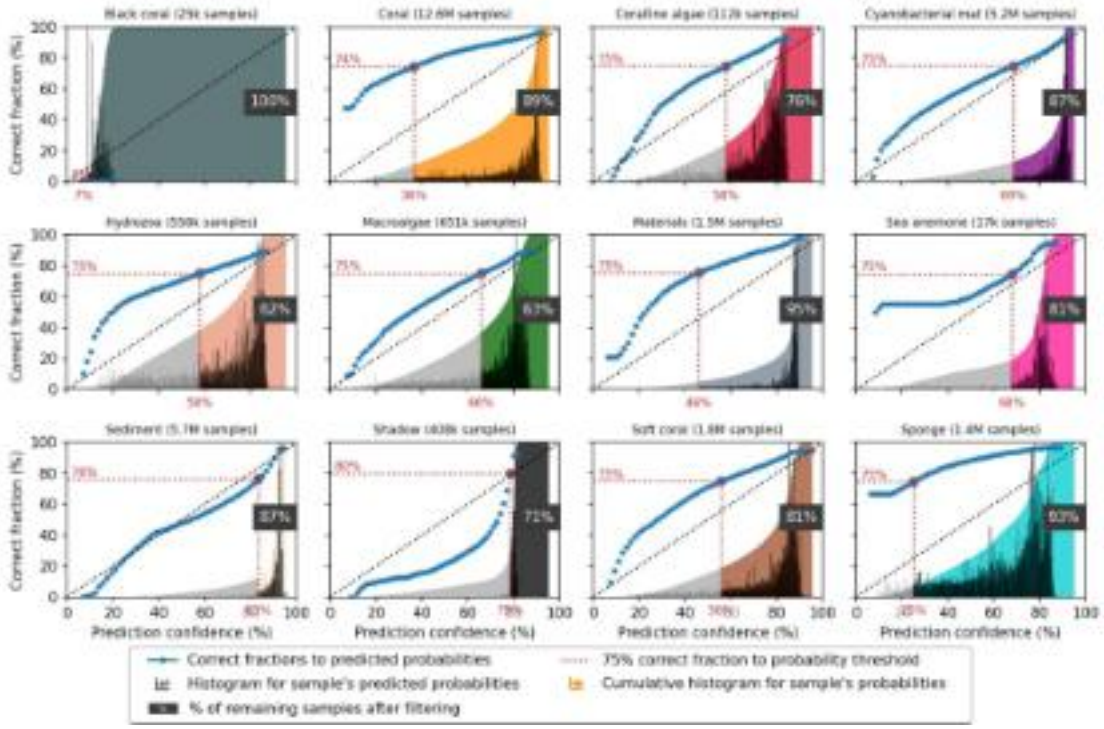

Figure 3.5 Sample filtering for reliability of predictions based on predicted probabilities. For each *reefgroups* class, we inspected the number of correct predictions that would remain after a certain probability threshold is applied. We settled on a 75% correct fraction value, then selected the corresponding probability threshold for each class and only retained all samples that were predicted with a probability that was higher than the threshold. This improved the confidence on the selected samples considerably, while providing a per-class expectation of correctness in the predictions.

3.3.3 Benthic community analysis

We calculated cover percentages for each label in the detailed, reefgroups and coral community separately, by dividing the number of pixels of each class by the total number of pixels in each site. We also provide a statistical multivariate analysis, in which nMDS was used as a tool to display benthic communities differences between sites. The nMDS analysis was implemented with the "R" programming language and the "Vegan" package, using a Bray-Curtis distance as a metric (Oksanen et al. 2022). We also plotted the pair-wise Bray-Curtis distance matrix for the 8 sites separately (Figure 3.8-3.10).

3.3.3.1 Diversity indices

To compare the diversity between sites we calculated 4 indices (Table 3.3). We calculated the Shannon diversity index (H), the Simpson diversity index (D), Gini-Simpson index (GS) and

Table 3.3 Diversity indices for all 3 labelsets over all sites.

	Reefgroups Diversity Indices				
	S	*H*	*D*	*GS*	*equitability*
Playa Kalki	10	2.42	0.23	0.77	0.44
Habitat	10	2.25	0.28	0.72	0.36
Kokomo	11	1.83	0.37	0.63	0.25
Carmabi	10	1.78	0.37	0.30	0.27
Water Factory	10	2.03	0.34	0.66	0.30
Marie Pampoen	11	1.75	0.40	0.60	0.23
Sea Aquarium	10	2.24	0.31	0.69	0.32
East Point	10	2.45	0.23	0.77	0.43
	Coral Community Diversity Indices				
	S	*H*	*D*	*GS*	*equitability*
Playa Kalki	16	2.93	0.18	0.82	0.35
Habitat	16	3.12	0.14	0.86	0.46
Kokomo	18	2.83	0.20	0.80	0.28
Carmabi	18	2.55	0.24	0.76	0.23
Water Factory	18	2.39	0.28	0.72	0.20
Marie Pampoen	18	2.13	0.34	0.66	0.16
Sea Aquarium	19	2.52	0.29	0.71	0.18
East Point	19	2.93	0.19	0.81	0.28
	Detailed Diversity Indices				
	S	*H*	*D*	*GS*	*equitability*
Playa Kalki	34	2.85	0.22	0.78	0.13
Habitat	33	2.71	0.23	0.77	0.13
Kokomo	37	2.36	0.33	0.67	0.08
Carmabi	37	1.96	0.38	0.62	0.07
Water Factory	34	3.28	0.15	0.85	0.19
Marie Pampoen	36	3.09	0.18	0.82	0.16
Sea Aquarium	36	3.48	0.14	0.86	0.19
East Point	35	3.77	0.10	0.90	0.30

S = Species number, H = Shannon index, D = Simpson index, GS = Gini-Simpson index, *equitability* = Simpson's evenness.

the Simpson's Eveness index (*equitability*):

$$H = -\sum_{i=1}^{S} p_i \log p_i$$

$$D = \sum_{i=1}^{S} p_i^2$$

$$GS = 1 - D$$

$$equitability = \frac{\frac{1}{D}}{S} = \frac{1}{D \times S}$$

Where S is species richness, p_i is the relative abundance of species i and log is the natural logarithm. The diversity indices were calculated using the scikit-bio Python package (Rideout et al. 2023).

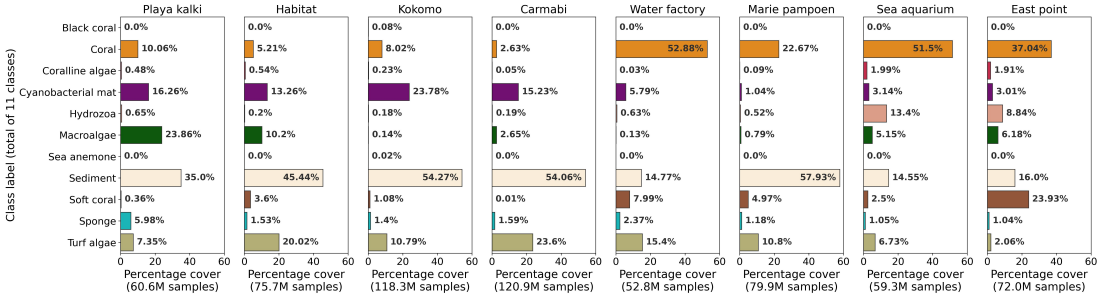

Figure 3.6 Dominant *reefgroups* coverage. East Point, Sea Aquarium, Marie Pampoen and Water Factory show a higher concentration of scleractinian corals. East Point had the most amount of *Soft coral* coverage and together with Sea Aquarium also present the highest cover of Hydrozoans. Water Factory, Carmabi, Kokomo, Habitat and Playa Kalki present the largest percentages of *Cyanobacterial mats* and *Turf algae*. Playa Kalki presented the highest abundance of *Macroalgae*, followed by Habitat. Playa Kalki also presents the highest abundance of *Sponge*.

3.3.3.2 Depth-wise distribution analysis

We compiled the depth-wise distribution for each class in the reefgroups labelset and for the 9 most dominant scleractinian corals in the coral-community labelset (*Acropora cervicornis*, *Diploria strigosa*, *Madracis auretenra*, *Meandrina meandrites*, *Montastrea cavernosa*, *Orbicella annularis*, *Orbicella faveolata*, *Porites asteroides and Siderastrea siderea*). To obtain the distribution we divided each habitat map transect into smaller segments or quadrats of size 40×640 pixels. The HyperDiver measured the hydrostatic pressure and the diving altitude from the seafloor for each hyperspectral push-broom line. The depth of the HyperDiver at image acquisition time was calculated from the hydrostatic pressure and then added to the altitude of the device from

the sea-floor, to obtain the total depth of the acquired pixel line. The median depth for each quadrat was calculated from the 40 acquisition lines that composed it. Within each quadrat the relative fraction of each label was calculated by dividing the number of pixels for the class by the size of the quadrat. The depth-wise distribution was then plotted using vertical ridge-plots for the whole island (Figure 3.11).

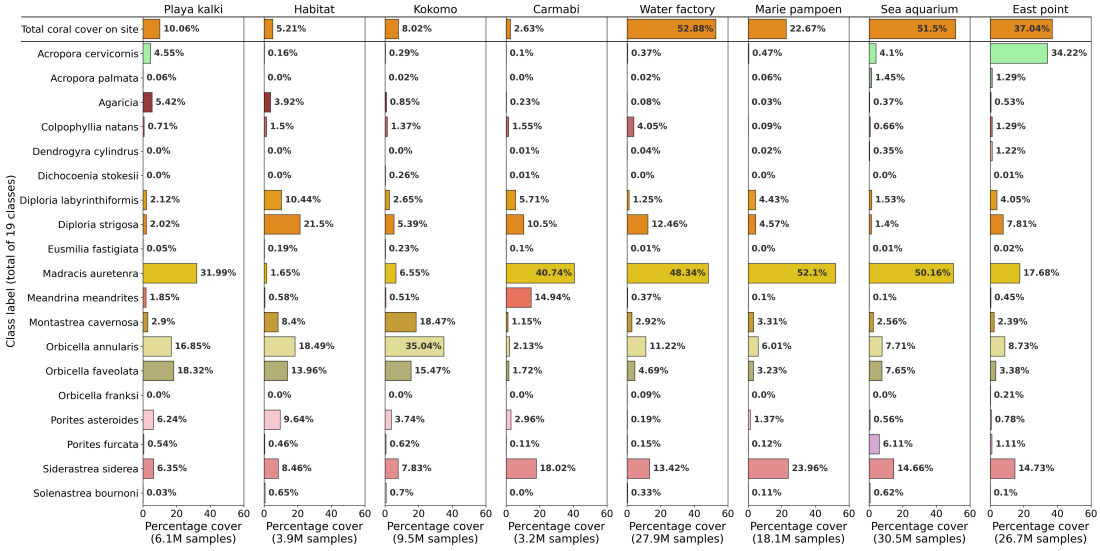

Figure 3.7 Coral communities coverage. The coral communities across the 8 sites were mostly dominated by the *Madracis auretenra* species. The second most dominating coral class was the *Orbicella annularis* species. *Orbicella faveolata*, *Siderastrea siderea* also appeared in mid-high percentage across sites. The brain corals *Diploria strigosa* and *Diploria labyrinthiformis* were abundant in Habitat, Carmabi and Water Factory. *Porites furcata* was highest in Sea Aquarium and *Meandrina meandrites* in Carmabi. *Porites asteroides* was more abundant towards the northern side of the island (Habitat and Playa Kalki). *Acropora cervicornis* was only dominant in East Point.

3.3.3.3 Environmental correlation analysis

Understanding the correlation between environmental variables and community distributions can elucidate drivers of increase and decline of certain species. The difference in reef communities across the island is mostly driven by external factors, such as physical, ecological and anthropogenic stressors. In this study we focused on the anthropogenic and ecological factors and their influence on the community distributions. To correlate our multivariate distribution and environmental variables, we apply GLLVM (Rabe-Hesketh 2004). GLLVMs extend generalized linear models to be used with multivariate data using a factor analytic approach. It incorporates a small number of latent variables for each site accompanied by species-specific factor loadings to model correlations between responses. One of the main advantages of GLLVMs is that they

can handle situations where there are many species, because the number of parameters in the covariance model scales linearly with the number of responses (Warton et al. 2015). We use the R package *gllvm* implementation (Niku et al. 2019) to calculate the GLLVM responses for our data. This package provides a flexible and fast implementation of GLLVMs to apply on ecological data.

We calculated the co-occurrence between the cover percentages of reefgroups and coral community classes and the environmental factors for each site, by running the *gllvm* package with a "negative.binomial" family, 3 latent variables and a random seed of 1234 (Figure 3.12&3.13). We fitted the model with and without environmental variables. When considering the environmental variables we used the formula: $\sim infrastructure + trash + sewage + diving\_pressure + fishing\_pressure + carnivorous\_fish\_biomass + herbivorous\_fish\_biomass$. We plotted the coefficients for each class with each environmental factor. We also plotted the occurrence correlation between benthic classes and scleractinian coral community classes controlled by the environmental variables.

3.4 Results

3.4.1 Reef community distribution and diversity

We calculated and compared the community composition per-site, for the *reefgroups*, as well as for the *coral community* (Figure 3.1).

3.4.1.1 *Reefgroups*

Sites closer to the southern end – East Point (37%), Sea Aquarium (52%), Marie Pampoen (23%) & Water Factory (53%) – of the island showed a higher abundance of *Coral* than on the sites in the northern part. A greater amount of *Hydrozoans* were found at East Point (9%) and Sea Aquarium (13%), and the greatest amount of *Soft coral* (23%) was found at East Point.

Sites located further north and close to urban areas presented the largest percentages of *Cyanobacterial mats* – Water Factory (6%), Carmabi (15%), Kokomo (24%), Habitat (13%) & Playa Kalki (16%). *Turf algae* followed a similar trend, with Water Factory (15%), Carmabi (24%) and Habitat (20%) showing high coverage of this class. The northern sites had higher abundance of *Macroalgae* with 24% in Playa Kalki, followed by Habitat with 10%. Playa Kalki also showed the highest abundance of *Sponges* (6%).

The nMDS and Bray-Curtis distance plots (Figure 3.8) show the similarities in dominant groups communities in the southern sites of East Point and Sea Aquarium. These sites also shared a similarly high Shannon diversity index of 2.49 and 2.3 for the reefgroups labelset. Marie

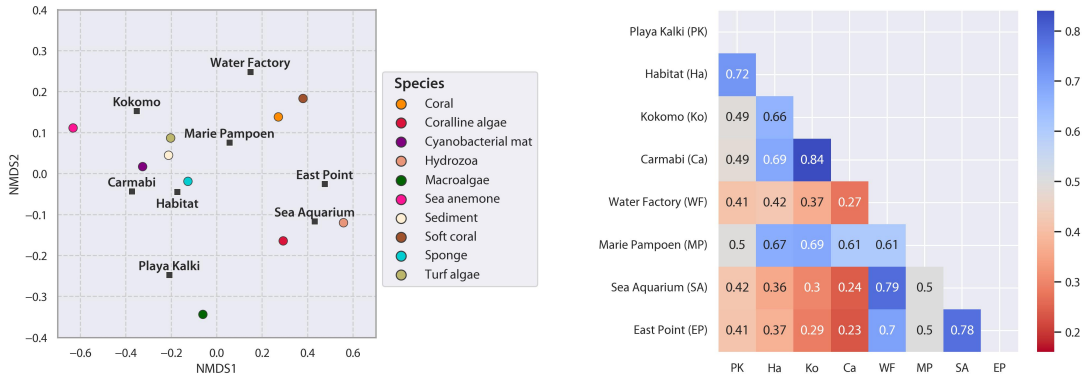

(**a**) nMDS Analysis (**b**) Bray-Curtis similarity

Figure 3.8 The nMDS and Bray-Curtis distance plots. East Point and Sea Aquarium show similar communities differentiating themselves through higher CCA, *Soft coral* and *Hydrozoa* coverage. Marie Pampoen and Water Factory cluster on the plot driven by the similar number of *Coral*, *Soft coral* and *Turf algae* cover. Playa Kalki and Habitat cluster because of similar *Macroalgae* and *Sponge* cover. Carmabi and Kokomo share similar community distributions dominated by *Cyanobacterial mat* and large areas of *Sediment*.

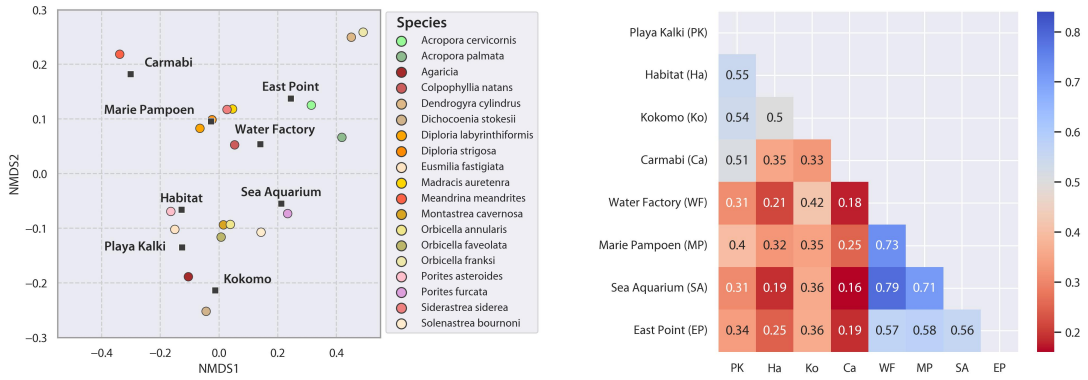

(**a**) nMDS Analysis (**b**) Bray-Curtis similarity

Figure 3.9 Coral community nMDS and Bray-Curtis plots. *Porites asteroides* and *Agaricia spp.* drive the communities in the northern site of the island (Playa Kalki and Habitat). The southern most sites loosely cluster together, with East Point showing a distinct community driven by the *Acropora spp.*, plus the rare species *Orbicella franksi* and *Dendrogyra cylindrus*. The Carmabi site war far from any cluster due to its large percentage of *Meandrina meandrites* species. The Bray-Curtis distances show that the closest communities were those in Sea Aquarium, Marie Pampoen and Water Factory, dominated by the *Madracis spp.*. Together with East Point, they were also the most distant from the Carmabi site community.

Pampoen and Water Factory sites have also similarities in their reefgroups communities, and are mostly affected by the similar number of *Coral*, *Soft coral* and *Turf algae* cover. Similarly, Playa

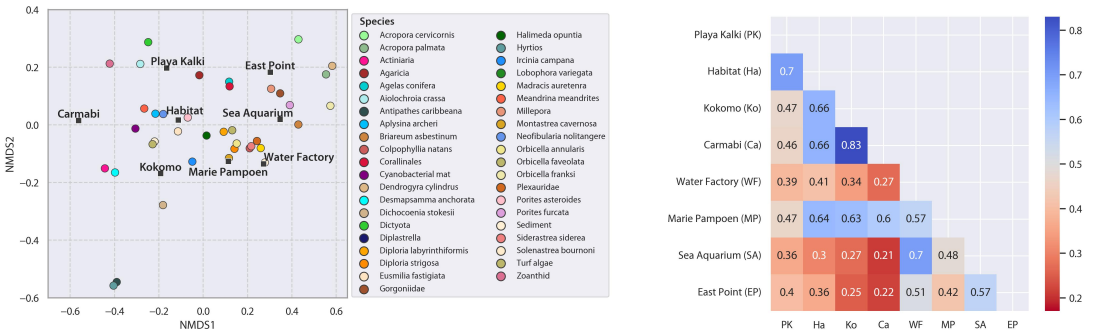

(**a**) nMDS Analysis (**b**) Bray-Curtis similarity

Figure 3.10 Detailed nMDS and Bray-Curtis plots, with 41 biotic and substrate labels.

Kalki and Habitat presented a similar community distribution and cluster together in the nMDS plot, distinguished mostly by macroalgal cover. Carmabi and Kokomo shared similar community distributions dominated by cyanobacterial mats and large areas of sediment.

The depth-wise distribution of reefgroups classes shows that cyanobacterial mats are located below 5 or 6 meters (Figure 3.11a). *Macroalgae* and *Soft coral* were located in shallower areas between 4 and 7 meters depth. Scleractinian corals were more evenly distributed along the depth gradient with a small conglomeration around 7 meters. *Sponge* and *Turf algae* were mostly found around 6 to 8 meters as well.

3.4.1.2 Scleractinian coral communities

The coral communities across the 8 sites were mostly dominated by the *Madracis auretenra* species. It covered around 52% of the coral community in Marie Pampoen, 50% in Sea Aquarium, 48% in Water Factory, 41% in Carmabi and 32% in Playa Kalki. Only in East Point (18%), Kokomo (7%) and Habitat (1.65%) was it not the most dominant species. In East Point was dominated by *Acropora cervicornis*, which otherwise only appeared in small percentages in Sea Aquarium (4.1%) and Playa Kalki (4.5%). The second most dominant coral class was the *Orbicella annularis* species, with 35% percentage cover in Kokomo and 18% in Habitat. *Orbicella faveolata*, *Siderastrea siderea* also appeared in mid-high percentage across sites. The brain corals *Diploria strigosa* and *Diploria labyrinthiformis* were abundant in Habitat, Carmabi and Water Factory. *Porites furcata* was relevant in the Sea Aquarium community with 6.11% and *Meandrina meandrites* in Carmabi with 15%. *Porites asteroides* was more abundant towards the northern side of the island with almost 10% cover in Habitat and 6% in Playa Kalki.

The nMDS analysis for the coral communities showed that sites towards the northern side of the island clustered together and thus showed a similar community, driven by *Porites asteroides* and *Agaricia spp.* (Figure 3.9a). The southern most sites loosely clustered together, with East

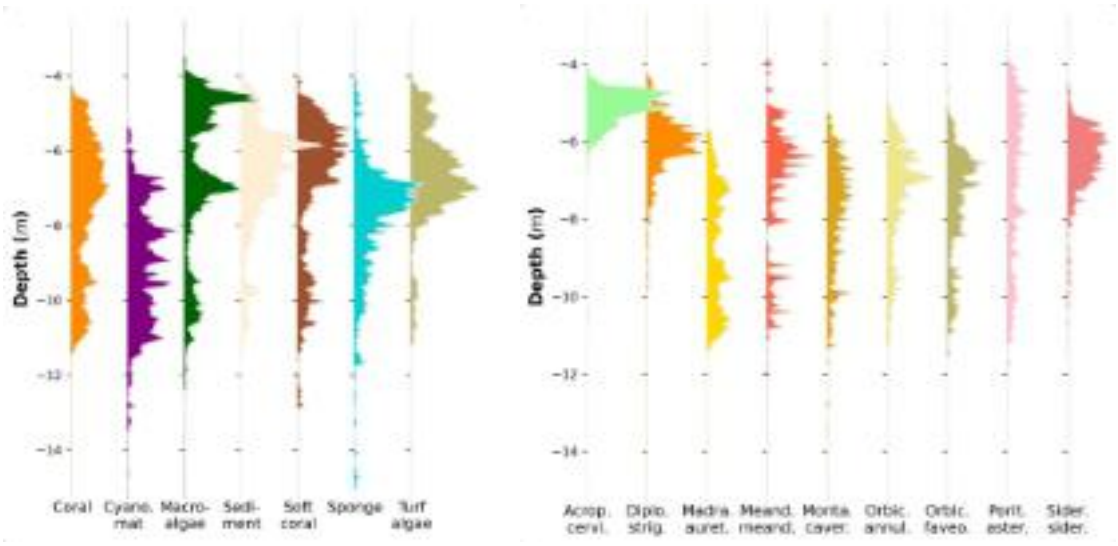

(**a**) Reefgroups (**b**) Coral community

Figure 3.11 Depth-wise distribution for the benthic *reefgroups* across all 8 sites. Cyanobacterial mats were mostly found below 6 meters. *Macroalgae* and *Soft coral* were located in shallower areas between 4 and 7 meters depth. *Coral* was more evenly distributed along the depth gradient with a small conglomeration around 7 meters. Sponges and turf algae were mostly found around 6 to 8 meters as well. *Acropora cervicornis* was mostly found between 4 and 6 meters depth. *Diploria strigosa* and *Siderastrea siderea* were mostly found between 4 and 8 meters. *Madracis auretenra*, *Orbicella annularis*, *Orbicella faveolata* and *Montastrea cavernosa* were distributed between 6 and 11 meters depth, with *Madracis auretenra* having a more evenly distribution even towards the deeper end of the range. The *Porites asteroides* species showed a more even distribution across all depths down to 12 meters. The *Meandrina meandrites* species was found mostly between 5 and 8 meters depth with sporadic occurrences in the shallower and deeper ends.

Point differentiated by the *Acropora spp.*, and the rare species *Orbicella franksi* and *Dendrogyra cylindrus*. The Carmabi site did not cluster to any other sites due to its large percentage of *Meandrina meandrites* species and low overall coral cover. The Bray-Curtis distances show that the closest communities were those in Sea Aquarium, Marie Pampoen and Water Factory, dominated by the *Madracis spp.* and together with East Point, they were also the most distant from the Carmabi site community (Figure 3.9b).

The depth-wise analysis shows that *Acropora cervicornis* was mostly found between 4 and 6 meters depth (Figure 3.11b). *Diploria strigosa* and *Siderastra siderea* were found between 4 and 8 meters. *Madracis auretenra*, *Orbicella annularis*, *Orbicella faveolata* and *Montastrea cavernosa* were distributed between 6 and 11 meters depth, with *Madracis auretenra* having a more evenly distribution even towards the deeper end of the range. The *Porites asteroides* species showed a more even distribution across all depths down to 12 meters. Finally, the *Meandrina meandrites* species was found mostly between 5 and 8 meters depth with sporadic occurrences in the shallower

and deeper ends.

3.4.2 Environmental drivers

We inspected the correlation of the environmental factors to the distribution of reef communities across the 8 surveyed sites.

3.4.2.1 Coefficient analysis

The GLLVM estimated coefficients for environmental predictors from the fitted model between environmental factors and the abundance of the *reefgroups* (Figure 3.12). Coastal infrastructure, as well as pollution by trash residue, positively correlated with *Turf algae* abundance with a coefficient of 0.5 and 0.9, respectively, followed closely by diving activity and biomass of herbivorous fish. Trash found on the reefs impacted negatively for *Coral*, *Hydrozoa* and *Macroalgae* abundances. Sewage output affected *Turf algae*, *Soft coral*, *Macroalgae* and *Hydrozoa* negatively, and *Sponge* and *Cyanobacterial mats* positively. Diving activity was positively correlated with *Hydrozoa*, *Macroalgae* and *Coral*. In places with high fishing activity the abundance of *Soft coral* and *Turf algae* were significantly reduced, while *Sponge* and *Cyanobacterial mat* benefited from it. Higher carnivorous fish biomass affected positively the abundance of *Hydrozoa*, *Coral* and *Sponge*, while affecting negatively the abundance of *Turf algae*, *Macroalgae*, and *Soft coral*. Higher herbivorous fish biomass correlated with lower *Macroalgae*, lower *Sponge* coverage.

3.4.2.2 Co-occurrence of dominant *reefgroups*

The co-occurrence of benthic classes was derived from the GLLVM, which factors in the weight of environmental drivers in each pair-wise co-occurrence value. *Coral*, *Soft coral* and *Hydrozoa* were mostly found in the same sites in higher abundance, together with *Coralline algae* (Figure 3.13a). *Macroalgae* was located in sites with high abundance of *Sediment* and *Turf algae*, *Coralline algae*. *Turf algae*, *Sponge* and *Cyanobacterial mat* co-occurred in many location as well. *Sediment* and *Turf algae* were found together in several sites. *Coral*, *Soft coral* and *Hydrozoa* did not co-occur often with *Sediment*, *Macroalgae*, *Turf algae*, *Sponge* and *Cyanobacterial mat*.

3.4.2.3 Co-occurrence of scleractinian coral species/genera

Scleractinian corals' co-occurrence was calculated from the GLLVM and controlled by the environmental factors of each site (Figure 3.13b). Some species, such as *Meandrina meandrites* and *Porites asteroides*, were only found near each other. *Dichocenia stokesii*, a rare species in the dataset, was found mostly near *Eusmilia fastigiata*, *Diploria labyrinthiformis* and *Dendrogyra*

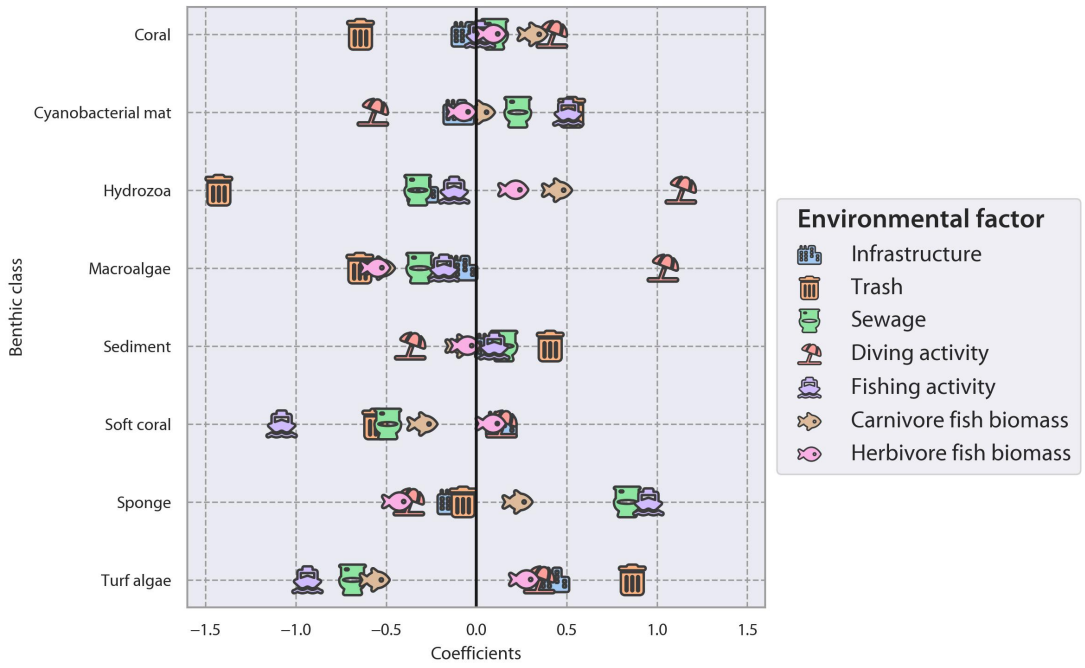

Figure 3.12 Environmental factors impact on the most dominant *reefgroups*. The coefficient plot was derived from the Generalized Linear Latent Variable Model (GLLVM), ran on 8 *reefgroups* and 7 environmental factors that have a different impact on each of the 8 surveyed sites. Trash found on the reefs impacted negatively for *Coral*, *Hydrozoa* and *Macroalgae* abundances. Diving activity was positively correlated with these 3 classes, as diving tourism usually seeks these more visually pleasing settings. Higher sewage output, fishing activity and trash presence correlated with higher *Cyanobacterial mats* abundance. Similarly, *Sponge* was found more in locations with higher sewage output and fishing activity.

cylindrus. Many species co-occurred quite often, for example, *Acropora palmata*, *Siderastrea siderea*, *Diploria strigosa*, *Orbicella franksi*, *Acropora cervicornis* and *Porites furcata*. Another cluster of co-occurrence include the species *Colpophyllia natans*, *Montastrea cavernosa*, *Solenastrea bournoni*, *Madracis auretenra* and *Orbicella annularis*. *Orbicella annularis* and *Orbicella faveolata* were often found together. Finally, corals of the *Agaricia* genus had the most evenly distributed co-occurrence values, being found often next to the *Orbicella* genus, *Madracis auretenra*, but not in the same sites as *Meandrina meandrites*, *Dichocenia stokesii*, *Eusmilia fastigiata* and *Dendrogyra cylindrus*.

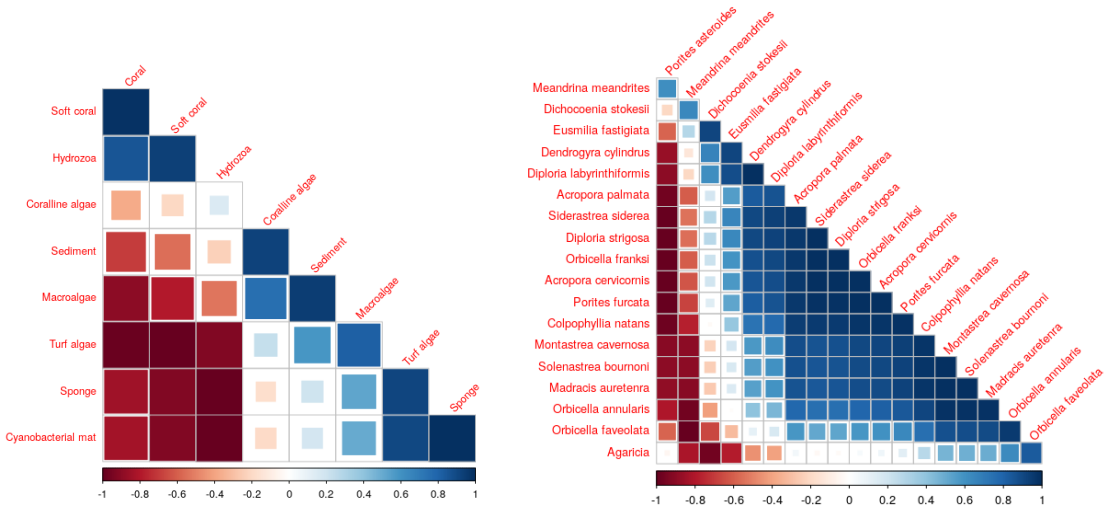

(**a**) Reefgroups (**b**) Coral community

Figure 3.13 Co-occurrence of the dominant benthic *reefgroups* and *coral community*, controlled by the environmental variables.

3.5 Discussion

Our detailed survey of 8 sites along the coast of Curaçao revealed a substantial variability in the overall community composition along the leeward coastline. Refining an AI workflow (Figure 3.2), 147 hyperspectral transects were converted into habitat maps (with 90% accuracy) containing about 640 million samples (pixels), each labelled to one of 42 habitat labels. Our detailed labelset comprised 39 biotic labels, which included 19 scleractinian coral species and genera, and 3 labels describing substrate types: cyanobacterial mats, bare sediment and turf algae. The detailed community labels were also abstracted to 12 labels describing functional benthic *reefgroups*, providing an aggregated view of the Curaçaoan reef communities. We compiled community composition and percentage coverage for each class over the 8 sites, as well as their depth-wise distribution. Finally, we analysed the possible driver factors for community composition across environmental gradients and stress variables taken from a thorough report conducted a year prior to our survey.

3.5.1 *Reefgroups* community shifts and their drivers

The community composition and coverage percentage values from our survey (in 2016) follow similar values to previous surveys in the region (in the years 2013–2015) (De Bakker, Meesters, et al. 2016; De Bakker, Van Duyl, et al. 2017; Sandin, Alcantar, et al. 2022), although the temporal, spatial and thematic scales in those studies differed from the ones used in our study. De Bakker et al 2016 (De Bakker, Meesters, et al. 2016) & de Bakker et al 2017 (De Bakker,

Van Duyl, et al. 2017) both had sparse spatial cover, both latitudinally as well as in the sampling density, as they covered 3 clustered sites close to the Carmabi station and one extra control site near East Point, and used a sparse sampling method on photoquadrats (Kohler et al. 2006). They provide a detailed temporal analysis of reef community shifts from 1973 to 2014 at 4 depth levels. Other studies and reports considered more sites across the coastline, with limited thematic detail (dominant benthic classes) (Sandin, Alcantar, et al. 2022) added to a reduced set of coral genera/species (WAITTS-Institute 2017).

Previous studies have shown that reef communities when deteriorated shift towards macroalgae and turf algae dominated reefs, and if further deteriorated, towards reefs dominated by benthic cyanobacterial mats (BCMs) (De Bakker, Van Duyl, et al. 2017). BCMs expand in degraded reefs and benefit from substrate-level nutrient release (Brocke et al. 2015; Haan, Huisman, et al. 2016). Together with turf algae, BCMs are the primary N_2 fixating benthic organisms. N_2 fixation by these organisms contributes to a positive feedback loop that accelerates the proliferation of both BCMs and turf algae, accelerating coral reef degradation (Gorgula et al. 2004; Haan, Visser, et al. 2014). Our results suggest that BCM and turf algae expansion continued into 2016 with 15% cover of cyanobacterial mats in Carmabi, and we provide more evidence that reefs further north present similarly shifted communities, with 24% BCM cover in Kokomo, 13% in Habitat and 16% in Playa Kalki. Turf algae covered 23.6% of the area surveyed in Carmabi and 20% covered in Habitat, being the most dominant class after bare sediment. Sandin et al. 2022 also show that turf algae covers a large areal percentage, average of 27% across 122 surveyed sites along the coastline of the island in November 2015 (Sandin, Alcantar, et al. 2022). They also show that the height of turf algae correlated with decreased coral cover. In our environmental drivers analysis, we noticed that the presence of trash (a proxy for pollution) correlated with low abundance of all corals types and of macroalgae, while correlating to high sediment, BCMs and turf algae coverage, all features of deteriorated reefs (Figure 3.12). Similarly, sewage output and fishing activity, correlated to higher sediment, BCMs and sponge coverage. Turf algae was negatively correlated with sewage output, given that with higher eutrophication levels BCMs become more dominant, as mentioned in previous studies in the area (De Bakker, Van Duyl, et al. 2017).

Some environmental factors, such as diving activity, correlate with features of a healthier coral reef, but as a consequence – rather than a driver of it. For example, coral, hydrozoa and macroalgae abundance was correlated with higher diving activity, because diving tourism generally seeks more visually attracting reefs as destinations and it is in the interest of the industry to keep the reef's status. Nonetheless, if the pressure is not managed properly, reefs can start to deteriorate due to physical contact from divers with corals, as well as an increase in littering and sewage output from tourism related infrastructure. Playa Kalki is a good example of this process, where much of Curaçao's diving tourism takes place, due to relatively extensive coral cover (10%), but having macroalgae coverage as dominant (23.9%), followed by BCMs (16.3%), hinting towards a

coral-macroalgae-cyanobacteria shift. Depth also played a role in the composition of *reefgroups* communities, with BCMs mostly found below 6 meters, while turf algae and macroalgae were located in shallower areas (4–8 meters) (Figure 3.11a). This could indicate different photosynthetic light requirements of these groups and the space sharing between BCMs and turf algae in deteriorated reefs. In healthier reefs, scleractinian and soft corals are also found in higher quantities in shallower areas.

The difference of the deteriorated reefs found from the center towards the north of the island is highlighted in the nMDS and Bray-Curtis plots of the *detailed* and *reefgroups* labelsets (Figure 3.10&3.8a). They show that the two sites considered in the (De Bakker, Meesters, et al. 2016) and (De Bakker, Van Duyl, et al. 2017) studies (Carmabi & East Point) show very different communities, with the rest of the sites in between these two extremes. The Carmabi and Kokomo sites were dominated by large stretches of bare sediment, turf algae and cyanobacterial mats, while the East Point community was more balanced and resembles a healthier reef, dominated by scleractinian corals, hydrozoans and soft corals (Figure 3.1&3.6). Further evidence is provided by the *reefgroups* co-occurrence plot (Figure 3.13a), where turf algae, BCMs and sponges have a higher probability to be found at the same site, while macroalgae and coralline algae start the transition towards healthier reefs, dominated by scleractinian-, soft- and hydrocorals. These results suggest that reefs close to human settlements (Carmabi, Kokomo), to aggro-industrial areas (Kokomo, Habitat) and tourism infrastructure (Playa Kalki) continue to deteriorate due to increased anthropogenic stressors.

3.5.2 Coral community shifts: opportunism on the rise

The coral community across the island varied as well, with sites such as Carmabi and East Point being the most different ones from each other (Figure 3.9b). The coral community in Carmabi was dominated by opportunistic fast-growing species such as *Madracis auretenra* and *Meandrina meandrites*; while the East Point site was dominated by more structurally complex corals such as *Acropora cervicornis*, *Orbicella* complexes and *Siderastrea siderea*, as well as by the *Madracis auretenra* species (Figure 3.7). Other survey efforts show a similar coral community compositions along the coastline, with higher *Acroporid* and *Orbicella spp.* coverage in the south of the island (WAITTS-Institute 2017). The absence of *Acroporid* species in previous studies (e.g., (De Bakker, Meesters, et al. 2016)) could be attributed to the depth of sampling, where the shallowest depth was 10 meters. In our study, *Acropora cervicornis* was mostly found between 4 and 6 meters depth (Figure 3.11b). Healthier reefs showed more complexity in their coral community providing a better habitat for other fauna, shown in the higher fish biomass correlated with corals and hydrozoans (Figure 3.12). Degraded reefs presented lower overall coral coverage and only sporadic appearances of small opportunistic colonies, having a clear winner in the *Madracis auretenra* coral species, being the dominant in 5 out of the 8 sites, with around

50% in 3 sites. Opportunistic-fast growing corals like *Madracis auretenra* do not provide enough hiding and nursery spaces for invertebrates and reef fish, lowering the overall diversity of reefs, reducing fish stocks and removing coastal protection from wave exposure (Carlot et al. 2023; Graham 2014).

3.5.3 The diversity is in the details

The combination of fine-grained benthic descriptions and abstracted functional classes allowed to compare the difference in community diversity indices between the 3 thematic scales we considered. Noteworthy was that, when using the *reefgroups* labelset with 10–11 habitat classes, the Shannon and Simpson diversity indices were very similar for the northernmost sites (Playa Kalki and Habitat) and the southernmost sites (East Point and Sea Aquarium) (Table 3.3). When calculating the indices using the detailed labelset (34–37 classes) the southernmost sites show a substantially higher diversity of up to 3.77 H in East Point, compared to 2.85 H in Playa Kalki. Even the Water Factory and Marie Pampoen sites show a higher diversity than the northern sites. When focusing specifically on scleractinian coral communities, the diversity shift as well, with more diversity (up to 0.86 GS) in the northern sites, although with lower total coral coverage (Figure 3.7). These findings reveal obscuring of true underlying diversity when labeling the survey data with abstracted high level classes, and the necessity of reporting diversity indices calculated from the lowest taxonomic level possible. Furthermore, the use of dense sampling with high thematic detail allows to consider rare species, usually neglected by sparse sampling studies (Hochberg et al. 2021; Pante et al. 2012; Schürholz et al. 2023).

3.6 Conclusions

Our study provides an in-depth description of 8 coral reef sites along the leeward coastline of Curaçao , continuing a large set of studies describing its reef communities and their shifts. We provide a detailed overview of the reefs, with dense habitat maps containing up to 42 community labels, many down to genera/species level. We show that many of the reefs continued to deteriorate, specially due to anthropogenic stressors in the center and north of the island, with BCMs and turf algae dominating many of the communities. Dense and detailed habitat sampling has the potential to provide in-depth information about reef communities and their shifts over time. The automatic creation of benthic habitat maps through AI creates consistent community composition and configuration descriptions, enabling thematic and spatial detail to scale up to an island-wide survey level. As demonstrated in this and other recent studies Mills et al. 2023; Teague et al. 2023, the advent of more accessible proximal sensing platforms, spectral imagers

and more powerful computing resources promises the democratization of automated and scalable workflows, leading to the standardization of coral reef mapping with unprecedented detail.

3.7 Acknowledgments

We would like to thank the IT departments at the Max Planck Institute for Marine Microbiology and the DataLab of the Leibniz Centre for Tropical Marine Research for the computational resources to run our workflows. We want to thank Anjleen Hannak, Alexandra Kler Lago and Ahmad Rafiuddin Rashid for the minutiose annotation work on the coral reef transects.

3.8 Author Contributions

Conceptualization: D.S., A.C.; Data Curation: D.S.; Investigation: D.S., A.C.; Methodology: D.S., A.C.; Formal analysis: D.S.; Software: D.S.; Supervision: A.C.; Validation: D.S., A.C.; Visualization: D.S., A.C.; Project Administration: D.S.; Resources: A.C.; Funding acquisition: A.C.; Writing original draft: D.S., Writing review and editing: A.C.. All authors have read and agreed to the published version of the manuscript.

References

Alemu, Jahson Berhane and Ysharda Clement (2014). "Mass Coral Bleaching in 2010 in the Southern Caribbean". In: *PLOS ONE* 9.1, e83829. DOI: *10.1371/journal.pone.0083829*.

Althaus, Franziska, Nicole Hill, Renata Ferrari, Luke Edwards, Rachel Przeslawski, Christine H. L. Schönberg, Rick Stuart-Smith, Neville Barrett, Graham Edgar, Jamie Colquhoun, Maggie Tran, Alan Jordan, Tony Rees, and Karen Gowlett-Holmes (2015). "A Standardised Vocabulary for Identifying Benthic Biota and Substrata from Underwater Imagery: The CATAMI Classification Scheme". In: *PLOS ONE* 10.10, e0141039. DOI: *10.1371/journal.pone.0141039*.

Aronson, R., W. Precht, M. Toscano, and K. Koltes (2002). "The 1998 bleaching event and its aftermath on a coral reef in Belize". In: *Marine Biology* 141.3, pp. 435–447. DOI: *10.1007/s00227-002-0842-5*.

Aronson, Richard B. and William F. Precht (2001). "White-band disease and the changing face of Caribbean coral reefs". In: *Hydrobiologia* 460.1, pp. 25–38. DOI: *10.1023/A:1013103928980*.

Bak, Rolf P. M. (1977). "Coral reefs and their zonation in the Netherlands Antilles | Dutch Caribbean Biodiversity Database". In: *Studies in Geology* 4. URL: *https://www.dcbd.nl/document/coral-reefs-and-their-zonation-netherlands-antilles* (visited on 12/10/2023).

Bak, Rolf P. M. and Brian E. Luckhurst (1980). "Constancy and change in coral reef habitats along depth gradients at Curaçao". In: *Oecologia* 47.2, pp. 145–155. DOI: *10.1007/BF00346812*.

Bak, Rolf P. M., Gerard Nieuwland, and Erik H. Meesters (2005). "Coral reef crisis in deep and shallow reefs: 30 years of constancy and change in reefs of Curacao and Bonaire". In: *Coral Reefs* 24.3, pp. 475–479. DOI: *10.1007/s00338-005-0009-1*.

Bries, Jill M., Adolphe O. Debrot, and David L. Meyer (2004). "Damage to the leeward reefs of Curaçao and Bonaire, Netherlands Antilles from a rare storm event: Hurricane Lenny, November 1999". In: *Coral Reefs* 23.2, pp. 297–307. DOI: *10.1007/s00338-004-0379-9*.

Brito-Millán, Marlene, Mark J. A. Vermeij, Esmeralda A. Alcantar, and Stuart A. Sandin (2019). "Coral reef assessments based on cover alone mask active dynamics of coral communities". In: *Marine Ecology Progress Series* 630, pp. 55–68. URL: *https://www.jstor.org/stable/26920540* (visited on 12/10/2023).

Brocke, Hannah J., Lubos Polerecky, Dirk de Beer, Miriam Weber, Joachim Claudet, and Maggy M. Nugues (2015). "Organic Matter Degradation Drives Benthic Cyanobacterial Mat Abundance on Caribbean Coral Reefs". In: *PLOS ONE* 10.5, e0125445. DOI: *10.1371/journal.pone.0125445*.

Camacho, Ruleo, Sophia Steele, Shanna Challenger, and Mark Archibald (2020). "Status of coral reefs in Antigua & Barbuda: using data to inform management". In: *PeerJ* 8, e9236. DOI: *10.7717/peerj.9236*.

Carlot, Jérémy, Michalis Vousdoukas, Alessio Rovere, Theofanis Karambas, Hunter S. Lenihan, Mohsen Kayal, Mehdi Adjeroud, Gonzalo Pérez-Rosales, Laetitia Hedouin, and Valeriano Parravicini (2023). "Coral reef structural complexity loss exposes coastlines to waves". In: *Scientific Reports* 13.1, p. 1683. DOI: *10.1038/s41598-023-28945-x*.

Chennu, Arjun, Paul Färber, Glenn De'ath, Dirk de Beer, and Katharina E. Fabricius (2017). "A diver-operated hyperspectral imaging and topographic surveying system for automated mapping of benthic habitats". In: *Scientific Reports* 7.1, pp. 1–12. DOI: *10.1038/s41598-017-07337-y*.

Corals of the World (2016). URL: *http://www.coralsoftheworld.org/* (visited on 11/23/2023).

Crabbe, M. James C. (2008). "Climate change, global warming and coral reefs: Modelling the effects of temperature". In: *Computational Biology and Chemistry* 32.5, pp. 311–314. DOI: *10.1016/j.compbiolchem.2008.04.001*.

Cramer, Katie L., Jeremy B. C. Jackson, Mary K. Donovan, Benjamin J. Greenstein, Chelsea A. Korpanty, Geoffrey M. Cook, and John M. Pandolfi (2020). "Widespread loss of Caribbean acroporid corals was underway before coral bleaching and disease outbreaks". In: *Science Advances* 6.17, eaax9395. DOI: *10.1126/sciadv.aax9395*.

Curaçao Tourist Board - Annual Report (2016). URL: *https://www.curacaotouristboard.com/monthly-statistics/* (visited on 11/20/2023).

De Bakker, Didier M., Erik H. Meesters, Rolf P. M. Bak, Gerard Nieuwland, and Fleur C. Van Duyl (2016). "Long-term Shifts in Coral Communities On Shallow to Deep Reef Slopes

of Curaçao and Bonaire: Are There Any Winners?" In: *Frontiers in Marine Science* 3. DOI: *10.3389/fmars.2016.00247*.

De Bakker, Didier M., Fleur C. Van Duyl, Rolf P. M. Bak, Maggy M. Nugues, Gerard Nieuwland, and Erik H. Meesters (2017). "40 Years of benthic community change on the Caribbean reefs of Curaçao and Bonaire: the rise of slimy cyanobacterial mats". In: *Coral Reefs* 36.2, pp. 355–367. DOI: *10.1007/s00338-016-1534-9*.

Donner, Simon D., Gregory J. M. Rickbeil, and Scott F. Heron (2017). "A new, high-resolution global mass coral bleaching database". In: *PLOS ONE* 12.4, e0175490. DOI: *10.1371/journal.pone.0175490*.

Eakin, C. Mark, Jessica A. Morgan, Scott F. Heron, Tyler B. Smith, Gang Liu, Lorenzo Alvarez-Filip, Bart Baca, Erich Bartels, Carolina Bastidas, Claude Bouchon, Marilyn Brandt, Andrew W. Bruckner, Lucy Bunkley-Williams, Andrew Cameron, Billy D. Causey, Mark Chiappone, Tyler R. L. Christensen, M. James C. Crabbe, Owen Day, Elena de la Guardia, Guillermo Díaz-Pulido, Daniel DiResta, Diego L. Gil-Agudelo, David S. Gilliam, Robert N. Ginsburg, Shannon Gore, Héctor M. Guzmán, James C. Hendee, Edwin A. Hernández-Delgado, Ellen Husain, Christopher F. G. Jeffrey, Ross J. Jones, Eric Jordán-Dahlgren, Les S. Kaufman, David I. Kline, Philip A. Kramer, Judith C. Lang, Diego Lirman, Jennie Mallela, Carrie Manfrino, Jean-Philippe Maréchal, Ken Marks, Jennifer Mihaly, W. Jeff Miller, Erich M. Mueller, Erinn M. Muller, Carlos A. Orozco Toro, Hazel A. Oxenford, Daniel Ponce-Taylor, Norman Quinn, Kim B. Ritchie, Sebastián Rodríguez, Alberto Rodríguez Ramírez, Sandra Romano, Jameal F. Samhouri, Juan A. Sánchez, George P. Schmahl, Burton V. Shank, William J. Skirving, Sascha C. C. Steiner, Estrella Villamizar, Sheila M. Walsh, Cory Walter, Ernesto Weil, Ernest H. Williams, Kimberly Woody Roberson, and Yusri Yusuf (2010). "Caribbean Corals in Crisis: Record Thermal Stress, Bleaching, and Mortality in 2005". In: *PLOS ONE* 5.11, e13969. DOI: *10.1371/journal.pone.0013969*.

Erftemeijer, Paul L. A., Bernhard Riegl, Bert W. Hoeksema, and Peter A. Todd (2012). "Environmental impacts of dredging and other sediment disturbances on corals: A review". In: *Marine Pollution Bulletin* 64.9, pp. 1737–1765. DOI: *10.1016/j.marpolbul.2012.05.008*.

Fabricius, Katharina E. (2005). "Effects of terrestrial runoff on the ecology of corals and coral reefs: review and synthesis". In: *Marine Pollution Bulletin* 50.2, pp. 125–146. DOI: *10.1016/j.marpolbul.2004.11.028*.

Ford, Amanda K., Sonia Bejarano, Maggy M. Nugues, Petra M. Visser, Simon Albert, and Sebastian C. A. Ferse (2018). "Reefs under Siege—the Rise, Putative Drivers, and Consequences of Benthic Cyanobacterial Mats". In: *Frontiers in Marine Science* 5. URL: *https://www.frontiersin.org/articles/10.3389/fmars.2018.00018* (visited on 11/19/2023).

Ganaie, M. A., Minghui Hu, A. K. Malik, M. Tanveer, and P. N. Suganthan (2022). "Ensemble deep learning: A review". In: *Engineering Applications of Artificial Intelligence* 115, p. 105151. DOI: *10.1016/j.engappai.2022.105151*.

Gardner, Toby A., Isabelle M. Côté, Jennifer A. Gill, Alastair Grant, and Andrew R. Watkinson (2003). "Long-Term Region-Wide Declines in Caribbean Corals". In: *Science* 301.5635, pp. 958–960. DOI: *10.1126/science.1086050*.

Gladfelter, W. B. (1982). "White-band Disease in Acropora Palmata: Implications for the Structure and Growth of Shallow Reefs". In: *Bulletin of Marine Science* 32.2, pp. 639–643.

Gorgula, Sonia K. and Sean D. Connell (2004). "Expansive covers of turf-forming algae on human-dominated coast: the relative effects of increasing nutrient and sediment loads". In: *Marine Biology* 145.3, pp. 613–619. DOI: *10.1007/s00227-004-1335-5*.

Graham, Nicholas A. J. (2014). "Habitat Complexity: Coral Structural Loss Leads to Fisheries Declines". In: *Current Biology* 24.9, R359–R361. DOI: *10.1016/j.cub.2014.03.069*.

Haan, Joost den, Jef Huisman, Hannah J. Brocke, Henry Goehlich, Kelly R. W. Latijnhouwers, Seth van Heeringen, Saskia A. S. Honcoop, Tanja E. Bleyenberg, Stefan Schouten, Chiara Cerli, Leo Hoitinga, Mark J. A. Vermeij, and Petra M. Visser (2016). "Nitrogen and phosphorus uptake rates of different species from a coral reef community after a nutrient pulse". In: *Scientific Reports* 6.1, p. 28821. DOI: *10.1038/srep28821*.

Haan, Joost den, Petra M. Visser, Anjani E. Ganase, Elfi E. Gooren, Lucas J. Stal, Fleur C. van Duyl, Mark J. A. Vermeij, and Jef Huisman (2014). "Nitrogen fixation rates in algal turf communities of a degraded versus less degraded coral reef". In: *Coral Reefs* 33.4, pp. 1003–1015. DOI: *10.1007/s00338-014-1207-5*.

Heery, Eliza C., Bert W. Hoeksema, Nicola K. Browne, James D. Reimer, Put O. Ang, Danwei Huang, Daniel A. Friess, Loke Ming Chou, Lynette H. L. Loke, Poonam Saksena-Taylor, Nadia Alsagoff, Thamasak Yeemin, Makamas Sutthacheep, Si Tuan Vo, Arthur R. Bos, Girley S. Gumanao, Muhammad Ali Syed Hussein, Zarinah Waheed, David J. W. Lane, Ofri Johan, Andreas Kunzmann, Jamaluddin Jompa, Suharsono, Daisuke Taira, Andrew G. Bauman, and Peter A. Todd (2018). "Urban coral reefs: Degradation and resilience of hard coral assemblages in coastal cities of East and Southeast Asia". In: *Marine Pollution Bulletin* 135, pp. 654–681. DOI: *10.1016/j.marpolbul.2018.07.041*.

Hochberg, Eric J. and Michelle M. Gierach (2021). "Missing the Reef for the Corals: Unexpected Trends Between Coral Reef Condition and the Environment at the Ecosystem Scale". In: *Frontiers in Marine Science* 8, p. 1191. DOI: *10.3389/fmars.2021.727038*.

Hughes, T. P., A. H. Baird, D. R. Bellwood, M. Card, S. R. Connolly, C. Folke, R. Grosberg, O. Hoegh-Guldberg, J. B. C. Jackson, J. Kleypas, J. M. Lough, P. Marshall, M. Nyström, S. R. Palumbi, J. M. Pandolfi, B. Rosen, and J. Roughgarden (2003). "Climate Change, Human Impacts, and the Resilience of Coral Reefs". In: *Science* 301.5635, pp. 929–933. DOI: *10.1126/science.1085046*.

Jackson, Jeremy B. C., Mary K. Donovan, Katie L. Cramer, and Vivian Lam (2015). *Status and trends of Caribbean coral reefs : 1970-2012 | IUCN*. URL: *https://www.iucn.org/content/status-and-trends-caribbean-coral-reefs-1970-2012* (visited on 11/18/2023).

Knowlton, Nancy and Jeremy B. C. Jackson (2008). "Shifting Baselines, Local Impacts, and Global Change on Coral Reefs". In: *PLOS Biology* 6.2, e54. DOI: *10.1371/journal.pbio.0060054*.

Kohler, Kevin E. and Shaun M. Gill (2006). "Coral Point Count with Excel extensions (CPCe): A Visual Basic program for the determination of coral and substrate coverage using random point count methodology". In: *Computers & Geosciences* 32.9, pp. 1259–1269. DOI: *10.1016/j.cageo.2005.11.009*.

Marine Species, World Register of (2023). *WoRMS Editorial Board World Register of Marine Species*. URL: *https://www.marinespecies.org* (visited on 11/13/2023).

Mills, Matthew S., Mischa Ungermann, Guy Rigot, Joost den Haan, Javier X. Leon, and Tom Schils (2023). "Assessment of the utility of underwater hyperspectral imaging for surveying and monitoring coral reef ecosystems". In: *Scientific Reports* 13.1, p. 21103. DOI: *10.1038/s41598-023-48263-6*.

Moberg, Fredrik and Carl Folke (1999). "Ecological goods and services of coral reef ecosystems". In: *Ecological Economics* 29.2, pp. 215–233. DOI: *10.1016/S0921-8009(99)00009-9*.

Mölder, Felix, Kim Philipp Jablonski, Brice Letcher, Michael B. Hall, Christopher H. Tomkins-Tinch, Vanessa Sochat, Jan Forster, Soohyun Lee, Sven O. Twardziok, Alexander Kanitz, Andreas Wilm, Manuel Holtgrewe, Sven Rahmann, Sven Nahnsen, and Johannes Köster (2021). *Sustainable data analysis with Snakemake*. 10:33. F1000Research. DOI: *10.12688/f1000research.29032.2*.

Muldrow, Milton, Edward C. M. Parsons, and Robert Jonas (2020). "Shifting baseline syndrome among coral reef scientists". In: *Humanities and Social Sciences Communications* 7.1, pp. 1–8. DOI: *10.1057/s41599-020-0526-0*.

Muñiz-Castillo, Aarón Israel, Andrea Rivera-Sosa, Iliana Chollett, C. Mark Eakin, Luisa Andrade-Gómez, Melanie McField, and Jesús Ernesto Arias-González (2019). "Three decades of heat stress exposure in Caribbean coral reefs: a new regional delineation to enhance conservation". In: *Scientific Reports* 9.1, p. 11013. DOI: *10.1038/s41598-019-47307-0*.

Niku, Jenni, Francis K. C. Hui, Sara Taskinen, and David I. Warton (2019). "gllvm: Fast analysis of multivariate abundance data with generalized linear latent variable models in r". In: *Methods in Ecology and Evolution* 10.12, pp. 2173–2182. DOI: *10.1111/2041-210X.13303*.

Nowosad, Jakub and Tomasz F. Stepinski (2019). "Information theory as a consistent framework for quantification and classification of landscape patterns". In: *Landscape Ecology* 34.9, pp. 2091–2101. DOI: *10.1007/s10980-019-00830-x*.

Oksanen, Jari, Gavin L. Simpson, F. Guillaume Blanchet, Roeland Kindt, Pierre Legendre, Peter R. Minchin, R.B. O'Hara, Peter Solymos, M. Henry H. Stevens, Eduard Szoecs, Helene Wagner, Matt Barbour, Michael Bedward, Ben Bolker, Daniel Borcard, Gustavo Carvalho, Michael Chirico, Miquel De Caceres, Sebastien Durand, Heloisa Beatriz Antoniazi Evangelista, Rich FitzJohn, Michael Friendly, Brendan Furneaux, Geoffrey Hannigan, Mark O. Hill, Leo Lahti, Dan McGlinn, Marie-Helene Ouellette, Eduardo Ribeiro Cunha, Tyler Smith, Adrian

Stier, Cajo J.F. Ter Braak, and James Weedon (2022). *vegan: Community Ecology Package*. URL: *https://CRAN.R-project.org/package=vegan*.

Paerl, Hans W. and Valerie J. Paul (2012). "Climate change: Links to global expansion of harmful cyanobacteria". In: *Water Research*. Cyanobacteria: Impacts of climate change on occurrence, toxicity and water quality management 46.5, pp. 1349–1363. DOI: *10.1016/j.watres.2011.08.002*.

Pante, Eric and Phillip Dustan (2012). "Getting to the Point: Accuracy of Point Count in Monitoring Ecosystem Change". In: *Journal of Marine Biology* 2012, e802875. DOI: *10.1155/2012/802875*.

Paszke, Adam, Sam Gross, Francisco Massa, Adam Lerer, James Bradbury, Gregory Chanan, Trevor Killeen, Zeming Lin, Natalia Gimelshein, Luca Antiga, Alban Desmaison, Andreas Kopf, Edward Yang, Zachary DeVito, Martin Raison, Alykhan Tejani, Sasank Chilamkurthy, Benoit Steiner, Lu Fang, Junjie Bai, and Soumith Chintala (2019). "PyTorch: An Imperative Style, High-Performance Deep Learning Library". In: *Advances in Neural Information Processing Systems 32*. Curran Associates, Inc., pp. 8024–8035. URL: *http://papers.neurips.cc/paper/9015-pytorch-an-imperative-style-high-performance-deep-learning-library.pdf*.

Pedregosa, F., G. Varoquaux, A. Gramfort, V. Michel, B. Thirion, O. Grisel, M. Blondel, P. Prettenhofer, R. Weiss, V. Dubourg, J. Vanderplas, A. Passos, D. Cournapeau, M. Brucher, M. Perrot, and E. Duchesnay (2011). "Scikit-learn: Machine Learning in Python". In: *Journal of Machine Learning Research* 12, pp. 2825–2830.

Pratchett, Morgan S, Andrew S Hoey, and Shaun K Wilson (2014). "Reef degradation and the loss of critical ecosystem goods and services provided by coral reef fishes". In: *Current Opinion in Environmental Sustainability*. Environmental change issues 7, pp. 37–43. DOI: *10.1016/j.cosust.2013.11.022*.

Rabe-Hesketh Sophia, Anders Skrondal (2004). *Generalized Latent Variable Modeling: Multilevel, Longitudinal, and Structural Equation Models*. New York: Chapman and Hall/CRC. 528 pp. DOI: *10.1201/9780203489437*.

Rashid, Ahmad Rafiuddin and Arjun Chennu (2020). "A Trillion Coral Reef Colors: Deeply Annotated Underwater Hyperspectral Images for Automated Classification and Habitat Mapping". In: *Data* 5.1, p. 19. DOI: *10.3390/data5010019*.

Rideout, Jai Ram, Greg Caporaso, Evan Bolyen, Daniel McDonald, Yoshiki Vázquez Baeza, Jorge Cañardo Alastuey, Anders Pitman, Jamie Morton, Jose Navas, Kestrel Gorlick, Justine Debelius, Zech Xu, llcooljohn, adamrp, Joshua Shorenstein, Laurent Luce, Will Van Treuren, charudatta-navare, Antonio Gonzalez, Colin J. Brislawn, Weronika Patena, Karen Schwarzberg, teravest, Jens Reeder, shiffer1, Igor Sfiligoi, nbresnick, Qiyun Zhu, Dr K. D. Murray, and Karan Sharma (2023). *biocore/scikit-bio: scikit-bio 0.5.9: Maintenance release*. Version 0.5.9. DOI: *10.5281/zenodo.8209901*.

Riitters, Kurt (2019). "Pattern metrics for a transdisciplinary landscape ecology". In: *Landscape Ecology* 34.9, pp. 2057–2063. DOI: *10.1007/s10980-018-0755-4*.

Riitters, Kurt and Peter Vogt (2023). "Mapping landscape ecological patterns using numeric and categorical maps". In: *PLOS ONE* 18.11, e0291697. DOI: *10.1371/journal.pone.0291697*.

Sandin, Stuart A., Esmeralda Alcantar, Randy Clark, Ramón de León, Faisal Dilrosun, Clinton B. Edwards, Andrew J. Estep, Yoan Eynaud, Beverly J. French, Michael D. Fox, Dave Grenda, Scott L. Hamilton, Heather Kramp, Kristen L. Marhaver, Scott D. Miller, Ty N. F. Roach, Gisette Seferina, Cynthia B. Silveira, Jennifer E. Smith, Brian J. Zgliczynski, and Mark J. A. Vermeij (2022). "Benthic assemblages are more predictable than fish assemblages at an island scale". In: *Coral Reefs* 41.4, pp. 1031–1043. DOI: *10.1007/s00338-022-02272-5*.

Sandin, Stuart A., Jennifer E. Smith, Edward E. DeMartini, Elizabeth A. Dinsdale, Simon D. Donner, Alan M. Friedlander, Talina Konotchick, Machel Malay, James E. Maragos, David Obura, Olga Pantos, Gustav Paulay, Morgan Richie, Forest Rohwer, Robert E. Schroeder, Sheila Walsh, Jeremy B. C. Jackson, Nancy Knowlton, and Enric Sala (2008). "Baselines and Degradation of Coral Reefs in the Northern Line Islands". In: *PLOS ONE* 3.2, e1548. DOI: *10.1371/journal.pone.0001548*.

Teague, Jonathan, John C. C. Day, Michael J. Allen, Thomas B. Scott, Eric J. Hochberg, and David Megson-Smith (2023). "A Demonstration of the Capability of Low-Cost Hyperspectral Imaging for the Characterisation of Coral Reefs". In: *Oceans* 4.3, pp. 286–300. DOI: *10.3390/oceans4030020*.

United Nations, Department of Economic and Population Division. Working Paper No. ESA/P/WP.241. Social Affairs (2015). *World Population Prospects: The 2015 Revision, Key Findings and Advance Tables*.

Van Duyl, Fleur C. (1985). *Duyl 1985 Atlas living reefs Caracao and Bonaire*.

WAITTS-Institute (2017). *MARINE SCIENTIFIC ASSESSMENT: The State of Curaçao's Coral Reefs*. URL: *https://www.waittinstitute.org/_files/ugd/47d1fd_b3e7537b9084480cbe31034de70ed7b8.pdf*.

Warton, David I., F. Guillaume Blanchet, Robert B. O'Hara, Otso Ovaskainen, Sara Taskinen, Steven C. Walker, and Francis K. C. Hui (2015). "So Many Variables: Joint Modeling in Community Ecology". In: *Trends in Ecology & Evolution* 30.12, pp. 766–779. DOI: *10.1016/j.tree.2015.09.007*.

Wilkinson, Clive R. (1999). "Global and local threats to coral reef functioning and existence: review and predictions". In: *Marine and Freshwater Research*. DOI: *10.1071/MF99121*.

Wyatt, Mathew, Ben Radford, Nikolaus Callow, Mohammed Bennamoun, and Sharyn Hickey (2022). "Using ensemble methods to improve the robustness of deep learning for image classification in marine environments". In: *Methods in Ecology and Evolution* 13.6, pp. 1317–1328. DOI: *10.1111/2041-210X.13841*.

Zhong, Zilong, Jonathan Li, Zhiming Luo, and Michael Chapman (2018). "Spectral–Spatial Residual Network for Hyperspectral Image Classification: A 3-D Deep Learning Framework". In: *IEEE Transactions on Geoscience and Remote Sensing* 56.2, pp. 847–858. DOI: *10.1109/TGRS.2017.2755542*.

Chapter 4

Seeing the Forest for the Trees: Mapping Cover and Counting Trees from Aerial Images of a Mangrove Forest Using Artificial Intelligence

Daniel Schürholz [1,2], *Gustavo Adolfo Castellanos-Galindo* [3,4,5], *Elisa Casella* [2,6], *Juan Carlos Mejía-Rentería* [7] *and Arjun Chennu* [2]

Manuscript status

Published as Daniel Schürholz, et al. (2023). "Seeing the Forest for the Trees: Mapping Cover and Counting Trees from Aerial Images of a Mangrove Forest Using Artificial Intelligence". In: *Remote Sensing* 15.13. Publisher: Multidisciplinary Digital Publishing Institute, p. 3334. DOI:10.3390/rs15133334.

[1]Max Planck Institute for Marine Microbiology, 28359 Bremen, Germany
[2]Leibniz Centre for Tropical Marine Research (ZMT), 28359 Bremen, Germany
[3]Leibniz Institute of Freshwater Ecology and Inland Fisheries (IGB), 12587 Berlin, Germany
[4]Institute of Biology, Freie Universität Berlin, 14195 Berlin, Germany
[5]Smithsonian Tropical Research Institute, Balboa, Republic of Panama
[6]Department of Environmental Sciences, Informatics and Statistics, Ca' Foscari University of Venice, 30172 Venice, Italy
[7]Grupo de Investigación en Ecología de Estuarios y Manglares, Departamento de Biología, Universidad del Valle, 25360 Cali, Colombia

4.1 Abstract

Mangrove forests provide valuable ecosystem services to coastal communities across tropical and subtropical regions. Current anthropogenic stressors threaten these ecosystems and urge researchers to create improved monitoring methods for better environmental management. Recent efforts that have focused on automatically quantifying the above-ground biomass using image analysis have found some success on high resolution imagery of mangrove forests that have sparse vegetation. In this study, we focus on stands of mangrove forests with dense vegetation consisting of the endemic *Pelliciera rhizophorae* and the more widespread *Rhizophora mangle* mangrove species located in the remote Utría National Park in the Colombian Pacific coast. Our developed workflow used consumer-grade Unoccupied Aerial System (UAS) imagery of the mangrove forests, from which large orthophoto mosaics and digital surface models are built. We apply CNNs for instance segmentation to accurately delineate (33% instance Average Precision) individual tree canopies for the *Pelliciera rhizophorae* species. We also apply CNNs for semantic segmentation to accurately identify (97% precision and 87% recall) the area coverage of the *Rhizophora mangle* mangrove tree species as well as the area coverage of surrounding mud and water land-cover classes. We provide a novel algorithm for merging predicted instance segmentation tiles of trees to recover tree shapes and sizes in overlapping border regions of tiles. Using the automatically segmented ground areas we interpolate their height from the digital surface model to generate a digital elevation model, significantly reducing the effort for ground pixel selection. Finally, we calculate a canopy height model from the digital surface and elevation models and combine it with the inventory of *Pelliciera rhizophorae* trees to derive the height of each individual mangrove tree. The resulting inventory of a mangrove forest, with individual *P. rhizophorae* tree height information, as well as crown shape and size descriptions, enables the use of allometric equations to calculate important monitoring metrics, such as above-ground biomass and carbon stocks.

4.2 Introduction

For the past decades, the global area covered by mangrove forests has receded because of direct and indirect anthropogenic causes such as land use changes, deforestation, pollution and climate change (Goldberg et al. 2020). The potential impacts of the disappearance of mangrove forests to local communities and adjacent ecosystems are manifold due to the critical services that these forests provide (coastal protection (Menéndez et al. 2020), fish nurseries (Castellanos-Galindo, Krumme, et al. 2013), feeding grounds (Carugati et al. 2018), carbon sequestration (Alongi 2012), etc.). The urgency of the current state of affairs has lead to the launch of many protection, rehabilitation and reforestation efforts of mangrove forests worldwide (Ellison et al. 2020; Friess et al. 2020). For these efforts to succeed, careful observation and detailed analysis of forest

conditions are required to identify problems, calibrate predictive models and enact mitigatory management actions (Innes 1994).

The condition of most forests can be assessed on different scales: individual trees, the collection of trees in a forest stand or the complete forest ecosystem (considering biotic and abiotic factors) (Ferretti 1997). An individual tree can be assessed in the field through many indicators such as nutritional status, presence of parasites/pathogens, crown transparency, DBH, crown length and crown width (m), to provide a few examples. Then, these indicators are collected for trees in several plots, aggregating the measurements in inventories and extrapolating for trees onto the forest stand. Creating inventories of a forest enables certain ecosystem indicators to be derived, which can be its biomass (above- and below-ground), canopy structure, tree species composition and community structure (Ding et al. 2021; Guo et al. 2023). For example, to calculate the AGB for a forest using allometric equations, the following variables must be collected for each individual tree: its species, height, DBH (Chave et al. 2005) and, to calculate the canopy structure, the crown size and shape must be acquired.

The manual in situ measurement of these variables is a labor-intensive task when a forest of several hectares is surveyed, even with advances in on-ground sensing technologies (Tockner et al. 2022; J. Wang et al. 2019). Thus, a limited number of small plots are surveyed depending on the aim, the sampling costs, the extent of the forest, the tree sizes and species diversity found in a patch of forest (e.g., 35×35 m plots for trees over 50 cm DBH) (Ravindranath et al. 2008). There is a trade-off between the sampling cost and the accepted uncertainties that appear when extrapolating the measurements to the complete forest area (Persson et al. 2022). Recent studies suggest that field surveys entail significant errors in measurement and plot positions (Persson et al. 2022; Zang et al. 2023). As in other intertidal systems, in-situ plot measurements in mangrove forests can be difficult to execute, given that tidal regimens, muddy terrain, pneumatophores and stilt roots, remote locations and other factors severely reduce the accessibility. Furthermore, DBH can be difficult to measure for some mangrove species (i.e., *Rhizophora mangle*), due to their complex trunk-growing structure (Clough et al. 1997), and correct crown size and shape is difficult to measure visually, given the irregular shape and clumpiness of the canopies (Yin et al. 2019).

In recent decades, researchers have used fly-over strategies to capture plane-view images of forests to use for inventory creation. This has been fueled by the advancements in remote sensing, image analysis and machine learning. These advancements have enabled analyses of mangrove forests and their dynamics across vast scales (Hai et al. 2022; Samanta et al. 2021; Thomas et al. 2018). In these studies, spectral indices, such as normalized difference vegetation index, are calculated for each pixel to describe and classify mangrove forests, being able to label the tree species and tree density within a pixel, as well as canopy width and forest fragmentation (Hai et al. 2022). The benefits of Earth-observation technologies are the large spatial coverage and frequent acquisition of images. Paired with machine learning automation, studies of long time-series of

images can be carried out. Recent improvements in satellite image resolutions (i.e., 0.031 m for the World-View 3 satellite) have allowed for more resolved classification of trees using semantic segmentation neural networks (Ulku et al. 2022; Z. Wang et al. 2023), detection of individual trees using instance segmentation networks (Flood et al. 2019; G. Braga et al. 2020; Khan et al. 2018; Lassalle, Ferreira, et al. 2022) and detection of mangrove forest clearings (Lassalle and Souza Filho 2022) on high-resolution RGB images. Nonetheless, the calculation of certain variables, such as the height of trees extracted from canopy height models (CHMs) is error-prone at the current resolution of satellite imagery and should be paired with low-flying platforms, such as planes or UASs (Lassalle, Ferreira, et al. 2022) for better validation and performance.

Several recent studies have pointed out and demonstrated the value offered by UASs for monitoring coastal environments, such as mangrove forests (Castellanos-Galindo, Casella, et al. 2019; Joyce et al. 2023; Otero et al. 2018; Ruwaimana et al. 2018). The imagery taken with UASs can be processed with SfM software to produce geo-referenced orthorectified photo-mosaics (orthomosaics) and DSMs. Paired with novel image segmentation techniques, precise area coverage of individual tree species in a forest are determined and other surrounding land cover classified (i.e., grass, shrubs, water, sand, mud, etc.) (Kattenborn, Eichel, et al. 2019; Schiefer et al. 2020). Certain terrain classes such as mud and sand are used to calculate the height of forest canopies or of individual trees by subtracting their elevation from the elevation of trees in the DSM (Miraki et al. 2021; Navarro et al. 2020). Furthermore, using hyperspectral and multispectral cameras yielding high-dimensional input data, the area covered by multiple tree species in a forest can be accurately segmented (La Rosa et al. 2021). Individual tree crown segmentation, delineation and classification can be facilitated by the advancement of machine learning algorithms on the high resolution RGB and LiDAR images of low-flying platforms (Weinstein et al. 2020). Recent studies segmented mangrove trees in forest plots using images from RGB or LiDAR sensors mounted on a consumer-grade UASs together with OBIA algorithms, and compare the predicted segments to on-ground measurements (Navarro et al. 2020; Wannasiri et al. 2013; Yin et al. 2019). Despite the success of OBIA algorithms on UAS images to detect mangrove trees, they rely upon tree crowns that are visually well separated and detailed elevation maps. The potential benefit of state-of-the-art instance segmentation techniques is to handle dense canopies and rely only on imaging data. A recent review (Kattenborn, Leitloff, et al. 2021) of deep learning applications for tree crown segmentation noted the potential of instance segmentation applications, hindered mainly due to the insufficient training data. The development of instance segmentation workflows of high resolution RGB images acquired from consumer-grade UASs is critical to be used as validation for global Earth-observation efforts and as preparation for improved resolution in future satellite sensors.

In this work, we develop and present a complete workflow to delineate individual trees of the *Pelliciera rhizophorae* mangrove species and calculate inventory measurements (i.e., tree height, crown shape and size, geo-location, etc.), as well as map the land cover for other classes: *Rhi-*

zophora mangle, water and mud (see Figure 4.1). The input data were a set of orthomosaics and DSMs created from images captured with consumer-grade UASs in three mangrove forest stands located in the Utría National Park on the Colombian Pacific coast (Figure 4.2). We implement two separate deep learning networks: (i) a semantic segmentation neural network to identify area coverage of the two mangrove species, mud and water classes and (ii) an instance segmentation neural network to delineate individual *Pelliciera rhizophorae* mangrove trees. We present a novel tiling/untiling algorithm (from here onwards, we refer to stitching or merging tiles together as "untiling") for the correct preservation of predicted tree instances located at the edges of tiles of large orthomosaics. We also provide a comparison of three different semantic segmentation untiling techniques to resolve the overlapping borders of tiles. We automate the calculation of a CHM, created from a Digital Elevation Model (DEM) using the classified ground pixels and compare it to a DEM created from manually selected ground areas. Finally, using the delineated trees and the CHM, we provide an inventory of the trees in the mangrove forest with their specific height, crown size and crown shape as well as area cover and height distribution values for the other tree classes.

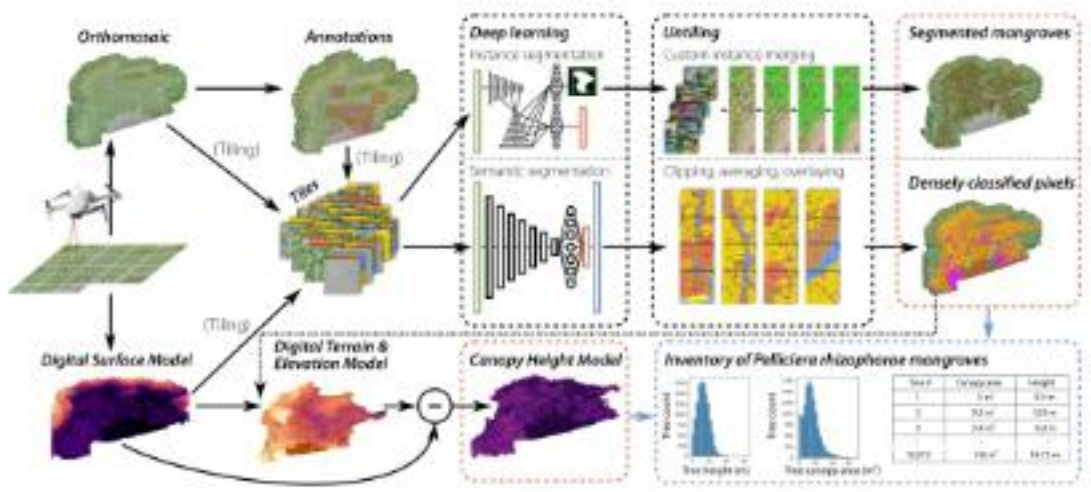

Figure 4.1 From airborne images to a detailed tree inventory: we present a workflow that creates a tree inventory for 35 hectares of a mangrove forest. The workflow starts with data acquisition using UASs flown over the mangrove forests. We then build top-down orthomosaic and DSM with SfM software. We implement a tiling and a novel untiling process of the orthomosaics and DEM images. Instance segmentation neural networks were used for detecting individual trees and semantic segmentation networks were used to map land cover. Using the classified ground regions, we created and interpolated the digital terrain model (DTM) into a DEM. Subtracting the DEM from the DSM yielded a comprehensive canopy height model. For each automatically segmented tree instance, the tree height was derived from the CHM. This creates an inventory of trees with their heights and crown areas, even in a dense forest canopy, and enables the calculation of Above Ground Biomass, an important measure for monitoring and carbon stock assessments.

4.3 Materials and Methods

The complete workflow, from data tiling to tree inventory, was developed in the Python programming language, using Snakemake (Mölder et al. 2021) to manage the analytical workflow.

4.3.1 Study Site and Input Data Structure

We focused on three mangrove forest sites of the Utría National Park: La Chunga North (LCN), Terron Colorado (TC) and Estero Grande Shore (EGS) (see Table 4.1 for area sizes). These mangrove forests are mainly comprised of two mangrove species: *Pelliciera rhizophorae* and *Rhizophora mangle*. *P. rhizophorae* is endemic to the East Pacific and Caribbean regions and is listed as vulnerable in the International Union for Conservation of Nature (IUCN) Red List for endangered species (Polidoro et al. 2010). It lives in intermediate to upstream estuarine environments with medium to high tidal ranges. The *R. mangle* species is more widespread across the Atlantic/East Pacific bio-geographic region and is listed as of "least concern" in the IUCN Red List for endangered species. It is found in downstream to intermediate estuarine environments with low to medium intertidal shifts.

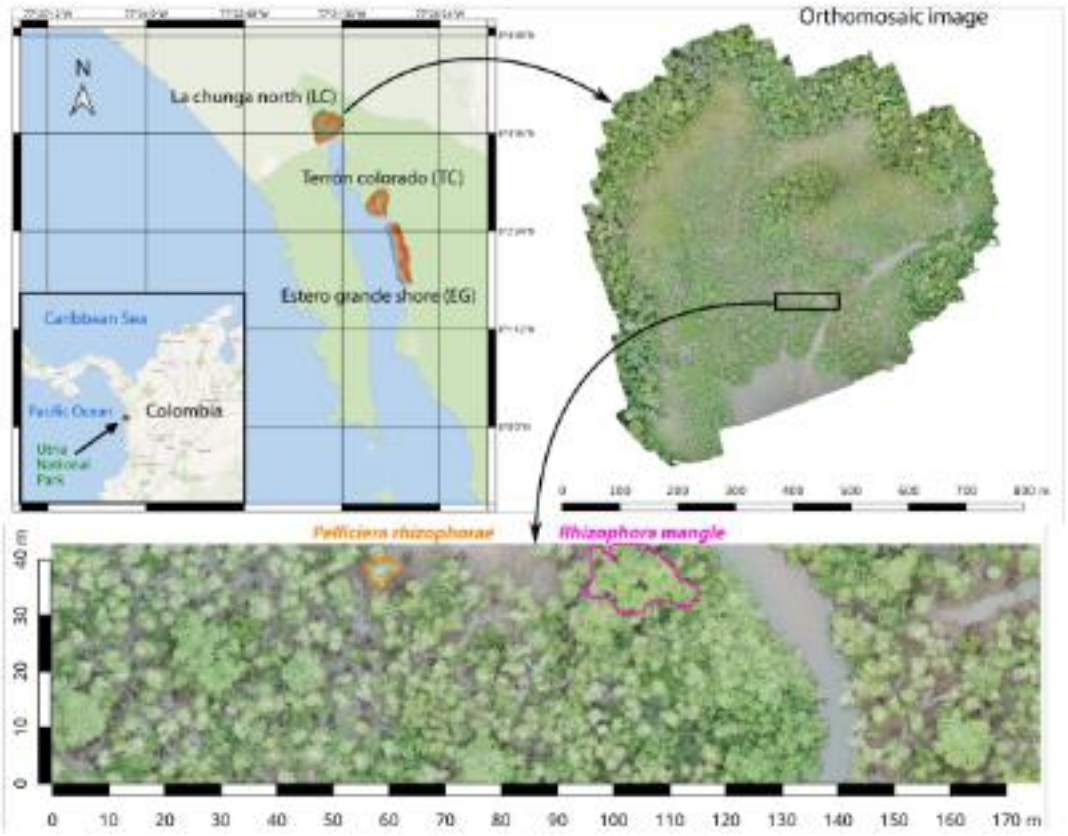

Figure 4.2 Surveying a dense canopy in a remote forest area: we used a consumer-grade UAS to survey a mangrove forest located in the Utría national park in the Colombian Pacific coast. Three surveyed plots of mangrove forests were used. For each plot large orthomosaic images were created, with fine spatial resolution (e.g., 3.64 cm/pixel) of the underlying mangrove trees. The two dominant species of mangrove trees are the *Pelliciera rhizophorae* species and the *Rhizophora mangle* species. Each of the three plots provide unique challenges for canopy segmentation, given that their conditions differ in ground composition, exposure, tidal level during the survey and lighting/blurring in the images.

The aerial footage of the sites was captured in 2019 (19–22 February) using two consumer-grade UASs the DJI Phantom 4 and DJI Mavic Pro (SZ DJI Technology Co., Ltd – Shenzhen, Guangdong, China). The DJI Phantom 4 has an integrated photo camera, the DJI FC330, which has a 1/2.3″ CMOS sensor with 12.4 M effective pixels, a focal length of 4 mm, a pixel size of $1.56 \times 1.56\ \mu m$ and a resolution of 4000×3000 pixels (px). The DJI Mavic Pro was equipped with the integrated DJI FC220 camera with 4000×3000 px resolution, 12.35 M effective pixels and 26 mm wide-angle lens. The flights were programmed to follow the trajectories in an automated mode by means of the commercial app "DroneDeploy". Ground control points (GCPs) were positioned in the field, and their geographic location was acquired. We used two single-band

Table 4.1 Mangrove forest study sites and digital products details.

	La Chunga North (LCN)	**Terron Colorado (TC)**	**Estero Grande Shore (EGS)**
UAS images			
Quantity	289	346	106
Areas			
Surveyed	367,806 m^2	241,752 m^2	425,851 m^2
Mangrove forest	223,456 m^2	120,726 m^2	110,960 m^2
Annotated	50,347 m^2	28,410 m^2	—
Resolutions			
Ortho. image	$19,855 \times 21,068$ px	$16,375 \times 18,923$ px	$10,478 \times 24,485$ px
Ortho. pixel	3.64 cm/px	3.27 cm/px	5.83 cm/px
DSM image	$15,145 \times 15,377$ px	$13,148 \times 13,454$ px	$6759 \times 15,468$ px
DSM pixel	7.29 cm/px	6.55 cm/px	11.7 cm/px
GCPs			
Quantity	3	2	4
*RMSE **	0.011 m	0.0097 m	1.13 m
Tiles **			
Total	3304	2438	2070
Annotated	196	168	—

* Root-mean-square error (RMSE) for ground control points (GCP) over all (X,Y,Z) coordinates. ** Tiles of size 512×512 pixels with 30% overlap.

global navigation satellite system (GNSS) receivers: an Emlid Reach RS+ single-band real-time kinematics (RTK) GNSS receiver (Emlid Tech Kft. – Budapest, Hungary) as a base station, and a Bad Elf GNSS Surveyor handheld GPS (Bad Elf, LLC – West Hartford, Arizona, USA). RINEX static data from the base station was processed with the Precise Point Positioning Service (PPP) of the Natural Resources of Canada (*https://webapp.csrs-scrs.nrcan-rncan.gc.ca/geod/tools-outils/ppp.php*, accessed on 26th June 2023), while rover position was processed using the RTKLib software (*https://rtklib.com/*, accessed on 26th June 2023) through a post processed kinematics (PPK) workflow. The final absolute positional accuracy of the products is below one meter because the results of the PPP workflow has a positional accuracy between 0.2 m and 1 m. The acquired images and GCPs were analyzed and used as inputs in the software Agisoft Metashape Professional 1.6.2 (*https://www.agisoft.com/*, accessed on 26th June 2023). With this SfM-MVS (structure from motion-multi-view stereo reconstruction) method we created an orthomosaic and a digital surface model for each site, similar to a previous study in the same

geographic region (Castellanos-Galindo, Casella, et al. 2019). Table 4.1 shows more details about the photogrammetric products.

4.3.2 Annotations

The preparation of the image data for machine learning started with the annotation of classes of interest. The LCN and TC sites were used for training and testing the deep neural networks; the EGS site was used as an out-of-distribution dataset. In the created orthomosaics it was easy to visually distinguish the regions of mangrove forest from the surrounding terrestrial forest. We delimited the area of the mangrove forest to only use this region during the prediction by the machine learning process (see orange outline in Figure 4.3 and Table 4.1 for area sizes). In LCN, 61% of the area is covered by mangrove forest, in TC 50% is covered by mangrove forest and in EGS 26% of the area is covered in mangrove forest. Inside the mangrove forest stands of LCN and TC, we selected three subplots per site to annotate the classes manually, specifically for the machine learning training process (see red outline in Figure 4.3; see Table 4.1 for the area sizes). In LCN, 22% of the mangrove forest area was annotated and in TC 24% was annotated.

Inside these subplots, different types of annotations were made for training semantic segmentation and instance segmentation CNNs (Figure 4.3). For semantic segmentation networks, pixel annotations were required. We selected *P. rhizophorae*, *R. mangle*, short-sized *R. mangle*, water and mud as our target classes (see Table 4.2A for annotation numbers). It was possible to visually differentiate between *P. rhizophorae* and *R. mangle* species in most cases. In some areas, distinct short-sized and shrub-like tree patches were visible. After comparing to on-ground images it was clear that these patches were comprised of short-sized *R. mangle*. Water pixels were also manually annotated. After these annotations were finished, the remaining non-annotated pixels were labeled as mud.

Tree instances were only marked for the *P. rhizophorae* species. Each tree was visually identified on the orthomosaic images and delineated using shapes in QGIS v3.12 (*https://www.qgis.org*, accessed on 26 June 2023). In total, 4611 *P. rhizophorae* trees were annotated, 2855 in LCN and 1756 in TC (Table 4.2B). Individual *R. mangle* trees were difficult to visually delineate, and therefore areas of contiguous canopy of this species were annotated.

4.3.3 Data tiling

The large sizes of the orthomosaic files (i.e., $21,068 \times 19,855$ pixels for LCN, 1.3 GB) are not directly suited for supervised learning with neural networks due to computational restrictions. In machine learning pipelines, the large orthomosaics are processed by taking smaller tiles as the processing unit. We implemented tiling with windows of a fixed size of 512×512 pixels (around

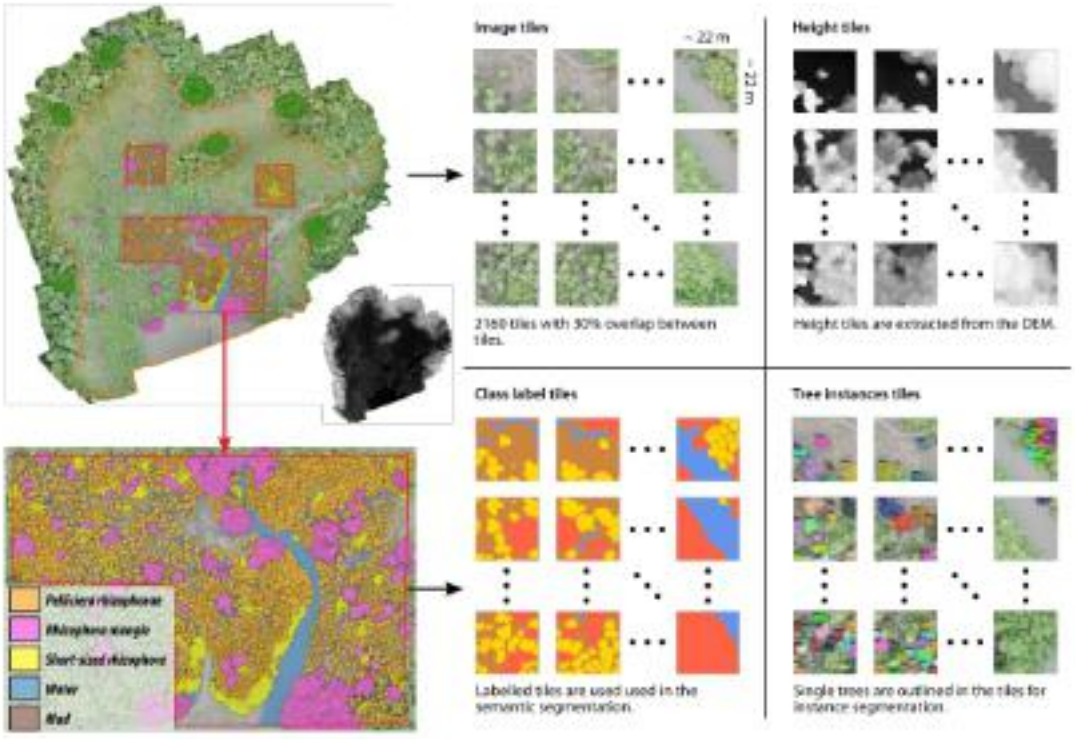

Figure 4.3 Annotating and tiling for AI: within the orthomosaics, working regions were marked, inside which the mangrove forests were considered for further classification (see orange lines). Inside sub-regions (red polygons), annotations were created for 5 classes (*Pelliciera rhizophorae*, *Rhizophora mangle*, short-sized *R. mangle*, water and mud). The areal annotations were used for semantic segmentation and the individual *P. rhizophorae* tree annotations were used in instance segmentation. The large orthomosaic images and their corresponding annotations were tiled using different strategies and allowed to downsize the classification problem to fit within the constraints of our computational resources. Different combinations of input signals from the plots were used by merging color pixels and the height information from the DSM.

17×17 m), which allows for an average of 30 trees of the *P. rhizophorae* species inside each tile. The tiling can be done with or without overlap between adjacent tiles to reduce uncertainties of predictions around tile borders by the CNNs. Using overlap also requires us to merge tree instances that are split between the borders of 2 or more tiles. We selected 30% overlap between tiles (154×512 pixels), allowing *P. rhizophorae* tree masks to maintain their complete shape in at least one tile. Identical tiling procedures were applied to all four linked layers of each study site: the orthomosaic, the elevation image (DSM), the class annotation regions and the tree annotations (Figure 4.3).

Table 4.2 (**A**) Pixel-wise and (**B**) tree-wise annotation details per site.

(A) Pixel-wise annotations for semantic segmentation			
Label	**La Chunga North**	**Terron Colorado**	**Total**
Pelliciera rhizophorae	24,304 m^2	10,268 m^2	34,572 m^2
	17,753,335 px	9,429,282 px	27,182,617 px
	(48%)	(35%)	(42%)
Rhizophora mangle	7998 m^2	6637 m^2	14,635 m^2
	5,842,042 px	6,094,429 px	11,936,471 px
	(16%)	(22%)	(19%)
Short-sized *Rhizophora mangle*	3716 m^2	629 m^2	4345 m^2
	2,714,167 px	577,334 px	3,291,501 px
	(8%)	(2%)	(5%)
Water	2214 m^2	1239 m^2	3453 m^2
	1,617,468 px	1,137,770 px	2,755,238 px
	(4%)	(4%)	(5%)
Mud	12,115 m^2	9637 m^2	21,752 m^2
	8,849,536 px	10,020,035 px	18,869,571 px
	(24%)	(37%)	(29%)
(B) Tree-wise annotations for instance segmentation			
Label	**La Chunga North**	**Terron Colorado**	**Total**
Pelliciera rhizophorae	2855 trees	1756 trees	4611 trees

* Pixel-wise annotation percentages are relative to the total annotated area in each plot.

4.3.4 Deep Learning: Semantic and Instance Segmentation Networks

We used two separate CNNs: a semantic segmentation network for dense pixel-wise predictions and an instance segmentation for delineation of *P. rhizophorae* trees (Figure 4.4). As input for both networks, we used the RGB tiles extracted from the orthomosaic images and the elevation tiles extracted from the DSM. We also ran the process with RGB + height tiles but a preliminary analysis showed no real benefit to considering the height information for the deep learning process. Thus, for the data experiments and final predictions, we only considered RGB tiles.

We implemented the DeepLabV3+ (Chen et al. 2018) semantic segmentation network with the Detectron2 Python library (Wu et al. 2019), which is build on the PyTorch machine learning library (Paszke et al. 2019). This algorithm has been successfully applied towards pixel-wise segmentation of natural habitats in top-down images (Alonso et al. 2019; Pavoni, Corsini, Callieri, et al. 2020). A recent study (La Rosa et al. 2021) used a modified version of DeepLab for

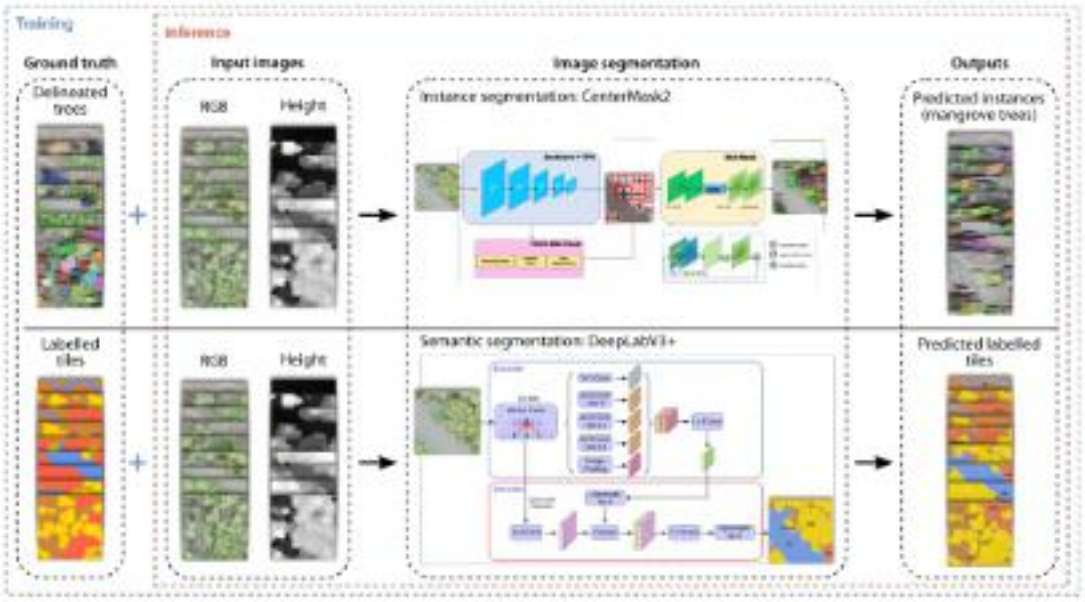

Figure 4.4 Two networks to rule them all: our workflow uses AI to convert orthomosaics of the mangrove forests into habitat maps and a tree inventory. The input of an RGB, height or RGB+height tile goes through a series of convolutional filters to extract deep features. The instance segmentation network CenterMask2 uses a spatial attention module to suggest prediction masks inside bounding boxes, which potentially delineate the canopy of individual *P. rhizophorae* trees. The semantic segmentation network uses an encoder and decoder framework to assign one of five semantic labels (see Figure 4.3) to each pixel. The network architecture illustrations are adapted from (Lee and Park 2020) for CenterMask2 and from (Chen et al. 2018) for DeepLabV3+.

semantic segmentation of hyperspectral images in Brazilian forests. We selected the ResNet-101 backbone for the DeepLabV3+ architecture, which also uses separate atrous convolutional layers to ensure higher-resolution outputs and reduce execution time. Starting from network weights from training with the ImageNet dataset, we retrained the whole network parameters with our image data. For training, we used 300 tiles in batches of 4, and employed 15,000 iterations in total. For the optimizer, we used a learning rate scheduler with polynomial decay (weight decay of 0.001) and warm-up period of 1000 iterations, developed for the DeepLab network. We use an initial learning rate of 0.01, a "hard pixel mining" loss function, and a loss weight of 1. The DeepLab network was trained on two NVIDIA RTX 2080 Ti GPUs (NVIDIA, Inc. – Santa Clara, California, USA) with 12 GB of memory each. The annotation input for the training of the network were densely annotated tiles (see Figure 4.3). The outputs of the semantic segmentation network were vectors of five class probabilities for each pixel in a tile. The highest probability value was selected as the class prediction in each pixel.

For instance segmentation, we implemented the CenterMask2 network on the Detectron2 framework, an improved version of the CenterMask instance segmentation network (Lee and Park

2020). The authors show that CenterMask2 outperforms the more commonly used MaskRCNN (mask region-based convolutional neural network), which has been recently used in tree segmentation studies (Chiang et al. 2020; G. Braga et al. 2020; Hao et al. 2021). CenterMask2 is an anchor-free one-stage instance segmentation network that implements a spatial attention-guided mask. The pretrained backbone (on the ImageNet dataset) we used was the VoVNetV2-99 network (Lee, Hwang, et al. 2019), and its stem and first residual module parameters were frozen. The network ran for 15,000 iterations with batches of 16 images. It used a warm-up multi-step learning rate scheduler, with 0.001 weight decay, 1000 warm-up iterations and steps at 10,000 and 13,000 iterations. The CenterMask2 network ran on two NVIDIA RTX 3090 Ti GPUs with 24 GB memory each. The annotation input for the training of the network were common objects in context (COCO)-style JSON files with tree shape descriptions and locations on the annotated tiles (see Figure 4.3). The output of the instance and segmentation networks were *P. rhizophorae* tree instance descriptions with bounding boxes, locations, masks and mask prediction scores (prediction confidence). On average, the training of the network took 3 h and 20 min for each experiment.

Given the low number of total training tiles (364) across sites, we used augmentations for both networks, with random flips of the images, cropping and rotations with the Detectron2 training pipeline. We analyzed the amount of data (before augmentation) needed for a better performance of the instance segmentation network. After separating 10% of the tiles as a testing dataset, we created several training datasets using 50%, 60%, 70%, 80% and 90% of the remaining tiles, thus ensuring a consistent testing dataset with no overlap with the training datasets (Figure 4.5a). We also compared the performance when considering "empty" tiles in the training set, in which no *P. rhizophorae* instance was present, to not over-fit the network. As a measure of performance for instance segmentation we used the mean Average Precision (AP) as defined by the COCO dataset (*https://cocodataset.org/#detection-eval*, accessed on 26 June 2023). This index measures the percentage of predicted instance masks for which the IoU (intersection over union) with the ground-truth annotation is larger than a list of 10 different thresholds. The thresholds go from 50% to 95% in steps of 5%, and then the percentages of masks with an IoU larger than the threshold at each step are averaged to get the final AP.

We trained the semantic segmentation network on 90% of the tiles and 10% testing tiles. We measured the performance of the network (Figure 4.5c) with precision (user's accuracy) and recall (producer's accuracy) confusion matrices and with the Cohen's Kappa score, overall accuracy, overall recall, overall precision and the F1-score (the harmonic mean of overall recall and precision values).

Additionally, we measured the agreement between *P. rhizophorae* and *R. mangle* predictions between the instance and semantic segmentation networks (Figure 4.5b). For this we calculated the area fraction inside instance predictions that is predicted as *P. rhizophorae* or *R. mangle* by the semantic segmentation network.

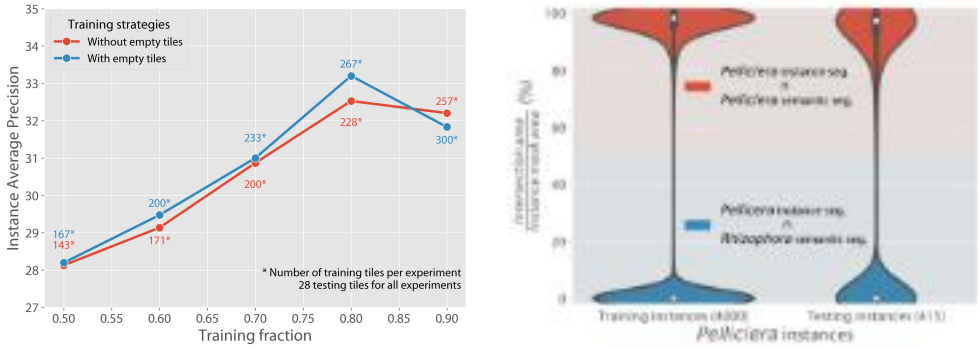

(**a**)

(**b**)

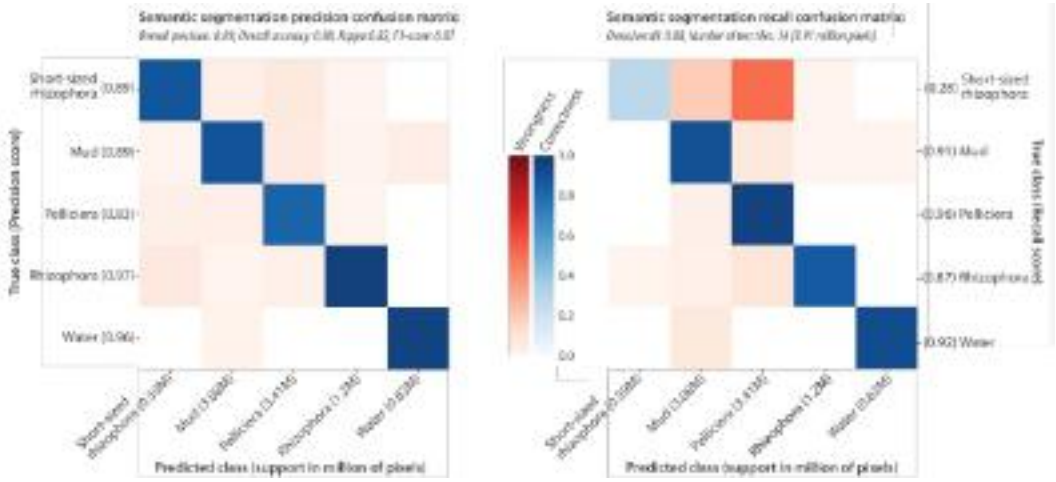

(**c**)

Figure 4.5 Evaluation of training modality: we trained the networks with 6 different classification regions annotated on 2 separate plots, looking for an optimal mix of annotation effort and generalization performance from the networks. The higher the number of tiles used in training the network the better the performance of the prediction (**a**). The best performance (33.1% instance Average Precision) was achieved with 80% of the training tiles (267), using datasets with empty tiles (tiles were no *P. rhizophorae* instance is found). In (**b**), we compared the agreement (or error) between predictions of instance and semantic segmentation networks. Agreement of *P. rhizophorae* predictions for both training and testing instances in both sites had a median of 97%. The error between *P. rhizophorae* instances and *R. mangle* areas was very low, with a mean of 2.6% overlap for training instances and 4.5% for testing instances. In (**c**), we show the semantic segmentation performance. All classes had a precision of over 80% and all classes except the short-sized *R. mangle* class had high recall scores (>87%). The low recall score of short-sized *R. mangle* (28%) shows a large confusion with the *P. rhizophorae* class.

4.3.5 Untiling Strategies

The predictions of the network on individual tiles had to be untiled back together to recover a consistent prediction over the complete mangrove forest area. Given that the tiling process was

done with overlap between the tiles, different strategies had to be applied to accurately recover and resolve the predictions in overlapping regions. The untiling process had to be implemented independently for instance segmentation and semantic segmentation predictions.

4.3.5.1 Untiling Instance Segmentation Tiles

Untiling the predicted instance tiles was done with a novel developed algorithm (see Algorithm 1 for the pseudo-code) to control the preservation of tree instances in border regions across tiles. The algorithm is controlled by two thresholds: one for the minimum predicted mask score and one for the overlap between two or more predicted instances, which intersect in the prediction. A schematic of the untiling steps is shown in Figure 4.6.

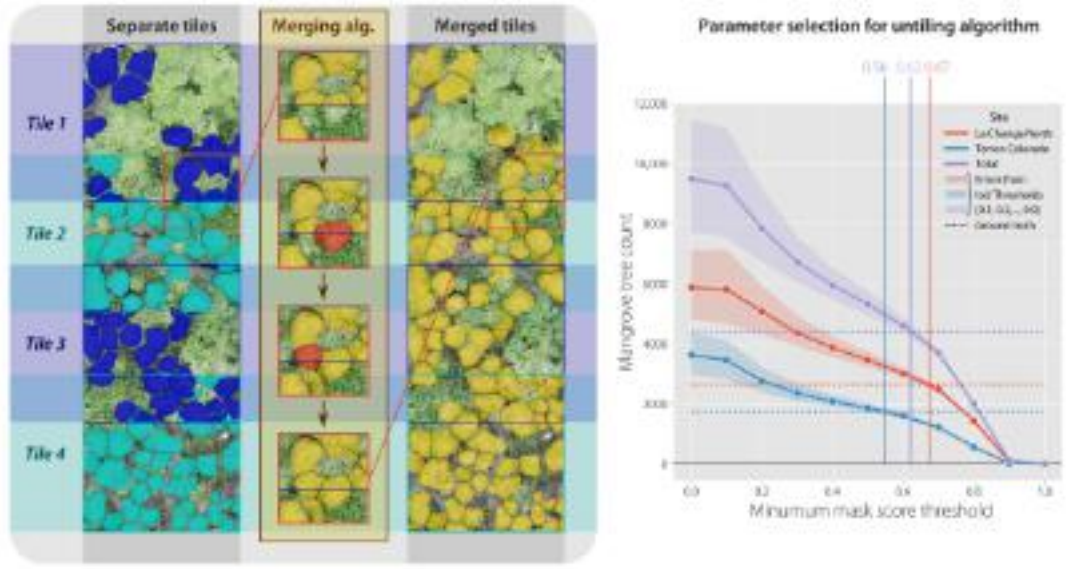

Figure 4.6 Instance untiling algorithm and parameters. We provide a heuristic algorithm for untiling the predicted instance segmentation within overlapping tiles. The algorithm works by filtering low-scoring predicted tree masks and handling overlapping tile sections with an overlap threshold to merge overlapping instances. In the illustration we show the process of merging two or more instances into one or more instance, such that a coherent shape and tree count is preserved. We calculated the ideal minimal mask score threshold and overlap threshold to preserve the original count of trees in annotated areas. For the overall scene reconstruction we found that a 0.62 minimum mask confidence threshold, together with a 0.5 overlap threshold predicted the same tree count as the original annotation count. Any change in minimum mask confidence needs an adjustment in the overlap threshold (error shown in shaded regions).

We first filter the tiles that do not have instances predicted in them. Then, we filter instances that have a prediction score (confidence) under a given threshold *mask_minimum_score* in the range $[0.0 - 1.0]$. We create an empty matrix the same size as the original orthomosaic

Algorithm 1 Tree instances untiling algorithm

```
tiles ← M(tile_width × tile_height × num_tiles × instances_per_tile)  ▷ M is a Matrix
mask_minimum_score ← α
overlap_threshold ← β
tiles ← RemoveTilesWithoutInstances(tiles)
tiles ← RemoveInstancesWithLowScores(tiles, mask_minimum_score)
untiled_map ← M0(orthomosaic_width × orthomosaic_height)  ▷ A matrix filled with zeroes
new_instance_id ← 0
for tile in tiles do
    for instance in tile.instances do
        new_instance_id ← new_instance_id + 1
        temp_tile ← Crop(untiled_map, tile.coordinates)
        intersected_instances ← temp_tile ∩ instance.mask
        merge_to_instance ← NULL
        intersected_instance ← NULL
        for intersected_instance in intersected_instances do
            intersection ← intersected_instance.mask ∩ instance.mask
            if intersection.size > (instance.size × overlap_threshold) then
                if !merge_to_instance || intersected_instance > merge_to_instance then
                    merge_to_instance ← intersected_instance
                end if
                temp_tile[intersection] ← intersected_instance.id
                instance.mask[intersection] ← False
            else
                if intersection.size > (intersected_instance.size × overlap_threshold) then
                    intersection ← intersected_instance
                    temp_tile[intersection.mask] ← new_instance_id
                    instance.mask[intersection] ← True
                end if
            end if
        end for
        if merge_to_instance ≠ NULL & intersected_instance ≠ NULL then
            temp_tile[instance.mask] ← merge_to_instance.id
            intersected_instance.size+ = intersection.size
            Delete(instance)
        else
            temp_tile[instance.mask] ← new_instance_id
        end if
        untiled_map[tile.coordinates] ← temp_tile
    end for
end for
```

image (*untiled_map*). We iterate over all remaining instances in all remaining tiles, creating a unique ID for any new instance that we keep. We crop the region corresponding to the tile in the large orthomosaic image and save it to *temp_tile*. We then calculate the overlap between the

new *instance* and every *intersected_instance*. We iterate over the overlapping instances and calculate the intersection size with the current *instance*. We compare this overlap with mask size of the current *instance* times a given *overlap_threshold* in the range [0.0–1.0] (Algorithm 1 line 17–23). If the overlap size is larger than this value, we assign the current instance pixels to one of the overlapping instances in *temp_tile*. To decide into which instance to merge, we first check that no *merge_to_instance* variable was set or that the *intersected_instance* size is larger than the previously saved instance in *merge_to_instance* (Algorithm 1 line 18–20). We then replace the intersection location in *temp_tile* with the ID of the current *intersected_instance*. We also remove the intersected area from the current *instance*. Otherwise, in case the *intersection.size* is larger than (*intersected_instance.size* × *overlap_threshold*), we assign the intersection to the current *instance* in *temp_tile* (Algorithm 1 line 24–28). Afterwards, if *merging_to_instance* is set, we assign all pixels in *temp_tile* of the current *instance* to that instance in *temp_tile* and delete the current *instance* (Algorithm 1 line 31–35), or else we just add the (remaining) parts of the current *instance* to its location in *temp_tile*. Finally, we merge the updated *temp_tile* back to the larger *untiled_map*, which after all iterations will contain tree instances without any overlap and clear crown boundaries. The algorithm's execution time is bound to the number of tiles (tile size and overlap) and number of instances predicted in each tile.

We measured the effects of the predicted mask score and overlap threshold variables by looking at which values make the count of trees closest to the original annotations in the annotation regions (Figure 4.6).

4.3.5.2 Untiling Semantic Segmentation Tiles

The predicted semantic tiles were untiled following three different strategies: overlaying, clipping and averaging (schematic in Figure 4.7). Overlaying simply places each new tile in its original position without considering any overlapped tile in that region. We overlaid tiles starting in the top left corner of the orthomosaic image, going from top to bottom, and moving to the subsequent column until the last tile is reached in the bottom right corner. This gives preference to predictions in tiles that are further down the list, where only the last tile to be untiled maintains its complete area and all other tiles maintain 49% of it (given a 30% overlap example). Clipping means that the half of the overlap region is clipped off the border of tiles and then placed in its original location on the orthomosaic. In a 30% overlap example, corner tiles retain 72% of their central area, tiles at the edge of the orthomosaic retain 60% and every other tile retains 49%. Averaging means taking the mean of network softmax values in the overlapping regions before the argmax function is used to select the predict class. In a 30% overlap example, corner tiles will have 28% of its area averaged, border tiles 40% and all other tiles 51%.

We measured the accuracy for each untiling strategies by dividing the total number of predicted pixels of every class (inside the annotation regions in each site) by the total number of pixels for

Figure 4.7 Semantic tile-merging strategies. For the semantic segmentation tiles we tried 3 different untiling strategies to recover the predicted habitat map: overlaying, clipping and averaging. We compared them to the ground truth densely annotated tiles and calculated their accuracies. No clear advantage was detected for any of the untiling strategies, which hints at the good prediction confidence of state-of-the-art semantic segmentation networks, even around borders of images.

that class in the manual annotation (Figure 4.7).

4.3.6 Digital Terrain Model, Digital Elevation Model and Canopy Height Model

After creating the untiled orthomosaics of semantic and instance segmentation predictions we created a digital terrain model, Digital Elevation Model and a canopy height model. In this study we reference DTM as a model only showing terrain features (i.e., mud and water pixels), selected from the DSM, which is the raw elevation model that considers all natural and artificial features on the map. The DEM is the result of interpolating the DTM to describe the elevation of the terrain below natural and built/artificial features. A CHM is the subtraction of a DEM from the DSM. In this study, we selected ground points in the orthomosaics to create a DTM and then interpolated the empty areas with smoothing, to generate a DEM (Miraki et al. 2021; Navarro et al. 2020).

We compared 2 strategies to select ground points and generate the DTMs. The first strategy was manually selecting ground points (in QGIS) that visually looked like mud or water region close to the mangrove trees. We corroborated that the selected region did not contain any higher elevation pixels in the DSM (corresponding to the surrounding trees), given that the initial resolutions of the orthomosaic and DSM were not identical. The manual selection of points took around 2 h for the TC site and 3 h for LCN.

The second strategy used our semantic segmentation predictions as they also contain ground pixels (mud and water classes). We use those regions to select the relevant points to interpolate into a DEM. Given that the predictions might contain errors, we used a threshold of 95% network confidence of the ground predictions to select pixels. This yields a very small number of ground predicted regions (under 0.5% of pixels). Finally, to remove residual pixels that may contain high elevation values in the DSM, we convolve a window of 2000×2000 pixels across the entire DSM and select pixels with elevation under a parameterized percentile value. The pixels that passed through this filtering were very likely to be only the ground level regions and were used as ground points for the DTM interpolation.

For both strategies, we use the Geo-spatial Data Abstraction Library's (GDAL) $fill\_no\_data$ function to interpolate and smooth out the DTM into a DEM. This function uses the inverse distance weighting (IDW) algorithm to interpolate missing values in a raster, followed by 3 smoothing passes with a 3×3 kernel. We then subtract the DSM elevation from the DEM elevation to obtain a CHM. We calculated the height of a tree by selecting the maximum elevation inside its contoured shape from the CHM.

We illustrate the complete process in Figure 4.8. We compared the resulting elevation of the trees using both strategies by plotting them against each other, and by comparing the bias of the mean and the 95% limit of agreement using Bland–Altman (or mean-difference) plots (Figure 4.8). We use the first "manual" ground pixel selection strategy as control for the second "automatic" ground pixel detection strategy.

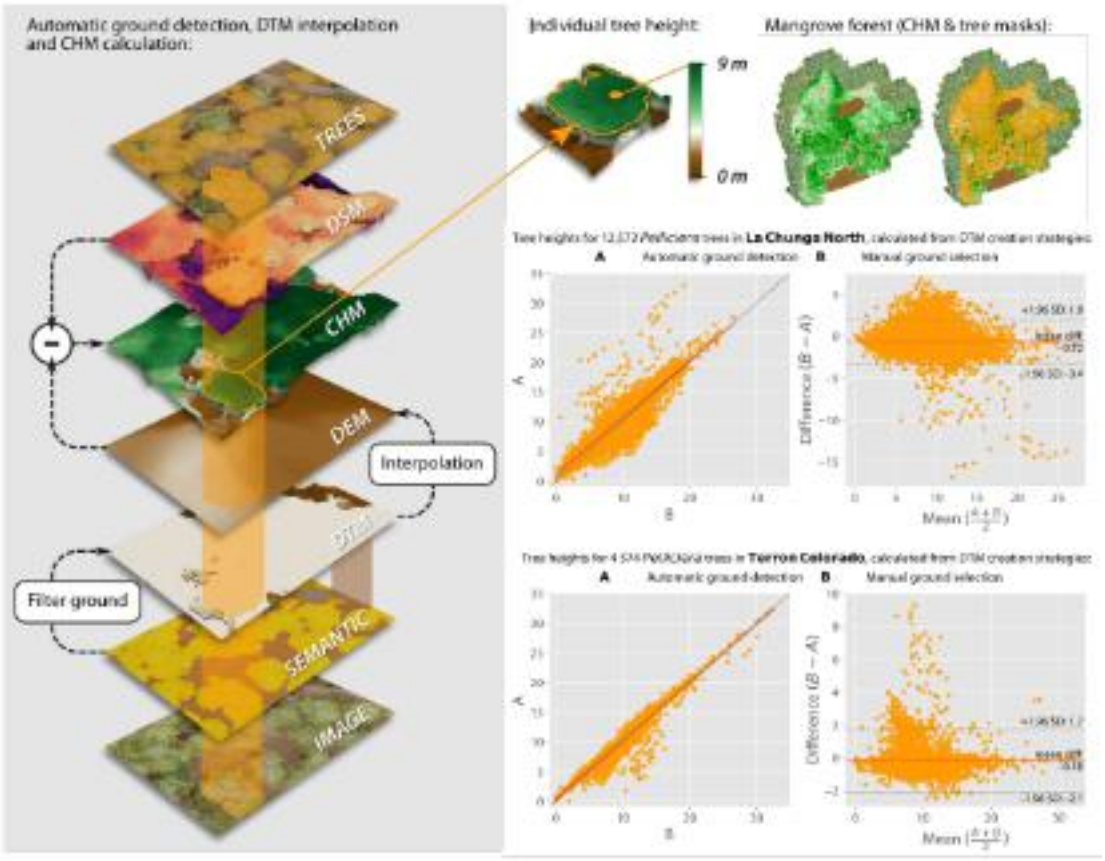

Figure 4.8 Digital Elevation Model (DEM) and canopy height model (CHM) strategy comparison: we illustrate our automatic ground selection and interpolation process. From the semantic segmentation predictions we select and filter high confidence ground pixels, which we then use to interpolate the DSM values in the corresponding ground locations. We subtract the DSM values from the DEM to generate a CHM. Finally we "cookie-cut" the predicted tree instances on the CHM to calculate height statistics of the tree crown. We check if the automatically extracted DEM is correlated to a DEM generated from manually selected ground regions in the plot. The tree heights from both methods did not show a significant bias for either technique as shown in the regression plots and mean-difference plots for both LCN and TC sites. Outliers can be caused by imperfections in the original DSM.

4.3.7 Forest Inventory

We summarize the attributes of the automatically delineated trees, such as crown shapes and heights, into an inventory of the forest (Figure 4.9). We calculate mean and maximum pixel heights inside predicted tree crown shapes for both DEM creation strategies. We also calculate and plot the tree crown diameter from the major axis of the ellipsis with the same second moment as the crown polygon. Other metrics calculated from the instance contour are the tree crown eccentricity, which is the ratio of the focal distance (distance between focal points on the ellipsis

covering the tree crown shape) over the major axis length (a value of 0 means the shape is a perfect circle), and tree crown area in square meters. We also plot the tree height in meters against the canopy area in square meters using a linear regression plot. These measurements were extracted with the "regionprops" function of the "scikit-image" Python library (Walt et al. 2014).

Finally, having the trained pipeline, we tile, predict the semantic and instance segmentation outputs and untile the out-of-distribution EGS site. In order to measure the scalability of the method, we then compare *P. rhizophorae* tree heights and tree crown areas for all three sites. We also compare the area cover of the *R. mangle* and the *P. rhizophorae* species as well as that of the short-sized *R. mangle* class from the semantic segmentation predictions. Finally, we calculate the pixel-wise height distributions in the CHMs for area-wise predictions of the three tree classes.

4.4 Results

The presented workflow allows for automatic delineation of individual *P. rhizophorae* trees and the segmentation of *R. mangle* canopy areas, as well as other land cover classes (mud and water). We review the accuracy of both instance and semantic segmentation networks, as well as of the untiling of the predicted tiles, and finally of the automatic calculation of tree measurements, such as height from the generated CHM.

4.4.1 Deep Learning Performance

We measured the performance of both instance and semantic segmentation networks separately but also compared their agreement on predictions for the *P. rhizophorae* class and overlap with the *R. mangle* class.

In Figure 4.5a, we show the performance of the CenterMask2 network when both tiles with *P. rhizophorae* instances and tiles without *P. rhizophorae* instances were considered in the training procedure. For both cases, the performance peaked with 80% of the training tiles (228 tiles without and 267 with empty tiles). When considering empty tiles, the AP was 33.2% and without the empty tiles it was 32.6%. With the 90% training fraction, the performance reduced by 1.2% when considering empty tiles and only by 0.3% when not. The best performing network was used for the final tile predictions.

The performance metrics for the semantic segmentation network are shown in Figure 4.5c. The overall precision for the network was 89%, the overall recall 88%, the F1-score was 87%, the overall accuracy was 88%, and the Kappa score was 82%. The precision confusion matrix also shows the per-class performance, where *R. mangle* has the highest score

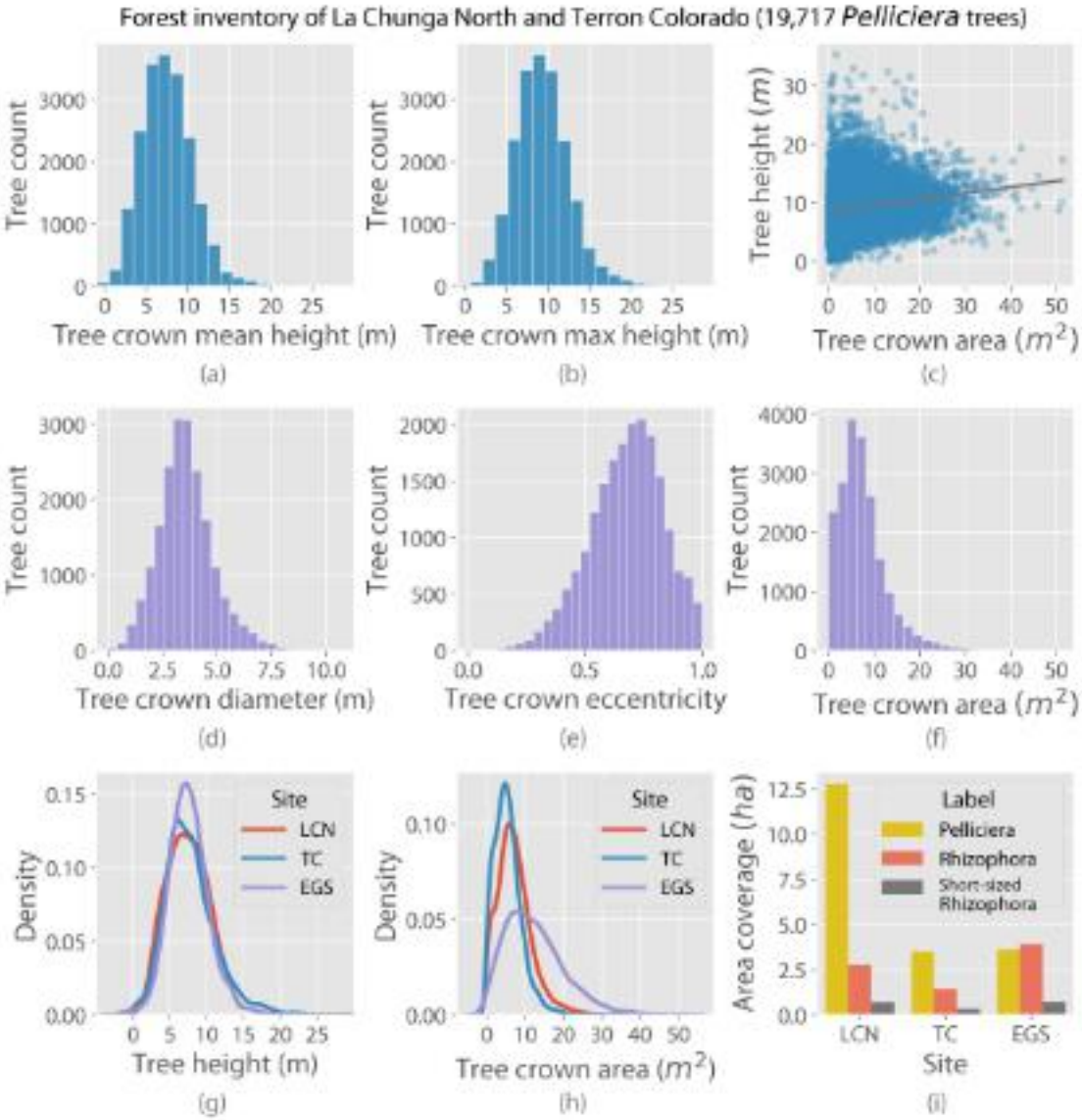

Figure 4.9 Combined inventory of the La Chunga North and Terron Colorado mangrove forest plots. We measured the (**a**) mean height and (**b**) maximum height in predicted *P. rhizophorae* instances as well as (**d**) tree crown diameter, (**e**) eccentricity and (**f**) area. We plotted (**c**) tree height against tree crown area. We compare (**g**) the tree heights and (**h**) tree crown areas of *P. rhizophorae* from the training sites LCN and TC with the out-of-distribution site Estero Grande Shore. We also compare the (**i**) area coverage of *P. rhizophorae*, *R. mangle* and short-sized *R. mangle* across the three sites.

(97%), followed by water (96%), mud (89%) and short-sized *R. mangle* (89%) and finally *P. rhizophorae* (83%). In the recall matrix, the highest value was for *P. rhizophorae* with 96%,

while by far the lowest was the short-sized *R. mangle*, with 28%. The major confusion that affected the recall values was between *P. rhizophorae*, mud and short-sized *R. mangle*. Other minor confusions occurred between water and mud and between short-sized *R. mangle* and *R. mangle*.

The two networks showed good overlap between their *P. rhizophorae* predictions, with median values of 98% for training instances and 97% for testing instances. Nonetheless, some *P. rhizophorae* tree crown instances in the testing tiles had fewer pixels predicted as *P. rhizophorae* by the semantic segmentation network inside their area (lower 25% quartile of 85% overlap). Similarly, there seemed to be little confusion between predictions of the two mangrove species. We found a median of 0.05% of all training and testing instances and a mean of 2.6% for training instances and 4.5% for testing instances. The instances in testing tiles showed higher overlap with up to 12% overlap for the upper 75% quartile.

4.4.2 Untiling Accuracy: Tree Instances

Our novel instance untiling algorithm (Algorithm 1) for tree crown masks can be modulated by two parameters: the mask prediction score and the overlap (IoU) threshold. To understand the interplay between the two parameters, we plot the mask score threshold value against the *P. rhizophorae* tree count after the untiling algorithm has been applied (Figure 4.6). The forest area used in this experiment is the sum of all the annotated regions in each site; hence, the dotted "ground truth" lines show the total number of manually annotated *P. rhizophorae* trees. The error, shown in shaded areas, corresponds to the different values obtained from changing the overlap threshold (from 10% to 90% overlap). For the LCN site, the ideal minimum mask score threshold was at 67% and an overlap threshold of 50%. For TC, the mask threshold was at 56% confidence and the overlap threshold at 50%. When combining both sites, the ideal mask score was 62% and an overlap threshold of 50%. The minimum mask score changed between 59% and 65% when the overlap threshold was changed from 10% to 90%, respectively. We used the ideal value of a 62% mask score threshold and 50% overlap threshold for the final predictions of the complete mangrove forest sites.

4.4.3 Untiling Accuracy: Semantic Labeling

Similar to the instance segmentation network, we measured the accuracy of untiling the results of semantic segmentation prediction on tiles with overlap while employing three different merging strategies (Figure 4.7). For each strategy and site, we calculate the accuracy by comparing the labeled pixels of each annotated regions against the labels in the untiled prediction. The accuracy variability was negligible for all strategies. In LCN the accuracy was 86.4% for the overlay and clip strategy and 86.6% for average, while in TC, it was 91.5%, 91.6% and 91.7%, respectively.

These accuracy values for the final untiled areas correlate with the accuracy reported for the testing tiles in the confusion matrices (Figure 4.5c). This portrays the great generalization capabilities of the semantic segmentation network, even in image borders.

4.4.4 Automatic Creation of Digital Elevation Model and Canopy Height Model

After untiling as described, we compared two ways to generate the needed DEM to accurately calculate the CHM: manually selecting ground pixels versus machine-predicted (semantic segmentation network) mud and water pixels. In Figure 4.8, we show that for a vast majority of the *P. rhizophorae* trees, the heights calculated from the CHMs from both DEMs correspond by staying close to the one-to-one line in the regression plots (Figure 4.8). We predicted and compared 12,572 *P. rhizophorae* trees in the LCN site and 4574 *P. rhizophorae* trees in TC. The Bland–Altman (mean-difference) plots show little bias in tree height predictions both in LCN (−0.72 m of mean difference) as in TC (−0.18 m of mean difference) from the automatic ground detection against the manual ground selection technique. In LCN, a small number of outliers were found outside of the −3.4 lower 95% limit of agreement (−1.96 SD line) standard deviation, where some trees were predicted as taller when using the automatic ground detection. Inversely, in TC, some trees were predicted as taller when using the manual ground selection strategy DEM, pushing the upper 95% limit of agreement (the +1.96 SD line) to 1.7, but the lower 95% limit was higher at 2.1.

4.4.5 Tree Inventory and Area Coverage

In Figure 4.9, we summarize the tree-level description of the forest stands created by our workflow. This includes the *P. rhizophorae* tree inventory and the area coverage of the *R. mangle* mangrove species and short-sized *R. mangle*. For the automatic ground detection CHM, the mean pixel height in *P. rhizophorae* predicted masks had a mean value of 7.58 m and the mean of maximum height values was 9.33 m (Figure 4.9a). The height values in the 25% and 75% quantile range were 5.35 m to 9.5 m for the automatic CHM, and 20.48% of trees had a maximum height over 10 m (Figure 4.9b).

We also calculated the tree crown diameter (major axis of ellipse), eccentricity and areas in square meters (Figure 4.9d–f). The mean of the crown diameters was 3.9 m. The distribution of eccentricity of the tree crowns tended towards 1.0 with a mean of 0.67, meaning that their shapes were more elongated and less circle shaped. The mean of tree crown areas was 6.77 m^2. The largest crowns measured up to 20 m^2. For the *P. rhizophorae* trees, we checked the correlation of tree height with the canopy areas (Figure 4.9c). We noticed that shorter trees did

not have larger crown areas (Figure 4.9c). The opposite was not the case, since we find small canopy areas with large heights.

We compared tree heights and tree crown areas of the two in-distribution sites (LCN and TC) with the out-of-distribution EGS site (Figure 4.9g,h). The calculated heights show an almost identical distribution, with very similar means and with 50% of the trees in the 5–10 m range. The tree crown areas present similar distributions between LCN and TC, with means around 7 m^2 and most trees having an area under 10 m^2. Trees in the EGS site show a wider distribution with a similar mean than the other two sites but with 40% of trees in the 10–20 m range.

Finally, we calculated the area coverage for *P. rhizophorae*, *R. mangle* and short-sized *R. mangle* from the semantic segmentation predictions. In LCN, the *P. rhizophorae* species was the most common class with 12.79 ha, followed by *R. mangle* with 2.8 ha and short-sized *R. mangle* with 0.6 ha. In TC, the difference was not as pronounced, with *P. rhizophorae* covering 3.49 ha and *R. mangle* covering 1.41 ha and short-sized *R. mangle* with 0.34 ha. In the out-of-distribution site, EGS, *P. rhizophorae* covered 3.63 ha and *R. mangle* covered 4.1 ha, and short-sized *R. mangle* covered 1.1 ha. The average height of *R. mangle* areas over the three sites had a range of 6–12 m with a mean of 10 m. The heights of short-sized *R. mangle* areas was lower, mostly in the 3.3–5.4 meter range.

4.5 Discussion

In this study, we propose a novel method for creating an inventory of mangrove forests and their surroundings. We also provide a technique for the automatic creation of a DEM and CHM, to calculate heights of individual trees and tree areas. We show that machine learning with deep neural networks has the potential to greatly increase the throughput and precision of surveys of hard-to-access forest areas. Furthermore, by detecting the contour of individual tree crowns and their respective heights, valuable information is obtained for allometric analysis. We show that the workflow can be scaled to handle large mangrove forest regions and generalizes well to new survey data that were not in the training dataset.

4.5.1 Effort Reduction of On-Ground Work and Annotation

Mangrove forests present difficult conditions for on-ground field surveys, given their complex root systems, tidal regimens and remote locations. The use of airborne imaging systems can alleviate the effort by covering large distances in a short time and not being hindered by the complex setting of the forest floor. UASs, in particular, provide a controllable platform for high resolution imaging of target areas from above. In this study, we used the photogrammetric

products (orthomosaic and DSM) constructed from aerial imagery captured with consumer-grade UASs in a remote and inaccessible area of Utría National Park on the Colombian Pacific coast. We used UASs with their default RGB cameras because this technology is easily accessible for local park authorities. Other studies, in contrast, have used more expensive sensors, such as multispectral or hyperspectral cameras, as well as LiDAR sensors (La Rosa et al. 2021; Yin et al. 2019).

We set out to establish that state-of-the-art deep learning techniques can enable even consumer-grade imagery to deliver information-rich survey output at the scale of entire mangrove forests. Given the large extent (103 hectares; Table 4.1) of the forests captured in the orthomosaics, we annotated subplots that would approximately represent 20% of the total mangrove area (Figure 4.3). To capture the variability in the sites, we used the following criteria when selecting annotation subplots: presence of both mangrove species, mud and water presence, location in the plot and height differences in the DSM. To train the semantic segmentation network, we densely annotated large areas such that no pixel was left un-annotated. To measure the performance of the untiling algorithms, we also selected rather larger regions to annotate (three per site) instead of directly annotating smaller-sized tiles that would fit in the network. The contouring of individual *P. rhizophorae* trees in QGIS was the most time consuming part of the process, but this time can be reduced by using novel annotation software designed for supervised learning with large orthomosaic images, such as TagLab (Pavoni, Corsini, Ponchio, et al. 2022).

The decision to not include the *R. mangle* species in the instance segmentation process was made due to the difficulty for the human annotators to visually identify individual tree crowns from each other. This could be overcome by using more specialized sensors that capture higher spatial and spectral resolutions and UASs with steadier flight control, considering the cost trade-off. Even so, the uneven growth patterns of mangrove crowns can be a limiting factor in comparison to other types of forests, where individual trees are easily distinguishable or where forest canopies have more spaced patterns (Schiefer et al. 2020).

We also included the short-sized *R. mangle* class, given that some parts of the forest had a shrub-like aspect that differed from surrounding trees. Most of these areas were exposed to incoming tide, and a smaller fraction were found in-between patches of *P. rhizophorae* trees. After comparing with on-ground images, we determined that those areas were covered in short-sized *R. mangle* trees. Given that it was not possible to visually identify individual tree crowns in the aerial images, we annotated area patches that covered one or more trees.

4.5.2 Instance and Semantic Segmentation

Using two deep neural networks that produce different outputs helped us achieve three distinct goals. First, the instance segmentation network CenterMask2 was trained to identify individual tree crowns for the *P. rhizophorae* mangrove species. Instance segmentation networks were

developed for detecting everyday objects in urban settings but have been successfully transferred to a variety of other fields, such as natural environments (Hafiz et al. 2020; Hoeser et al. 2020). Our implementation achieved an AP of 33% using over 80% of our annotated regions for training. This a good performance considering some quality artifacts in the orthomosaics of the images, such as blurring and the reduced training samples. Another source of error was the contour of annotations, given that mangrove canopies were not always 100% distinguishable between species and between trees of the same species. Furthermore, AP is a very stringent metric of performance as it heavily penalizes small errors in the mask overlap.

The second goal that our automation pipeline achieved was to annotate *R. mangle* areas with recall of 87% and precision of 97% (Figure 4.5c). We were not able to annotate individual trees for this species but were able to describe the area cover. In such cases, where individual trees cannot be detected, area cover and its height distribution can be used to monitor the species AGB (Urbazaev et al. 2018). By using the detected trees from instance segmentation and the areas from the semantic segmentation, we can account for every species in the mangrove forest. In Figure 4.5b, we show that *P. rhizophorae* and *R. mangle* have little to no overlap between the semantic and instance segmentation predictions, indicating a robust separation of these two classes.

The third goal of our workflow was to retrieve ground pixels (i.e., mud and water) to produce a DTM and a subsequent interpolated DEM. The semantic segmentation network predicted areas of the mud and water classes with high precision (89% and 96%, respectively), allowing for accurate detection of ground areas surrounding the mangrove trees.

4.5.3 Automating the Canopy Height Model

The creation of a DEM from accurately detected ground areas allowed us to extract a consistent CHM, from where individual tree heights could be estimated. The automatization reduces the time effort of manually selecting ground pixels by 3 h per plot. In the created DEM, nonetheless, we found small imperfections noticeable in the outliers of the mean-difference comparison in Figure 4.8. This was the result of artefacts from the difference in resolution of the DSM and orthomosaic. For example, some pixels in the bordering regions of mangrove trees and ground pixels were predicted as ground but had an elevation value in the DSM that corresponded to the trees. We reduced these errors by selecting only predicted ground pixels with high confidence (>95%) and further filtering pixels under a certain elevation in tiles along the scene (see Methods). After this filtering, the error in the heights of *P. rhizophorae* trees between the two methods was not significant. The outliers can be further corrected by checking and correcting small imperfections in the automatically generated DEM, which still takes only a couple of minutes compared to hours of selecting ground pixels for a manual DEM. Furthermore, in long-time monitoring settings, the time gain of automating CHM creation is additive. Finer CHM

calculations with closer-to-ground sensing techniques can be used for global-scale canopy height estimation studies (Simard et al. 2019).

4.5.4 From Pixels to Tiles to Trees

In our workflow, we propose a novel instance untiling algorithm that minimizes errors on tile borders (Algorithm 1; Figure 4.6). By tiling the forest plots with overlap, we enhance the probability that trees in border regions will be recovered correctly. Nonetheless, it also complicates the untiling process since the decision has to be made if two or more overlapping masks represent the same or different trees. The two settable parameters in our algorithm allow for adjusting the untiling process to match available on ground data (count of trees). The mask prediction score threshold reduces the number of trees considered for the final prediction by discarding low-confidence predictions such that less overlap occurs in the borders. Then, the overlap threshold parameter handles the case when two or more instances do overlap, and depending on the sizes of their masks and their intersection, we consider merging or dividing the masks. The algorithm gives preference for the already existing tiles in the final prediction because it checks first the existing instances for their size versus the intersection size. The algorithm also works if multiple instances are overlapping with the incoming instance, and each is merged into, merged together or split accordingly. In our study case, we utilize an overlap of 30% between tiles, but this algorithm works on any overlap sizes.

Similarly, for the semantic segmentation predictions, we combine the tiles using different strategies (Figure 4.7). In contrast to the large size of the mangrove forest plots, the benefits of different strategies seem negligible, but it can be relevant if the overlap is larger. We found that averaging was the best way to reconstruct the underlying scene more accurately, similar to what is recommended in (Huang et al. 2018). If the overlap is larger (over 50%) and tile sizes smaller, this strategy is also better suited to combine tiles (La Rosa et al. 2021). Nonetheless, with newer state-of-the-art semantic segmentation CNNs, tiling with overlap might no longer be required, given their high confidence predictions, even in border-adjacent pixels.

4.5.5 Seeing the Forest for the Trees: An Inven(s)tory

The final output of our workflow was an inventory of individual *P. rhizophorae* trees and area cover and height distribution for *R. mangle* and short-sized *R. mangle* (Figure 4.9). The distribution of heights of *P. rhizophorae* trees in our automated inventory fell within the range found in the literature, with most trees in the 5–10 m range and 15–20% larger trees in the 10–20 m range (Fuchs 1970). The regions classified as *R. mangle* trees had slightly taller values (6–12 m), with a larger Section (38%) of trees surpassing 10 m, which also correlates to literature descriptions of the species' height (Allen 2002). Our decision to separate the short-sized *R. mangle*

regions to another category was confirmed to be helpful for the class predictions, given the lower height (3.3–5.4 m) for regions of this category. As mentioned previously, these regions hold shorter trees of the *R. mangle* species, which grow like shrubs compared to taller *R. mangle* trees in more protected areas. Separating these two growth forms of the *R. mangle* species could help tailor the allometric equations for calculating AGB to be more precise.

Describing tree crown shapes and sizes from aerial imagery is a complicated task that has been tried with different methods (Suhardiman et al. 2016). By using instance segmentation networks on well-defined training data, the task can be seemingly simplified (Kattenborn, Leitloff, et al. 2021). Our workflow allows for individual tree crown predictions, and the possible descriptions go beyond tree crown diameters. We calculate tree crown areas and eccentricity, which are parameters that can be used for further understanding growth patterns of mangrove tree species in response to environmental factors (e.g, tide shifts, terrain rugosity, wind direction and speed, etc.).

The semantic segmentation prediction also enables us to study the gaps between trees or those separating forest stands. This helps to understand the growth patterns of the whole mangrove forest and the species distributions, depending on environmental variables, such as distance to shore, tidal locations, forest cover loss and water channel formation (Lassalle and Souza Filho 2022). It can also aid in detecting deforestation incidents or other disturbances in the environment.

4.5.6 Scaling Up: Limitations and Future Work

Our dual-network workflow was able to create a detailed inventory of large mangrove area plots. We show that it can scale and be applied onto new large mangrove forest plots (see height comparison plots in Figure 4.9), with the only condition being that the potential mangrove forest area in the new plot is delineated. In future work, our workflow will be applied onto seven large mangrove plots in the Utría National Park to analyze patterns in the forests. We extract critical information from medium-quality data and show that with consumer-grade technology (UAS and RGB images), complex analyses of forests can be supported for short-term studies or long-term monitoring.

Nonetheless, with better spatial and spectral resolution in the orthomosaics and better spatial and height precision in the DSM, the errors in the predictions could be improved. For example, the use of multi/hyper-spectral cameras mounted on low-flying platforms can improve class separability (La Rosa et al. 2021), and the use of LiDAR sensors can improve the CHM precision (Alon et al. 2020; Wannasiri et al. 2013; Yin et al. 2019). This richer data improves predictions in natural environments, even when more complex communities are targeted (La Rosa et al. 2021; Schürholz et al. 2023). Additionally, advancements in earth-observation technologies are allowing us to apply instance segmentation networks on satellite imagery (Lassalle, Ferreira,

et al. 2022). Research on imagery from low-flying platforms can, in the short-term, be used as detailed monitoring tools and validation information for global studies and, in the long-term, prepare the data-pipelines for enhanced satellite imagery.

The exponential improvement in machine learning platforms also promises to improve the performance of automated monitoring workflows. Both instance and semantic segmentation networks are constantly improving, and as more computational resources are made available, larger and more capable models will be used routinely. Furthermore, the current development of panoptic segmentation networks will allow us to simplify workflows such as ours by classifying foreground and background objects/classes at the same time, removing the need for inter-network comparisons (Cheng et al. 2020).

We use two networks to describe parts of a mangrove forest scene in different ways: pixel-wise and object-wise. We did not include ground measured data in this study, both due to the inaccessibility of the location and to establish the possibility for a quick aerial survey to support rich survey output. Additionally, the scale of the forest area predicted compared to the area that could be manually measured was very large. By comparing the two networks' predictions to each other, we can assure that the underlying scene was consistently described. For the application on new sites, the community composition of the forest must be assessed, and the prediction classes must be adapted accordingly. This constitutes a known drawback of multi-class supervised learning. Nonetheless, the backbone weights of the networks can be reused for training given that top-down forest features do not change significantly between mangrove trees, providing a starting point for new forest surveys using aerial data.

Our workflow provides a blueprint for automatic forest inventory creation, facilitating rapid automated assessments of large areas of mangrove forests with consumer-grade technology. It benefits from the advancements in UAS technology and artificial intelligence, enabling unprecedented detail in forest-wide inventories, especially in inaccessible areas such as remote mangrove forests.

4.6 Acknowledgements

We would like to thank the IT departments at the Max Planck Institute for Marine Microbiology and the Leibniz Center of Tropical Marine Research for implementing and maintaining the computational resources to run our workflows. Photographs were obtained under permit No. PFFO NO. 003-19 from the Colombian National Park Authority. We thank J.D. Osorio for participating in the field survey and A. Rovere for providing an Emlid Reach RS+ GNSS Receiver during field surveys. Finally, we would like to thank Svea Franke for her detailed and rigorous efforts to annotate the large orthomosaic images.

4.7 Author contributions

Conceptualization: D.S., A.C., G.A.C.-G.; Data Curation: D.S., J.C.M.-R.; Investigation: D.S., E.C., G.A.C.-G., J.C.M.-R.; Methodology: D.S., A.C.; Formal analysis: D.S., A.C.; Software: D.S.; Supervision: A.C.; Validation: D.S., A.C.; Visualization: D.S.; Project Administration: D.S.; Resources: A.C.; Funding acquisition: A.C., G.A.C.-G., J.C.M.-R.; Writing—original draft: D.S., Writing—review and editing: A.C., E.C., G.A.C.-G., J.C.M.-R. All authors have read and agreed to the published version of the manuscript.

References

Allen, James A. (2002). "Rhizophora mangle L". In: *In: Vozzo, J., ed. Tropical Tree Seed Manual: Part II, Species Descriptions. Agric. Handb. 712. Washington, DC: U.S. Department of Agriculture: 690-692*, pp. 690–692. URL: *https://www.fs.usda.gov/research/treesearch/45149* (visited on 04/19/2023).

Alon, Alvin, Enrique Festijo, and Cherry Casuat (2020). "Tree Extraction of Airborne LiDAR Data Based on Coordinates of Deep Learning Object Detection from Orthophoto over Complex Mangrove Forest". In: *International Journal of Emerging Trends in Engineering Research* 8, p. 2107. DOI: *10.30534/ijeter/2020/103852020*.

Alongi, Daniel M (2012). "Carbon sequestration in mangrove forests". In: *Carbon Management* 3.3, pp. 313–322. DOI: *10.4155/cmt.12.20*.

Alonso, Iñigo, Matan Yuval, Gal Eyal, Tali Treibitz, and Ana C. Murillo (2019). "CoralSeg: Learning coral segmentation from sparse annotations". In: *Journal of Field Robotics* 36.8, pp. 1456–1477. DOI: *https://doi.org/10.1002/rob.21915*.

Carugati, Laura, Beatrice Gatto, Eugenio Rastelli, Marco Lo Martire, Caterina Coral, Silvestro Greco, and Roberto Danovaro (2018). "Impact of mangrove forests degradation on biodiversity and ecosystem functioning". In: *Scientific Reports* 8.1, p. 13298. DOI: *10.1038/s41598-018-31683-0*.

Castellanos-Galindo, Gustavo A., Elisa Casella, Juan Carlos Mejía-Rentería, and Alessio Rovere (2019). "Habitat mapping of remote coasts: Evaluating the usefulness of lightweight unmanned aerial vehicles for conservation and monitoring". In: *Biological Conservation* 239, p. 108282. DOI: *10.1016/j.biocon.2019.108282*.

Castellanos-Galindo, Gustavo A., Uwe Krumme, Efrain A. Rubio, and Ulrich Saint-Paul (2013). "Spatial variability of mangrove fish assemblage composition in the tropical eastern Pacific Ocean". In: *Reviews in Fish Biology and Fisheries* 23.1, pp. 69–86. DOI: *10.1007/s11160-012-9276-4*.

Chave, J., C. Andalo, S. Brown, M. A. Cairns, J. Q. Chambers, D. Eamus, H. Fölster, F. Fromard, N. Higuchi, T. Kira, J.-P. Lescure, B. W. Nelson, H. Ogawa, H. Puig, B. Riéra, and T. Yamakura (2005). "Tree allometry and improved estimation of carbon stocks and balance in tropical forests". In: *Oecologia* 145.1, pp. 87–99. DOI: *10.1007/s00442-005-0100-x*.

Chen, Liang-Chieh, Yukun Zhu, George Papandreou, Florian Schroff, and Hartwig Adam (2018). *Encoder-Decoder with Atrous Separable Convolution for Semantic Image Segmentation*. DOI: *10.48550/arXiv.1802.02611*. arXiv: *1802.02611[cs]*.

Cheng, Bowen, Maxwell D. Collins, Yukun Zhu, Ting Liu, Thomas S. Huang, Hartwig Adam, and Liang-Chieh Chen (2020). "Panoptic-DeepLab: A Simple, Strong, and Fast Baseline for Bottom-Up Panoptic Segmentation". In: *arXiv:1911.10194 [cs]*. arXiv: *1911.10194*. URL: *http://arxiv.org/abs/1911.10194* (visited on 02/18/2021).

Chiang, Chia-Yen, Chloe Barnes, Plamen Angelov, and Richard Jiang (2020). "Deep Learning-Based Automated Forest Health Diagnosis From Aerial Images". In: *IEEE Access* 8, pp. 144064–144076. DOI: *10.1109/ACCESS.2020.3012417*.

Clough, B. F., P. Dixon, and O. Dalhaus (1997). "Allometric Relationships for Estimating Biomass in Multi-stemmed Mangrove Trees". In: *Australian Journal of Botany* 45.6, pp. 1023–1031. DOI: *10.1071/bt96075*.

Ding, Zhaowei, Ruonan Li, Patrick O'Connor, Hua Zheng, Binbin Huang, Lingqiao Kong, Yi Xiao, Weihua Xu, and Zhiyun Ouyang (2021). "An improved quality assessment framework to better inform large-scale forest restoration management". In: *Ecological Indicators* 123, p. 107370. DOI: *10.1016/j.ecolind.2021.107370*.

Ellison, Aaron M., Alexander J. Felson, and Daniel A. Friess (2020). "Mangrove Rehabilitation and Restoration as Experimental Adaptive Management". In: *Frontiers in Marine Science* 7. URL: *https://www.frontiersin.org/articles/10.3389/fmars.2020.00327* (visited on 03/30/2023).

Ferretti, Marco (1997). "Forest Health Assessment and Monitoring – Issues for Consideration". In: *Environmental Monitoring and Assessment* 48.1, pp. 45–72. DOI: *10.1023/A:1005748702893*.

Flood, Neil, Fiona Watson, and Lisa Collett (2019). "Using a U-net convolutional neural network to map woody vegetation extent from high resolution satellite imagery across Queensland, Australia". In: *International Journal of Applied Earth Observation and Geoinformation* 82, p. 101897. DOI: *10.1016/j.jag.2019.101897*.

Friess, Daniel A., Erik S. Yando, Guilherme M. O. Abuchahla, Janine B. Adams, Stefano Cannicci, Steven W. J. Canty, Kyle C. Cavanaugh, Rod M. Connolly, Nicole Cormier, Farid Dahdouh-Guebas, Karen Diele, Ilka C. Feller, Sara Fratini, Tim C. Jennerjahn, Shing Yip Lee, Danielle E. Ogurcak, Xiaoguang Ouyang, Kerrylee Rogers, Jennifer K. Rowntree, Sahadev Sharma, Taylor M. Sloey, and Alison K. S. Wee (2020). "Mangroves give cause for conservation optimism, for now". In: *Current biology: CB* 30.4, R153–R154. DOI: *10.1016/j.cub.2019.12.054*.

Fuchs, H. P. (1970). "Ecological and palynological notes on Pelliciera rhizophorae". In: *Acta botanica neerlandica* 19.6, pp. 884–894. URL: *https://natuurtijdschriften.nl/pub/539736* (visited on 04/19/2023).

G. Braga, José R., Vinícius Peripato, Ricardo Dalagnol, Matheus P. Ferreira, Yuliya Tarabalka, Luiz E. O. C. Aragão, Haroldo F. de Campos Velho, Elcio H. Shiguemori, and Fabien H. Wagner (2020). "Tree Crown Delineation Algorithm Based on a Convolutional Neural Network". In: *Remote Sensing* 12.8, p. 1288. DOI: *10.3390/rs12081288*.

Goldberg, Liza, David Lagomasino, Nathan Thomas, and Temilola Fatoyinbo (2020). "Global declines in human-driven mangrove loss". In: *Global Change Biology* 26.10, pp. 5844–5855. DOI: *10.1111/gcb.15275*.

Guo, Ke, Bing Wang, and Xiang Niu (2023). "A Review of Research on Forest Ecosystem Quality Assessment and Prediction Methods". In: *Forests* 14.2, p. 317. DOI: *10.3390/f14020317*.

Hafiz, Abdul Mueed and Ghulam Mohiuddin Bhat (2020). "A Survey on Instance Segmentation: State of the art". In: *International Journal of Multimedia Information Retrieval* 9.3, pp. 171–189. DOI: *10.1007/s13735-020-00195-x*. arXiv: *2007.00047[cs,eess]*.

Hai, Pham Minh, Pham Hong Tinh, Nguyen Phi Son, Tran Van Thuy, Nguyen Thi Hong Hanh, Sahadev Sharma, Do Thi Hoai, and Vu Cong Duy (2022). "Mangrove health assessment using spatial metrics and multi-temporal remote sensing data". In: *PLOS ONE* 17.12, e0275928. DOI: *10.1371/journal.pone.0275928*.

Hao, Zhenbang, Lili Lin, Christopher J. Post, Elena A. Mikhailova, Minghui Li, Yan Chen, Kunyong Yu, and Jian Liu (2021). "Automated tree-crown and height detection in a young forest plantation using mask region-based convolutional neural network (Mask R-CNN)". In: *ISPRS Journal of Photogrammetry and Remote Sensing* 178, pp. 112–123. DOI: *10.1016/j.isprsjprs.2021.06.003*.

Hoeser, Thorsten and Claudia Kuenzer (2020). "Object Detection and Image Segmentation with Deep Learning on Earth Observation Data: A Review-Part I: Evolution and Recent Trends". In: *Remote Sensing* 12.10, p. 1667. DOI: *10.3390/rs12101667*.

Huang, Bohao, Daniel Reichman, Leslie M. Collins, Kyle Bradbury, and Jordan M. Malof (2018). "Tiling and Stitching Segmentation Output for Remote Sensing: Basic Challenges and Recommendations". In: URL: *https://arxiv.org/abs/1805.12219v3* (visited on 09/14/2020).

Innes, J. L. (1994). "Design of an intensive monitoring system for swiss forests". In: *Mountain Environments in Changing Climates*. Routledge.

Joyce, Karen E., Kate C. Fickas, and Michelle Kalamandeen (2023). "The unique value proposition for using drones to map coastal ecosystems". In: *Cambridge Prisms: Coastal Futures* 1, e6. DOI: *10.1017/cft.2022.7*.

Kattenborn, Teja, Jana Eichel, and Fabian Ewald Fassnacht (2019). "Convolutional Neural Networks enable efficient, accurate and fine-grained segmentation of plant species and communities from high-resolution UAV imagery". In: *Scientific Reports* 9.1, p. 17656. DOI: *10.1038/s41598-019-53797-9*.

Kattenborn, Teja, Jens Leitloff, Felix Schiefer, and Stefan Hinz (2021). "Review on Convolutional Neural Networks (CNN) in vegetation remote sensing". In: *ISPRS Journal of Photogrammetry and Remote Sensing* 173, pp. 24–49. DOI: *10.1016/j.isprsjprs.2020.12.010*.

Khan, A., U. Khan, M. Waleed, A. Khan, T. Kamal, S. N. K. Marwat, M. Maqsood, and F. Aadil (2018). "Remote Sensing: An Automated Methodology for Olive Tree Detection and Counting in Satellite Images". In: *IEEE Access* 6, pp. 77816–77828. DOI: *10.1109/ACCESS.2018.2884199*.

La Rosa, Laura Elena Cué, Camile Sothe, Raul Queiroz Feitosa, Cláudia Maria de Almeida, Marcos Benedito Schimalski, and Dário Augusto Borges Oliveira (2021). "Multi-task fully convolutional network for tree species mapping in dense forests using small training hyperspectral data". In: *ISPRS Journal of Photogrammetry and Remote Sensing* 179, pp. 35–49. DOI: *10.1016/j.isprsjprs.2021.07.001*.

Lassalle, Guillaume, Matheus Pinheiro Ferreira, Laura Elena Cué La Rosa, and Carlos Roberto de Souza Filho (2022). "Deep learning-based individual tree crown delineation in mangrove forests using very-high-resolution satellite imagery". In: *ISPRS Journal of Photogrammetry and Remote Sensing* 189, pp. 220–235. DOI: *10.1016/j.isprsjprs.2022.05.002*.

Lassalle, Guillaume and Carlos Roberto de Souza Filho (2022). "Tracking canopy gaps in mangroves remotely using deep learning". In: *Remote Sensing in Ecology and Conservation* 8.6, pp. 890–903. DOI: *10.1002/rse2.289*.

Lee, Youngwan, Joong-won Hwang, Sangrok Lee, Yuseok Bae, and Jongyoul Park (2019). "An Energy and GPU-Computation Efficient Backbone Network for Real-Time Object Detection". In: *Proceedings of the IEEE Conference on Computer Vision and Pattern Recognition Workshops*.

Lee, Youngwan and Jongyoul Park (2020). *CenterMask : Real-Time Anchor-Free Instance Segmentation*. DOI: *10.48550/arXiv.1911.06667*.

Menéndez, Pelayo, Iñigo J. Losada, Saul Torres-Ortega, Siddharth Narayan, and Michael W. Beck (2020). "The Global Flood Protection Benefits of Mangroves". In: *Scientific Reports* 10.1, p. 4404. DOI: *10.1038/s41598-020-61136-6*.

Miraki, Mojdeh, Hormoz Sohrabi, Parviz Fatehi, and Mathias Kneubuehler (2021). "Individual tree crown delineation from high-resolution UAV images in broadleaf forest". In: *Ecological Informatics* 61, p. 101207. DOI: *10.1016/j.ecoinf.2020.101207*.

Mölder, Felix, Kim Philipp Jablonski, Brice Letcher, Michael B. Hall, Christopher H. Tomkins-Tinch, Vanessa Sochat, Jan Forster, Soohyun Lee, Sven O. Twardziok, Alexander Kanitz, Andreas Wilm, Manuel Holtgrewe, Sven Rahmann, Sven Nahnsen, and Johannes Köster (2021). *Sustainable data analysis with Snakemake*. 10:33. F1000Research. DOI: *10.12688/f1000research.29032.2*.

Navarro, Alejandro, Mary Young, Blake Allan, Paul Carnell, Peter Macreadie, and Daniel Ierodiaconou (2020). "The application of Unmanned Aerial Vehicles (UAVs) to estimate above-ground biomass of mangrove ecosystems". In: *Remote Sensing of Environment* 242, p. 111747. DOI: *10.1016/j.rse.2020.111747*.

Otero, Viviana, Ruben Van De Kerchove, Behara Satyanarayana, Columba Martínez-Espinosa, Muhammad Amir Bin Fisol, Mohd Rodila Bin Ibrahim, Ibrahim Sulong, Husain Mohd-

Lokman, Richard Lucas, and Farid Dahdouh-Guebas (2018). "Managing mangrove forests from the sky: Forest inventory using field data and Unmanned Aerial Vehicle (UAV) imagery in the Matang Mangrove Forest Reserve, peninsular Malaysia". In: *Forest Ecology and Management* 411, pp. 35–45. DOI: *10.1016/j.foreco.2017.12.049*.

Paszke, Adam, Sam Gross, Francisco Massa, Adam Lerer, James Bradbury, Gregory Chanan, Trevor Killeen, Zeming Lin, Natalia Gimelshein, Luca Antiga, Alban Desmaison, Andreas Kopf, Edward Yang, Zachary DeVito, Martin Raison, Alykhan Tejani, Sasank Chilamkurthy, Benoit Steiner, Lu Fang, Junjie Bai, and Soumith Chintala (2019). "PyTorch: An Imperative Style, High-Performance Deep Learning Library". In: *Advances in Neural Information Processing Systems 32*. Curran Associates, Inc., pp. 8024–8035. URL: *http://papers.neurips.cc/paper/9015-pytorch-an-imperative-style-high-performance-deep-learning-library.pdf*.

Pavoni, Gaia, Massimiliano Corsini, Marco Callieri, Giuseppe Fiameni, Clinton Edwards, and Paolo Cignoni (2020). "On Improving the Training of Models for the Semantic Segmentation of Benthic Communities from Orthographic Imagery". In: *Remote Sensing* 12.18, p. 3106. DOI: *10.3390/rs12183106*.

Pavoni, Gaia, Massimiliano Corsini, Federico Ponchio, Alessandro Muntoni, Clinton Edwards, Nicole Pedersen, Stuart Sandin, and Paolo Cignoni (2022). "TagLab: AI-assisted annotation for the fast and accurate semantic segmentation of coral reef orthoimages". In: *Journal of Field Robotics* 39.3, pp. 246–262. DOI: *10.1002/rob.22049*.

Persson, Henrik Jan, Magnus Ekström, and Göran Ståhl (2022). "Quantify and account for field reference errors in forest remote sensing studies". In: *Remote Sensing of Environment* 283, p. 113302. DOI: *10.1016/j.rse.2022.113302*.

Polidoro, Beth A., Kent E. Carpenter, Lorna Collins, Norman C. Duke, Aaron M. Ellison, Joanna C. Ellison, Elizabeth J. Farnsworth, Edwino S. Fernando, Kandasamy Kathiresan, Nico E. Koedam, Suzanne R. Livingstone, Toyohiko Miyagi, Gregg E. Moore, Vien Ngoc Nam, Jin Eong Ong, Jurgenne H. Primavera, Severino G. Salmo Iii, Jonnell C. Sanciangco, Sukristijono Sukardjo, Yamin Wang, and Jean Wan Hong Yong (2010). "The Loss of Species: Mangrove Extinction Risk and Geographic Areas of Global Concern". In: *PLOS ONE* 5.4, e10095. DOI: *10.1371/journal.pone.0010095*.

"Methods for Estimating Above-Ground Biomass" (2008). In: *Carbon Inventory Methods Handbook for Greenhouse Gas Inventory, Carbon Mitigation and Roundwood Production Projects*. Ed. by N. H. Ravindranath and Madelene Ostwald. Advances in Global Change Research. Dordrecht: Springer Netherlands, pp. 113–147. DOI: *10.1007/978-1-4020-6547-7_10*.

Ruwaimana, Monika, Behara Satyanarayana, Viviana Otero, Aidy M. Muslim, Muhammad Syafiq A, Sulong Ibrahim, Dries Raymaekers, Nico Koedam, and Farid Dahdouh-Guebas (2018). "The advantages of using drones over space-borne imagery in the mapping of mangrove forests". In: *PLOS ONE* 13.7, e0200288. DOI: *10.1371/journal.pone.0200288*.

Samanta, Sourav, Sugata Hazra, Partho P. Mondal, Abhra Chanda, Sandip Giri, Jon R. French, and Robert J. Nicholls (2021). "Assessment and Attribution of Mangrove Forest Changes in

the Indian Sundarbans from 2000 to 2020". In: *Remote Sensing* 13.24, p. 4957. DOI: *10.3390/rs13244957*.

Schiefer, Felix, Teja Kattenborn, Annett Frick, Julian Frey, Peter Schall, Barbara Koch, and Sebastian Schmidtlein (2020). "Mapping forest tree species in high resolution UAV-based RGB-imagery by means of convolutional neural networks". In: *ISPRS Journal of Photogrammetry and Remote Sensing* 170, pp. 205–215. DOI: *10.1016/j.isprsjprs.2020.10.015*.

Simard, Marc, Lola Fatoyinbo, Charlotte Smetanka, Victor H. Rivera-Monroy, Edward Castañeda-Moya, Nathan Thomas, and Tom Van der Stocken (2019). "Mangrove canopy height globally related to precipitation, temperature and cyclone frequency". In: *Nature Geoscience* 12.1, pp. 40–45. DOI: *10.1038/s41561-018-0279-1*.

Suhardiman, Ali, Satoshi Tsuyuki, and Yunianto Setiawan (2016). "Estimating Mean Tree Crown Diameter of Mangrove Stands Using Aerial Photo". In: *Procedia Environmental Sciences*. The 2nd International Symposium on LAPAN-IPB Satellite (LISAT) for Food Security and Environmental Monitoring 33, pp. 416–427. DOI: *10.1016/j.proenv.2016.03.092*.

Thomas, Nathan, Peter Bunting, Richard Lucas, Andy Hardy, Ake Rosenqvist, and Temilola Fatoyinbo (2018). "Mapping Mangrove Extent and Change: A Globally Applicable Approach". In: *Remote Sensing* 10.9, p. 1466. DOI: *10.3390/rs10091466*.

Tockner, Andreas, Christoph Gollob, Ralf Kraßnitzer, Tim Ritter, and Arne Nothdurft (2022). "Automatic tree crown segmentation using dense forest point clouds from Personal Laser Scanning (PLS)". In: *International Journal of Applied Earth Observation and Geoinformation* 114, p. 103025. DOI: *10.1016/j.jag.2022.103025*.

Ulku, Irem, Erdem Akagündüz, and Pedram Ghamisi (2022). "Deep Semantic Segmentation of Trees Using Multispectral Images". In: *IEEE Journal of Selected Topics in Applied Earth Observations and Remote Sensing* 15, pp. 7589–7604. DOI: *10.1109/JSTARS.2022.3203145*.

Urbazaev, Mikhail, Christian Thiel, Felix Cremer, Ralph Dubayah, Mirco Migliavacca, Markus Reichstein, and Christiane Schmullius (2018). "Estimation of forest aboveground biomass and uncertainties by integration of field measurements, airborne LiDAR, and SAR and optical satellite data in Mexico". In: *Carbon Balance and Management* 13.1, p. 5. DOI: *10.1186/s13021-018-0093-5*.

Walt, Stéfan van der, Johannes L. Schönberger, Juan Nunez-Iglesias, François Boulogne, Joshua D. Warner, Neil Yager, Emmanuelle Gouillart, Tony Yu, and the scikit-image contributors (2014). "scikit-image: image processing in Python". In: *PeerJ* 2, e453. DOI: *10.7717/peerj.453*.

Wang, Jiamin, Xinxin Chen, Lin Cao, Feng An, Bangqian Chen, Lianfeng Xue, and Ting Yun (2019). "Individual Rubber Tree Segmentation Based on Ground-Based LiDAR Data and Faster R-CNN of Deep Learning". In: *Forests* 10.9, p. 793. DOI: *10.3390/f10090793*.

Wang, Zhenhua, Jing Li, Zhilian Tan, Xiangfeng Liu, and Mingjie Li (2023). "Swin-UperNet: A Semantic Segmentation Model for Mangroves and Spartina alterniflora Loisel Based on UperNet". In: *Electronics* 12.5, p. 1111. DOI: *10.3390/electronics12051111*.

Wannasiri, Wasinee, Masahiko Nagai, Kiyoshi Honda, Phisan Santitamnont, and Poonsak Miphokasap (2013). "Extraction of Mangrove Biophysical Parameters Using Airborne LiDAR". In: *Remote Sensing* 5.4, pp. 1787–1808. DOI: *10.3390/rs5041787*.

Weinstein, Ben G., Sergio Marconi, Stephanie A. Bohlman, Alina Zare, and Ethan P. White (2020). "Cross-site learning in deep learning RGB tree crown detection". In: *Ecological Informatics* 56, p. 101061. DOI: *10.1016/j.ecoinf.2020.101061*.

Wu, Yuxin, Alexander Kirillov, Francisco Massa, Wan-Yen Lo, and Ross Girshick (2019). *Detectron2*. *https://github.com/facebookresearch/detectron2*.

Yin, Dameng and Le Wang (2019). "Individual mangrove tree measurement using UAV-based LiDAR data: Possibilities and challenges". In: *Remote Sensing of Environment* 223, pp. 34–49. DOI: *10.1016/j.rse.2018.12.034*.

Zang, Jingrong, Shichao Jin, Songyin Zhang, Qing Li, Yue Mu, Ziyu Li, Shaochen Li, Xiao Wang, Yanjun Su, and Dong Jiang (2023). "Field-measured canopy height may not be as accurate and heritable as believed: evidence from advanced 3D sensing". In: *Plant Methods* 19.1, p. 39. DOI: *10.1186/s13007-023-01012-2*.

Chapter 5

Removing the turbid veil: are turbid reefs a refugia for corals in an adverse future?

Daniel Schürholz [1,2]*, Andi Muh. Agung Pratama* [3]*, Gunawan Syafruddin* [3]*, Puspita Lestari Kanna* [3]*, Estradivari Estradivari* [2]*, Dino Angelo Ramos* [4] *and Arjun Chennu* [2]

Manuscript status

In preparation for submission to *Coral Reefs*.

5.1 Abstract

In recent decades, evidence has pointed to turbid reefs as possible refugia for scleractinian corals to weather the adverse conditions of the Anthropocene. Rapid human population expansion in coastal urban settlements has increased the negative impact from human activity on coral reefs. As one of the consequences, elevated turbidity and sedimentation levels are repeatedly being measured in shallow coral reefs located close to large urban settlements and agricultural land. Investigating the coral community shifts that are triggered by the these environmental changes, is key to understand the future trajectories of these ecosystems, and to provide evidence about the role of turbid reefs as a haven for scleractinian corals. This study focuses on the Spermonde Archipelago in South Sulawesi - Indonesia, located within the Coral Triangle, the region with

[1]Max Planck Institute for Marine Microbiology, 28359 Bremen, Germany
[2]Leibniz Centre for Tropical Marine Research (ZMT), 28359 Bremen, Germany
[3]Hasanuddin University (UNHAS), Makassar, South Sulawesi, Indonesia
[4]University of Granada (UGR), Granada, Spain

the highest taxonomic diversity of scleractinian corals worldwide. Coral reefs in Spermonde are found in a steep turbidity gradient. Extreme eutrophication and sedimentation levels have been measured in the islands close to the metropolis of Makassar and the agricultural land north of it. Turbidity decreases towards the outer-shelf, where corals live in clear oligotrophic waters. It is believed that scleractinian corals living in clear waters are more susceptible to bleaching as a consequence of increasingly warmer water temperatures, given that they also have to withstand high incident UV light.

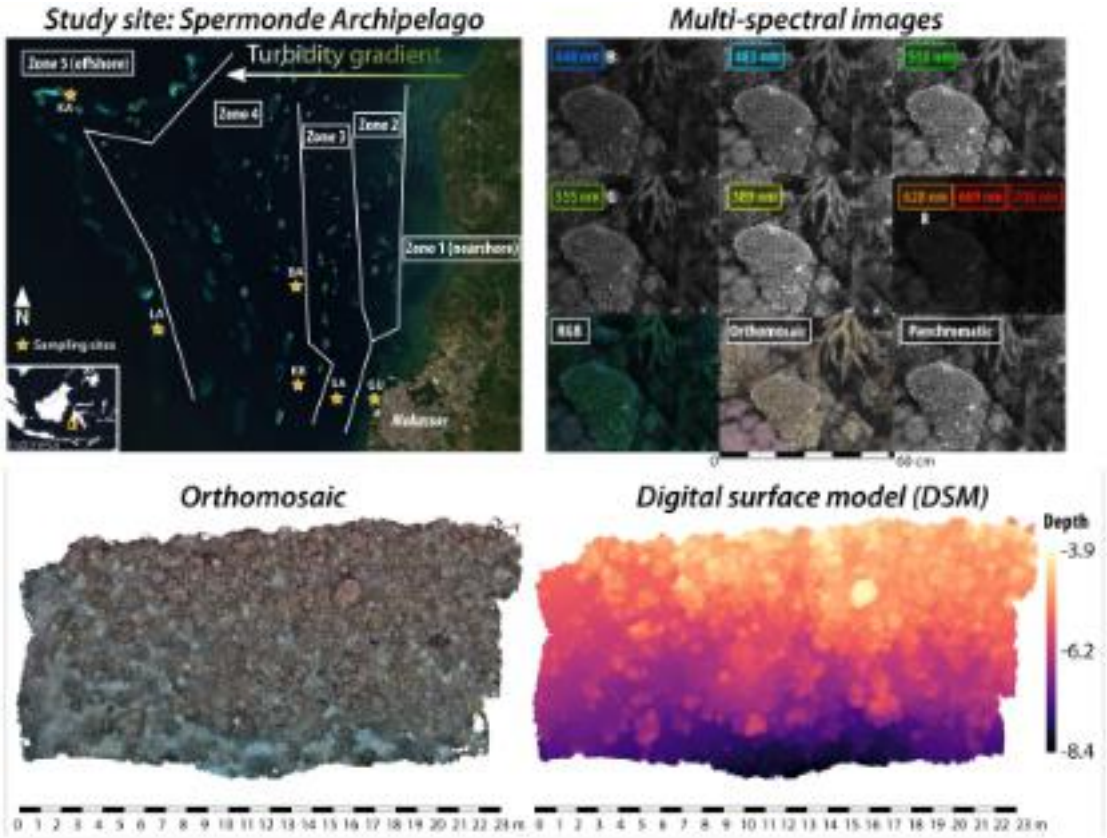

Figure 5.1 Overview of study site and acquired data products. The Spermonde Archipelago is located in front of the city of Makassar in South Sulawesi, Indonesia, and experiences a steep turbidity gradient correlated to the distance to the main land. 13 coral reef plots ($\sim 15 \times 20m$) across 6 islands at 3 different depth levels (reef flat/crest, reef slope middle & reef slope deep) were surveyed by acquiring color and multispectral images with the HyperDiver device. Color images were then used to produce orthomosaic and digital surface models of the reefs with SfM software. A co-registration between color- and multispectral orthomosaics is planed for future work. The multispectral images capture 8 spectral bands (wavelengths between 448 nm and 708 nm) and 1 panchromatic band.

We surveyed benthic communities in 13 coral reef plots ($\sim 15 \times 20m$) in 6 islands across the turbidity gradient, and locally at each island, across a depth gradient from (approx. 3–12 m

depth). The HyperDiver device was used to capture high-resolution spatial and spectral images of the benthic environment from an altitude of $\sim$ 1.5 meters from the seafloor. One multi-spectral and one hyperspectral camera (with 8 and 480 spectral bands respectively) were used to capture fine spectral detail. Two stereo color cameras were used to capture overlapping images with high spatial resolution. The color and multi-spectral images were used to create orthomosaic- and digital surface models of the seafloor. These photogrammetric models were geo-referenced with a handheld Garmin eTrex GPS device, that marked 6 ground control points from the surface. To produce training data for AI workflows, six coral reef biologists annotated over 1600 polygons of interest on the 3 of the color-image orthomosaics. In total, 577 individual scleractinian coral colonies were contoured and labeled with one of 34 genera. Other biotic elements like sponges, soft corals, sea urchins, macroalgae, coralline algae and anemones were annotated to the finest taxonomic level possible. Substrate elements were also annotated as cyanobacterial mats, sediment, turf algae or coral rubble.

A preliminary analysis of the annotated sites suggests that reefs closer to the city of Makassar have experienced more deterioration, showing only scattered small-sized coral colonies, with most of the area covered by abundant macro- and turf algae, due to high eutrophication levels. Reefs in the mid-turbidity zones (Zone 3,4) show the healthiest reefs, with dense patches of *Acroporid* and *Porites* colonies and high coral diversity. Reefs on the outer-shelf present smaller patches of large colonies, with large stretches of bare sediment in-between. This suggests that a moderate level of turbidity may protect scleractinian corals from high radiation levels and help them withstand increased water temperatures. Further correlative analysis must be done to separate turbidity and sedimentation from other possible stressors present in the region, such as blast fishing, over-fishing and tourism. The detailed spatial and spectral data facilitates manual and automatic classification of benthic communities in coral reefs capturing the high taxonomic diversity of the region and with individual biotic organisms delineated. Scaling up the classification to larger coral reef areas with the same spatial and thematic detail, will allow to unveil more fine-grained patterns in the coral community distribution across a turbid gradient.

5.2 Author contributions

Conceptualization: D.S., A.C.; Data Curation: D.S., A.M.A.P, G.S., P.L.K., E.E., D.A.R.; Investigation: D.S., A.M.A.P, G.S., P.L.K., E.E., D.A.R.; Methodology: D.S., A.C.; Formal analysis: D.S., A.C.; Software: D.S.; Supervision: A.C.; Validation: D.S., A.C.; Visualization: D.S.; Project Administration: D.S.. A.C.; Resources: A.C.; Funding acquisition: A.C.; Writing—original draft: D.S., Writing—review and editing: A.C. All authors have read and agreed to the publication of this abstract.

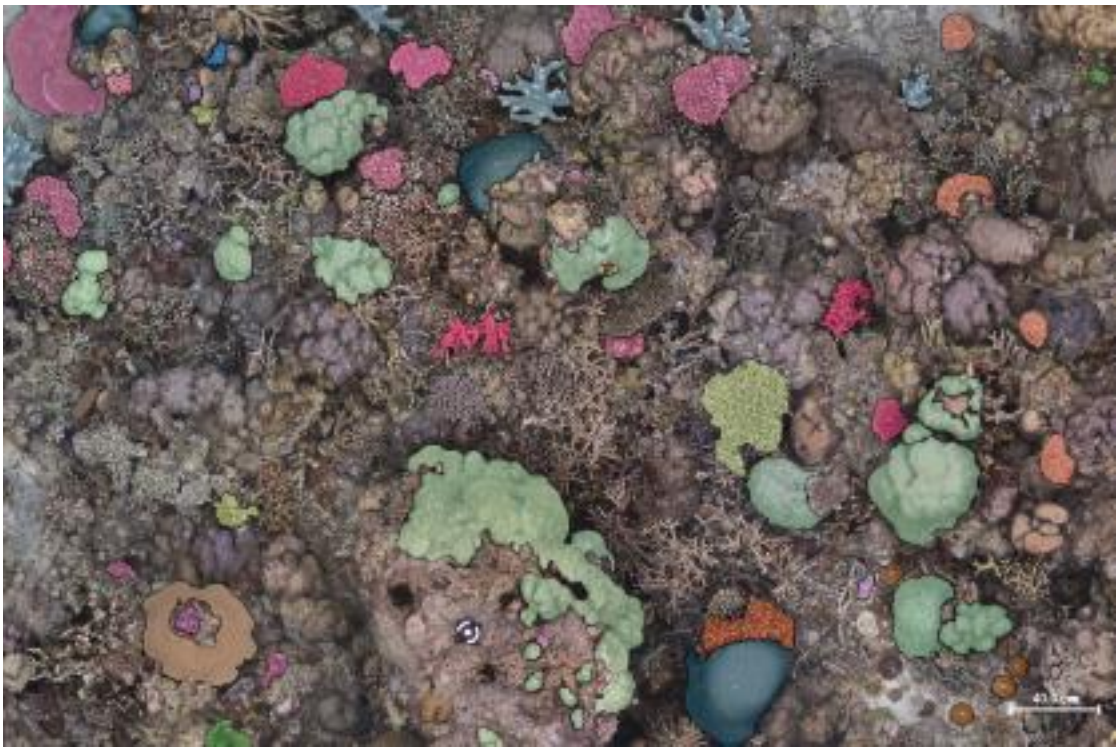

(**a**)

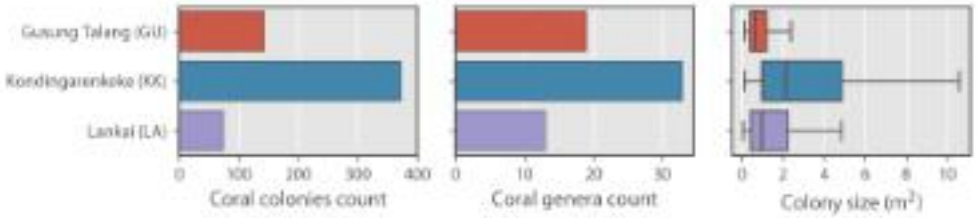

(**b**)

Figure 5.2 Scleractinian coral colonies annotations overview. (a) Example of manually delineated and labelled coral colonies, which were selected in stratified manner across subplots and covered as much taxonomic diversity as identifiable from the images (generally to genus level). The annotations are suitable for training of AI workflows. (b) The site Kondingarenkeke (KK) is located in Zone 4 of the turbidity gradient (see Figure 5.1). The sampled plot was located between 4 and 8 meters of depth. The number of coral colonies was the highest in this reef. It was the most taxonomically diverse community, dominated by *Porites*, *Galaxea* and *Acropora* colonies (Figure C.1). KK presented the largest coral colonies. Site Gusung Talang (GU) is located in Zone 1 with high levels of turbidity. The sampled plot was located on the reef flat almost entirely at 3 meters depth. The coral count and diversity were the second highest (dominated by small *Favia* and *Fungia* colonies), but most colonies were small in size and scattered. Finally, Lankai (LA) is located in Zone 5 with clear waters. The sampled plot was located on the deep end of the reef slope (5.5–8.5 meters). The coral count was the lowest, but some larger colonies were located. The diversity was the lowest as well (dominated by small *Acropora* and *Pocillopora* colonies).

Part III

Perspective

Chapter 6

Discussion and Outlook

6.1 Discussion

Shallow coastal ecosystems play a critical role in global and local natural processes. They provide invaluable services to the coastal human populations and other adjacent ecosystems, as well as helping to regulate the global climate. In recent decades, coral reefs and mangrove forests have been under constant stress, due to direct and indirect consequences of anthropogenic activities. Thus, protecting and restoring these environments has become a central focus of many international and domestic regulatory efforts. This has prompted an urge to understand the baselines and current states of these remote and under-researched ecosystems, to be able to continue monitoring them through time (Muldrow et al. 2020). However, for conservation efforts to be effective, our scientific knowledge of these ecosystems has to be constantly updated through consistent and scalable monitoring (Lecours 2017; Sparrow et al. 2020).

Recent monitoring efforts are providing constant surveillance of shallow coastal ecosystems at a global scale, by using Earth observation systems (B. Lyons et al. 2020; Goldberg et al. 2020; Kennedy et al. 2021). Their use of satellite imagery enables coverage of large areas, but the distance to the targets and the atmospheric and aquatic interfaces, limit the spatial and thematic detail that can be extracted from their data products. Relying only on broad-scale analyses of these ecosystems, which often times have not been locally validated, can mask important small-scale processes and miss-inform management efforts (Brito-Millán et al. 2019; Hochberg et al. 2021). Thus, standardised field methods need to be available as validation for these global efforts, whilst also targeting testable hypotheses over defined areas to determine the causes of changes in ecosystem community composition and configuration (Riitters 2019; Sparrow et al. 2020). This entails that survey methodologies should output products that can be scaled spatially and abstracted thematically to meet the specifications of both global surveillance efforts and local ecological investigations.

6.1.1 Scaling-up and refining survey products with proximal sensing and AI

Proximal sensing technologies, such as the HyperDiver and UAS platforms, provide the perfect scale for detailed monitoring of shallow coastal ecosystems through fine-grain spatial and spectral imaging (Chennu et al. 2017; Joyce et al. 2023). On the spatial scale these platforms can cover several hectares of an ecosystem during a survey campaign with millimeter pixel resolution. This allows for easy visual identification of biotic targets to detailed taxonomic levels, and for the discernability between different substrate types. On the spectral scale, hyper- and multi-spectral sensors can be used to add richness to the data. However, to truly scale up the annotation of terabytes of raw image data, human expert effort rapidly becomes the bottleneck, prompting the need for the automation of ecosystem mapping.

In this doctoral project, end-to-end AI workflows are designed, developed and validated, to automate ecosystem mapping processes. The developed workflows were designed to cover the requirements of each shallow coastal ecosystem that was the target of the mapping process. In (Chapter 2 & Chapter 3), the mapping targets are 8 coral reefs on an island-wide survey. Coral reefs generally have biotic communities that are taxonomically and morphologically very diverse. In the surveyed reef 42 biotic and abiotic labels were identified, with 19 coral species/genera, 10 sponge species, 4 soft coral species/genera, 3 macroalgae species/genera and 3 substrate types, among other classes. For ML algorithms to automatically and accurately classify the variability in the mapping targets, rich spatial and spectral data was required. Thus, the underwater diver-operated HyperDiver device was used, which can capture hyperspectral transects with 480 spectral bands and centimeter pixel resolution ($\sim 2.5 cm^2/pixel$).

To automatically classify these rich datasets, a spectral-spatial deep learning algorithm for remote sensing work with hyperspectral data from satellite observations was selected (Zhong et al. 2018). The algorithm was optimized and adapted to underwater hyperspectral transects of coral reef habitats. In (Chapter 2) a detailed inspection of the performance of the algorithm was explained, even comparing to another traditional ML algorithm. More importantly, a detailed assessment of the resulting habitat maps was executed, to determine the fidelity of the mapping products to the true reef community composition and configuration. In (Chapter 3) the AI workflow was optimized using ensemble network techniques to provide more robust and unbiased classification (Wyatt et al. 2022). The resulting predictions were very accurate with 90% prediction accuracy for 48 labels, an unprecedented level of automatically predicted thematic detail in underwater mapping. Recently, a mapping effort in an Indo-Pacific coral reef, has used underwater hyperspectral transects and AI workflows and achieved even higher thematic detail (91 benthic classes) (Mills et al. 2023). The authors expanded on the same deep learning algorithm as the one used in (Chapter 2) and produced a similar prediction reliability analysis as presented in (Chapter 3) (Figure 3.5 & Figure B.1). Automated hyperspectral mapping of underwater habitats is a recent field of study, and thus it requires detailed inspection of the mapping products and applied AI models. This doctoral project adds valuable information with

detailed mapping product assessment, the comparison to traditional methods and CNN prediction reliability analyses. As the costs of hyperspectral cameras sinks and they become more accessible (Teague, Day, et al. 2023), emerging users will have good understanding and guidelines to produce automated mapping workflows with AI, providing a valuable tool for detailed mapping of shallow coastal ecosystems.

Current hyperspectral imagers provide enough detail for detailed thematic mapping, but they lack enough spatial resolution to allow for accurate individual-organism detection. Organism detection is an important tool for automatic inventorization of ecosystems, as it can provide detail accounting for very large habitats, while relieving managers and researchers from arduous in-situ tasks (Tucker et al. 2023). Organism detection has been achieved on satellite imagery and from UAS platforms, but it has usually been applied only in ecosystems that present a sparse configuration of the target individuals (Lassalle et al. 2022; Otero et al. 2018; Tucker et al. 2023). In contrast, certain mangrove forests present very dense canopies and bush-like morphologies that make individual tree crowns hard to identify. (Chapter 4) presents an end-to-end AI workflow that uses a consumer-grade UAS and instance segmentation CNNs to segment individual mangrove trees in a forests with dense canopies. The spatial detail from photogrammetric models built with SfM software from color images is detailed enough to allow the AI model to delineate individual trees. Furthermore, the workflow automatically categorizes surrounding forest, mud and water areas, providing habitat context to the targeted and detected organisms. These predicted mud and water areas are used to build a DTM and a DEM that subtracted from the photogrammetric DSM allows to automatically create a CHM. The resulting tree-wise predictions are supplemented with accurate height information and tree crown size and shape, enabling the use of allometric equations for carbon stocks accounting of whole mangrove ecosystems. As UASs become more accessible and relevant in coastal ecosystem monitoring (Joyce et al. 2023), the novel automated inventorization tool presented in (Chapter 4) promises to allow for regular surveillance monitoring of large stretches of mangrove forests, facilitating accurate blue carbon accounting (Macreadie et al. 2019; Song et al. 2023).

As mentioned in the "Limitations and outlook" section of (Chapter 2), it is imperative that the original images and annotations of habitat mapping efforts be made publicly available so that they can be re-evaluated independently, to disentangle the effects of changes in AI methods and data. Observing this recommendation, the complete source code for the AI workflow for detailed coral reef classification (Chapter 2) has been published in an open repository (Schürholz and Chennu 2022b) (Appendix D.1). In parallel, the raw input data and finalized habitat maps have been published in an open data repository (Schürholz and Chennu 2022a) (Appendix D.2). Similarly, the raw input data products and finalized inventories of mangrove forests (Chapter 4) have been published in a separate repository (Schürholz, Castellanos-Galindo, et al. 2023) (Appendix D.3). Furthermore, in this last repository the AI workflow was applied on 4 new mangrove forest plots and these are included in the data repository, providing predictions for

over 40 hectares of these remote habitats.

6.1.2 Ecological insights

The unprecedented thematic detail achieved in the underwater habitat maps with dense sampling provided abundant evidence for the current state of reef communities and dynamics in coral reefs on the Caribbean island of Curaçao. By densely mapping 20 hectares in 8 sites distributed along the leeward coast of the island, a clear gradient in coral reef community compositions emerged (Chapter 3). The comparisons with an array of previous studies of Curaçaoan reefs confirmed the validity of the maps and the community composition and configuration that they depicted. The ability to detect and map substrate classes such as benthic cyanobacterial mats (BCMs), turf algae and bare sediment proved to be very helpful in determining the states of these reefs. As shown in previous temporal studies on reefs in Curaçao (Bak et al. 2005; De Bakker et al. 2017), the reef communities close to urban settlements and aggro-industrial land were very deteriorated and had started shifting towards BCM and turf algae dominated environments. Other reefs in the north of the island, and under intense diving and fishing pressures, had also started deteriorating and shifting towards macroalgae and turf algae dominated habitats. Reefs in the south showed the healthiest communities, still dominated by scleractinian, soft and hydrocorals. Another benefit of dense sampling is the statistical power provided by having millions of samples. The environmental correlation and co-occurrence analyses (using GLLVMs) provided a clear pattern of deteriorated vs. healthy reefs on the island's reefs, and the possible drivers of community shifts. Sewage output, trash presence and over-fishing were the most prominent drivers of community shifts towards BCM and turf algae dominance.

The thematic detail in the habitat maps also allowed for reporting clearer biodiversity indexes and community composition plots. When diversity indexes are reported on abstracted or incomplete labelsets and sparse samples, true diversity is masked (Cao et al. 2002; Hochberg et al. 2021). (Table 3.3) provides a view of biodiversity indices produced by using an abstracted *reef-groups* labelset, a coral community subset, and a *detailed* labelset. Only the latter represents a biodiversity view that is consistent with the environmental gradient along the 8 sites. Thematic detail also facilitates focusing on intra-group communities, such as the scleractinian coral community depicted in (Figure 3.7). Although many of the reefs in the mid-southern side of Curaçao's leeward coastline show high abundance of corals, only one is not dominated by the opportunistic *Madracis auretenra* species. Neglecting this fact, by abstracting every species/-genera to a single *Coral* class, would disregard the issue of low functional redundancy present in many Caribbean reefs. The low structural complexity of *Madracis* species, for example, reduces the available hideouts and nursery space for reef invertebrates and fish, producing a decline in fisheries output, besides reducing the coastal protection from wave energy (Carlot et al. 2023; Graham 2014; Rogers et al. 2014). Only one site in the southern most tip of the island showed

higher complexity with large coverage of *Acroporids* and *Orbicella* complexes. These insights are only possible if classifications are done to deep taxonomic levels and with enough sampling to give statistical weight to predictions and reduce uncertainty. Furthermore, as shown in (Chapter 2) the ability to abstract to a *reefgroups* labelset also provides the ability to compare and validate global monitoring efforts, that usually use broad-groups labelsets (B. Lyons et al. 2020; Hochberg et al. 2021).

Moving from pixel-wise towards organism-focused predictions, further improves the possible insights attainable with ecosystem mapping products. In (Chapter 4) individual trees of the endemic *Pelliciera rhizophorae* mangrove species are delineated and their heights calculated. This provides a detailed geo-referenced inventory of mangrove forests, that can enable temporal tracking of individual trees, and more precise ecosystem accounting through allometric equations. Using the finalized predictions and data products, collaborators in the Universidad del Valle in Colombia are calculating the AGB and above ground carbon stocks for these valuable shallow coastal ecosystems, similar to a process done for other more sparse mangrove forests (Jones et al. 2020; Navarro et al. 2020; Wirasatriya et al. 2022). Previous studies used to rely on extrapolation methods, from sparse in-situ measurements to large satellite predicted mangrove areas, generating large uncertainty in the final calculations. Proximal sensing with effective AI workflows promise to reduce uncertainty by densely sampling forests and producing consistent inventories through time.

Providing the combination of thematic detail and organism-focused predictions is the next step in ecosystem mapping on the proximal sensing scale. (Chapter 5) presents an initial setup for this scenario. Merging spatially detailed color- and spectrally rich multi-spectral images, the acquired dataset promises to provide enough detail to enable organism detection (e.g., coral colonies) and thematic detail (e.g., classification of detected organism to genus/species). The type of habitat description attainable is shown in (Figure 5.2b), depicting what would be possible from detailed inventories of coral colonies in 3 reefs in the Coral Triangle, a region known for its vast biodiversity. The ability to connect coral reef community distributions with organism phenotypes on a large scale can elucidate key ecological questions, for example, the response of coral species reproduction strategies and phenotype plasticity to external stressors throughout their life-cycle. These hypothesis have been tested in focused studies done in a controlled settings with subsets of representative samples (Brito-Millán et al. 2019; Drury et al. 2022; Durante et al. 2019), but could benefit from the statistical backing of large thematic and spatial scales. With an initial and reduced annotation set, an example analysis of the deterioration status and adaptation of corals to turbidity and sedimentation was possible in (Chapter 5). Developing an AI workflow that can scale automated dense and detailed mapping up to the 13 surveyed sites in the turbid reefs of the Spermonde Archipelago would facilitate the gain of deeper ecological insights.

6.1.3 Methodological features and limitations

Spatial and thematic detailed mapping was performed through the acquisition of rich spatial and spectral data, with the use of proximal sensing platforms and novel AI workflows. The automation capabilities of these workflows allow to allocate the human expert effort to more meaningful tasks (i.e., ecological analyses), relieving them from tedious and repetitive work (i.e., annotating or measuring whole ecosystems) (Beijbom et al. 2015). Trained AI models can be used again in the same surveyed region with no extra effort required, facilitating temporal studies with consistent and comparable mapping products. The consistency of the predictions is maintained, given that if a bias was introduced into the AI model at training time, it will carry this bias throughout every application on new datasets, making products comparable. The true benefit of automation thus becomes palpable when spatial and temporal scales are extended. Also, by using AI for classification and a carefully designed protocol for creating the training set, the bias of human annotators can be substantially reduced and generalization improved (Hänsch et al. 2017). The human effort is reduced and focused to the initial stage of the mapping process, and the trained models can then be applied to larger areas and out-of-distribution sets. In contrast, human bias is more volatile, as experts are usually replaced throughout the life-cycle of monitoring efforts. With the advancements in AI methods and image-sensing technologies a widespread adoption of automated approaches is expected in ecological studies (Pichler et al. 2023; Xu et al. 2021).

Despite their rapid adoption, there are some limitations for current proximal sensing technologies. Imaging sensors with advanced capabilities, such as hyperspectral imagers, can have prohibitive costs for monitoring efforts. Even multispectral snapshot cameras are still very expensive. Some studies are making spectral technologies available through ad-hoc modifications to regular color cameras, but the capabilities of these sensors are limited (Teague, Day, et al. 2023; Teague, Willans, et al. 2019). Certain proximal sensing platforms are also very costly (e.g., AUVs or underwater rovers) and only large projects with sufficient funding can access such resources. Some UASs have become accessible to a broader audience (such as the ones used in Chapter 4), but as more carrying capacity is required for heavier and more advanced sensors, the price and complexity of the platforms rise.

Similarly to sensing platforms, AI workflows can be inaccessible for certain monitoring efforts. Specially, when using complex deep learning networks that are computationally demanding and can require expensive CPU, disk, memory and GPU settings to process large quantities of data in reasonable time. Cloud computing provides a cost-efficient alternative, but carries its own caveats, such as the need for an internet connection, expensive subscription plans and out-of-house data hosting. Further technological advancements in all these areas will be required for a true democratization of automated environmental mapping.

The thematic detail that can be attained with current technologies for automated mapping is

also limited, simply because of the visual discernability of biotic organisms. Since ML algorithms are trained from human annotations, it follows that if the human expert cannot identify an organism in an image to the most detailed taxonomic level possible, then the AI algorithm will not achieve this either. Molecular and/or spectroscopic methods could be used to identify organisms, but annotating on a large scale is still not possible due to logistical and time constraints. Thematic detail also varies across biogeographic regions and hinders interoperability of AI models. Scleractinian coral diversity in the Caribbean, for example, is far lower than in the Indo-Pacific. A method, such as the one presented in (Chapter 2) could not be applied "out-of-the-box" to a coral reef in another region. The parameters in the CNN can be reused, but the model has to be retrained with training data from the target region. Current advances in ML algorithms are allowing for smoother transitions between datasets, but human annotations are still always required.

Despite the current limitations, the production of detailed maps of ecosystem communities with their composition and configuration portrayed is a valuable tool in most monitoring/survey efforts. The effort of planning a mapping product to cater to a broad audience, by designing abstractable thematic and spatial scales, facilitates the effective reuse of data products in different contexts. The focus of future mapping workflows should be aimed at detailed and dense products, that use standardized labelsets and are publicly available.

6.2 Outlook

6.2.1 Future ecosystem community descriptions

Proximal sensing tools and AI workflows can be further expanded to provide more thematically detailed dense habitat maps, with ecosystem features described.

6.2.1.1 Future proximal sensing platforms

(Chapter 5) provides a glimpse into the future of ecosystem mapping. Complex shallow coastal ecosystems, such as Indo-Pacific coral reefs, can be mapped to great detail, using spectral and color imaging sensors in unison. The final goal is to delineate individual organisms (i.e., corals) and classify them to the most detailed taxonomic level possible (i.e., genus). As part of this doctoral project, and to achieve spatial and spectral detail, the HyperDiver device ((Chennu et al. 2017)) was expanded with two stereo color-imagers and one multi-spectral camera, in preparation for the survey described in (Chapter 5). The high spatial detail from the color sensors allows for organism segmentation, while spectral detail from the multi-spectral camera boosts the class-separation capabilities of AI workflows. Multi-spectral cameras were preferred to

hyperspectral ones, because as shown in (Chapter 2), far less spectral bands than those provided in hyperspectral imagers (10–25 instead of >100) are required for accurate thematically detailed predictions (Figure 2.3). Furthermore, the selected multi-spectral imager has the added benefit of capturing snapshot images (instead of images generated by stitching single-line scans) allowing for SfM software to produce photogrammetric models. This eases the co-registration to the spatially detailed color photogrammetric models. The co-registered orthomosaic model will contain 3 color bands from regular RGB-imagers, added to the 9 spectral bands from the multi-spectral imager, providing enough spatial and spectral detail to facilitate dense and detailed inventorization of coral reefs (Figure 5.1).

Other photogrammetric models, that were not directly used in any of the studies presented in this doctoral project, are 3D-models, such as triangular meshes and point clouds. Many studies have used these models to measure the structural complexity of ecosystems (Casella et al. 2017; D'Urban Jackson et al. 2020; Fukunaga et al. 2019; Lepczyk et al. 2021), to predict benthic community composition and configuration (Hopkinson et al. 2020), to measure individual coral colony growth (Lange et al. 2020) and to elucidate the cover of cryptic sessile fauna in reefs (Kornder et al. 2021). To have a complete habitat description, 3D complexity has to be described, and due to the spatially detailed dataset available through the expanded HyperDiver setting, such descriptions are achievable.

6.2.1.2 Future AI workflows for ecosystem mapping

The core of future AI workflows for shallow coastal ecosystem inventorization should be instance segmentation networks, as they provide the necessary tools to do both segmentation and classification tasks. Nowadays, open source libraries and publicly available software with great segmentation capabilities exist, such as Segment Anything Model (SAM)[1] and the TagLab annotation tool (Pavoni et al. 2022). (Figure 6.1) presents an example of applying the SAM model on the coral reef data presented in (Chapter 5) and (Figure 5.2) an example of semi-automatic annotations done with the TagLab tool. Many coral colonies were accurately delineated. These masks can be used in an AI workflow to train another ML classifier or to prompt human experts that can classify them semi-automatically.

In (Chapter 4) two deep learning CNNs build the core of the AI workflow, one network is used for instance segmentation (tree delineation) and one is used for semantic segmentation (pixel-wise classification). In recent years, networks that can do both tasks simultaneously have been developed, and are called panoptic segmentation networks (Cheng et al. 2020). These networks provide the benefits of segmenting individuals for a given class, while densely mapping background or contextual classes. In the dataset shown in (Chapter 5) for example, corals and sponges could be marked to be individually segmented, while substrate classes, such as BCMs

[1] A product of Meta – Inc, Available on https://segment-anything.com/, (visited on: 27/12/2023)

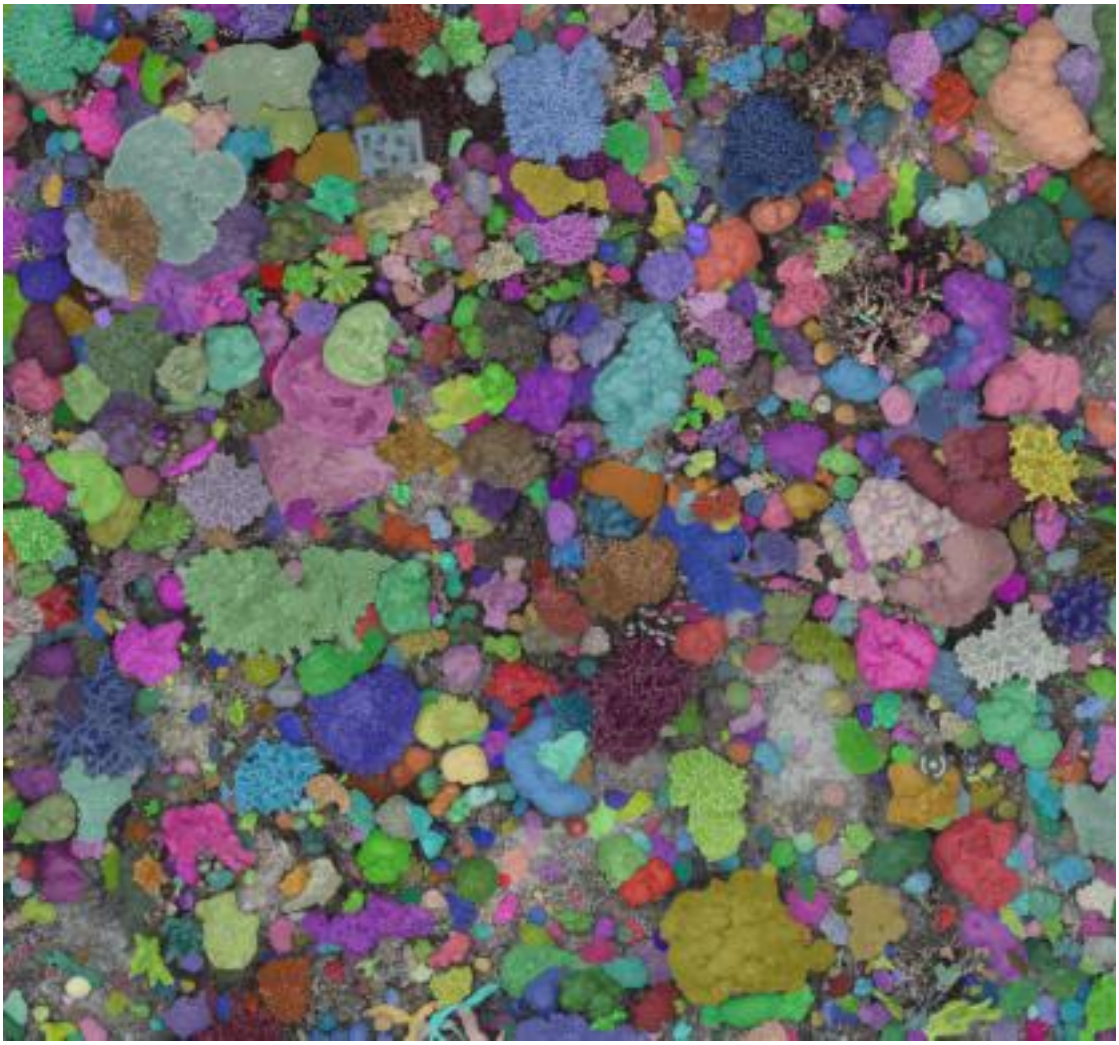

Figure 6.1 Example of coral reef instance segmentation using the Segment Anything Model (SAM) from Meta, Inc. Many coral colonies are perfectly segmented, without any previous training on the dataset. Branching corals are sometimes erroneously segmented or incomplete. Nonetheless, it provides good data points for further classification, by human experts or automated classifiers.

and turf algae, would be classified on a per-pixel basis. These networks show promising results, but further development is still required for them to be applicable to complex settings such as shallow coastal ecosystems (Kattenborn et al. 2021).

6.2.2 Future research

This doctoral project has attempted to provide evidence that shallow coastal ecosystem mapping should consider dense sampling and thematic detail on a proximal sensing scale to produce valuable analysis tools and to elucidate critical mechanisms of biotic and abiotic communities in these habitats. Through a few applications of AI-enabled automated and scalable ecosystem mapping, the benefits of detailed descriptions of these complex ecosystems were shown. However, great scope for further development and improvement remains. A great avenue of study, that was not explored in this body of work, is the validation of global monitoring reports on shallow coastal ecosystems (e.g., (B. Lyons et al. 2020; Goldberg et al. 2020)) through survey-scale mapping efforts (e.g., Chapter 3). There has been effort done in this direction in terrestrial applications (Tsendbazar et al. 2021), but local surveys in coastal ecosystems have lacked the coverage, sampling resolution and precise geo-referencing (in underwater surveying), to accurately compare the two scales of measurement. Further research is required to provide good mechanisms to compare both methods, and specially to geo-reference underwater habitat maps. As image resolution from satellite platforms becomes finer, many of the methodologies applied in the examples of this doctoral project could be applied on this emerging image data. For example, mangrove canopy mapping with tree instance segmentation has already been achieved using high-resolution satellite imagery (Lassalle et al. 2022). Given that satellites can revisit the same site frequently, this would allow for detailed organism tracking through time. In turn, these prompts interesting research possibilities, to determine the changes and the location of organisms across two or more time points.

One of the aims of the studies in this doctoral thesis has been the creation of detailed habitat maps through the use of spectrally rich data. A complementary application of spectral information is photopigment analysis. Further research can focus on the role of relevant photopigments (e.g., Chlorophyll) and their distribution across environmental gradients within the biotic communities in shallow coastal ecosystems. The availability of detailed thematic maps would even allow to carry out this analysis on a per-species or per-genera level, elucidating the drivers for community composition and configuration across gradients. Photopigment analysis could also determine the health of organisms and identify stages of deterioration, for example during coral bleaching or coral band-diseases (Fabricius 2006; Kuta et al. 2002).

In conclusion, shallow coastal ecosystem ecology and detailed ecosystem mapping through proximal sensing and AI workflows are active fields of research, undergoing rapid improvement leading to astounding new insights. Improvements in proximal sensing platforms and AI algorithms will help gather large datasets of shallow coastal ecosystem biotic communities, allowing to set baselines in remote under-studied habitats and to provide much needed consistency for accurate temporal studies. Spatial and thematic scales that were not possible to achieve in the near past, can elucidate patterns that were not considered before, providing new knowledge and challenging previous beliefs. The automated and scalable analysis of composition, configuration, structure

and function of biotic and abiotic elements in ecosystems further deepens our understanding of natural and anthropogenic processes, that affect coral reefs and mangrove forests, facilitating more informed protection and restoration efforts to be taken, for the benefit of these valuable habitats and the populations depending on them.

References

B. Lyons, Mitchell, Chris M. Roelfsema, Emma V. Kennedy, Eva M. Kovacs, Rodney Borrego-Acevedo, Kathryn Markey, Meredith Roe, Doddy M. Yuwono, Daniel L. Harris, Stuart R. Phinn, Gregory P. Asner, Jiwei Li, David E. Knapp, Nicholas S. Fabina, Kirk Larsen, Dimosthenis Traganos, and Nicholas J. Murray (2020). "Mapping the world's coral reefs using a global multiscale earth observation framework". In: *Remote Sensing in Ecology and Conservation*. Ed. by Nathalie Pettorelli and Vincent Lecours, rse2.157. DOI: *10.1002/rse2.157*.

Bak, Rolf P. M., Gerard Nieuwland, and Erik H. Meesters (2005). "Coral reef crisis in deep and shallow reefs: 30 years of constancy and change in reefs of Curacao and Bonaire". In: *Coral Reefs* 24.3, pp. 475–479. DOI: *10.1007/s00338-005-0009-1*.

Beijbom, Oscar, Peter J. Edmunds, Chris Roelfsema, Jennifer Smith, David I. Kline, Benjamin P. Neal, Matthew J. Dunlap, Vincent Moriarty, Tung-Yung Fan, Chih-Jui Tan, Stephen Chan, Tali Treibitz, Anthony Gamst, B. Greg Mitchell, and David Kriegman (2015). "Towards Automated Annotation of Benthic Survey Images: Variability of Human Experts and Operational Modes of Automation". In: *PLOS ONE* 10.7, e0130312. DOI: *10.1371/journal.pone.0130312*.

Brito-Millán, Marlene, Mark J. A. Vermeij, Esmeralda A. Alcantar, and Stuart A. Sandin (2019). "Coral reef assessments based on cover alone mask active dynamics of coral communities". In: *Marine Ecology Progress Series* 630, pp. 55–68. URL: *https://www.jstor.org/stable/26920540* (visited on 12/10/2023).

Cao, Yong, D. Dudley Williams, and David P. Larsen (2002). "Comparison of Ecological Communities: The Problem of Sample Representativeness". In: *Ecological Monographs* 72.1, pp. 41–56. DOI: *10.1890/0012-9615(2002)072[0041:COECTP]2.0.CO;2*.

Carlot, Jérémy, Michalis Vousdoukas, Alessio Rovere, Theofanis Karambas, Hunter S. Lenihan, Mohsen Kayal, Mehdi Adjeroud, Gonzalo Pérez-Rosales, Laetitia Hedouin, and Valeriano Parravicini (2023). "Coral reef structural complexity loss exposes coastlines to waves". In: *Scientific Reports* 13.1, p. 1683. DOI: *10.1038/s41598-023-28945-x*.

Casella, Elisa, Antoine Collin, Daniel Harris, Sebastian Ferse, Sonia Bejarano, Valeriano Parravicini, James L. Hench, and Alessio Rovere (2017). "Mapping coral reefs using consumer-grade drones and structure from motion photogrammetry techniques". In: *Coral Reefs* 36.1, pp. 269–275. DOI: *10.1007/s00338-016-1522-0*.

Cheng, Bowen, Maxwell D. Collins, Yukun Zhu, Ting Liu, Thomas S. Huang, Hartwig Adam, and Liang-Chieh Chen (2020). "Panoptic-DeepLab: A Simple, Strong, and Fast Baseline for Bottom-Up Panoptic Segmentation". In: *arXiv:1911.10194 [cs]*. arXiv: *1911.10194*. URL: *http://arxiv.org/abs/1911.10194* (visited on 02/18/2021).

Chennu, Arjun, Paul Färber, Glenn De'ath, Dirk de Beer, and Katharina E. Fabricius (2017). "A diver-operated hyperspectral imaging and topographic surveying system for automated mapping of benthic habitats". In: *Scientific Reports* 7.1, pp. 1–12. DOI: *10.1038/s41598-017-07337-y*.

D'Urban Jackson, Tim, Gareth J. Williams, Guy Walker-Springett, and Andrew J. Davies (2020). "Three-dimensional digital mapping of ecosystems: a new era in spatial ecology". In: *Proceedings of the Royal Society B: Biological Sciences* 287.1920, p. 20192383. DOI: *10.1098/rspb.2019.2383*.

De Bakker, Didier M., Fleur C. Van Duyl, Rolf P. M. Bak, Maggy M. Nugues, Gerard Nieuwland, and Erik H. Meesters (2017). "40 Years of benthic community change on the Caribbean reefs of Curaçao and Bonaire: the rise of slimy cyanobacterial mats". In: *Coral Reefs* 36.2, pp. 355–367. DOI: *10.1007/s00338-016-1534-9*.

Drury, Crawford, Jenna Dilworth, Eva Majerová, Carlo Caruso, and Justin B. Greer (2022). "Expression plasticity regulates intraspecific variation in the acclimatization potential of a reef-building coral". In: *Nature Communications* 13.1, p. 4790. DOI: *10.1038/s41467-022-32452-4*.

Durante, Meghann K., Iliana B. Baums, Dana E. Williams, Sam Vohsen, and Dustin W. Kemp (2019). "What drives phenotypic divergence among coral clonemates of Acropora palmata?" In: *Molecular Ecology* 28.13, pp. 3208–3224. DOI: *10.1111/mec.15140*.

Fabricius, Katharina E. (2006). "Effects of irradiance, flow, and colony pigmentation on the temperature microenvironment around corals: Implications for coral bleaching?" In: *Limnology and Oceanography* 51.1, pp. 30–37. DOI: *10.4319/lo.2006.51.1.0030*.

Fukunaga, Atsuko, John H. R. Burns, Brianna K. Craig, and Randall K. Kosaki (2019). "Integrating Three-Dimensional Benthic Habitat Characterization Techniques into Ecological Monitoring of Coral Reefs". In: *Journal of Marine Science and Engineering* 7.2, p. 27. DOI: *10.3390/jmse7020027*.

Goldberg, Liza, David Lagomasino, Nathan Thomas, and Temilola Fatoyinbo (2020). "Global declines in human-driven mangrove loss". In: *Global Change Biology* 26.10, pp. 5844–5855. DOI: *10.1111/gcb.15275*.

Graham, Nicholas A. J. (2014). "Habitat Complexity: Coral Structural Loss Leads to Fisheries Declines". In: *Current Biology* 24.9, R359–R361. DOI: *10.1016/j.cub.2014.03.069*.

Hänsch, R., A. Ley, and O. Hellwich (2017). "Correct and still wrong: The relationship between sampling strategies and the estimation of the generalization error". In: *2017 IEEE International Geoscience and Remote Sensing Symposium (IGARSS)*. 2017 IEEE International Geoscience and Remote Sensing Symposium (IGARSS), pp. 3672–3675. DOI: *10.1109/IGARSS.2017.8127795*.

Hochberg, Eric J. and Michelle M. Gierach (2021). "Missing the Reef for the Corals: Unexpected Trends Between Coral Reef Condition and the Environment at the Ecosystem Scale". In: *Frontiers in Marine Science* 8, p. 1191. DOI: *10.3389/fmars.2021.727038*.

Hopkinson, Brian M., Andrew C. King, Daniel P. Owen, Matthew Johnson-Roberson, Matthew H. Long, and Suchendra M. Bhandarkar (2020). "Automated classification of three-dimensional reconstructions of coral reefs using convolutional neural networks". In: *PLOS ONE* 15.3, e0230671. DOI: *10.1371/journal.pone.0230671*.

Jones, Alice R., Ramesh Raja Segaran, Kenneth D. Clarke, Michelle Waycott, William S. H. Goh, and Bronwyn M. Gillanders (2020). "Estimating Mangrove Tree Biomass and Carbon Content: A Comparison of Forest Inventory Techniques and Drone Imagery". In: *Frontiers in Marine Science* 6. URL: *https://www.frontiersin.org/articles/10.3389/fmars.2019.00784* (visited on 12/27/2023).

Joyce, Karen E., Kate C. Fickas, and Michelle Kalamandeen (2023). "The unique value proposition for using drones to map coastal ecosystems". In: *Cambridge Prisms: Coastal Futures* 1, e6. DOI: *10.1017/cft.2022.7*.

Kattenborn, Teja, Jens Leitloff, Felix Schiefer, and Stefan Hinz (2021). "Review on Convolutional Neural Networks (CNN) in vegetation remote sensing". In: *ISPRS Journal of Photogrammetry and Remote Sensing* 173, pp. 24–49. DOI: *10.1016/j.isprsjprs.2020.12.010*.

Kennedy, Emma V., Chris M. Roelfsema, Mitchell B. Lyons, Eva M. Kovacs, Rodney Borrego-Acevedo, Meredith Roe, Stuart R. Phinn, Kirk Larsen, Nicholas J. Murray, Doddy Yuwono, Jeremy Wolff, and Paul Tudman (2021). "Reef Cover, a coral reef classification for global habitat mapping from remote sensing". In: *Scientific Data* 8.1, p. 196. DOI: *10.1038/s41597-021-00958-z*.

Kornder, Niklas A., Jose Cappelletto, Benjamin Mueller, Margaretha J. L. Zalm, Stephanie J. Martinez, Mark J. A. Vermeij, Jef Huisman, and Jasper M. de Goeij (2021). "Implications of 2D versus 3D surveys to measure the abundance and composition of benthic coral reef communities". In: *Coral Reefs* 40.4, pp. 1137–1153. DOI: *10.1007/s00338-021-02118-6*.

Kuta, K. and L. Richardson (2002). "Ecological aspects of black band disease of corals: relationships between disease incidence and environmental factors". In: *Coral Reefs* 21.4, pp. 393–398. DOI: *10.1007/s00338-002-0261-6*.

Lange, Ines D. and Chris T. Perry (2020). "A quick, easy and non-invasive method to quantify coral growth rates using photogrammetry and 3D model comparisons". In: *Methods in Ecology and Evolution*. Ed. by Natalie Cooper, pp. 2041–210X.13388. DOI: *10.1111/2041-210X.13388*.

Lassalle, Guillaume, Matheus Pinheiro Ferreira, Laura Elena Cué La Rosa, and Carlos Roberto de Souza Filho (2022). "Deep learning-based individual tree crown delineation in mangrove forests using very-high-resolution satellite imagery". In: *ISPRS Journal of Photogrammetry and Remote Sensing* 189, pp. 220–235. DOI: *10.1016/j.isprsjprs.2022.05.002*.

Lecours, Vincent (2017). "On the Use of Maps and Models in Conservation and Resource Management (Warning: Results May Vary)". In: *Frontiers in Marine Science* 4, p. 288. DOI: *10.3389/fmars.2017.00288*.

Lepczyk, Christopher A, Lisa M Wedding, Gregory P Asner, Simon J Pittman, Tristan Goulden, Marc A Linderman, Jeanne Gang, and Rosalie Wright (2021). "Advancing Landscape and Seascape Ecology from a 2D to a 3D Science". In: *BioScience* 71.6, pp. 596–608. DOI: *10.1093/biosci/biab001*.

Macreadie, Peter I., Andrea Anton, John A. Raven, Nicola Beaumont, Rod M. Connolly, Daniel A. Friess, Jeffrey J. Kelleway, Hilary Kennedy, Tomohiro Kuwae, Paul S. Lavery, Catherine E.

Lovelock, Dan A. Smale, Eugenia T. Apostolaki, Trisha B. Atwood, Jeff Baldock, Thomas S. Bianchi, Gail L. Chmura, Bradley D. Eyre, James W. Fourqurean, Jason M. Hall-Spencer, Mark Huxham, Iris E. Hendriks, Dorte Krause-Jensen, Dan Laffoley, Tiziana Luisetti, Núria Marbà, Pere Masque, Karen J. McGlathery, J. Patrick Megonigal, Daniel Murdiyarso, Bayden D. Russell, Rui Santos, Oscar Serrano, Brian R. Silliman, Kenta Watanabe, and Carlos M. Duarte (2019). "The future of Blue Carbon science". In: *Nature Communications* 10.1, p. 3998. DOI: *10.1038/s41467-019-11693-w*.

Mills, Matthew S., Mischa Ungermann, Guy Rigot, Joost den Haan, Javier X. Leon, and Tom Schils (2023). "Assessment of the utility of underwater hyperspectral imaging for surveying and monitoring coral reef ecosystems". In: *Scientific Reports* 13.1, p. 21103. DOI: *10.1038/s41598-023-48263-6*.

Muldrow, Milton, Edward C. M. Parsons, and Robert Jonas (2020). "Shifting baseline syndrome among coral reef scientists". In: *Humanities and Social Sciences Communications* 7.1, pp. 1–8. DOI: *10.1057/s41599-020-0526-0*.

Navarro, Alejandro, Mary Young, Blake Allan, Paul Carnell, Peter Macreadie, and Daniel Ierodiaconou (2020). "The application of Unmanned Aerial Vehicles (UAVs) to estimate above-ground biomass of mangrove ecosystems". In: *Remote Sensing of Environment* 242, p. 111747. DOI: *10.1016/j.rse.2020.111747*.

Otero, Viviana, Ruben Van De Kerchove, Behara Satyanarayana, Columba Martínez-Espinosa, Muhammad Amir Bin Fisol, Mohd Rodila Bin Ibrahim, Ibrahim Sulong, Husain Mohd-Lokman, Richard Lucas, and Farid Dahdouh-Guebas (2018). "Managing mangrove forests from the sky: Forest inventory using field data and Unmanned Aerial Vehicle (UAV) imagery in the Matang Mangrove Forest Reserve, peninsular Malaysia". In: *Forest Ecology and Management* 411, pp. 35–45. DOI: *10.1016/j.foreco.2017.12.049*.

Pavoni, Gaia, Massimiliano Corsini, Federico Ponchio, Alessandro Muntoni, Clinton Edwards, Nicole Pedersen, Stuart Sandin, and Paolo Cignoni (2022). "TagLab: AI-assisted annotation for the fast and accurate semantic segmentation of coral reef orthoimages". In: *Journal of Field Robotics* 39.3, pp. 246–262. DOI: *10.1002/rob.22049*.

Pichler, Maximilian and Florian Hartig (2023). "Machine learning and deep learning—A review for ecologists". In: *Methods in Ecology and Evolution* 14.4, pp. 994–1016. DOI: *10.1111/2041-210X.14061*.

Riitters, Kurt (2019). "Pattern metrics for a transdisciplinary landscape ecology". In: *Landscape Ecology* 34.9, pp. 2057–2063. DOI: *10.1007/s10980-018-0755-4*.

Rogers, Alice, Julia L. Blanchard, and Peter J. Mumby (2014). "Vulnerability of Coral Reef Fisheries to a Loss of Structural Complexity". In: *Current Biology* 24.9, pp. 1000–1005. DOI: *10.1016/j.cub.2014.03.026*.

Schürholz, Daniel, Gustavo Adolfo Castellanos-Galindo, Elisa Casella, Juan Carlos Mejía-Rentería, and Arjun Chennu (2023). *Detailed tree inventory and area coverage of remote mangrove*

forests (species: Pelliciera rhizophorae and Rhizophora mangle) in the Utría National Park in the Colombian Pacific Coast. DOI: *10.1594/PANGAEA.962229*.

Schürholz, Daniel and Arjun Chennu (2022a). *Dense and taxonomically detailed habitat maps of coral reef benthos machine-generated from underwater hyperspectral transects in Curaçao*. DOI: *10.1594/PANGAEA.946315*.

– (2022b). *Digitizing the coral reef: a complete workflow for dense taxonomic mapping of benthic habitats with machine learning of underwater hyperspectral images*. DOI: *10.5281/zenodo.7185108*.

Song, Shanshan, Yali Ding, Wei Li, Yuchen Meng, Jian Zhou, Ruikun Gou, Conghe Zhang, Shengbin Ye, Neil Saintilan, Ken W. Krauss, Stephen Crooks, Shuguo Lv, and Guanghui Lin (2023). "Mangrove reforestation provides greater blue carbon benefit than afforestation for mitigating global climate change". In: *Nature Communications* 14.1, p. 756. DOI: *10.1038/s41467-023-36477-1*.

Sparrow, Ben D., Will Edwards, Samantha E.M. Munroe, Glenda M. Wardle, Greg R. Guerin, Jean-Francois Bastin, Beryl Morris, Rebekah Christensen, Stuart Phinn, and Andrew J. Lowe (2020). "Effective ecosystem monitoring requires a multi-scaled approach". In: *Biological Reviews* 95.6, pp. 1706–1719. DOI: *10.1111/brv.12636*.

Teague, Jonathan, John C. C. Day, Michael J. Allen, Thomas B. Scott, Eric J. Hochberg, and David Megson-Smith (2023). "A Demonstration of the Capability of Low-Cost Hyperspectral Imaging for the Characterisation of Coral Reefs". In: *Oceans* 4.3, pp. 286–300. DOI: *10.3390/oceans4030020*.

Teague, Jonathan, Jack Willans, Michael J. Allen, Thomas B. Scott, and John C. C. Day (2019). "Hyperspectral imaging as a tool for assessing coral health utilising natural fluorescence". In: *Journal of Spectral Imaging* 8. DOI: *10.1255/jsi.2019.a7*.

Tsendbazar, N., M. Herold, L. Li, A. Tarko, S. de Bruin, D. Masiliunas, M. Lesiv, S. Fritz, M. Buchhorn, B. Smets, R. Van De Kerchove, and M. Duerauer (2021). "Towards operational validation of annual global land cover maps". In: *Remote Sensing of Environment* 266, p. 112686. DOI: *10.1016/j.rse.2021.112686*.

Tucker, Compton, Martin Brandt, Pierre Hiernaux, Ankit Kariryaa, Kjeld Rasmussen, Jennifer Small, Christian Igel, Florian Reiner, Katherine Melocik, Jesse Meyer, Scott Sinno, Eric Romero, Erin Glennie, Yasmin Fitts, August Morin, Jorge Pinzon, Devin McClain, Paul Morin, Claire Porter, Shane Loeffler, Laurent Kergoat, Bil-Assanou Issoufou, Patrice Savadogo, Jean-Pierre Wigneron, Benjamin Poulter, Philippe Ciais, Robert Kaufmann, Ranga Myneni, Sassan Saatchi, and Rasmus Fensholt (2023). "Sub-continental-scale carbon stocks of individual trees in African drylands". In: *Nature* 615.7950, pp. 80–86. DOI: *10.1038/s41586-022-05653-6*.

Wirasatriya, Anindya, Rudhi Pribadi, Sigit Bayhu Iryanthony, Lilik Maslukah, Denny Nugroho Sugianto, Muhammad Helmi, Raditya Rizki Ananta, Novi Susetyo Adi, Terry Louise Kepel, Restu N. A. Ati, Mariska A. Kusumaningtyas, Rempei Suwa, Raghab Ray, Takashi Nakamura, and Kazuo Nadaoka (2022). "Mangrove Above-Ground Biomass and Carbon Stock in

the Karimunjawa-Kemujan Islands Estimated from Unmanned Aerial Vehicle-Imagery". In: *Sustainability* 14.2, p. 706. DOI: *10.3390/su14020706*.

Wyatt, Mathew, Ben Radford, Nikolaus Callow, Mohammed Bennamoun, and Sharyn Hickey (2022). "Using ensemble methods to improve the robustness of deep learning for image classification in marine environments". In: *Methods in Ecology and Evolution* 13.6, pp. 1317–1328. DOI: *10.1111/2041-210X.13841*.

Xu, Yongjun, Xin Liu, Xin Cao, Changping Huang, Enke Liu, Sen Qian, Xingchen Liu, Yanjun Wu, Fengliang Dong, Cheng-Wei Qiu, Junjun Qiu, Keqin Hua, Wentao Su, Jian Wu, Huiyu Xu, Yong Han, Chenguang Fu, Zhigang Yin, Miao Liu, Ronald Roepman, Sabine Dietmann, Marko Virta, Fredrick Kengara, Ze Zhang, Lifu Zhang, Taolan Zhao, Ji Dai, Jialiang Yang, Liang Lan, Ming Luo, Zhaofeng Liu, Tao An, Bin Zhang, Xiao He, Shan Cong, Xiaohong Liu, Wei Zhang, James P. Lewis, James M. Tiedje, Qi Wang, Zhulin An, Fei Wang, Libo Zhang, Tao Huang, Chuan Lu, Zhipeng Cai, Fang Wang, and Jiabao Zhang (2021). "Artificial intelligence: A powerful paradigm for scientific research". In: *The Innovation* 2.4, p. 100179. DOI: *10.1016/j.xinn.2021.100179*.

Zhong, Zilong, Jonathan Li, Zhiming Luo, and Michael Chapman (2018). "Spectral–Spatial Residual Network for Hyperspectral Image Classification: A 3-D Deep Learning Framework". In: *IEEE Transactions on Geoscience and Remote Sensing* 56.2, pp. 847–858. DOI: *10.1109/TGRS.2017.2755542*.

Part IV

Appendix

Appendix A

Supplementary material for Chapter 2: Digitizing The Coral Reef

A.1 Spectral-spatial neural network parameters and machine learning libraries

The parameters used for training the spectral-spatial neural network were: a batch size of 32, a number of epochs of 32 and an input patch size of 13×13 pixels. Cross entropy loss with weight balancing based on class abundance was used as the loss function during network training. The optimizer was a rectified Adam function with a weight decay value of 1.5 and had a β of 0.999 (Liu et al. 2021). The learning rate value was adjusted by a cyclic learning rate scheduler, oscillating from $1e^{-8}$ to $1e^{-3}$ in triangular ramps with a step of 250 batches of data samples. The whole network training workflow was built with the PyTorch library (Paszke et al. 2019), the Skorch machine learning workflow management library (https://github.com/skorch-dev/skorch) and the Mlflow training visualization tool (https://github.com/mlflow/mlflow/). Training was performed on a machine with two Nvidia RTX2080 GPUs, each with 12Gb of dedicated memory.

The principal component analysis done for the segmented method was implemented using the scikit-learn library (Pedregosa et al. 2011). Furthermore, the watershed algorithm from the scikit-image library was used (Walt et al. 2014). Dense conditional random fields (DCRF) were implemented with the pyDenseCRF python library (https://github.com/lucasb-eyer/pydensecrf).

References

Liu, Xue, Temilola E. Fatoyinbo, Nathan M. Thomas, Weihe Wendy Guan, Yanni Zhan, Pinki Mondal, David Lagomasino, Marc Simard, Carl C. Trettin, Rinki Deo, and Abigail Barenblitt (2021). "Large-Scale High-Resolution Coastal Mangrove Forests Mapping Across West Africa With Machine Learning Ensemble and Satellite Big Data". In: *Frontiers in Earth Science* 8. URL: *https://www.frontiersin.org/articles/10.3389/feart.2020.560933* (visited on 05/01/2023).

Paszke, Adam, Sam Gross, Francisco Massa, Adam Lerer, James Bradbury, Gregory Chanan, Trevor Killeen, Zeming Lin, Natalia Gimelshein, Luca Antiga, Alban Desmaison, Andreas Kopf, Edward Yang, Zachary DeVito, Martin Raison, Alykhan Tejani, Sasank Chilamkurthy, Benoit Steiner, Lu Fang, Junjie Bai, and Soumith Chintala (2019). "PyTorch: An Imperative Style, High-Performance Deep Learning Library". In: *Advances in Neural Information Processing Systems 32*. Curran Associates, Inc., pp. 8024–8035. URL: *http://papers.neurips.cc/paper/9015-pytorch-an-imperative-style-high-performance-deep-learning-library.pdf*.

Pedregosa, F., G. Varoquaux, A. Gramfort, V. Michel, B. Thirion, O. Grisel, M. Blondel, P. Prettenhofer, R. Weiss, V. Dubourg, J. Vanderplas, A. Passos, D. Cournapeau, M. Brucher, M. Perrot, and E. Duchesnay (2011). "Scikit-learn: Machine Learning in Python". In: *Journal of Machine Learning Research* 12, pp. 2825–2830.

Walt, Stéfan van der, Johannes L. Schönberger, Juan Nunez-Iglesias, François Boulogne, Joshua D. Warner, Neil Yager, Emmanuelle Gouillart, Tony Yu, and the scikit-image contributors the scikit-image (2014). "scikit-image: image processing in Python". In: *PeerJ* 2, e453. DOI: *10.7717/peerj.453*.

A.2 Supplementary Figures

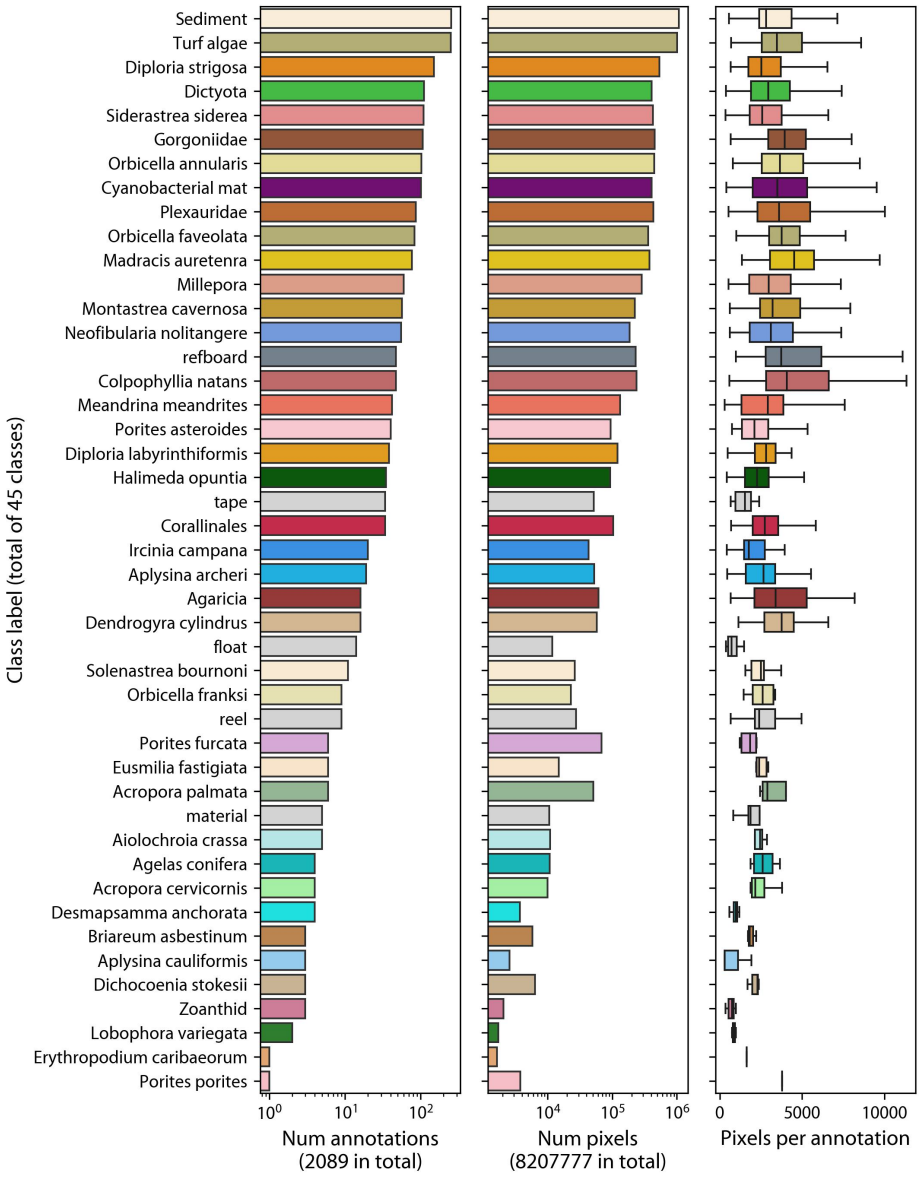

Figure A.1 Class distributions of detailed annotations. The dataset shows a large class imbalance in annotation regions in learning and validation transects. Classes such as Sediment and Turf algae are abundant in almost every transect with over 200 regions and covering around one million pixels. Rare classes such as *Lobophora variegata* and *Zoanthid* have only 2 and 3 regions respectively, covering only around 2000 pixels. The annotations across classes were of similar sizes in term of number of pixels contained, except for rare species.

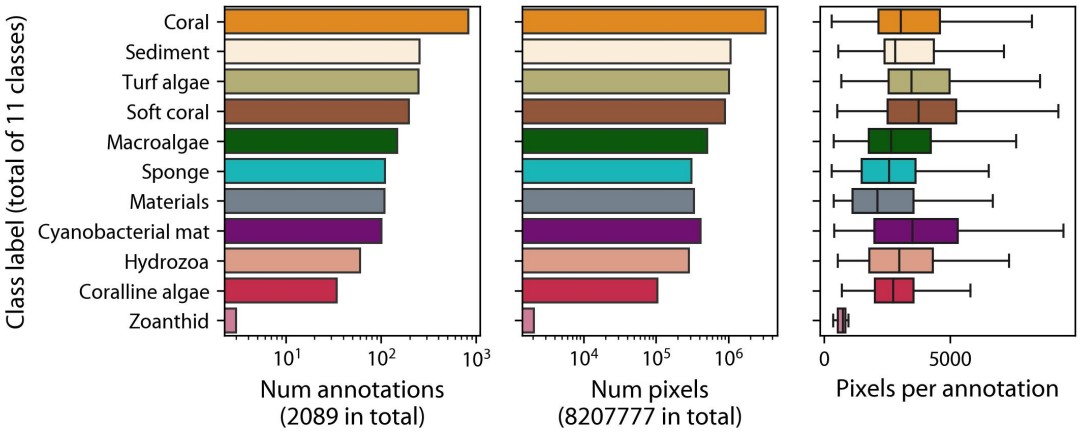

Figure A.2 Class distributions of reefgroups annotations. The reefgroups dataset less class imbalance than the detailed labelspace learning and validation transects. Classes such as *Coral*, *Sediment* and *Turf algae* are abundant in almost every transect with over 200 regions and covering around one million pixels. Rare classes such as *Zoanthid* have only 2 and 3 regions respectively, covering only around 2000 pixels. The annotations across classes were of similar sizes in term of number of pixels contained.

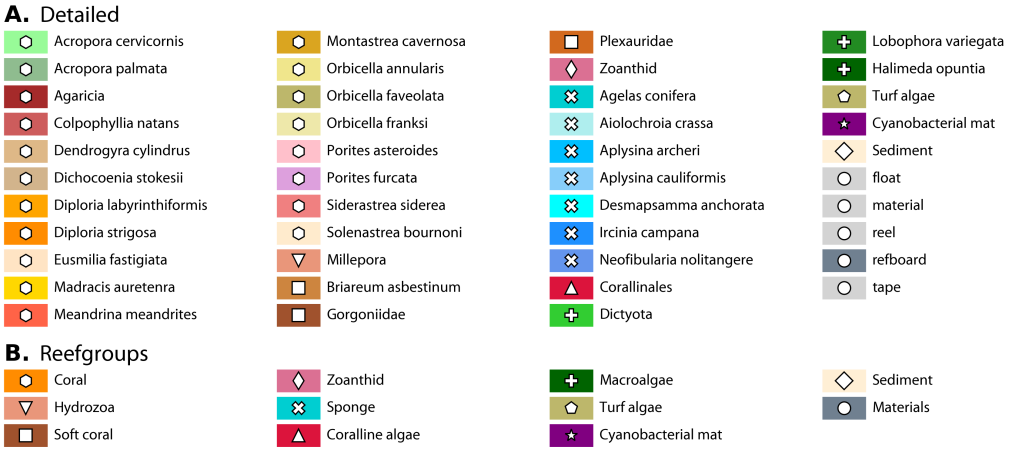

Figure A.3 Detailed and reefgroups labelspaces. (**A**) Detailed labelspace consisting of 43 classes, representing the deepest possible taxonomic definition of targets in visual annotation of underwater transects. (**B**) Reefgroups labelspace consisting of 11 labels for broad reef groups and abiotic elements. Some of the reefgroups classes are divided into two or more classes in the detailed labelspace. Shapes within the color boxes are provided for easier identification between labelspaces.

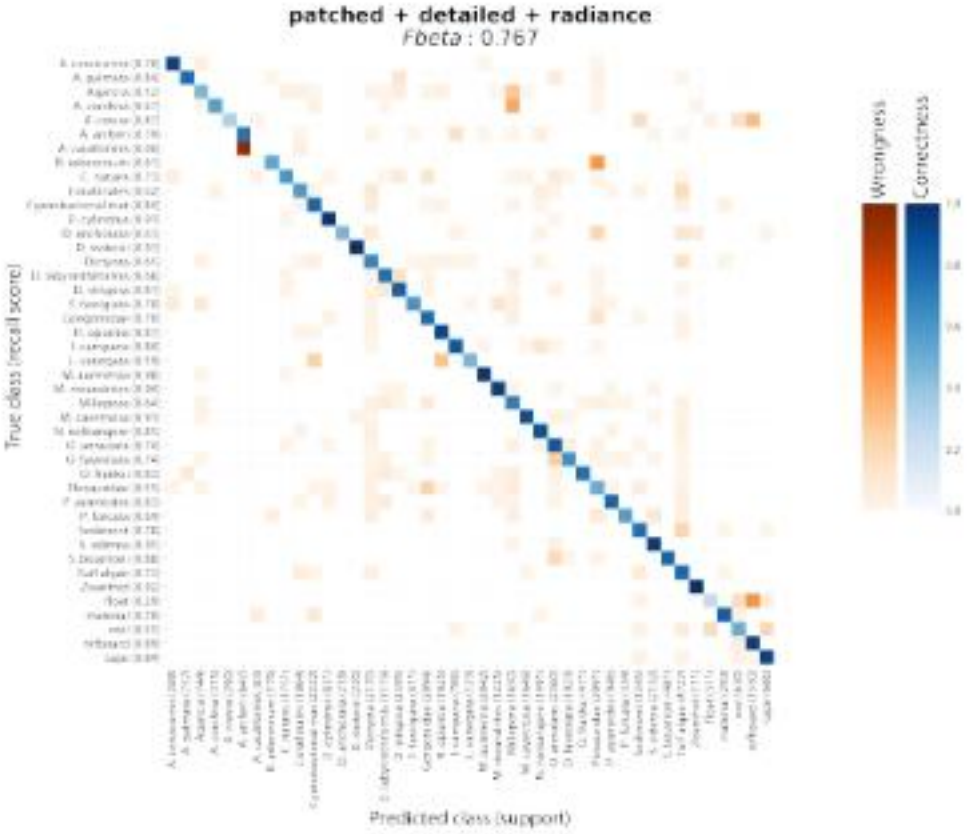

Figure A.4 Recall confusion matrix for patched classifier predicting into the detailed labelspace from radiance images.

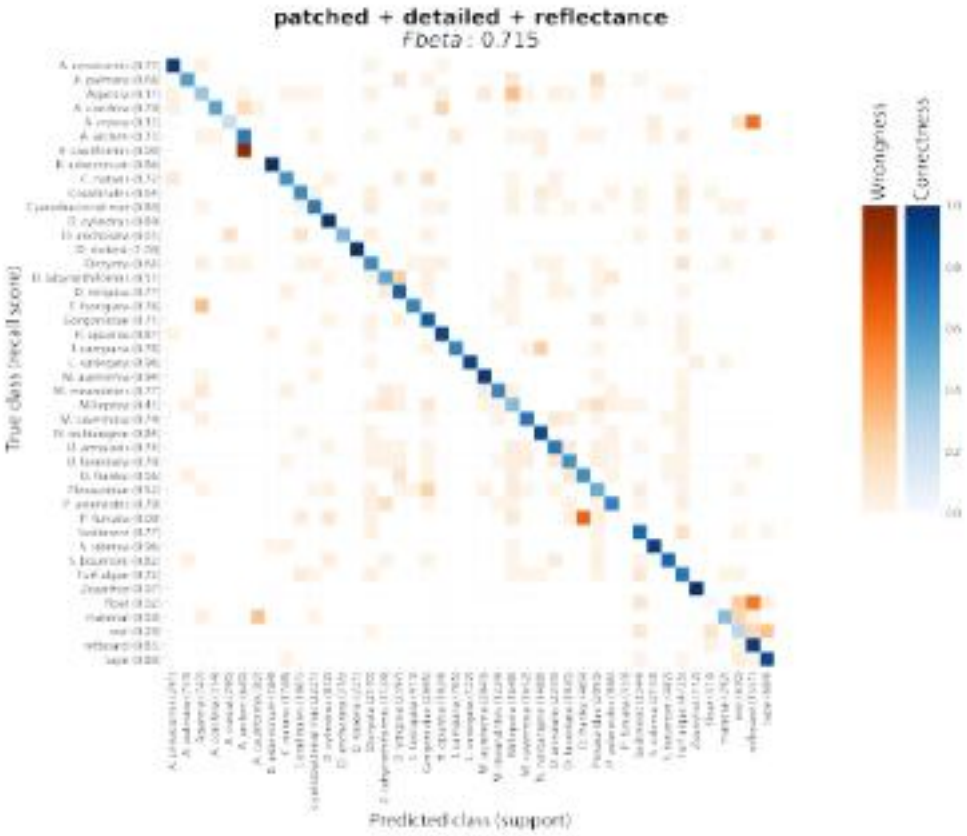

Figure A.5 Recall confusion matrix for patched classifier predicting into the detailed labelspace from reflectance images.

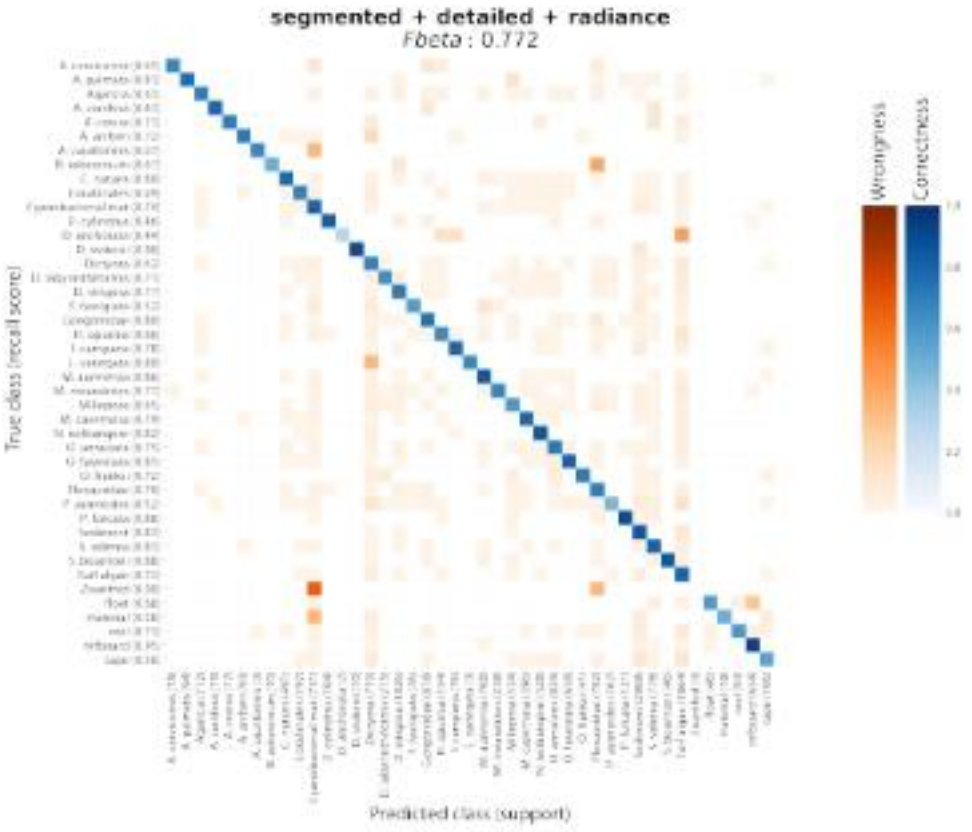

Figure A.6 Recall confusion matrix for segmented classifier predicting into the detailed labelspace from radiance images.

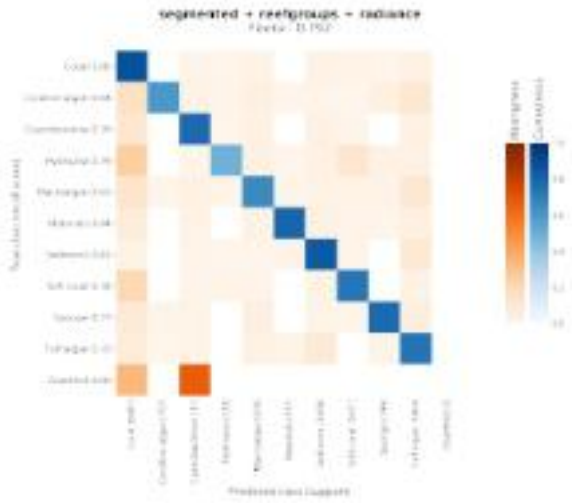

Figure A.7 Recall confusion matrix for segmented classifier predicting into the reefgroups labelspace from radiance images.

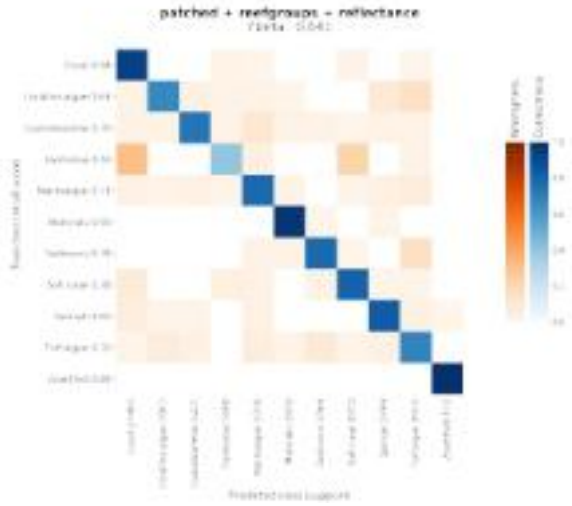

Figure A.8 Recall confusion matrix for patched classifier predicting into the reefgroups labelspace from reflectance images.

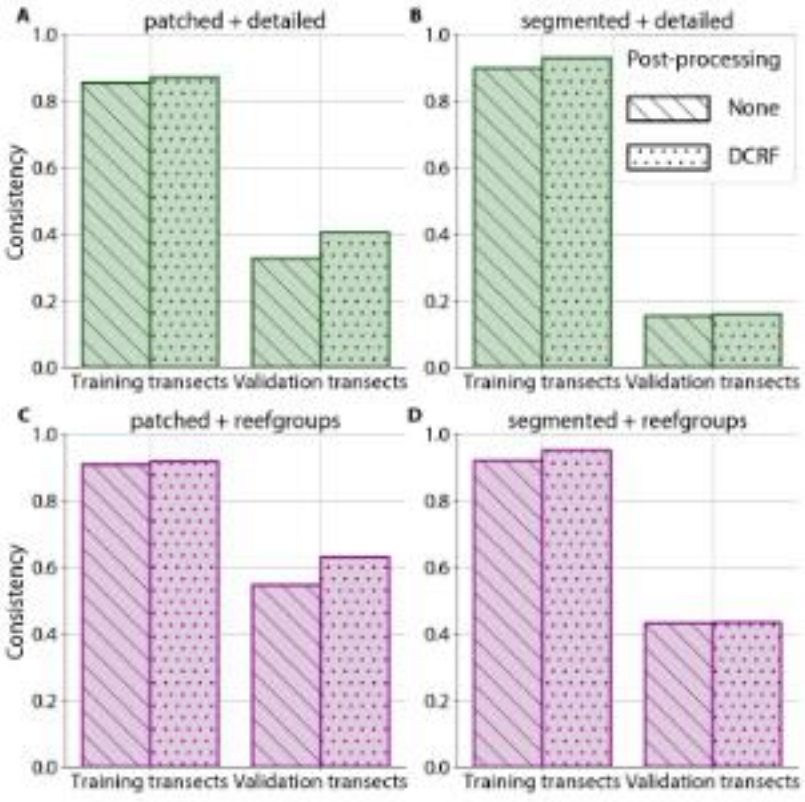

Figure A.9 Classification consistency for combinations of ML methods and labelspaces as in Figure 2.4, but using reflectance data.

Figure A.10 Habitat maps montage with workflow patched+detailed+radiance. Middle section of 23 learning transects. Size of each section is 640x19920 pixels.

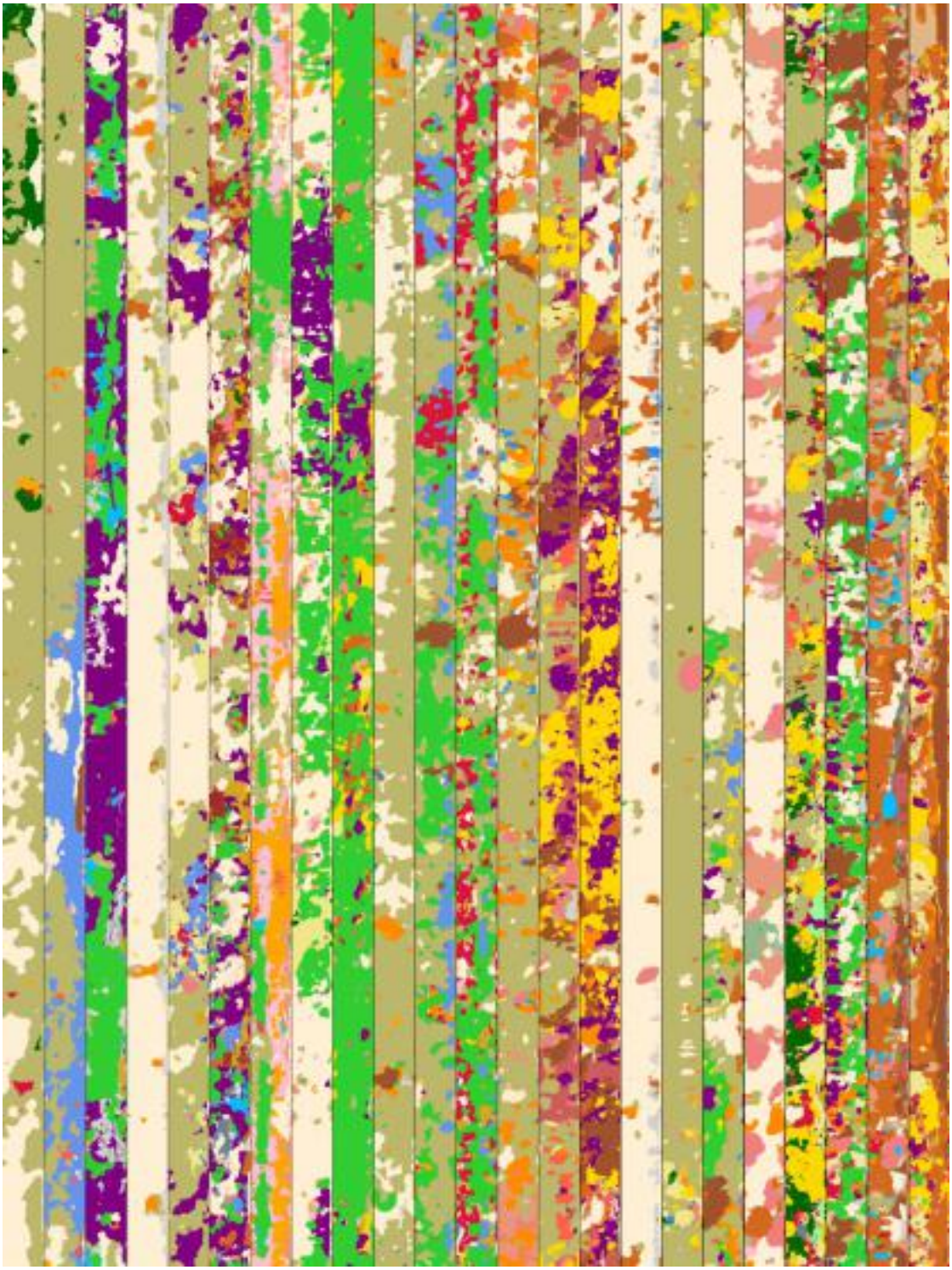

Figure A.11 Habitat maps with workflow segmented+detailed+reflectance. Middle section of 23 learning transects. Size of each section is 640x19920 pixels.

Figure A.12 Habitat maps montage with workflow patched+reefgroups+radiance. Middle section of 23 learning transects. Size of each section is 640x19920 pixels.

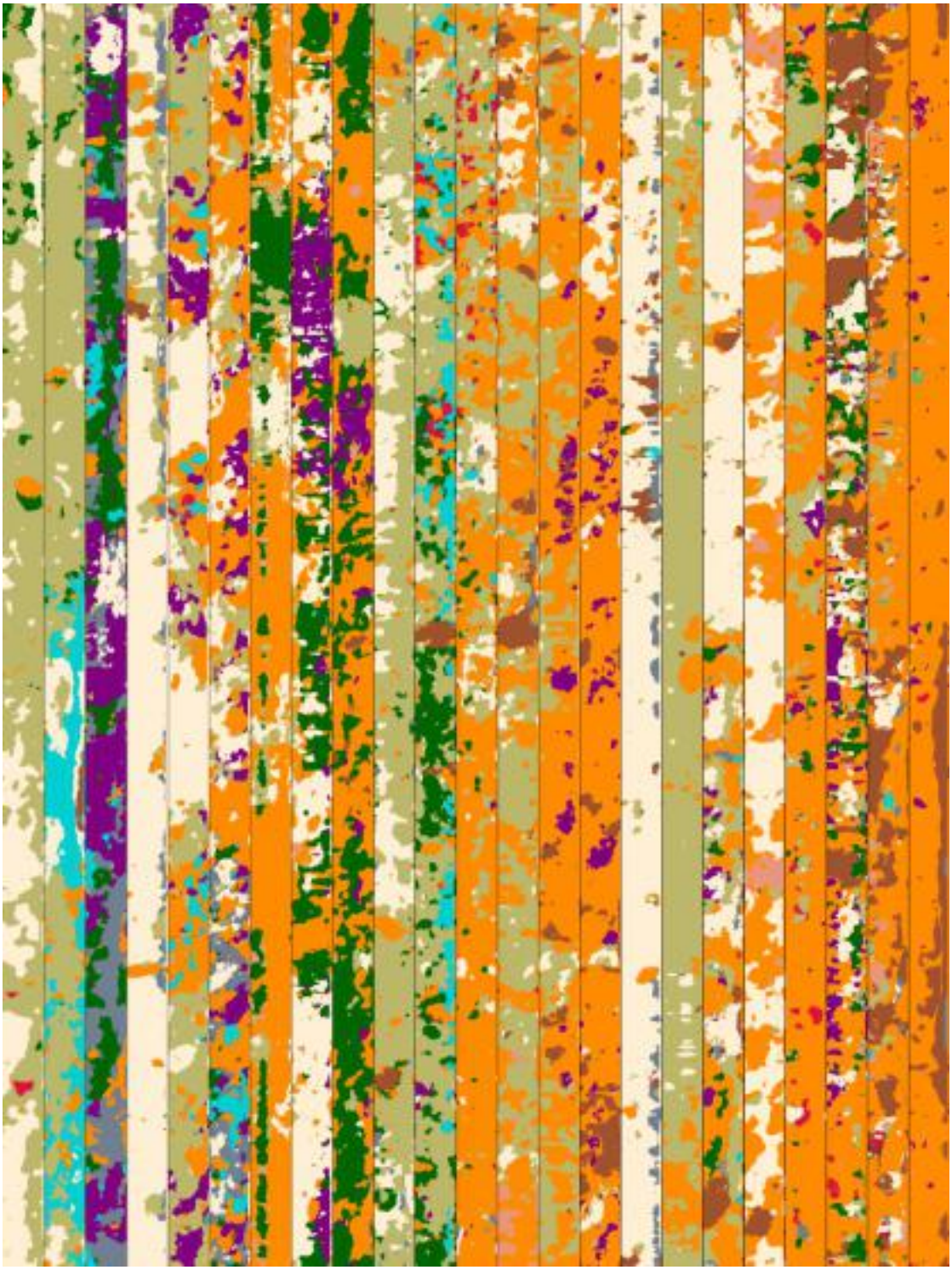

Figure A.13 Habitat maps montage with workflow segmented+reefgroups+radiance. Middle section of 23 learning transects. Size of each section is 640x19920 pixels.

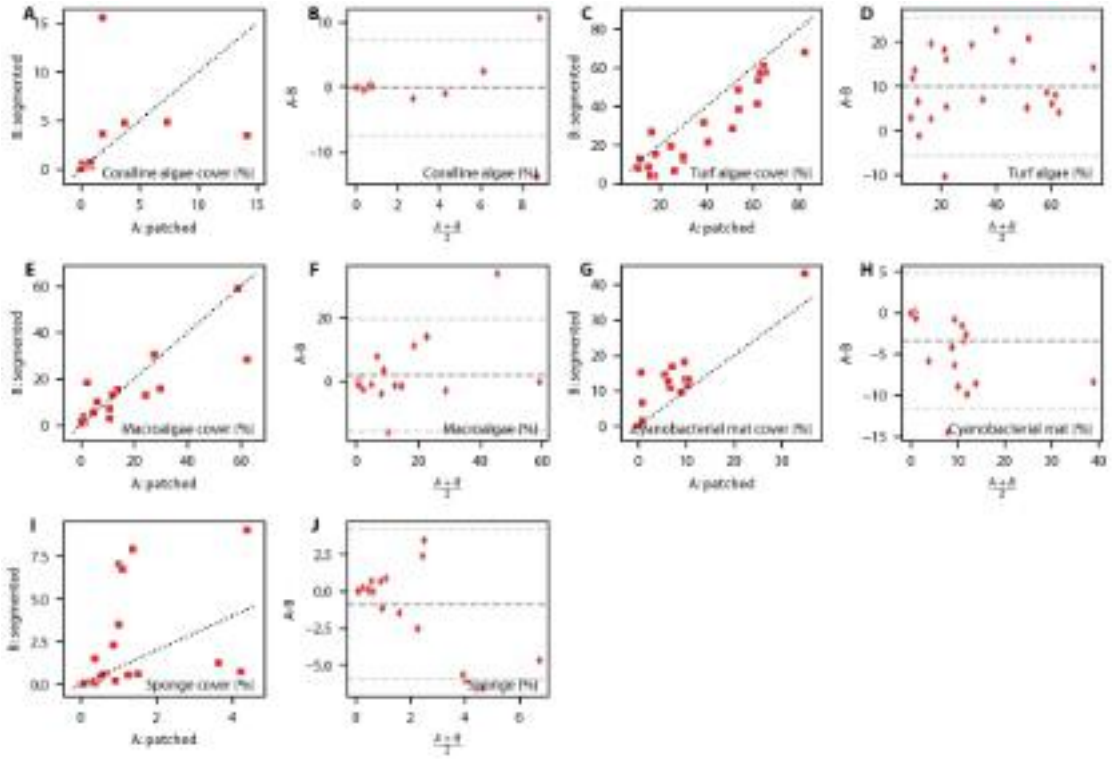

Figure A.14 Correlation and mean-difference (Bland-Altmann) plots of percent coverage from 22 transects for 5 dominant reef classes (see Figure 2.6 for Coral and Sediment plots). The coralline algae cover correlation plot (**A**) shows good correlation of both methods in transects with low coralline algae coverage and disagreement on transects with more than 15% coverage. The mean-difference plot (**B**) show no bias towards any of the methods, with only two transects showing high differences between the methods. The turf algae cover correlation plot (**C**) shows a slight over-estimation by the patched method in almost all transects, which is confirmed by a bias of 10% in the in the mean-difference plot (**D**). The Macroalgae cover correlation plot (**E**) shows agreement between the methods in all 21 transects, and the mean-difference plot (**E**) shows no bias towards any of the methods. The cyanobacterial mat cover correlation plot (**G**) shows slight over-estimation of cover from the segmented method, but overall good alignment of the methods. The mean-difference plot (**H**) shows the bias of 4% towards the segmented method. The sponge cover correlation plot (**I**) shows disagreement between the methods, specially in transects with higher sponge cover. From visual inspection of the maps, it appears that the segmented classifier predicted darkened areas of the transects (which have much lower prediction confidence) as sponges. Due to the low overall cover of the sponge class in the dataset, the mean-difference plot (**J**) does not show a big bias towards any of the two methods.

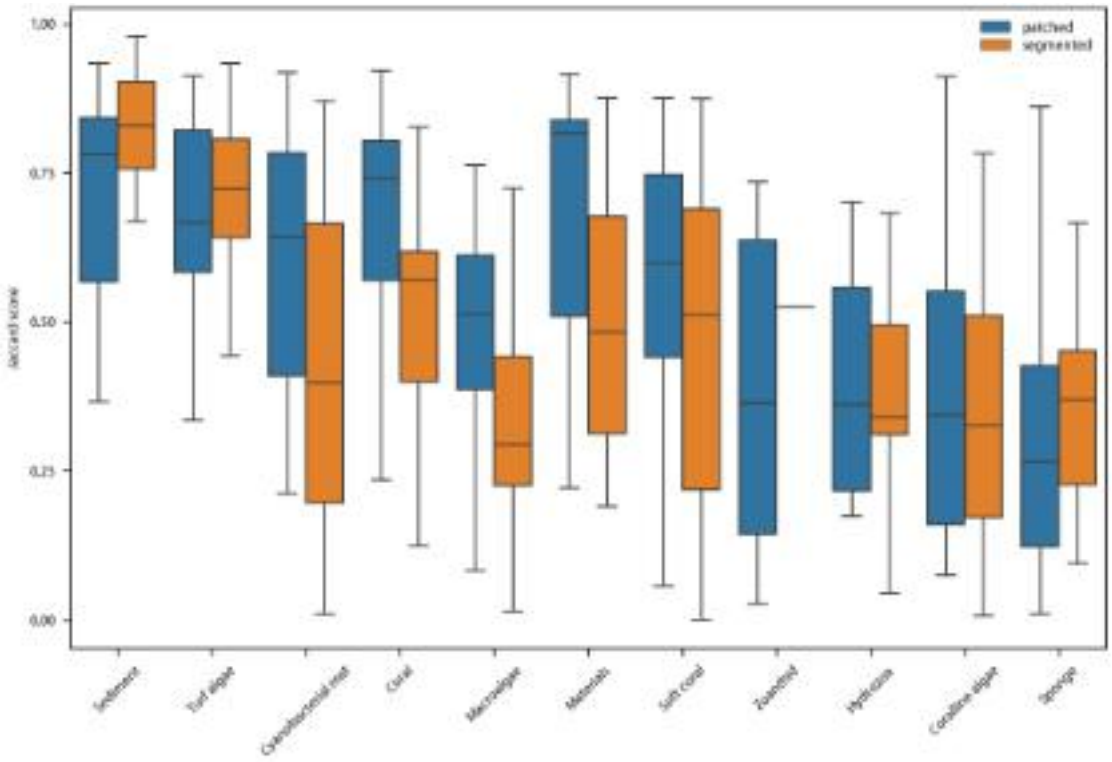

Figure A.15 Configurational similarity assessed using the Jaccard index between the reefgroups and detailed-to-reefgroups habitat maps for all dominant classes, expanding on panel **F** of Figure 2.6. The patched method produces more spatially congruent predictions between the two labelspaces for most of the dominant classes (as shown by the median values): Cyanobacterial mat, Coral, Macroalgae, Materials, Soft coral, Hydrozoa and Coralline algae. Maps produced with the segmented method showed higher configurational similarity between both labelspaces for the remaining classes: Sediment, Turf algae, Zoanthid and Sponge.

Appendix B

Supplementary material for Chapter 3: Curaçao reefs under the hyperspectral lens

B.1 Supplementary figures

Figure B.1 Sample filtering for reliability based on predicted probabilities. For each class in the detailed labelset, we inspected the number of correct predictions that would remain after a certain probability threshold is applied. We settled on a 75% correct fraction value, then selected the corresponding probability threshold for each class and only retained all samples that were predicted with a probability that was higher than the threshold. This improved the confidence on the selected samples considerably.

Appendix C

Supplementary material for Chapter 5: Removing the turbid veil to count corals

C.1 Supplementary figures

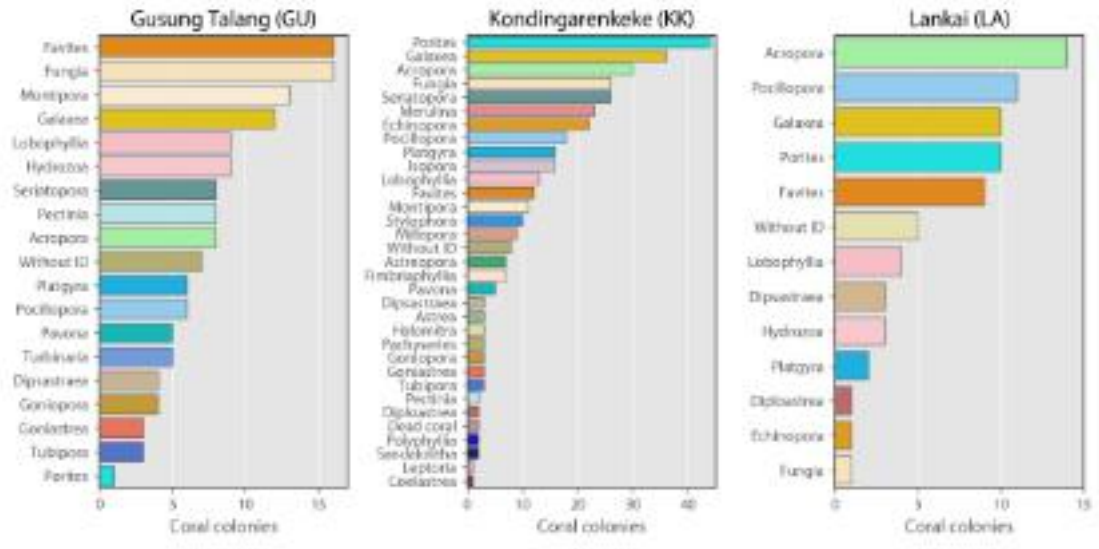

Figure C.1 Scleractinian coral community across the turbidity and depth gradient of 3 coral reefs in the Spermonde Archipelago.

Appendix D

Published source code and datasets

D.1 (Source code) Digitizing the coral reef: a complete workflow for dense taxonomic mapping of benthic habitats with machine learning of underwater hyperspectral images (1.0.0)

Published as Schürholz, Daniel & Chennu, Arjun. (2022). Digitizing the coral reef: a complete workflow for dense taxonomic mapping of benthic habitats with machine learning of underwater hyperspectral images (1.0.0). Zenodo. DOI: 10.5281/zenodo.7185108

D.1.1 Source code repository description

This repository contains the source code to reproduce the work presented in "Digitizing the coral reef: machine learning of underwater spectral images enables dense taxonomic mapping of benthic habitats", written and developed by Daniel Schürholz and Arjun Chennu. The work describes the survey scale mapping of hyperspectral data acquired in the coral reefs of Curacao island in the Caribbean. The repository contains the complete workflow for the creation of habitat maps of benthic communities from underwater hyperspectral scans, and can be adapted to new survey sites.

D.2 (Dataset) Dense and taxonomically detailed habitat maps of coral reef benthos machine-generated from underwater hyperspectral transects in Curaçao

Published as Schürholz, Daniel & Chennu, Arjun (2022). Dense and taxonomically detailed habitat maps of coral reef benthos machine-generated from underwater hyperspectral transects in Curaçao. PANGAEA. DOI: 10.1594/PANGAEA.946315

D.2.1 Dataset description

This dataset contains 248 benthic habitat maps, that were created from 31 underwater hyperspectral images captured with the HyperDiver device in 8 reef sites across the western coastline of Curacao (see https://doi.org/10.3390/data5010019 for information on the acquisition of the transects). The maps were produced by 8 combinations of two semantic labelspaces (detailed and reefgroups), two machine learning classifiers (patched and segmented), and two spectral signals (radiance and reflectance). Maps in the detailed labelspace have each pixel assigned to one of 43 labels, which are taxonomic labels at family, genus and species levels for biotic components of the reef (corals, sponges, macroalgae, etc.), as well as substrate labels (sediment, cyanobacterial mats, turf algae) and survey material labels (transect tape, reference board, etc.). The set of maps in the reefgroups labelspace cluster the labels in the detailed labelspace into 11 classes that describe reef functional groups (i.e. corals, sponges, algae, etc.). All habitat maps were produced with high accuracy (Fbeta 87%), by two different machine learning methods: a random forest ensemble classifier (segmented method) and a deep learning neural network classifier (patched method). The maps are further divided by the signal type from the hyperspectral image that was used, either radiance or reflectance (the latter was calculated with a reference board located at the beginning and end of each transect). These benthic habitat maps can be used to obtain accurate descriptions of the benthic community and habitat structure of coral reef sites in Curacao. The dataset also contains: an assessment of the accuracy and data efficiency of the machine learning methods, a consistency assessment of the mapped regions, a comparison of habitat metrics (class coverage, biodiversity indices, composition and configuration) between habitat maps produced by each method, and an effort-vs-error analysis of sparse sampling techniques on the densely classified maps.

D.3 (Dataset) Detailed tree inventory and area coverage of remote mangrove forests (species: Pelliciera rhizophorae and Rhizophora mangle) in the Utría National Park in the Colombian Pacific Coast

Published as Schürholz, Daniel; Castellanos-Galindo, Gustavo Adolfo; Casella, Elisa; Mejía-Rentería, Juan Carlos; Chennu, Arjun (2023). Detailed tree inventory and area coverage of remote mangrove forests (species: Pelliciera rhizophorae and Rhizophora mangle) in the Utría National Park in the Colombian Pacific Coast. PANGAEA. DOI: 10.1594/PANGAEA.962229

D.3.1 Dataset description

This dataset contains detailed inventories of 7 large plots of mangrove forests in the Utría National Park in the Colombian Pacific Coast. The inventory consists of individual geo-referenced tree masks for the endemic Pelliciera rhizophorae species, and area coverages for the Rhizophora mangle species, as well as Mud and Water areas. For each individual tree of the Pelliciera rhizophorae species we provide the predicted height, crown diameter and crown area. We also provide the cover area of the other predicted classes. The inventories were automatically produced with trained Artificial Intelligence (AI) algorithms. The algorithms were trained with orthomosaic images and digital surface models (DSMs) produced from Unoccupied Aerial System (UAS) imagery with Structure-from-Motion software, both paired with expert annotations of the trees and areas. In this dataset we provide all the input data for the algorithms, as well as the predicted geo-referenced data products, such as: predicted Pelliciera rhizophorae tree masks, Rhizophora mangle areas, Water areas, Mud areas, canopy height models (CHM), digital elevation models (DEM), digital terrain models (DTM) and various ancillary images. We also provide the initial orthomosaic files and the DSM files, that were produced with SfM software Agisoft Metashape v1.6.2 from the aerial footage captured in 2019 (19–22 February) using two consumer-grade UASs: the DJI Phantom 4 and DJI Mavic Pro (SZ DJI Technology Co., Ltd—Shenzhen, China). The DJI Phantom 4 has an integrated photo camera, the DJI FC330 and the DJI Mavic Pro was equipped with the integrated DJI FC220. The flights were programmed to follow the trajectories in an automated mode by means of the commercial application "DroneDeploy". Ground control points (GCPs) were positioned in the field, and their geographic location was acquired. We used two single-band global navigation satellite system (GNSS) receivers: an Emlid Reach RS+ single-band real-time kinematics (RTK) GNSS receiver (Emlid Tech Kft.—Budapest, Hungary) as a base station, and a Bad Elf GNSS Surveyor handheld GPS (Bad Elf, LLC—West Hartford, AZ, USA). RINEX static data from the base station was processed with

the Precise Point Positioning Service (PPP) of the Natural Resources of Canada, while rover position was processed using the RTKLib software through a post processed kinematics (PPK) workflow. The final absolute positional accuracy of the products is below one meter because the results of the PPP workflow has a positional accuracy between 0.2 m and 1 m.